

For Reference

NOT TO BE TAKEN FROM THIS ROOM

For Reference

NOT TO BE TAKEN FROM THIS ROOM

Ex LIBRIS
UNIVERSITATIS
ALBERTAENSIS





Digitized by the Internet Archive
in 2019 with funding from
University of Alberta Libraries

<https://archive.org/details/Quadir1962>

Thesis
1962
#80

THE UNIVERSITY OF ALBERTA

STUDIES ON THE HYDRATES OF NICKEL CHLORIDE

A THESIS

SUBMITTED TO THE FACULTY OF GRADUATE STUDIES
IN PARTIAL FULFILMENT OF THE REQUIREMENTS FOR
THE DEGREE OF DOCTOR OF PHILOSOPHY

DEPARTMENT OF CHEMISTRY

by

SYED JAMAL QUADIR

EDMONTON, ALBERTA
FEBRUARY, 1962.

TABLE OF CONTENTS

	Page
ABSTRACT	i
ACKNOWLEDGEMENTS	iv
LIST OF TABLES	v
LIST OF ILLUSTRATIONS	ix
INTRODUCTION	
General	1
Equilibrium Studies	4
The Hydration Number of Nickel Ions in Solution	9
Kinetic Studies	16
Structural Studies	35
Objectives of the Present Work	53
EXPERIMENTAL	
Equilibrium Studies	
The $\text{NiCl}_2 - \text{H}_2\text{O}$ System	54
The $\text{NiCl}_2 - \text{H}_2\text{O-en}$ System	63
Kinetic Studies	68
Infrared and X-ray Studies	72
RESULTS	
Equilibrium Studies	75
Kinetic Studies	106
Infrared and X-ray Studies	147

	Page
DISCUSSION	
Equilibrium Studies	162
Kinetic Studies	176
Structural Studies	193
SUMMARY	222
BIBLIOGRAPHY	223

ABSTRACT

Investigations on the nickel chloride-water system have revealed that the stable hydrates are: $\text{NiCl}_2 \cdot 6\text{H}_2\text{O}$, $\text{NiCl}_2 \cdot 4\text{H}_2\text{O}$ and $\text{NiCl}_2 \cdot 2\text{H}_2\text{O}$ in contradistinction to the suggestions of Castor and Basolo. Thermodynamic, kinetic, infrared absorption and X-ray diffraction studies confirm this contention.

The thermodynamic measurements on the $\text{NiCl}_2\text{-H}_2\text{O}$ system revealed a stepwise character of the isotherm. The transition temperatures for the conversion of $\text{NiCl}_2 \cdot 6\text{H}_2\text{O}$ to $\text{NiCl}_2 \cdot 4\text{H}_2\text{O}$, and $\text{NiCl}_2 \cdot 4\text{H}_2\text{O}$ to $\text{NiCl}_2 \cdot 2\text{H}_2\text{O}$ have been determined. From the isotherms the solubility limits at different temperatures were obtained. From the temperature dependence of solubility the heats of solution for $\text{NiCl}_2 \cdot 6\text{H}_2\text{O}$ and $\text{NiCl}_2 \cdot 4\text{H}_2\text{O}$ were calculated. For obtaining absolute binding energies for the water addenda, lattice energies for NiCl_2 , $\text{NiCl}_2 \cdot 2\text{H}_2\text{O}$, $\text{NiCl}_2 \cdot 4\text{H}_2\text{O}$ and $\text{NiCl}_2 \cdot 6\text{H}_2\text{O}$ were calculated.

The atmosphere of the Ni(II) ion in aqueous solution and in the solid state has been found to be different. The temperature induced transitions observed in the solid state were not detectable in solution. In aqueous solution six

water molecules are symmetrically disposed around the Ni(II) ion; whereas in the solid state the structural unit is $[\text{Ni}(\text{H}_2\text{O})_4\text{Cl}_2] \cdot 2\text{H}_2\text{O}$. This has been confirmed by the recent appearance of the structure of $\text{NiCl}_2 \cdot 6\text{H}_2\text{O}$.

The kinetics of the dehydration of $\text{NiCl}_2 \cdot 6\text{H}_2\text{O}$ at different temperatures and with different desiccants of varying efficiency were determined. A model for the mechanism of dehydration has been proposed. From the temperature dependence of the rate of dehydration the activation energy for the conversion of $\text{NiCl}_2 \cdot 6\text{H}_2\text{O}$ to $\text{NiCl}_2 \cdot 4\text{H}_2\text{O}$ was calculated.

The infrared spectra of $\text{NiCl}_2 \cdot 6\text{H}_2\text{O}$, $\text{NiCl}_2 \cdot 4\text{H}_2\text{O}$ and $\text{NiCl}_2 \cdot 2\text{H}_2\text{O}$ reveal certain distinct features. From the gradual emergence and disappearance of certain absorption bands it is evident that the only stable hydrates are $\text{NiCl}_2 \cdot 6\text{H}_2\text{O}$, $\text{NiCl}_2 \cdot 4\text{H}_2\text{O}$ and $\text{NiCl}_2 \cdot 2\text{H}_2\text{O}$. The bands at the O-H stretching, O-H bending and coordinated water regions have been explained in terms of hydrogen bonding of the types O-H--O and O-H--Cl. From the frequency displacements, the O-H--O and O-H--Cl bond distances have been computed and compared with those reported in the literature. The O-H--O and O-H--Cl distances for $\text{NiCl}_2 \cdot 2\text{H}_2\text{O}$ and $\text{NiCl}_2 \cdot 6\text{H}_2\text{O}$ have been found to agree reasonably with the literature values. Infrared spectra of some iso-

morphous hydrates of divalent metal chloride of the first transition series were taken to determine the relation between isomorphism and the infrared spectra. It seems quite probable from the infrared absorption evidence that $\text{NiCl}_2 \cdot 4\text{H}_2\text{O}$ is isomorphous with $\text{MnCl}_2 \cdot 4\text{H}_2\text{O}$.

The stability of different hydrates in atmospheres of different relative humidity was examined to establish exact conditions for obtaining $\text{NiCl}_2 \cdot 6\text{H}_2\text{O}$, $\text{NiCl}_2 \cdot 4\text{H}_2\text{O}$ and $\text{NiCl}_2 \cdot 2\text{H}_2\text{O}$ at room temperature.

ACKNOWLEDGEMENTS

The author wishes to express his appreciation for the guidance and inspiration of Dr. William J. Wallace who initiated and supervised this work.

The author acknowledges his indebtedness to Dr. G. R. Freeman for many important suggestions which improved the presentation of this work.

The author is indebted to External Aid Office (Canada) (Economic and Technical Assistance Branch - Department of Trade and Commerce) for the award of a Colombo Plan scholarship and to Pakistan Council of Scientific and Industrial Research for considering him on duty and financial support.

Advice and encouragement of Dr. K. P. Singh of the Department of Mining and Metallurgy of the University of Alberta is gratefully acknowledged.

Finally, the author expresses his appreciation and gratitude to his wife, Bibha, for her patience and understanding and her willing sacrifices which made this work possible.

LIST OF TABLES

Table		Page
1	Vapour Pressure of Ethylenediamine at Different Temperatures	63
2	Vapour Pressure - Composition Data for $\text{NiCl}_2\text{-H}_2\text{O}$ System at 27, 30, 35 and 36°C	76
3	Vapour Pressure - Composition Data for $\text{NiCl}_2\text{-H}_2\text{O}$ System at 37, 40, 45, 50 and 55°C	78
4	Vapour Pressure - Composition Data for $\text{NiCl}_2\text{-H}_2\text{O}$ System at 60, 65 and 70°C	80
5	Vapour Pressure - Composition Data for $\text{NiCl}_2\text{-H}_2\text{O}$ System at 75°C	81
6	Logarithm of Vapour Pressure - $1/T$ Data for $\text{NiCl}_2\text{-H}_2\text{O}$ System for $\text{NiCl}_2\text{:H}_2\text{O}$ Ratios of 23.83, 16.38, 12.82 and 10.97	84
7	Logarithm of Vapour Pressure - $1/T$ Data for $\text{NiCl}_2\text{-H}_2\text{O}$ System for $\text{NiCl}_2\text{:H}_2\text{O}$ Ratios of 9.66, 8.38, 7.35 and 6.15	86
8	Logarithm of Vapour Pressure - $1/T$ Data for $\text{NiCl}_2\text{-H}_2\text{O}$ System for $\text{NiCl}_2\text{:H}_2\text{O}$ Ratios of 5.58, 5.08, 4.68, 4.37 and 4.28	89
9	Logarithm of Vapour Pressure - $1/T$ Data for $\text{NiCl}_2\text{-H}_2\text{O}$ System for $\text{NiCl}_2\text{:H}_2\text{O}$ Ratios of 3.89, 3.58, 3.30, 2.52 and 2.16	92

Table		Page
10	Vapour Pressure Data for $\text{NiCl}_2\text{-H}_2\text{O}$ System at Different Temperatures for $\text{NiCl}_2\text{:H}_2\text{O}$ Ratio of 3.89	93
11	Solubility Limits of NiCl_2 in Water	96
12	Vapour Pressure - Composition Data for Aqueous $\text{NiCl}_2\text{-en}$ System at 23, 25, 27 and 30°C	99
13	Vapour Pressure - Composition Data for Aqueous $\text{NiCl}_2\text{-en}$ System at 35, 40, 45 and 50°C	101
14	Vapour Pressure of Aqueous Solution of Nickel Chloride at Different Temperatures for a Composition $\text{H}_2\text{O/NiCl}_2 = 13.49$	104
15a	Dehydration of $\text{NiCl}_2\cdot 6\text{H}_2\text{O}$ at Room Tempe- rature $\cong 25^\circ\text{C}$ for a Sample 2.8542 gm. in a Desiccator Containing P_2O_5 Desiccant	107
15b	Dehydration of $\text{NiCl}_2\cdot 6\text{H}_2\text{O}$ at Room Tempe- rature $\cong 25^\circ\text{C}$ for a Sample 1.6892 gm. in a Desiccator Containing Phosphorous Pent- oxide Desiccant	111
16	Dehydration of $\text{NiCl}_2\cdot 6\text{H}_2\text{O}$ at Room Tempe- rature $\cong 25^\circ\text{C}$ for a Sample 132.3 mg. over a Quartz Spiral Balance Containing $\text{Mg}(\text{ClO}_4)_2$ Desiccant	115

Table		Page
17	Dehydration of $\text{NiCl}_2 \cdot 6\text{H}_2\text{O}$ at 25°C for a Sample 475.5 mg. over a Quartz Spiral Balance in Vacuum	120
18	Dehydration of $\text{NiCl}_2 \cdot 6\text{H}_2\text{O}$ at 35°C for a Sample 476.0 mg. over a Quartz Spiral Balance in Vacuum	123
19	Dehydration of $\text{NiCl}_2 \cdot 6\text{H}_2\text{O}$ at 45°C for a Sample 479.0 mg. over a Quartz Spiral Balance in Vacuum	126
20	Rate of Loss of Water for $\text{NiCl}_2 \cdot 6\text{H}_2\text{O}$ at Different Temperatures	134
21	Dehydration of $\text{NiCl}_2 \cdot 6\text{H}_2\text{O}$ at Different Relative Humidities at Room Temperature $\cong 25^\circ\text{C}$	136
22	Rate of Dehydration of $\text{NiCl}_2 \cdot 6\text{H}_2\text{O}$ under Different Relative Humidities	142
23	Stable Hydrates of Nickel Chloride in the Atmospheres of Different Relative Humidi- ties	145
24	Prominent Bands of the Infrared Spectra of the Hydrates of Nickel Chloride in cm^{-1}	154
25	Prominent O-H Stretching Frequencies of Different Hydrates in cm^{-1}	155

Table		Page
26	Enthalpy and Entropy of Decomposition of the Hydrates of Nickel Chloride	165
27	Release of Water to the Medium by the Reaction of Ethylenediamine with Aqueous Nickel Chloride Solution at Different Temperatures	173
28	Lattice Energy Values of Nickel Chloride Hydrates	217

LIST OF ILLUSTRATIONS

Figure		Page
1	The Stepwise Dehydration	8
2	The Continuous Dehydration	8
3	Schematic Representation of Ni(en)_3 and $\text{Ni(H}_2\text{O)}_6$	12
4	Model of Interface	15
5	Effect of Water Vapour Pressure on Nucleation	20
6	Dehydration Curve for $\text{CuSO}_4 \cdot 5\text{H}_2\text{O}$ in Presence of Increasing Pressures of Water Vapour	21
7	Dehydration Curve for $\text{MnC}_2\text{O}_4 \cdot 2\text{H}_2\text{O}$ in Presence of Increasing Pressures of Water Vapour	21
8	Differential Rate Curves for the Dehydration of $\text{CuSO}_4 \cdot 5\text{H}_2\text{O}$ (Crowther & Coutts)	23
9	Dehydration of Calcium Chloride (Castor & Basolo)	28
10	Dehydration of Zirconyl Chloride (Castor & Basolo)	28
11	Differential Rate Curves (Castor & Basolo)	32
12	The Schematic Representation of the Crystal Structure of $\text{CoCl}_2 \cdot 6\text{H}_2\text{O}$	37

Figure		Page
13	The Environment of the Fifth H_2O Molecule in $\text{CuSO}_4 \cdot 5\text{H}_2\text{O}$	38
14	The Structure of $\text{CuCl}_2 \cdot 2\text{H}_2\text{O}$	38
15	The Structure of $\text{CoCl}_2 \cdot 2\text{H}_2\text{O}$	41
16	Potential Energy Curve	44
17	Experimental Set-up of Stock Type High Vacuum Line	55
18	Experimental Set-up for the Thermodynamic Measurements on the $\text{NiCl}_2\text{-H}_2\text{O}$ System	56
19	Weighing Tube	59
20	Fractionation Train for the Purification of Ethylenediamine	64
21	Sodium Mirror Bulb for the Purification of Ethylenediamine	65
21a	Experimental Set-up for Dehydration over Quartz Spiral Balance	71
22	Vapour Pressure - Composition Diagrams for $\text{H}_2\text{O-NiCl}_2$ System at 27°C , 30°C , 33°C , 35°C and 36°C	77
23	Vapour Pressure - Composition Diagrams for $\text{H}_2\text{O-NiCl}_2$ System at 36°C , 37°C , 40°C , 45°C , 50°C and 55°C	79
24	Vapour Pressure - Composition Diagrams for $\text{H}_2\text{O-NiCl}_2$ System at 60°C , 65°C , 70°C , and 75°C	82

Figure		Page
25	Log P as a function of $1/T$ for $H_2O/NiCl_2$ Ratio of 23.83, 16.38, 12.82 and 10.97	85
26	Log P as a function of $1/T$ for $H_2O/NiCl_2$ Ratio of 9.66	87
27	Log P as a function of $1/T$ for $H_2O/NiCl_2$ Ratio of 8.38, 7.35 and 6.15	88
28	Log P as a function of $1/T$ for $H_2O/NiCl_2$ Ratio of 5.58, 5.08, 4.68, 4.37 and 4.28	90
29	Log P as a function of $1/T$ for $H_2O/NiCl_2$ Ratio of 3.89, 3.58, 3.30, 2.52 and 2.16	94
30	Log N as a function of $1/T$ for $NiCl_2 - H_2O$ System	97
31	Vapour Pressure - Composition Diagrams for Aqueous Nickel Chloride - en System at $23^\circ C$, $25^\circ C$, $27^\circ C$ and $30^\circ C$	100
32	Vapour Pressure - Composition Diagrams for Aqueous Nickel Chloride - en System at $35^\circ C$, $40^\circ C$ and $45^\circ C$	102
33	Vapour Pressure - Composition Diagrams for Aqueous Nickel Chloride - en System at $50^\circ C$	103
34	Log P as a function of $1/T$ for an Aqueous Solution of Nickel Chloride of $H_2O/NiCl_2$ Ratio of 13.49	105

Figure		Page
35	Dehydration Curve for $\text{NiCl}_2 \cdot 6\text{H}_2\text{O}$ Desiccated over Phosphorous Pentoxide in a Desiccator	113
36	Differential Rate Curves	114
37	Dehydration Curve for $\text{NiCl}_2 \cdot 6\text{H}_2\text{O}$ over a Quartz Spiral Balance Containing $\text{Mg}(\text{ClO}_4)_2$ at $\approx 25^\circ\text{C}$	118
38	Differential Rate Curves	119
39	Dehydration Curve for $\text{NiCl}_2 \cdot 6\text{H}_2\text{O}$ over a Quartz Spiral Balance in Vacuum at 25°C	128
40	Dehydration Curve for $\text{NiCl}_2 \cdot 6\text{H}_2\text{O}$ over a Quartz Spiral Balance in Vacuum at 35°C	129
41	Dehydration Curve for $\text{NiCl}_2 \cdot 6\text{H}_2\text{O}$ over a Quartz Spiral Balance in Vacuum at 45°C	130
42	Differential Rate Curves at 25°C	131
43	Differential Rate Curves at 35°C	132
44	Differential Rate Curves at 45°C	133
45	Log K as a function of $1/T$	135
46	Decomposition Curve for $\text{NiCl}_2 \cdot 6\text{H}_2\text{O}$ at Room Temperature $\approx 25^\circ\text{C}$ for Sulphuric Acid Desiccants of Specific Gravity 1.40, 1.50 and 1.60	140

Figure		Page
47	Decomposition Curve for $\text{NiCl}_2 \cdot 6\text{H}_2\text{O}$ at Room Temperature $\approx 25^\circ\text{C}$ for Sulphuric Acid Desiccants of Specific Gravity 1.60, 1.70 and 1.80, and $\text{Mg}(\text{ClO}_4)_2$ and P_2O_5	141
48	Rate of Loss of Water as a Function of Desiccant Efficiency	144
49	Reproducibility of Infrared Absorption Spectra	149
50	Infrared Absorption Spectra of $\text{NiCl}_2 \cdot 6\text{H}_2\text{O}$, $\text{NiCl}_2 \cdot 4\text{H}_2\text{O}$ and $\text{NiCl}_2 \cdot 2\text{H}_2\text{O}$ in the O-H Stretching Region	150
51	Infrared Absorption Spectra of $\text{NiCl}_2 \cdot 6\text{H}_2\text{O}$, $\text{NiCl}_2 \cdot 4\text{H}_2\text{O}$ and $\text{NiCl}_2 \cdot 2\text{H}_2\text{O}$ in the O-H Bending Region	151
52	Infrared Absorptions Spectra of $\text{NiCl}_2 \cdot 6\text{H}_2\text{O}$, $\text{NiCl}_2 \cdot 4\text{H}_2\text{O}$ and $\text{NiCl}_2 \cdot 2\text{H}_2\text{O}$ in the 800 cm^{-1} Region	152
53	Infrared Absorption Spectra of Nickel Chloride at Different Stages of Hydration in $3500 - 3000\text{ cm}^{-1}$ Region (Normal)	156
54	Infrared Absorption Spectra of Nickel Chloride at Different States of Hydration in $1650 - 1550\text{ cm}^{-1}$ Region (Normal)	157

Figure		Page
55	Infrared Absorption Spectra of Nickel Chloride Hydrates at Different Stages of Hydration in $3500 - 3000 \text{ cm}^{-1}$ Region (Five Times Expansion)	158
56	X-ray Diffractometer Traces for $\text{NiCl}_2 \cdot 6\text{H}_2\text{O}$, $\text{NiCl}_2 \cdot 4\text{H}_2\text{O}$ and $\text{NiCl}_2 \cdot 2\text{H}_2\text{O}$	159
57	X-ray Diffractometer Traces for Nickel Chloride Hydrates $\text{NiCl}_2 \cdot 5\text{H}_2\text{O}$, $\text{NiCl}_2 \cdot 4\text{H}_2\text{O}$ and $\text{NiCl}_2 \cdot 3\text{H}_2\text{O}$	160
58	X-ray Diffractometer Traces for Nickel Chloride Hydrates $\text{NiCl}_2 \cdot 2.5\text{H}_2\text{O}$ and $\text{NiCl}_2 \cdot 2\text{H}_2\text{O}$	161
59a	Vapour Pressure - Composition Diagram for H_2O -en System	170
59b	Decomposition Curve for $\text{NiCl}_2 \cdot 6\text{H}_2\text{O}$ at 25°C (Castor & Basolo)	181
60	$\frac{d[A]}{dt}$ as a function of $[C]$	189
61	Different Values of k_5 between 0.1 to 1.0 as a function of $[C]$	191
62	Diagrammatic Representation of $\text{CoCl}_2 \cdot 6\text{H}_2\text{O}$	194
63	Diagrammatic Representation of $\text{NiCl}_2 \cdot 4\text{H}_2\text{O}$	196
64	Diagrammatic Representation of $\text{NiCl}_2 \cdot 2\text{H}_2\text{O}$	196

Figure		Page
65	Structural Relation between $\text{NiCl}_2 \cdot 6\text{H}_2\text{O}$, $\text{NiCl}_2 \cdot 4\text{H}_2\text{O}$ and $\text{NiCl}_2 \cdot 2\text{H}_2\text{O}$	198
66	Infrared Absorption Spectra of $\text{NiCl}_2 \cdot 6\text{H}_2\text{O}$, $\text{NiCl}_2 \cdot 5.5\text{H}_2\text{O}$, $\text{NiCl}_2 \cdot 5\text{H}_2\text{O}$, and $\text{NiCl}_2 \cdot 4.5\text{H}_2\text{O}$ in 800 cm^{-1} Region	200
67	Infrared Absorption Spectra of $\text{NiCl}_2 \cdot 6\text{H}_2\text{O}$ and $\text{CoCl}_2 \cdot 6\text{H}_2\text{O}$	206
68	Infrared Absorption Spectra of $\text{NiCl}_2 \cdot 4\text{H}_2\text{O}$ and $\text{MnCl}_2 \cdot 4\text{H}_2\text{O}$	207
69	Infrared Absorption Spectra of $\text{NiCl}_2 \cdot 2\text{H}_2\text{O}$, $\text{CoCl}_2 \cdot 2\text{H}_2\text{O}$ and $\text{MnCl}_2 \cdot 2\text{H}_2\text{O}$	208
70	Infrared Absorption Spectra of $\text{NiCl}_2 \cdot 6\text{H}_2\text{O}$ Heated to Different Temperatures	210
71	The Position of Hydrogen in $\text{NiCl}_2 \cdot 6\text{H}_2\text{O}$ Estimated on the Basis of Infrared Obser- vation	211
72	Density of Cobalt and Nickel Chloride Hydrates as a Function of Water Content	219

STUDIES ON THE HYDRATES OF NICKEL CHLORIDE

INTRODUCTION

General

Within the field of metal ion chemistry there is probably not a more widely recognized phenomenon than the tendency of the metal ions to attract and associate with other polar species. These species may range from ions of opposite charge through uncharged but polar Lewis acids to non-polar but polarizable Lewis acids. Within the group of compounds formed in this way none is more prevalent than the compounds formed by the interaction of metal ions with water and referred to as hydrates. For the purpose of discussion it is convenient to divide the hydrates into two subdivisions. Those which occur in solution and those which occur in the solid state. In solution the concept of hydrated metal ions is generally applied whereas in the solid state it is usual to speak of salt hydrates. The difference between these two situations is undoubtedly more apparent than real. Probably the principal difference is that the situation is much less clear in solution. Here the actual arrangement of

the water molecules with respect to the metal ion depends upon the charge density on the metal ion and its consequent ability to break down the water structure. This ability will, of course, vary from large monovalent cations where disruption of the water structure is negligible and the ion fits into the normal water structure by displacement of a water molecule to small polyvalent cations where the water molecules are pulled in to the extent that the resulting complex is, at least formally, analogous to an ammonia complex. The fuzziness in this picture results from the high lability of the associated water molecules, the ability of the fundamental aquo-complex to influence the surrounding water structure and the current uncertainty about the mode of attachment of the water molecules. Thus, recent studies have shown that the half time of exchange of water molecules in non-ligand field stabilized systems is of the order of 10^{-3} seconds (1). A variety of methods of estimating hydration numbers have been reported over the years and these have yielded values ranging from 2 or 3 water molecules to as many as 30 or 40 (2). It has been such studies as these which have led to the concept of first, second, third, etc., solvation sheaths. In view of Taube's observations (3) upon chromium(III) aquo ions in solution it would seem reasonable to accept as valid the concept of an inner or first solvation sheath which gives to the ion the properties of a

normal complex ion of the ammine type. Subsequent solvation sheaths must then be interpreted in terms of the influence of this ion upon the remainder of the water structure. This may range from highly oriented molecules in the immediate vicinity of the ion to those which are not significantly affected by the presence of the metal ion and are in normal water structure positions. These latter molecules might be described as free in comparison with those which do lie under the influence of the field of the metal ions. The final uncertainty is associated with the attachment of the water molecules. Spectroscopic studies on the same system are not in agreement concerning the attachment of water molecules. The ESR results seem to indicate unsymmetrical attachment in the form of normal electron pair overlap. Whereas polarized infrared measurements indicated symmetrical attachment along the axis of the water dipole (4).

Despite these difficulties some progress has been made toward estimating the energy of interaction of single water molecules with ions in solution (5). It seems rather more likely that information of this kind could be obtained from studies in which the atmosphere of the metal ion is known and constant. This then suggests a study of the solid hydrated salts in an effort to determine such information. In the course of such a study it is necessary to be able to isolate, identify and study all the hydrated salts that a

metal ion will form.

Most of the studies which have been made with a view to isolating and identifying salt hydrates originate in an equilibrium study which has its basis in the phase rule. However, over the years there have been efforts to use kinetic studies for the identification of unusual or unstable phases. Studies of both of these kinds have been reported in the literature and will be discussed below. Once the systems for study have been identified it is necessary to know something of their structural relationships before proceeding to draw conclusions with respect to the energetics of the transformation of one form into another. Until relatively recently there has been little structural information on the salt hydrates. Currently, however, there is an increasing volume of such information becoming available in the literature. These studies too will be discussed below.

Studies such as these which lead to an understanding of the nature and properties of salt hydrates with particular reference to those of the divalent ions of the first transition metal series will form the bulk of this introductory section.

Equilibrium Studies

With the advent of the crystal field theory some attempts have been made to correlate the hydration energies of the divalent transition metal ions on the basis of purely

electrostatic interaction effects (6). In the divalent and trivalent ions of the first transition series the heats of hydration vary in an irregular manner. However, when the estimated crystal field corrections are subtracted from the total heats, the residual values fall on a smooth curve in the so-called "natural order" (7). In view of the uncertainty associated with solvation energies it was thought worthwhile to attempt to estimate the metal-water interaction energy under circumstances where the environment of the metal ion was more nearly fixed and understood. This objective suggested that the most easily dissociable metal complexes, metal hydrates, were worthy of examination. Thus, the nickel chloride-water system was chosen and has been examined by a simple, static vapour pressure-composition technique. The vapour pressure-composition behaviour of the $\text{NiCl}_2\text{-H}_2\text{O}$ system has not been extensively studied. However, Derby and Yngve (8) studied the vapour pressures of the systems containing water and magnesium(II), copper (II), cobalt(II) and nickel(II) chlorides in an isosteniscope in an effort to determine the number of hydrates in each system and their transition temperatures. For the nickel chloride-water systems only four compositions corresponding to mole ratios of $\text{H}_2\text{O}/\text{NiCl}_2$ of 6, 5.74, 4 and 3.78 were studied. From the vapour pressure-temperature curves the transition temperature for the conversion of $\text{NiCl}_2\cdot 6\text{H}_2\text{O}$ to $\text{NiCl}_2\cdot 4\text{H}_2\text{O}$

was reported to be 36.25°C and from extrapolation of vapour pressure-temperature curves for $\text{NiCl}_2 \cdot 4\text{H}_2\text{O}$ -saturated vapour and $\text{NiCl}_2 \cdot 4\text{H}_2\text{O}$ - $\text{NiCl}_2 \cdot 2\text{H}_2\text{O}$ -saturated vapour the transition of $\text{NiCl}_2 \cdot 4\text{H}_2\text{O}$ into $\text{NiCl}_2 \cdot 2\text{H}_2\text{O}$ was estimated to be "about" 75° .

From the solubility measurements of Benrath, and Boye (9b) the hydrates reported were $\text{NiCl}_2 \cdot 2\text{H}_2\text{O}$, $\text{NiCl}_2 \cdot 4\text{H}_2\text{O}$, $\text{NiCl}_2 \cdot 6\text{H}_2\text{O}$ and $\text{NiCl}_2 \cdot 7\text{H}_2\text{O}$. The transition temperatures for the conversion of $\text{NiCl}_2 \cdot 6\text{H}_2\text{O}$ to $\text{NiCl}_2 \cdot 4\text{H}_2\text{O}$ and $\text{NiCl}_2 \cdot 4\text{H}_2\text{O}$ to $\text{NiCl}_2 \cdot 2\text{H}_2\text{O}$ were reported by Benrath and Boye (9b) to be 29°C and 64°C .

In a study of the ternary system of nickel chloride-hydrochloric acid-water Foote (10) confirmed $\text{NiCl}_2 \cdot 6\text{H}_2\text{O}$, $\text{NiCl}_2 \cdot 4\text{H}_2\text{O}$ and $\text{NiCl}_2 \cdot 2\text{H}_2\text{O}$ as the only identifiable species.

Pearce and Eckstrom (9a) determined the solubility of nickel chloride in water at 25°C and calculated the activity of the solvent and the partial and apparent molal volumes of the dissolved salt.

It is apparent that the thermodynamic functions for the conversion of $\text{NiCl}_2 \cdot 6\text{H}_2\text{O}$ to $\text{NiCl}_2 \cdot 4\text{H}_2\text{O}$ and $\text{NiCl}_2 \cdot 4\text{H}_2\text{O}$ to $\text{NiCl}_2 \cdot 2\text{H}_2\text{O}$ have not been reported. Thus, a careful study of the nickel(II) chloride-water system appears justified.

The phase rule states that for a system of C components and P phases

$$F = C - P + 2$$

where F is the number of degrees of freedom. A complete

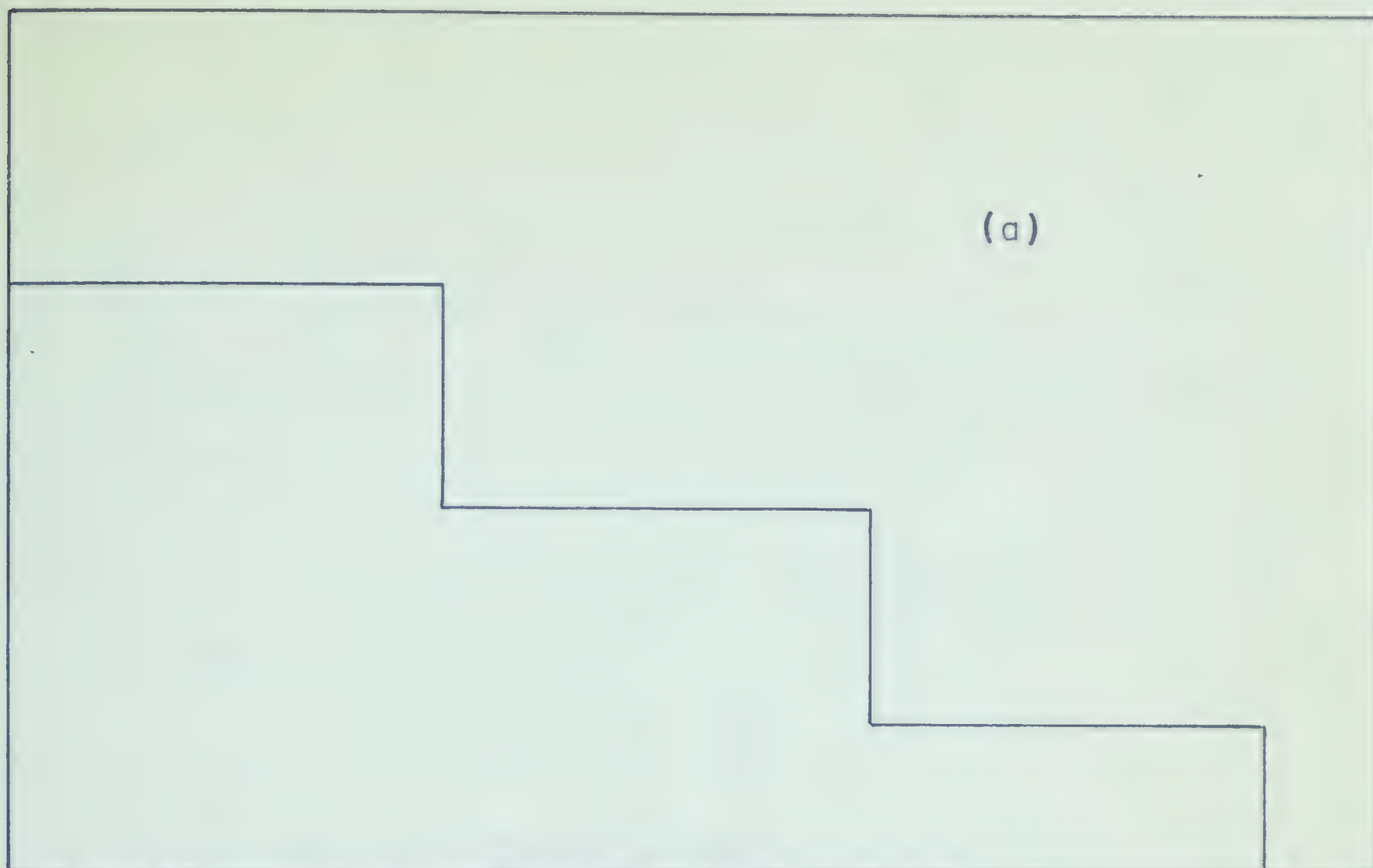
description of a two component system in a single phase would require three variables. These are most commonly pressure, temperature and composition. Isothermal variation of pressure with composition would lead to a diagram which shows the existence of specific phases. If such measurements are carried out at different temperatures then the effect of change of temperature on the system is observable also.

Within specific temperature and pressure limits a particular metal hydrate is stable. Outside the temperature and pressure region of stability the hydrate in question is transformed irreversibly into some other form which is stable under the then existing conditions.

Crystal hydrates may be classified into two extreme types from the standpoint of the shape of the dehydration isotherm (11,12). These are continuous dehydration and step-wise dehydration as shown in Figs. 1 and 2. Zeolites invariably exhibit continuous dehydration. When a pair of hydrates are structurally so similar that they are able to form solid solutions the behaviour observed is that shown by solutions generally, i.e. a continuous variation in vapour pressure which corresponds to the continuous change in the composition of the solution. It is only when there are distinct and separate phases that a marked discontinuity is observed upon transformation of one hydrate into another.

DEHYDRATION PRESSURE

(a)

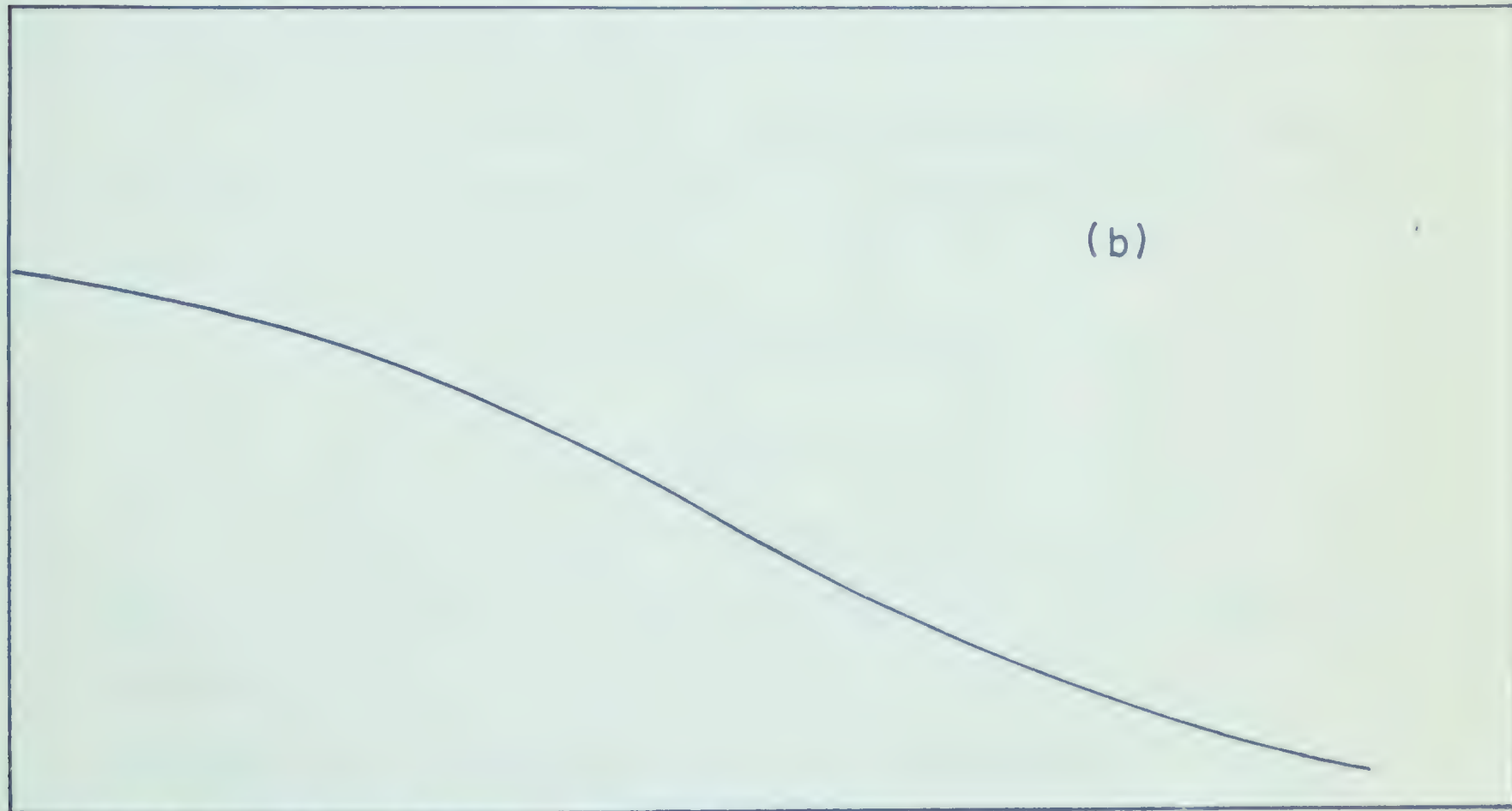


AMOUNT OF WATER DEHYDRATED

Fig. 1

DEHYDRATION PRESSURE

(b)

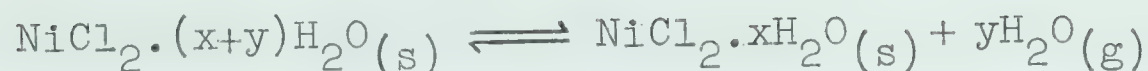


AMOUNT OF WATER DEHYDRATED

Fig. 2

TWO EXTREME TYPES OF DEHYDRATION ISOTHERM. (a) THE STEPWISE DEHYDRATION, (b) THE CONTINUOUS DEHYDRATION.

For the reaction:



the equilibrium constant is just the pressure of water over the solid.

$$K_p = P^y$$

Van't Hoff isochore can now be applied. It is expressed as:

$$\frac{d \ln K}{dT} = \frac{-\Delta H^\circ}{RT^2}$$

$$\text{or} \quad \frac{d \ln P^y}{dT} = \frac{-\Delta H^\circ}{RT^2}$$

By measuring the dissociation pressures at a series of temperatures ΔH° can be determined.

The integration of the above equation with respect to temperature (considering ΔH° as independent of temperature) would give:

$$\ln P = \frac{-\Delta H^\circ}{RT} + \text{constant}$$

$$\log P = \frac{-\Delta H^\circ}{4.576T} + C$$

By plotting $\log P$ against $1/T$ a straight line should be obtained with slope = $-\Delta H^\circ/4.576$. From this relationship ΔH° can be calculated.

The Hydration Number of Nickel Ions in Solution

The heats of solution of the various nickel chloride hydrates were estimated at different temperatures

during the present work. It was therefore desirable to determine whether the hydration sheath of the nickel ions in solution remained the same over the range of temperatures used in the study.

Grunwald and Bacarella have shown that the dissociation of a salt in the mixed solvent water-dioxane produced a change in composition of the solution which was reflected in the composition of the vapour (13). This change corresponded to preferential solvation of the salt by one of the components of the mixture. Thermodynamic treatment of the data indicated that the sodium ions in the solution were appreciably solvated.

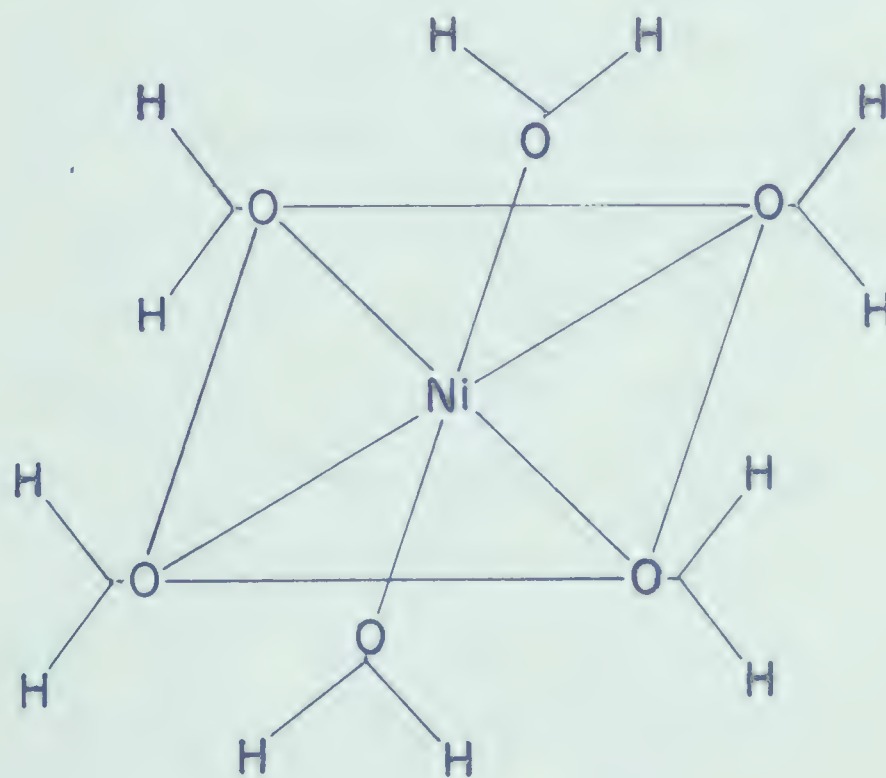
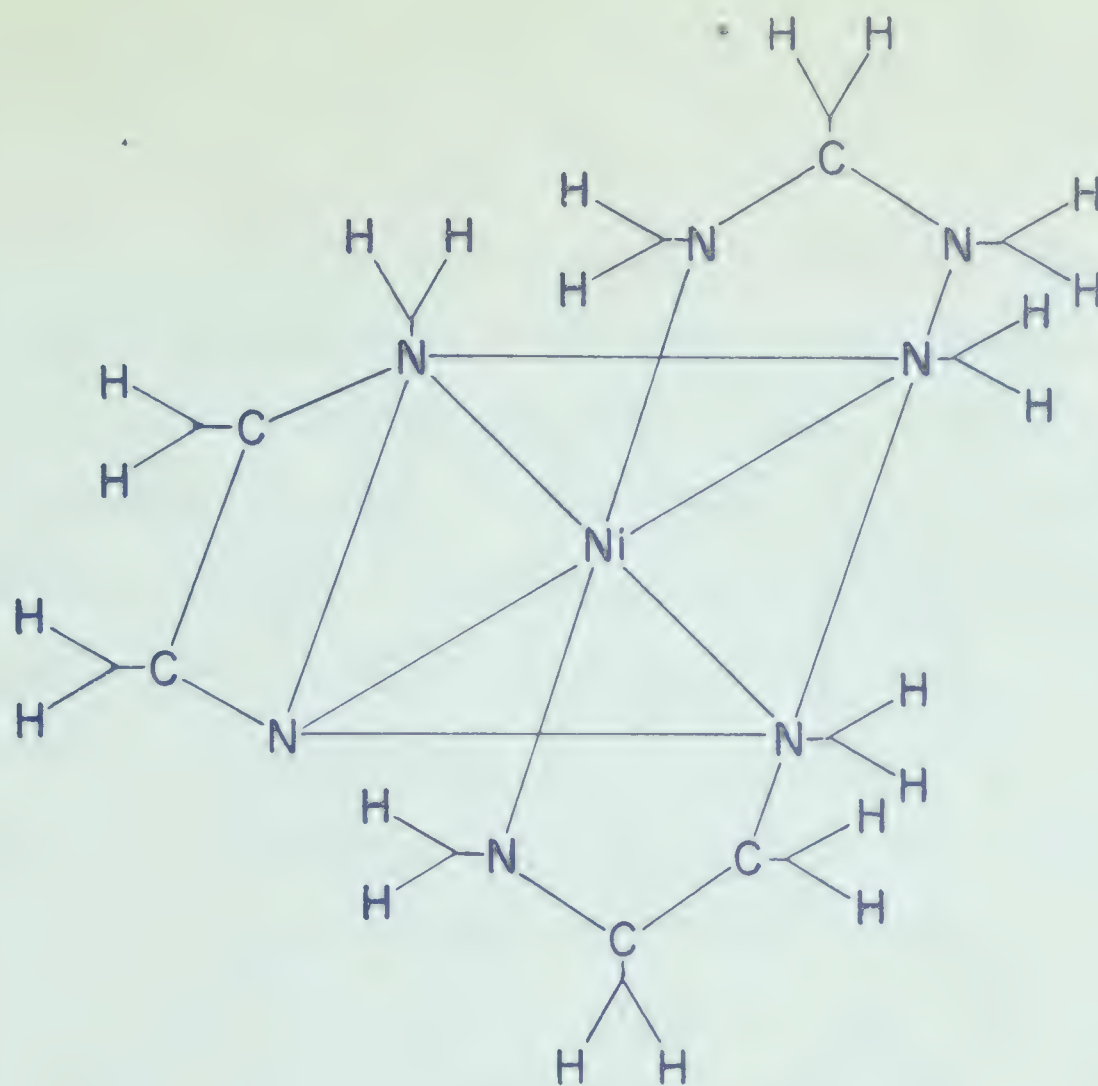
The mixed solvent method could also be used to investigate the atmosphere in the vicinity of nickel ions in solution.

A solution of nickel chloride in water may be considered to contain an aquo Ni(II) complex immersed in the water. It is assumed that a certain amount of water is bound to a Ni(II) ion in some symmetrical fashion, constituting the primary solvation sheath. Outside this sheath the water molecules become less oriented to the nickel ion as the molecule-ion distance increases.

At a distance of a few molecular diameters from the ion, the water may be considered as bulk solvent. Suppose now that a complexing agent is introduced into the

medium which displaces the water molecules from the solvation sheath. Such a process would yield a solution possessing effectively more water molecules than before. Due to the presence of the complexing agent, bound water would be released to the medium as free water. To satisfy such a picture the complexing agent has to fulfill certain requirements. The two basic requirements are that the change in solvation energy is minimum and the size and shape of the new complex does not materially differ from the aquo complex. It is known that the energy per bond with solvent water is not too different for water and ethylenediamine (14), that the sizes of the nickel aquo complex, presumed to be $\text{Ni}(\text{H}_2\text{O})_6^{++}$, and $\text{Ni}(\text{en})_3^{++}$ are quite comparable, and that their shapes are spherically symmetrical. The other similarity between $\text{Ni}(\text{H}_2\text{O})_6^{++}$ and $\text{Ni}(\text{en})_3^{++}$ is the disposition of hydrogens. In both cases the hydrogens are protruding into the medium, as shown in Fig. 3. Thus, ethylenediamine satisfies, to a first approximation, both the energetic and steric requirements.

The addition of ethylenediamine to an aqueous solution of nickel chloride would liberate water and the system would become effectively more dilute with the addition of more ethylenediamine. The extent of dilution should be revealed by measurement of any property of the solution which depends upon the activities of the solution



SCHEMATIC REPRESENTATION OF $\text{Ni}(\text{en})_3$ AND $\text{Ni}(\text{H}_2\text{O})_6$

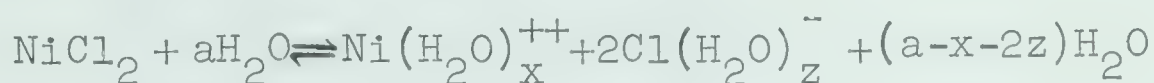
Fig. 3

constituents. The vapour pressure of a solution is such a property. If the vapour pressure of the solution is determined as a function of ethylenediamine added, there should be a gradual increase as the water is being released, followed by a gradual decrease as soon as ethylenediamine in excess of that required to displace water from the primary solvation sheath appears in the solution. Thus, the position of inflection should indicate the number of ethylenediamine molecules in immediate association with nickel. By following the change of vapour pressure as a function of the ethylenediamine concentration the primary solvation number can be obtained. Such a vapour pressure-composition diagram at different temperatures would reveal changes in solvation number, if any, due to change of temperature. It is generally conjectured that at higher temperature the number of oriented water molecules in the immediate vicinity of the metal ion decreases (15).

Thus, the preferential binding of ethylenediamine by the nickel ion results in the liberation of water molecules from the primary solvation sheath. If a pair of solutions has the same vapour pressure, one containing ethylenediamine and the other not, then: $a_w = a_{en}$, where "a" represents activity. Assume that the ions in solution which are of the same charge type are approximately of the same size, and to a first approximation,

have the same solvent interaction characteristics. Then, in all probability, they will have the same activity coefficients, e.g. $\text{Ni}(\text{H}_2\text{O})_x^{++}$ as opposed to $\text{Ni}(\text{en})_3(\text{H}_2\text{O})_y^{++}$. If this assumption is correct it is likely that the water has the same activity coefficient in both the solutions and hence $C_W = C_{\text{en}}$.

Supposing the Ni(II) iceberg to be representable, on the average, as $\text{Ni}(\text{H}_2\text{O})_x^{++}$ and the $\text{Ni}(\text{en})_3^{++}$ iceberg as $\text{Ni}(\text{en})_3(\text{H}_2\text{O})_y^{++}$ the following sequence of reaction will be correct:

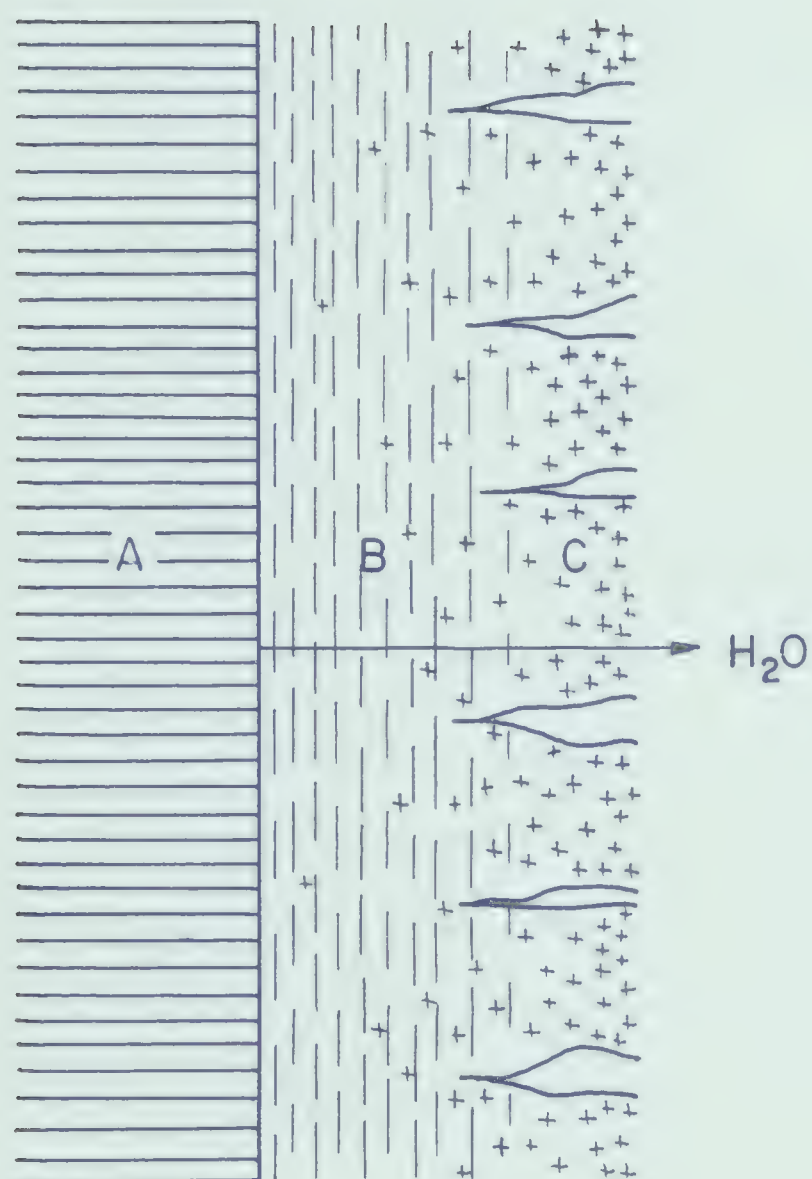


In NiCl_2 -water mixture the free water would be $(a_1 - x - 2z)$ moles and in NiCl_2 -water-ethylenediamine mixture $(a_2 - y - 2z)$ moles. If two solutions which have equal concentration of water molecules are now compared:

$$a_1 - x - 2z = a_2 - y - 2z$$

$$a_1 - a_2 = x - y$$

If the outer solvation sheaths of $\text{Ni}(\text{H}_2\text{O})_x^{++}$ and $[\text{Ni}(\text{en})_b(\text{H}_2\text{O})_y]^{++}$ are not very different then the molar difference of the original water concentration should give the number of water molecules released per mole of ethylenediamine added. Thus, this offers a method to estimate the average number of water molecules associated



MODEL OF INTERFACE

Fig. 4

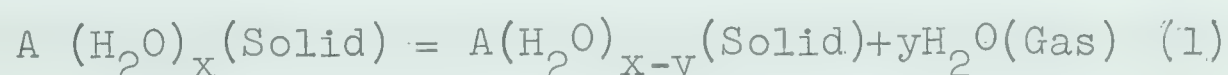
with the inner solvation sphere of the metal ion.

Kinetic Studies

Many attempts have been made to offer a mechanism for dehydration of specific hydrates (16-43). It appears from the observations reported in the literature that a general mechanism to explain the behavior of all salt hydrates is difficult to envisage.

One model for the dehydration process has been proposed by Topley (44) and is shown in Fig. 4. The process of dehydration might be imagined as evaporation of water molecules from the surface of the hydrate, leading to a dehydrated unstable phase possessing no clearly defined crystal structure (Fig. 4(B)). The rearrangement of this phase results in a new crystalline phase (Fig. 4 (C)) (45). The presence of water vapour has been shown to accelerate this rearrangement (46). Presumably, adsorption of water on the surface leads to a condensed phase in which recrystallization can occur with a reduced activation energy.

Depending on the structure of the original solid phase, a number of alternative processes can occur during the dehydration of a system by reaction (1).



An ideal zeolite is the simplest case. Here the water molecules can pass in or out of the crystal lattice without

changing its structure appreciably. A second possibility occurs when the crystal structure of the dehydrated form is different from the original one but is so related to it that a contact between two crystalline faces will not cause any discontinuity. A final possibility occurs when the dehydrated crystalline form cannot be accommodated within the original lattice. The second and third cases are considered to be limiting. A certain thickness of the dehydrated product can always be formed on the parent substance without dislocation of the structure, but beyond this critical thickness breakdown would, except in the limiting case, always occur. During the process of dehydration a layer of dehydrated product may be deposited on the parent substance and its transformation to a grossly or micro crystalline phase may be either immediate, gradual or delayed. Slow rearrangement to a new crystalline phase may be due to a high activation energy for the process. Usually a high activation energy in such a step occurs when significant migration of the lattice units is necessary to produce the new phase.

The rate of dehydration of a salt hydrate may be governed by any of the following: the rate of nucleus formation, the rate of loss of water from the reactant/product interface, the rate of propagation of the reaction throughout the bulk of the solid or the rate of diffusion of water molecules through the solid product.

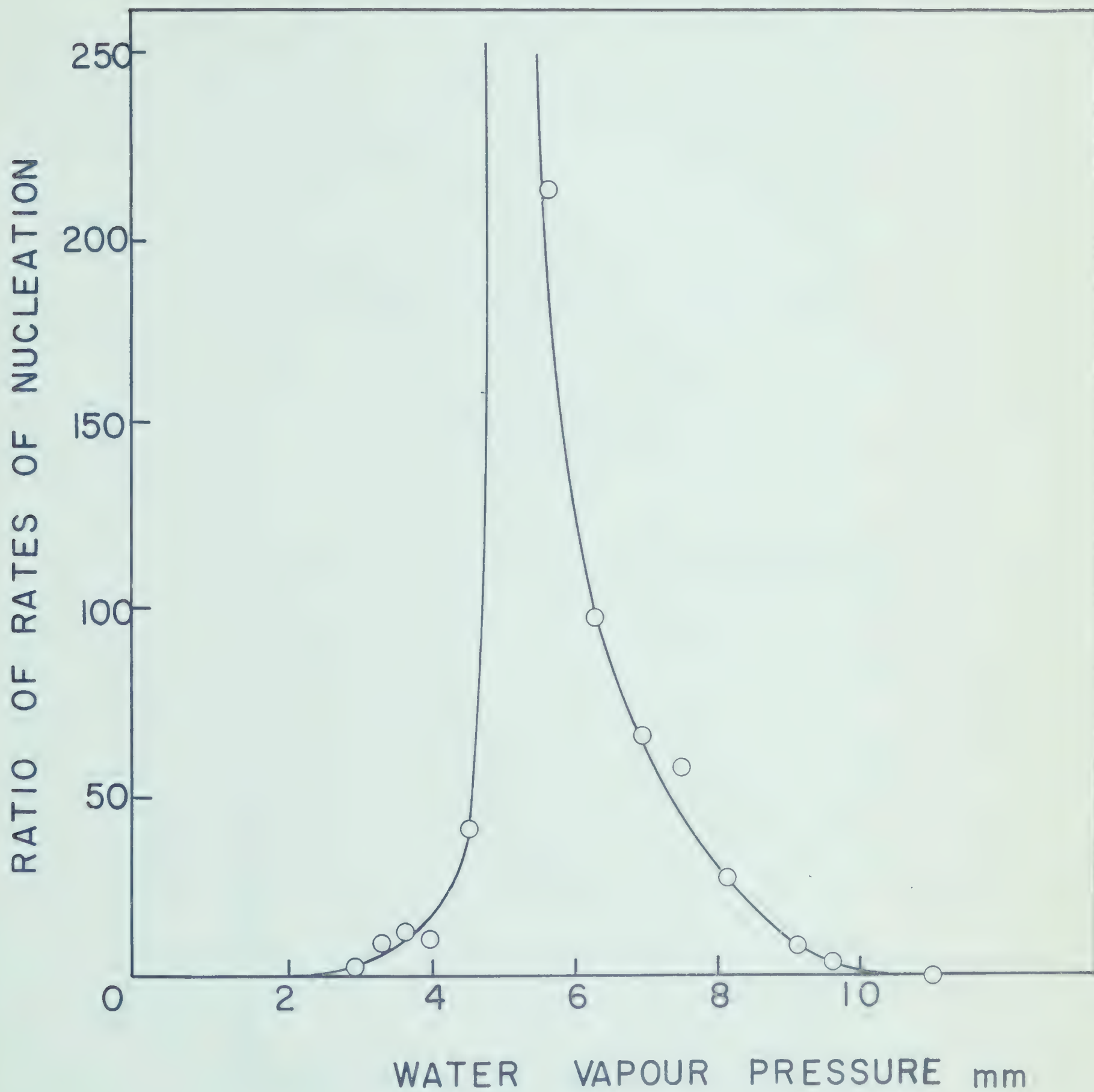
In a perfect crystal of a salt hydrate there is no dislocation or crystal imperfection where reaction can occur. In the case of a real crystal, containing imperfections, the free energy of formation is slightly less and the sites of imperfection are favourable for the growth of a new nucleus (47). The induction period is dependent upon the number of sites available. If there is an infinite number of sites the induction period disappears completely. When a nucleus of the dehydrated phase is formed on the surface the reaction proceeds from it symmetrically. According to Garner and Jennings (48) the sites where nucleus formation takes place are limited and probably are the areas where there is some discontinuity in the lattice. These discontinuities may be normal crystal dislocations or other crystal imperfections or they may be mobile or immobile lattice vacancies formed due to the loss of water molecules. Mobile imperfections are formed when the water molecules are lost from the whole surface of the hydrate. The vacancies so formed diffuse to dislocations to form nuclei. Alternatively, water may be lost only from the disturbed areas.

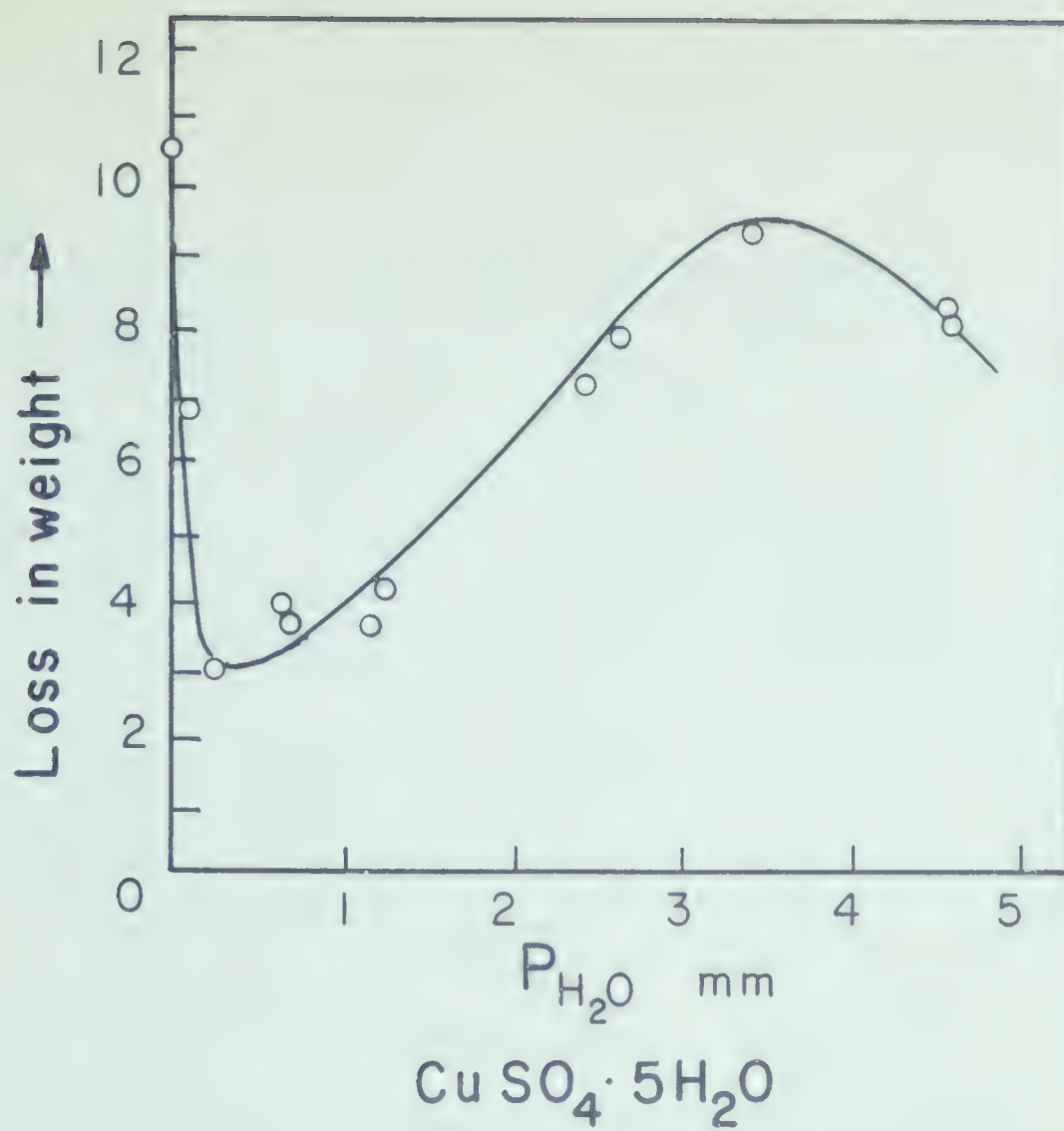
In the majority of hydrates the stability of the residual lattice on dehydration is low. The loss of water molecules produces a collapsed lattice on the surface. In hard vacuum the product of dehydration consists of disorganized minute crystallites having a large internal surface (49).

When dehydration takes place in the presence of relatively small amounts of water vapour, smaller than the dissociation pressure of the hydrate, the crystallites grow sufficiently in size to be able to diffract X-rays. Under the influence of water vapour the collapsed lattice crystallizes. The rate of this transformation from a collapsed to a crystalline phase is critically dependent on the water vapour pressure as shown by Garner and Jennings (47), see Fig. 5. The water vapour can effect the restoration of the lattice structure of the original hydrate, as seen in common alum, or it can effect the formation of a new crystalline phase, as in copper sulphate pentahydrate (48).

The dehydration curve observed for $\text{CuSO}_4 \cdot 5\text{H}_2\text{O}$ (50) and $\text{Mn}(\text{C}_2\text{O}_4) \cdot 2\text{H}_2\text{O}$ (51), in presence of increasing pressures of water vapour show a minimum and a maximum as shown in Figs. 6 and 7. The initial decrease in rate has been interpreted as resulting from the adsorption of water vapour in the capillaries. The subsequent increase in rate is considered due to catalytic influence of water vapour in forming nuclei of a new phase which facilitates escape of water vapour. A minimum in the rate is observed because subsequent adsorption of the water vapour on the surface causes the back reaction to become important.

The retardation of the growth of nuclei has been accounted for by Garner and Jennings (48) in terms of blocking





6

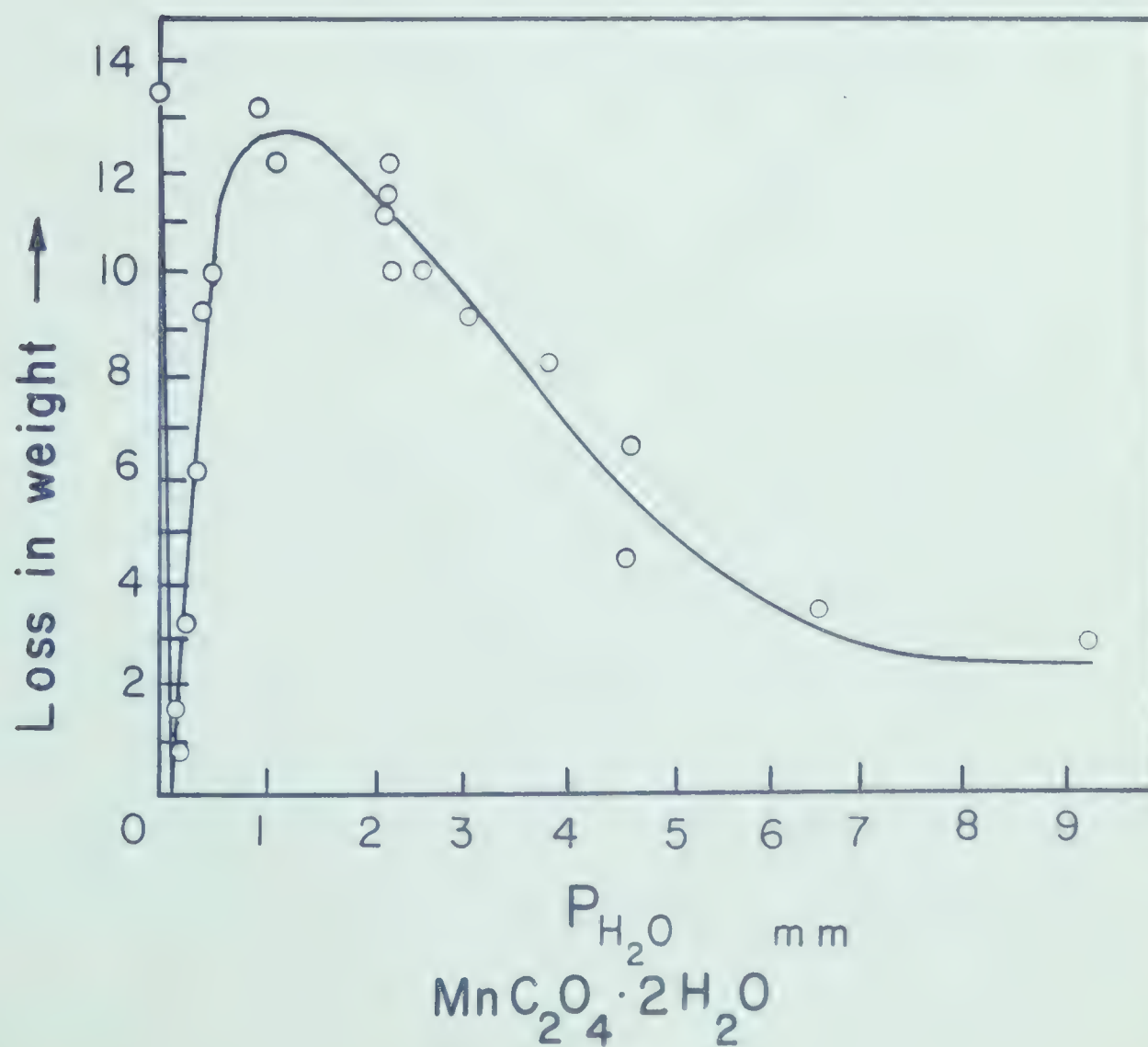


Fig 7

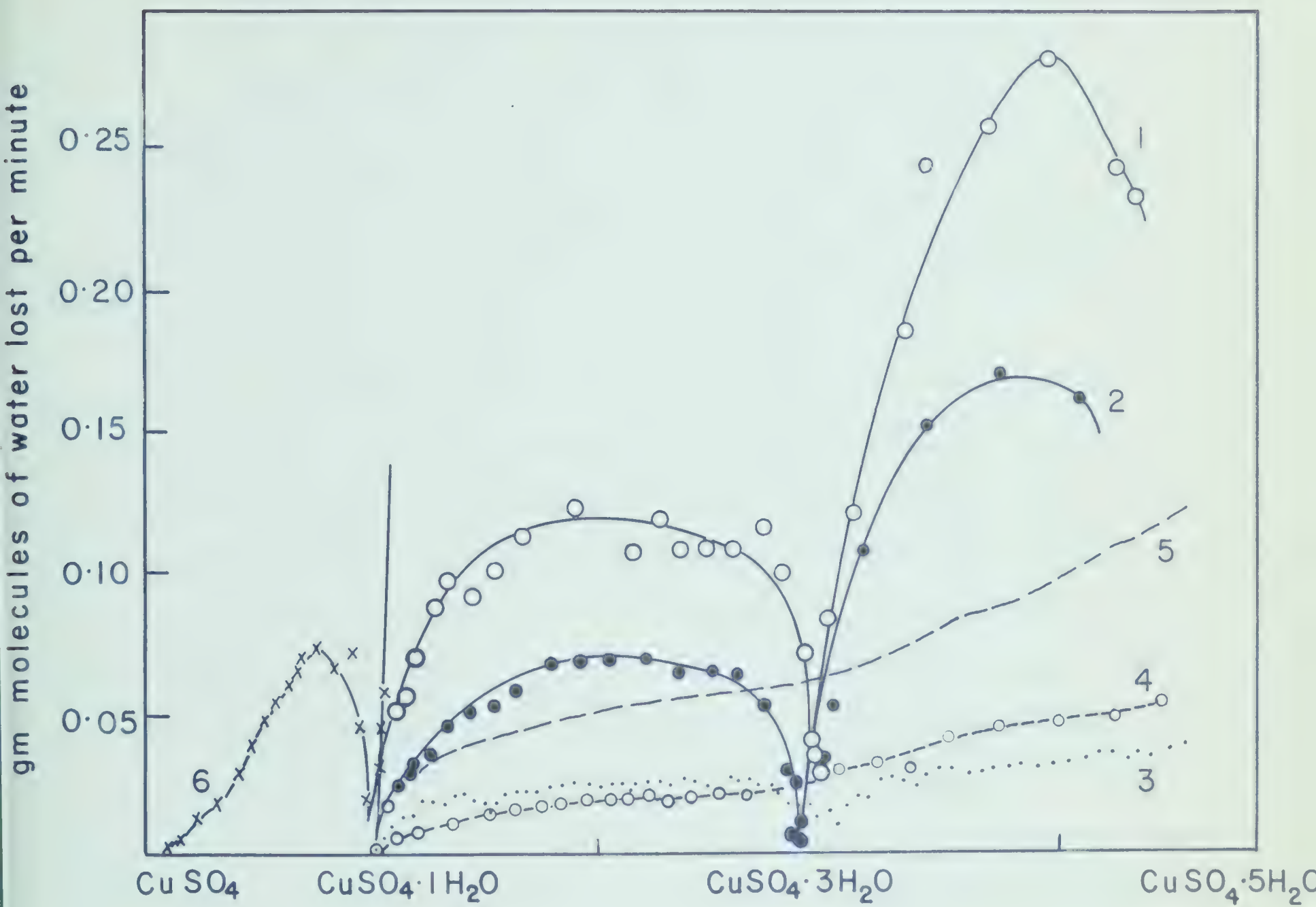
the reaction at the interface by adsorbed water molecules which obeys a Langmuir adsorption isotherm. The relation is:

$$\frac{p_{\text{H}_2\text{O}}}{R_0 - R_p} = k_{p_{\text{H}_2\text{O}}} + \text{const.}$$

where R_0 is the rate in vacuo and R_p the rate at $p_{\text{H}_2\text{O}}$, hence a plot of $\frac{p_{\text{H}_2\text{O}}}{R_0 - R_p}$ versus $p_{\text{H}_2\text{O}}$ gives a straight line.

Thus, the changes in the rate of dehydration in the presence of water vapour may occur in two stages. The first process consists of the separation of an amorphous phase and the second, the crystallization of this phase. The process of crystallization of the amorphous phase is accelerated by the water vapour. The rate of crystallization is the determining factor for the type of decomposition curve obtained. Since the concentration of water vapour is an important factor for the crystallization process, the rate of dehydration depends very much on the concentration of water vapour.

The dehydration of salt hydrates has been studied by a number of methods. Crowther and Coutts (52) studied the dehydration of salt hydrates on an automatic recording balance at 100°C . Under the same experimental conditions in the dehydration of $\text{CuSO}_4 \cdot 5\text{H}_2\text{O}$ and $\text{BaCl}_2 \cdot 2\text{H}_2\text{O}$, discontinuities in the rate/composition curve were observed. The curves obtained under different conditions for $\text{CuSO}_4 \cdot 5\text{H}_2\text{O}$ are shown in Fig. 8.



- 1 & 2 Fine crystals, thinly spread; 100°C
 3 Fine crystals, in thick layer; 100°C
 4 Fine crystals; in layer in weighing bottle; 100°C
 5 Single large crystal; 100°C
 6 Fine crystals, thinly spread; 220°C

For thinly spread, fine crystals there is a discontinuity corresponding to a definite hydrate. In the other cases a smooth curve resulted. The positions of discontinuities were however dependent upon the size and placement of the hydrate particles. The same type of discontinuities were not observed for the dehydration of the hydrates of magnesium, manganese, nickel, cobalt and zinc sulphates and strontium, cobalt and manganese chlorides.

Crowther and Coutts recognized three types of behaviour in the dehydration of crystalline salts forming more than one hydrate. When the dehydration proceeds slowly at ordinary temperatures, approximately equilibrium conditions are present. Under these circumstances the rate of evaporation is practically constant and is proportional to the fixed vapour pressure. When the evaporation takes place at a higher temperature there is continuous reduction of the rate of loss of water due to the slowness of removal of water vapour from the surface. This slowness may be diffusion controlled. When dehydration is carried out at a higher temperature and the removal of water is facilitated by using small crystals in thin layers, there is a distinct discontinuity.

The reason for the distinction between one hydrate and the other was not advanced due to the lack of knowledge of the space lattice of the crystals and the forces involved

in the separation of water molecules from the crystal surface. A tentative explanation for the discontinuity in $\text{CuSO}_4 \cdot 5\text{H}_2\text{O}$ and $\text{BaCl}_2 \cdot 2\text{H}_2\text{O}$ was offered on the basis of Langmuir's theory of heterogeneous reactions which proceed only at the actual phase boundary.

Tate and Warren (53) studied the dehydration of the salt hydrates by entrainment distillation with liquids immiscible with water. By plotting the water collected during dehydration against time three types of curves were obtained: (a) uniform dehydration from the initial to the final states; the rate remaining either approximately constant or falling rather steadily to become negligible when the end product is reached, (b) dehydration proceeded at a constant or gradually decreasing rate up to a certain composition at which a sudden decrease occurred in the rate of dehydration, (c) dehydration proceeded smoothly to a certain point at which a sudden increase in the rate of dehydration occurred.

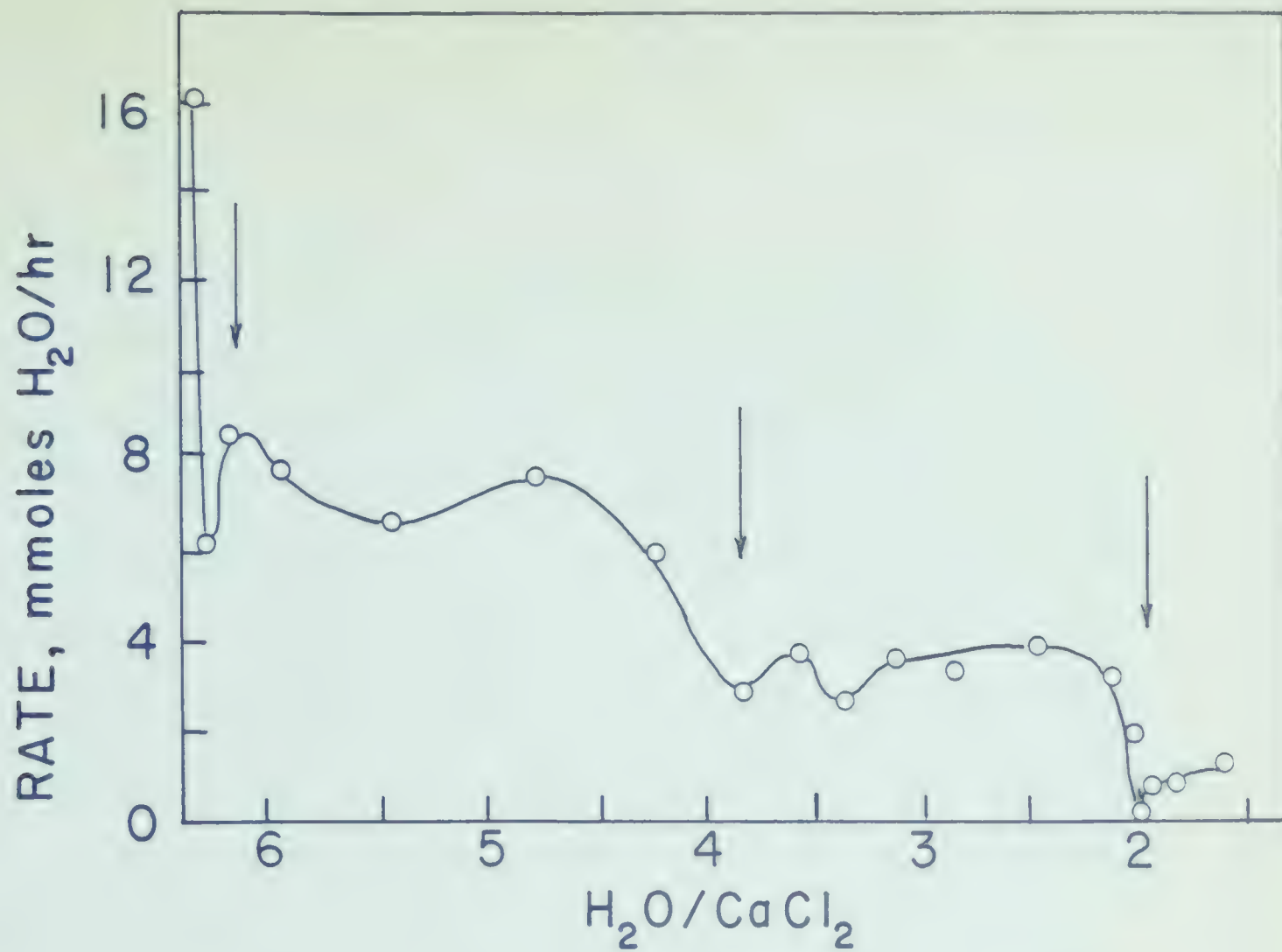
The discontinuities have been observed to occur at the composition of a definite intermediate hydrate. Tate and Warren remarked that although a discontinuity in a dehydration curve may be an evidence for the formation of a hydrate, the absence of a discontinuity is not to be taken to indicate that the intermediate hydrates are not formed. The situation is analogous to that found by Crowther and Coutts (52), where formation of lower hydrates was not revealed in certain

hydrates where they were known on the basis of independent evidence. Contrarywise, discontinuities have been observed by Ghosh (54) for $\text{NiSO}_4 \cdot 6\text{H}_2\text{O}$ corresponding to 1, 2, 3, 4, and 5 water molecules. This does not necessarily mean that these hydrates exist.

An attempt to revive the kinetic procedure for the identification of hydrates has been made recently by Castor and Basolo (55). A general theory has been proposed to account for the discontinuities observed in the rate/composition curves. The heterogeneous reaction of the type represented by equation (1) may proceed autocatalytically due to the availability of local energy as a result of the rapid reorganization to a more stable crystal lattice. In an autocatalytic reaction the gross rate of decomposition is very small both near the beginning and near the end of the reaction and rises to a maximum between these extremities. In the region corresponding to the intermediate compound, the rate of the first decomposition process slows down due to smaller concentration of the reactant and the second decomposition process is slow due to a smaller number of nuclei present for the progress of the reaction. Thus, the gross rate of reaction shows a minimum at or near the composition of the intermediate, regardless of the possibility of some overlap of the two bounding decomposition curves. As long as the overlap is not too large either due to simultaneous occurrence

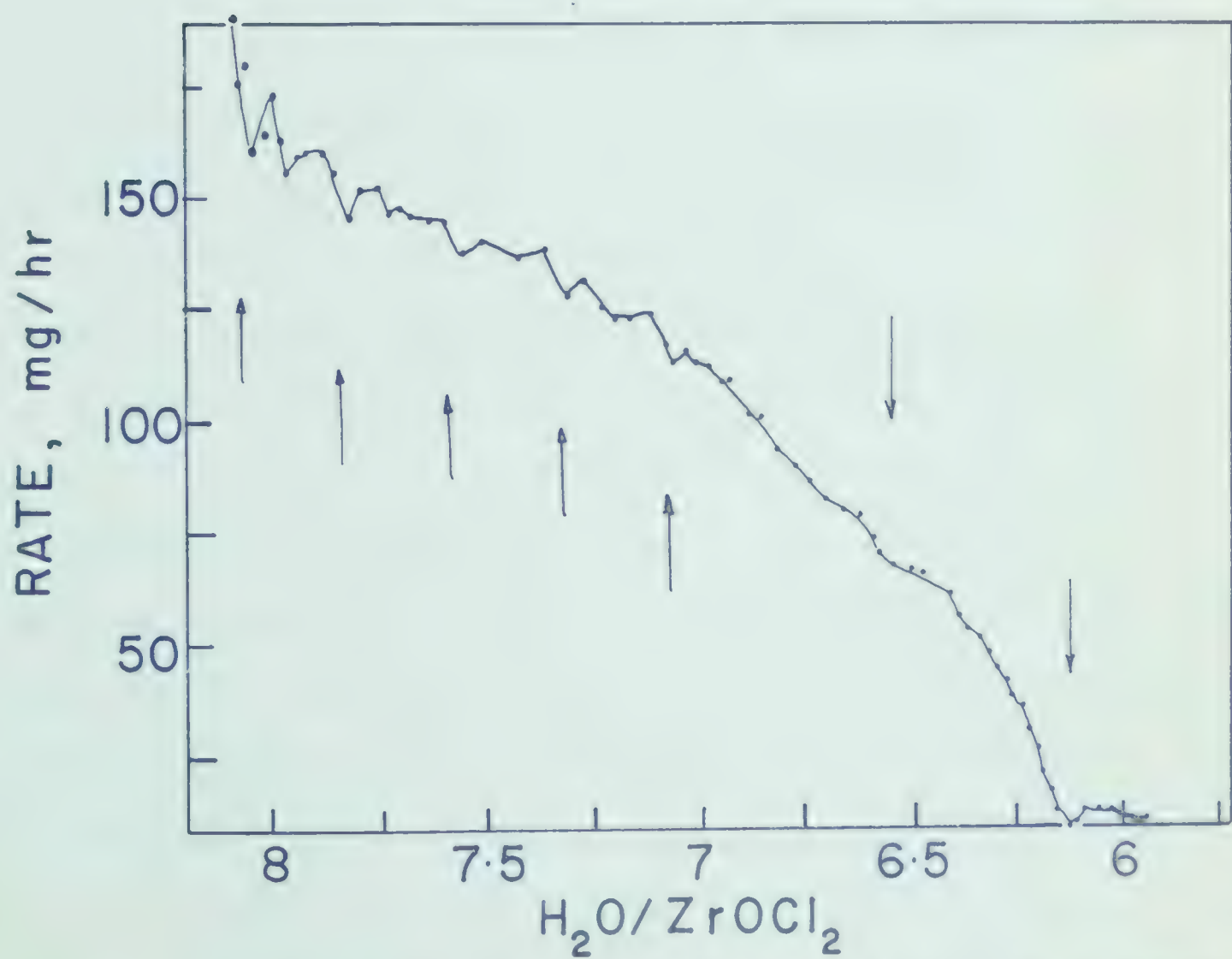
of two reactions over a considerable composition range or due to less frequent observations, the minimum is detectable. The rate versus composition curve is an integral curve and approaches the true differential curve when the time or composition increment is made to approach an infinitesimal value. The observed shape of the dehydration curves was found to resemble inverted parabola as anticipated from the theoretical considerations. By this technique hydrates of correct composition and some hitherto unknown hydrates were revealed. The reason proposed for some of these unknown hydrates not having been detected by other means was their close similarity with known hydrates and the general insensitivity of thermodynamic measurements.

The types of discontinuities observed by Castor and Basolo (55) are shown in Figs. 9 and 10. The basis on which some of these hydrates are reported leave room for criticism. It appears that the discontinuities are carefully selected. From the rate versus composition curves it can be seen that some minima have been assigned to a particular hydrate whereas other minima have been neglected. As an example such is the case for calcium chloride hydrate as shown in Fig. 9. The rate minimum at $\text{H}_2\text{O}/\text{CaCl}_2 \simeq 4$ has been considered resulting from the existence of $\text{CaCl}_2 \cdot 4\text{H}_2\text{O}$, whereas an exactly similar minimum at $\text{H}_2\text{O}/\text{CaCl}_2 \simeq 3.5$ has been neglected. The dehydration curve for zirconyl chloride



DEHYDRATION OF CALCIUM CHLORIDE

119



DEHYDRATION OF ZIRCONYL CHLORIDE

hydrate shown in Fig. 10 exhibits ill defined minima and it seems difficult to justify the existence of hydrates on the basis of these minima alone. The monotonous decrease in the rate of dehydration strongly suggests that the dehydration is occurring from a mixture of hydrates. It is rather uncertain to associate these minima with hydrates of fractional water content. From the spread of the experimental points it does not seem unreasonable to draw a smooth curve through them. The picture presented by Castor and Basolo (55) seems to be oversimplified.

The dehydration of a salt hydrate in a closed system in a desiccator in the presence of a desiccant would depend not only on the rate of loss of water from the hydrate but also on the rate at which the desiccant absorbs water. The process of dehydration for such a system may be considered to consist of liberation of water from the hydrate and the pressure build up due to such a process. In the presence of a desiccant the water liberated may either go back to the original hydrate or remain adsorbed on the dehydrated surface or disappear by absorption in the desiccant. Where the desiccant has an aqueous tension much lower than the vapour pressure of the hydrate, the probability of water returning to the original hydrate is reduced. However, the adsorption of water on the dehydrated surface probably does occur and this may slow down the process of dehydration. The

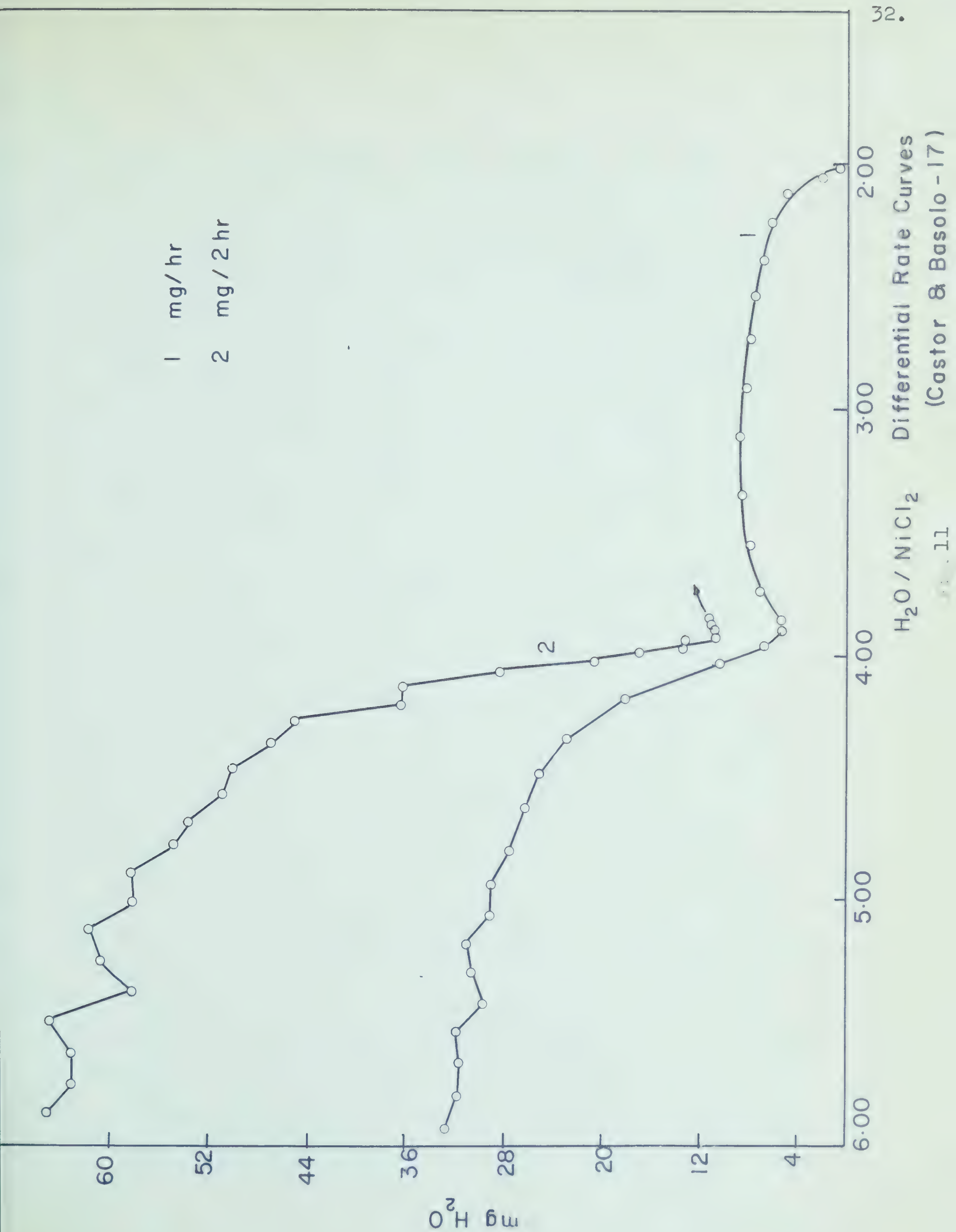
other process which influences the dehydration rate is the diffusion of the water molecules through the bulk of the solid substance.

For a very simple case it can be assumed that the rate determining step is either the rate of liberation of water from the hydrate or the rate of hydration of the desiccant. In the case of desiccants like magnesium perchlorate and phosphorous pentoxide the rate of absorption of liberated water is very fast and the result is that the rate determining step must be the rate of liberation of water from the hydrate. This picture is very simple and may not be applicable to all systems. There could be other competing processes such as recrystallization and lattice rearrangement which can influence the rate determining step.

If the rate determining step is the liberation of water from the hydrate then the other conditions to be fulfilled for the reaction to be autocatalytic are that the locally available energy accelerates the dehydration and the free energy of the product phase be less than the reactant phase. When this is the situation the differential rate versus composition curve would be similar to that suggested by Castor and Basolo (55) where minima occur corresponding to a definite phase. However, effectiveness of the method for the identification of hydrates is questionable. Minima do not always occur at the exact composition corresponding to

an intermediate hydrate due to considerable overlap of the decomposition curves arising from different decomposing species. Thus, the placement of the minima with respect to a certain position would depend on the competing reactions taking place in the system. Even if it is assumed that the process taking place is as simple as proposed by Castor and Basolo (55), it can be seen from their graphs that there are many essentially equivalent minima. Some were taken to indicate the formation of a particular hydrate, whereas others were said to be meaningless. The time interval chosen for following the progress of reaction is an important consideration. For longer time intervals the minima may not be detectable due to an averaging of the size of the increments which would make the differential decomposition curve appear smooth, whereas smaller time intervals would reveal the structure of the differential decomposition curve manifested by the interplay of other competing processes. The choice would however depend on the limits of the experimental precision and the velocity of the reaction.

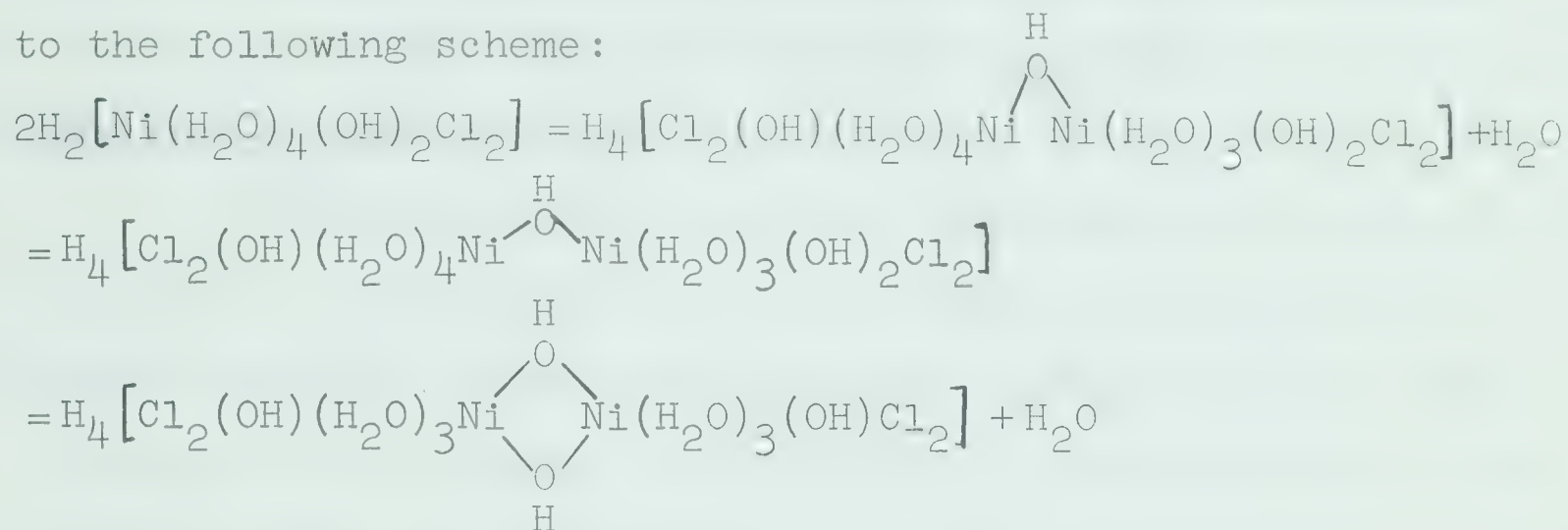
The differential dehydration curve for nickel chloride hydrate following Castor and Basolo (55), is shown in Fig. 11(1), plotted as the rate of loss of water per hour versus composition. When the rate of loss of water per two hours is plotted versus composition, the curve assumes the form shown in Fig. 11(2). As predicted above, the increase of time interval makes the curve appear more smooth. Since



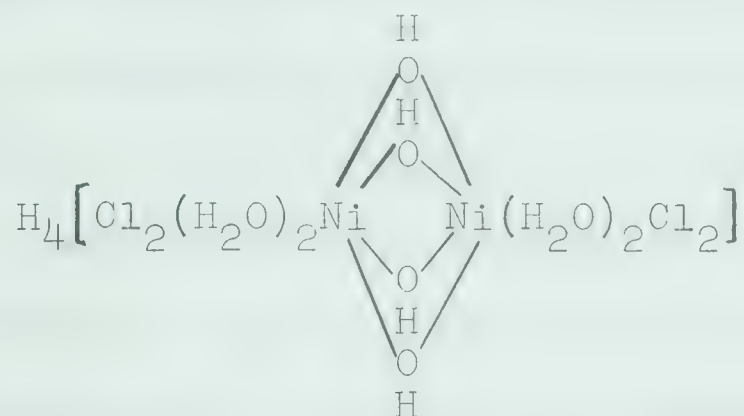
there are no data for smaller time intervals (56) it is impossible to determine the form the decomposition curve assumes under these conditions. The plot in Fig. 11(1), is not justifiable since all these are not the experimentally determined points but an average value of longer time intervals. Factors which have a pronounced effect on the appearance and placement of the minima are the adsorption of water on the dehydrated surface, which decreases the rate of dehydration, and the migration of the interface, neither of which can be controlled experimentally.

The hydrates suggested by Castor and Basolo (55) for nickel chloride are: $\text{NiCl}_2 \cdot 6\text{H}_2\text{O}$, $\text{NiCl}_2 \cdot 5.5\text{H}_2\text{O}$, $\text{NiCl}_2 \cdot 5\text{H}_2\text{O}$, $\text{NiCl}_2 \cdot 4\text{H}_2\text{O}$ and $\text{NiCl}_2 \cdot 2\text{H}_2\text{O}$. It is very interesting to see how the existence of the unusual hydrates has been rationalized. Meerwein (cf. ref. 56) had studied the reaction of concentrated aqueous and alcoholic solutions of $\text{NiCl}_2 \cdot 6\text{H}_2\text{O}$, and found that solutions of "sufficient" concentration exhibited acidic properties. Meerwein explained this as due to the coordination of water molecule to form a metal-oxygen bond with resultant weakening of the oxygen-hydrogen bond and an increase of the acidity of the hydrogens. The resultant species was formulated as $\text{H}[\text{M}(\text{OH})]$. Castor and Basolo invoked this formulation to write the preliminary structural formula for $\text{NiCl}_2 \cdot 6\text{H}_2\text{O}$ as $\text{H}[\text{Ni}(\text{H}_2\text{O})_5(\text{OH})\text{Cl}_2]$ or $\text{H}_2[\text{Ni}(\text{H}_2\text{O})_4(\text{OH})_2\text{Cl}_2]$.

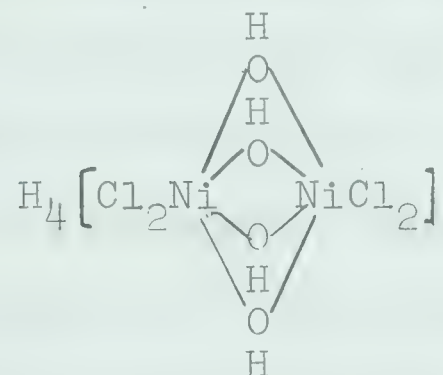
The compound $\text{H}_2[\text{Ni}(\text{H}_2\text{O})_4(\text{OH})_2\text{Cl}_2]$ oligates and di-oligates to $\text{NiCl}_2 \cdot 5.5\text{H}_2\text{O}$ and $\text{NiCl}_2 \cdot 5\text{H}_2\text{O}$ respectively according to the following scheme:



The resulting dimer again condenses to $\text{NiCl}_2 \cdot 4\text{H}_2\text{O}$:



which on further dehydration becomes:



with the resulting octahedral coordination of four $\text{O}1$ -linkages between any two nickel atoms which is impossible due to steric reasons. Thus, the colour change for $\text{NiCl}_2 \cdot 4\text{H}_2\text{O}$ from green to yellow $\text{NiCl}_2 \cdot 2\text{H}_2\text{O}$ has been ascribed to a change

of coordination number from 6 to 4. The half hydrates, colour change, constitutional water ($\text{NiCl}_2 \cdot 2\text{H}_2\text{O}$) and acidity of aqueous solution were correlated on the basis of the condensation hypothesis.

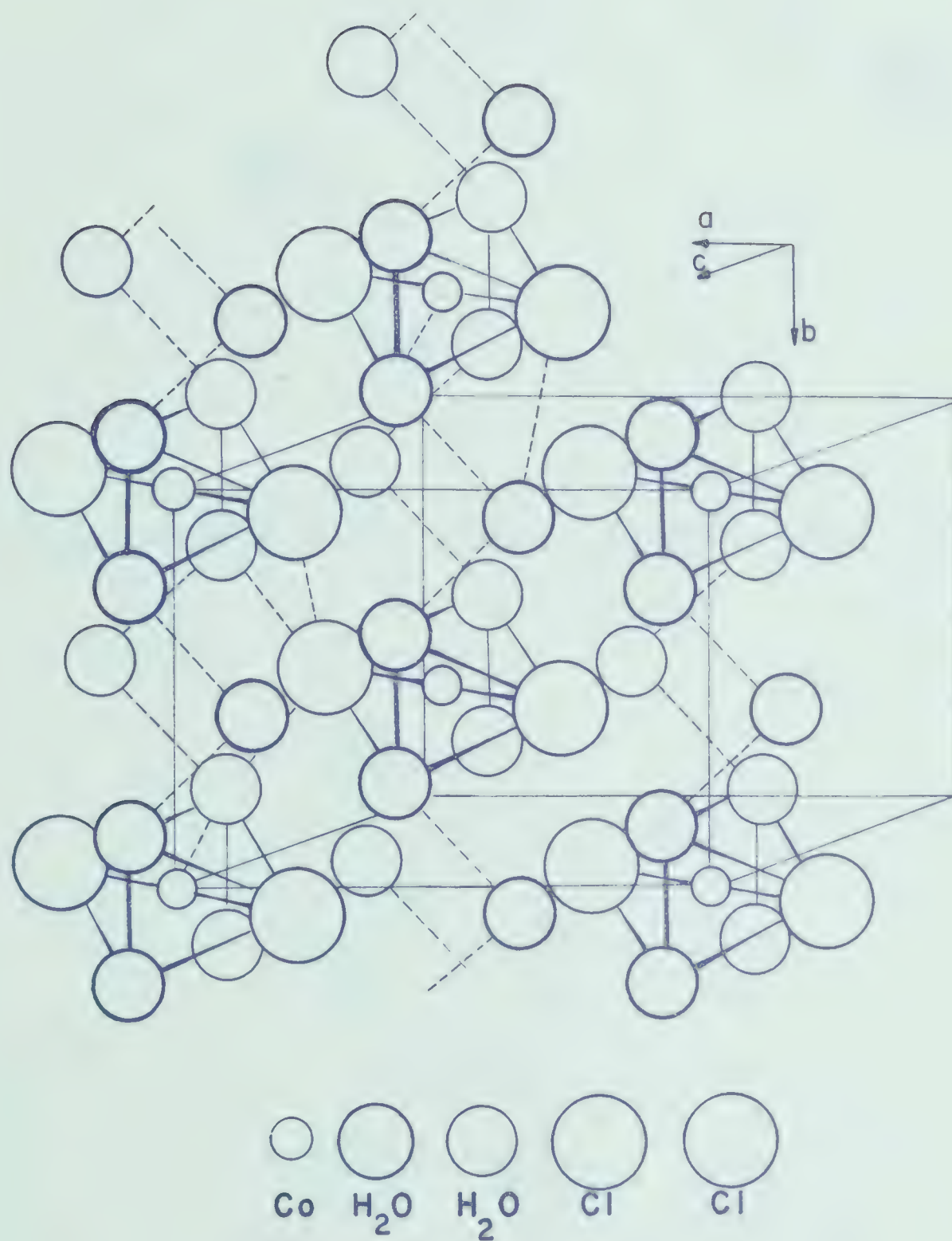
To determine the nature of the dehydration process for nickel chloride hydrates, measurements were made in different desiccants without any elaborate precaution. In order to obtain a true measure of the extent of decomposition it was essential that the water liberated during the decomposition was removed immediately from the mass of crystals. Under atmospheric pressure the water remains entangled in the crystals and evaporates much more slowly than the true reaction rate. Thus, the dehydration rate was also followed in vacuum, on a quartz spiral balance, under controlled conditions at different temperatures to obtain the temperature dependence of the reaction rate and calculate the activation energy of the process. A distinction may be made between the vacuum and non-vacuum methods used in the present study. When water is removed from the interface by the use of vacuum, rapid diffusion of water molecules takes place. In non-vacuum system removal of water vapour influences the kinetics of the process.

Structural Studies

The actual arrangement of water molecules in the hydrates was classically inferred from their dehydration behaviour under varying circumstances. On this basis water molecules within crystalline hydrates were classified as water

of constitution, co-ordinated water, anion water, lattice water and zeolitic water. Because this approach did not yield fundamental information about the placement of water molecules within the crystal lattice it has been superceded by an approach based upon structure determination. In the final analysis there is no better approach to relating behaviour to structure than by actually determining the structure.

It is expected on the basis of general considerations that the environment of the metal ion would be governed by the usual factors affecting crystal structure. These are radius ratio, electroneutrality and minimum energy. The familiar criteria may be modified in the case of metal ions which contain unfilled d orbitals by the interaction of potential ligands with these potential bonding orbitals. The high incidence of hexahydrates among divalent ions of the first transition series lead to the conjecture that $M(H_2O)_6^{++}$ was present as a separate and identifiable unit in the crystal lattice. This, however, is dispelled by the structure for $CoCl_2 \cdot 6H_2O$ shown in Fig. 12, possessing a $Co(H_2O)_4Cl_2 \cdot 2H_2O$ unit (57). This general structure appears not to be unusual. Another example of this general sort of structure is shown in Fig. 13, where it is seen that in $CuSO_4 \cdot 5H_2O$, the fifth water molecule is differently situated than the other four (58). Four of the water molecules are arranged in a plane

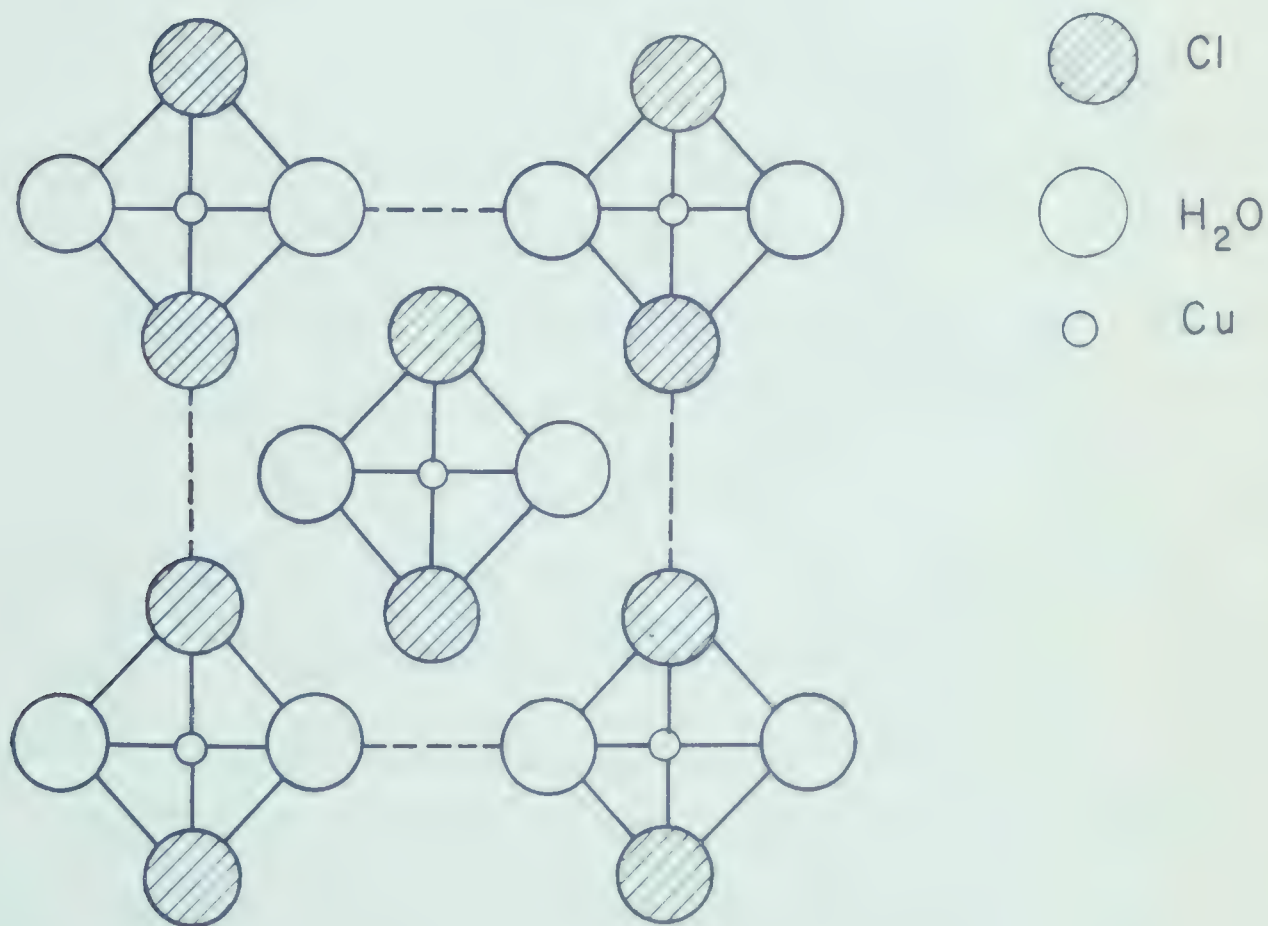


THE SCHEMATIC REPRESENTATION OF THE
CRYSTAL STRUCTURE OF $\text{CoCl}_2 \cdot 6\text{H}_2\text{O}$



The Environment of the Fifth H₂O Molecule (Centre) in CuSO₄·5H₂O

Fig. 13



The Structure of CuCl₂·2H₂O

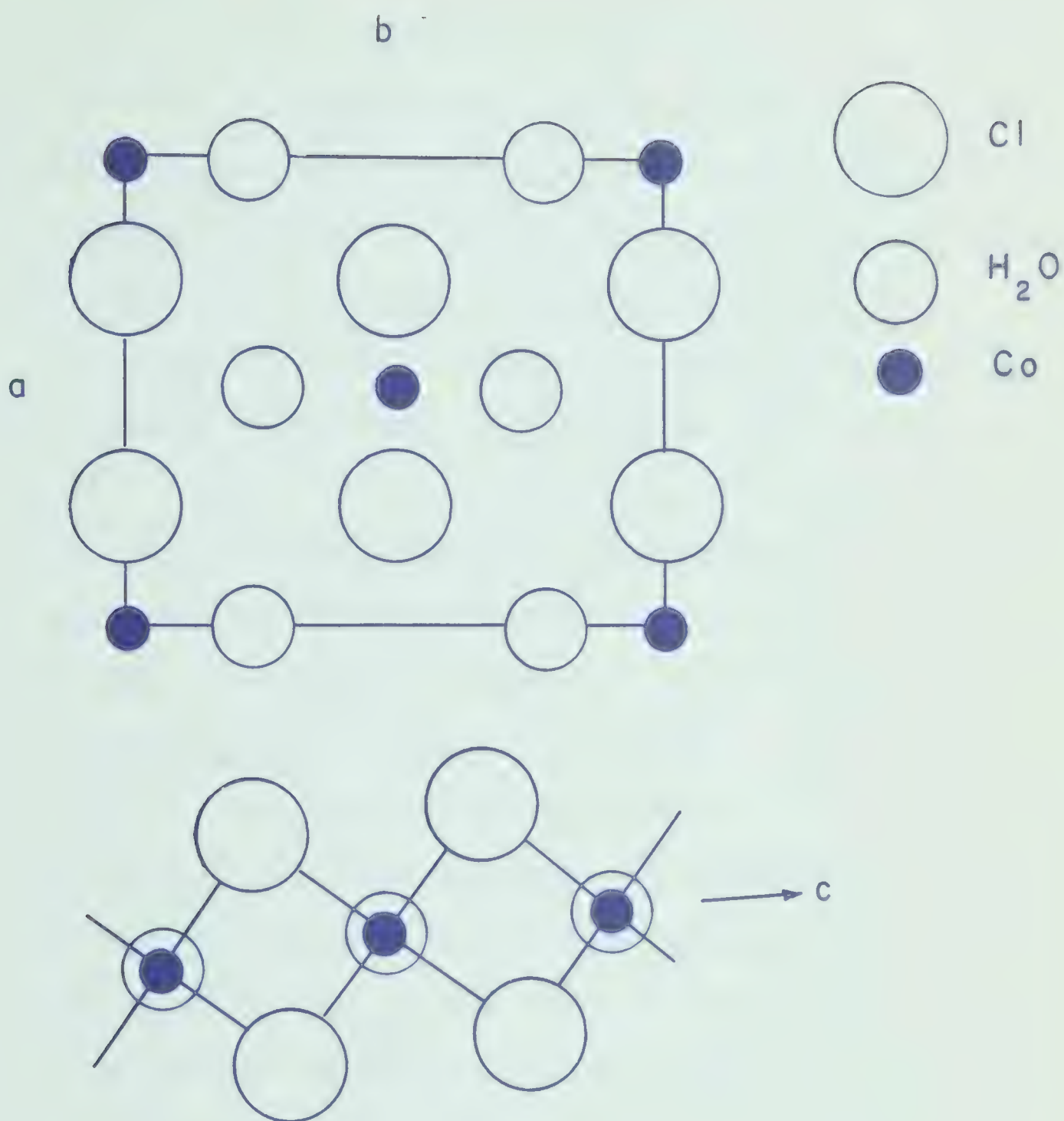
around the metal ion, and are directly associated with it. The fifth water molecule is attached to two oxygens of SO_4^{--} and to two of the water molecules directly associated with the copper ion. There are then two environments for water molecules in these two hydrates which are not equivalent in terms of binding energy within the crystal lattice. The lattice water may or may not be most strongly bound, but whatever the binding energy for these water molecules it has no relation to the strength of interaction between metal ions and water molecules. In the case of $\text{CuCl}_2 \cdot 2\text{H}_2\text{O}$, shown in Fig. 14, the water molecules are directly co-ordinated to the metal ion and are structurally equivalent (59,60).

In these examples the structure of the hydrates have been influenced to a greater extent by the co-ordination number of the metal ion than by any other single factor. It would appear, on the basis of a limited number of examples, that in a series of hydrates of the same metal ion the structure is governed to a large extent by the tendency of the metal ion to maintain the same co-ordination number. When a higher hydrate loses water and is converted to a lower hydrate the remaining groups migrate to compensate for the water which is lost. The structure and composition of the new hydrate depends upon maintenance of the co-ordination number of the metal ion, minimum migration of the remaining ligands and minimum energy for the new system. Consequently, the struc-

tures in a series of hydrates ought to be related to one another by simple translation of groups. The structure of $\text{CoCl}_2 \cdot 6\text{H}_2\text{O}$ is very different from $\text{CoCl}_2 \cdot 2\text{H}_2\text{O}$, because four co-ordination positions are occupied by water molecules and two co-ordination positions by chloride ions in the former case whereas in the latter, four co-ordination positions are occupied by chloride ions and two co-ordination positions by water molecules. However, it is possible to convert one into the other in a fairly straight-forward manner. The structure of $\text{CoCl}_2 \cdot 2\text{H}_2\text{O}$ is shown in Fig. 15 (61).

The influence of anions is evident from a comparison of the structures of $\text{NiCl}_2 \cdot 6\text{H}_2\text{O}$ and $\text{NiSO}_4 \cdot 7\text{H}_2\text{O}$. In $\text{NiSO}_4 \cdot 7\text{H}_2\text{O}$ there is one water molecule more than is required to fill the co-ordination sphere around the metal ion. In the hydrated salts of oxy-ions, such as sulphate, additional water molecules can be held between the nickel water units and the oxy-ions by means of O-H...O bonds. This arrangement may be similar to that shown in Fig. 13 for $\text{CuSO}_4 \cdot 5\text{H}_2\text{O}$. The hydrogen bonding of the type O-H...O is stronger than that of O-H...Cl, and, as a consequence, the oxy-ions can more easily accommodate the extra water molecule than can the simple anions like chloride.

Comparison of the infrared spectrum of a compound in the solid with that in the liquid or gaseous states reveals that both the frequency and the number of the absorption



Top - Structure of $\text{CoCl}_2 \cdot 2\text{H}_2\text{O}$ Projected Along c -axis

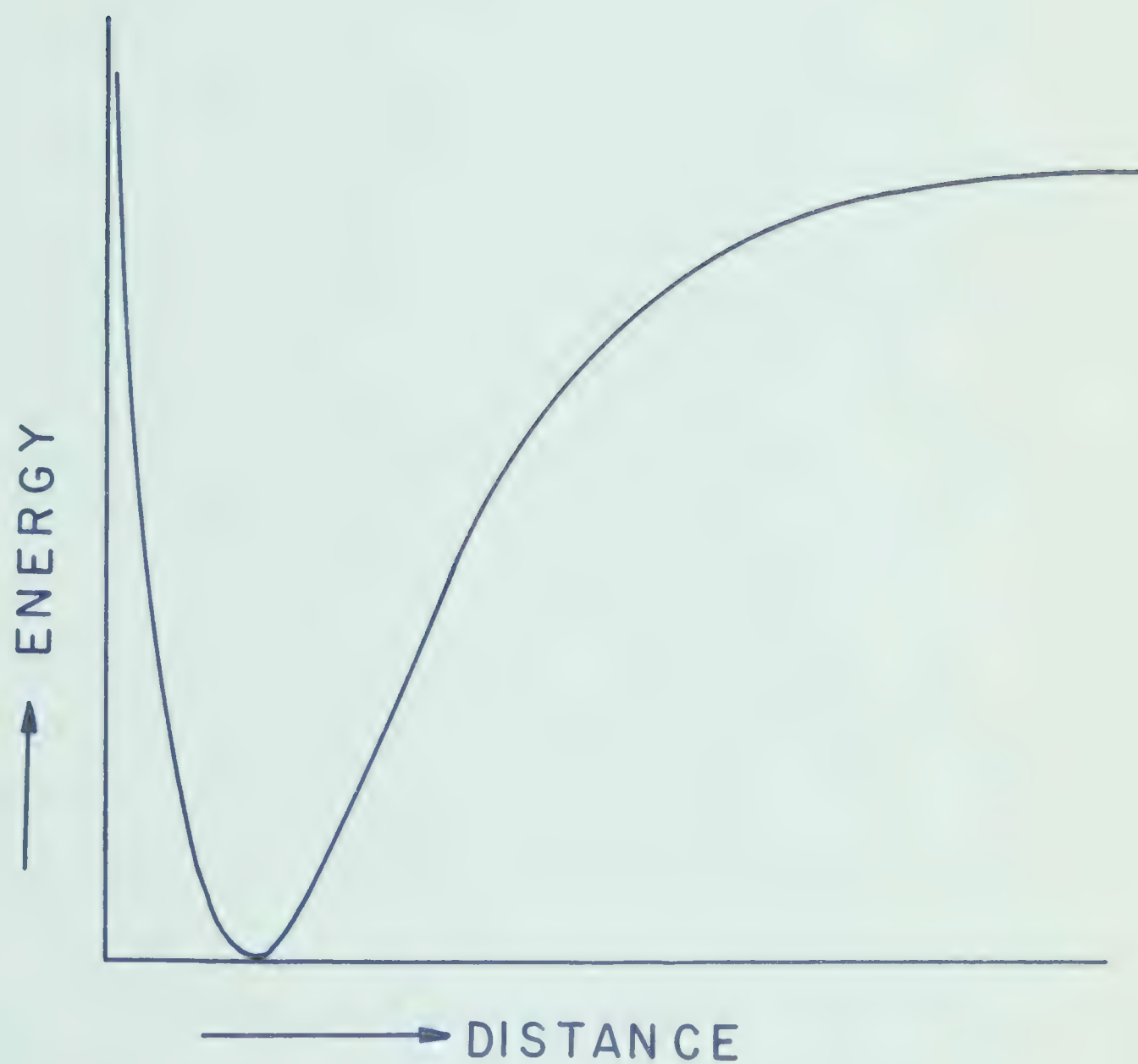
Bottom - Structure of $\text{CoCl}_2 \cdot 2\text{H}_2\text{O}$ Projected Along b -axis

bands may change. The frequency changes which occur upon entering the solid state generally result from the increase in the intensity of interactions of the vibrating units with the atoms of neighbouring molecules, which are in closer proximity in the solid phase. These changes may become important in those cases where hydrogen bonding is possible.

A hydrogen bond exists between two atoms when the hydrogen atom of an X-H bond is located between them in such a manner that it can interact with the second atom R to form an X-H...R unit. The two hydrogen bonded atoms may be the same or different and may be in the same or different molecules. The properties which they must have in common are negative character and relatively small size. The more electronegative the atoms the stronger will be the electrostatic interaction with the hydrogen. Although the residual charge on the bonding atoms is of primary importance, the X...R distance will also play a role in determining the magnitude of the effect produced. This is really a dipole-dipole or ion-dipole interaction, and as a consequence will fall off rapidly with distance.

In considering the influence of hydrogen bonding upon infrared absorption frequency it is convenient to take as an example the interaction of an O-H bond with a neighbouring oxygen. A free O-H group has a sharp absorption band at 3680 cm^{-1} (62), which is due to the normal stretching

vibration of the O-H bond. When an electronegative atom, such as oxygen, is placed in sufficiently close proximity to an O-H group that hydrogen bonding can contribute to the energy of the system, the O-H group is no longer free. The vibration frequencies characteristic of a molecule depends on the masses of the vibrating atoms and on the restoring forces which operate when the molecule is distorted from its equilibrium configuration (63). These restoring forces may be assumed to be proportional to the distortion in the molecule (64), and the proportionality constant relating the restoring force to the distortion is called the force constant. It has been used to estimate the bond strength (65). A simple potential energy diagram is shown in Fig. 16. The potential energy is dependent on the interatomic distance, and is a minimum at the equilibrium distance. Thus, the bond strength is maximum at the normal equilibrium distance. If the equilibrium distance is increased for any reason the potential energy curve becomes both broader and shallower. This corresponds to a decrease in the bond strength and since there is a relationship between bond strength and characteristic band frequency, the frequency of vibration decreases. Thus, any potential field which can modify the bond strength due to change in bond length leads to a shift in the frequency of vibration. When the free O-H bond becomes a part of an O-H...O system it is weakened as a result of stretching of



POTENTIAL ENERGY CURVE

Fig. 16

the bond, and change in the effective electron density associated with the bond which affects both the ionic bond character and the dissociation energy (66). Both of these effects can cause the absorption frequency to decrease. The magnitude of the frequency shift provides a tool in estimating the interaction energy (67) associated with the hydrogen bond.

Hydrogen bond formation causes changes in both the frequency and intensity of absorption. The frequency behaviour is indicative of the potential function maintaining the equilibrium configuration. The intensity behaviour is indicative of the charge movement due to the distortion of this configuration. The frequencies influenced by hydrogen bonding are shifted and broadened or split. The explanations advanced for both broadening and splitting of bands have been controversial for many years. The broadening was considered to be associated with the sensitivity of hydrogen bonds to intermolecular influences. In the case of weak hydrogen bonding there are fewer hydrogen bonded forms interacting to influence the breadth of the band. Consequently at lower temperatures, due to quenching of some of the hydrogen bonded forms, or in the vapour state, where only small (two or three molecule)hydrogen bonded units can form, the discrete structure of the band was observed. In the case of strong hydrogen bonding, due to the greater number of hydrogen bonded configurations, the width of the band is less dependent on

the state of aggregation. Presumably this results from the larger numbers of hydrogen bonded configurations not being sufficiently sharpened by the reduction in temperature to remove the overlap of adjacent bands and reveal the structure of the band envelope or from the larger aggregates permissible in the gas phase. Another intermolecular mechanism has been suggested (68). It is suggested that one of the bands is the true hydrogen stretching band and the others are combination bands arising as the result of the simultaneous excitation of more than one mode of vibration which distorts the potential energy surface. When the potential energy surface departs from a simple harmonic form it gives rise to strong combination bands which are very sensitive to intermolecular influences. Molecules are deformed by intermolecular forces and the nuclei vibrate around new equilibrium positions. If the potential energy surface is anharmonic the potential constants differ for different equilibrium positions. Thus, the bands merge into a broad hydrogen stretching band.

The changes in intensity have been ascribed to either altered ionic character of the bond (69) or altered contributions of charge transfer forms (70). Huggins and Pimental (71) have shown that a choice between the two models may be made on the basis of a study of the O-H bending modes. If an increase in intensity in the stretching region is due to increased ionic character of the bond then a similar effect

should be observed in the bending region. The charge transfer model attributes no unusual charge properties to the proton, and consequently intensity increase will not be expected in the bending region. The intensity changes in the two regions support the charge transfer model.

When the number of bands changes, the change may take the form of disappearance of existing bands or the appearance of new bands. Any new bands which appear are characteristically dependent upon the structure of the particular phase being considered. In the solid state disappearance of bands may be due to the rigid orientation of the molecules which eliminates rotational isomerism. For example *p*-chloroacetophenone has two carbonyl absorption bands in the liquid state but only one in the solid state (72).

The appearance of additional bands is a more common phenomenon. Kletz and Price (73) have proposed several explanations for such a behaviour. In the solid state the environment is fixed and stronger intermolecular forces exist. That shoulder observed in the liquid state became a doublet in the solid state was explained as probably due to higher resolution of the spectra in the solid state. Splitting of the energy levels, or transitions forbidden in one state becoming allowed in another due to crystal symmetry, may give rise to a new band. But the explanation preferred by Kletz and Price for their observations of the infrared spectra of

various solid and liquid alkylphenols is that two isomeric forms may exist in the liquid state of which one is more stable than the other. The nature of packing in the crystal may require the formation of a considerable proportion of both forms despite their difference in thermodynamic stability. Another important factor is that in a crystal the same molecules occur in different environments. Then, even though all the molecules in the unit cell are isomeric, a difference in their molecular environment may cause a difference in the frequency of absorption of two otherwise identical molecules. Those which are susceptible to intermolecular hydrogen bonding are particularly sensitive to the effect of environment. Thus, the unit cells may be packed in such a way that intermolecular hydrogen bonding is favoured in one case but not in another. For instance, the splitting of the original single band due to in-phase and out-of phase vibrations of the same groups in different molecules has been observed for the $-(CH_2)_n$ rocking mode in polyethylene (74).

Evidently then the spectral differences in the solid state as opposed to the liquid or gaseous state are, as a first approximation, consequences of the influence of the environment of the molecules in the crystal lattice. This is, however, an oversimplification of the situation for there is now only qualitative understanding of the interplay of the factors which produce spectral changes in the solid state (75).

There are some practical difficulties in obtaining spectra of the solid phase. The most important of these are control of sample thickness and elimination of reflection and scattering of light from the surface of the solid. The methods available are thinly spliced or deposited solid mounted directly on the cell window, suspension in a high boiling petroleum oil (Nujol), polytrifluorovinyl chloride (Fluorolube), or hexachlorobutadiene etc., dispersing in a powdered alkali halide, particularly KBr, and pressing into a clear disc. These methods all have both advantages and disadvantages.

The first method has been traditionally used for minerals which are easy to handle as thin polished sections (76). However, very fine powders may be spread fairly uniformly on the surface of an alkali halide window either by hand or allowing a suspension to settle out slowly (77). In this latter case sample preparation is tedious, uniform sample thickness is difficult to achieve, preferred orientation of the particles on the surface can give erroneous intensity ratios. Reproducibility and the general quality of the spectra are poor. Because of these shortcomings the matrix-free technique is now little used.

A mull is a paste of the sample material in an oil prepared by grinding the ingredients together. Most solids can be studied in this manner. In order that an oil be a useful mulling agent it must have high density, viscosity,

refractive index and low absorbance in the spectral region of interest. However, it is difficult to obtain and maintain a uniform suspension of the sample, and the length of the optical path cannot be accurately controlled. Hence for qualitative work mulls are very useful but they are of limited usefulness for quantitative intensity measurements.

The KBr-pellet technique (78) yields quantitative and reproducible spectra of solids. It has the advantage of the absence of an absorption band of the dispersing or suspending medium and the possibility of controlling the sample weight accurately. Unfortunately there are disadvantages associated with this medium which are now becoming understood. These difficulties have been critically reviewed by Duyckaerts (79). The influence of KBr on the spectrum of a solid may be caused by a number of factors which range from simple adsorption to chemical reaction. It is very difficult to eliminate moisture in preparing KBr discs even with dry box techniques. At the very least water gives rise to a band and might even cause hydrate formation or hydrolysis of compounds. When the region of interest happens to be the O-H frequencies, it does not seem to be suitable. The close contact during grinding, vibrating and pressing, between the dispersing medium and the substance may give rise to chemical reaction as in the equation:



Benzoic acid mixed with potassium bromide is transformed into

potassium benzoate in a ball mill (80). Mixed crystal formation can take place as in the case of alkali bifluorides (81). The distortion of the crystal structure can take place to produce spectra identical with those of liquids as in benzil (82). Complex formation between KBr and the substance may lead to frequency shifts and band splitting as in the case of thiourea (83). Baker (84) has critically evaluated the factors which influence the changes in pellet spectra. The basis of choice between mulling and pelleting depends on the region of the spectrum of interest and also the kind of information desired.

Early in this century Coblentz (85) studied the infrared spectra of minerals in an effort to distinguish between water of crystallization and water of constitution. The criterion used for distinguishing water of crystallization from water of constitution was the presence of all the absorption bands of water in the former case and absence of some in the latter case. Liquid water absorbs strongly at about 3.2μ and 6.3μ and it was found that in all crystalline compounds containing water of crystallization these bands were present. From the spectra reported by Coblentz it can be seen that the band at 3.2μ broadens depending on the amount of water. Coblentz also showed that the frequencies of absorption differed from those of liquid water. There was also some variation from one compound to another, since the water groups

were not free in the crystal but vibrated in the fields of force of the other constituents. Because of the breadth of the infrared bands for the hydrates and of lower resolution of the spectrometers most of the early work was observational in nature. Infrared spectra of many hydrated metal salts have been reported by Miller and Wilkins (86). Frederickson (87) characterized hydrated aluminas by the difference in the absorption patterns in the O-H stretching and deformation regions. Corbridge and Lowe (88) studied some hydrated phosphates and tried without success to correlate some characteristic of the water absorption bands with the number of water molecules in a hydrate. Lucchesi and Glasson (89) investigated the infrared absorption spectrum of bound water in metal hydrates in which the cation charge varied from 1 to 4, and the size, shape and charge of the anion and the water content varied. Shifts in the frequency of the O-H stretching and bending regions were reported. There was, however, no obvious correlation between absorption spectra of water in hydrates and the nature and strength of binding of the water.

The infrared spectrum of a solid hydrate should give an insight into the nature of intermolecular forces, the extent of inter-and intramolecular hydrogen bonding and the binding of water molecules in the crystalline solid. The possibility of using the infrared spectra to study these factors has not been explored to any great extent. The position,

shape and intensity of the water bands of solid hydrates depends on the interaction of the water molecules with their crystalline environment. The extent of hydrogen bonding will depend upon the orientation of water molecules relative to one another and to the other ions in the crystal lattice. Thus, the shape of the band is an indication of the environment of the absorbing molecules. The sharpness of the band is an indication of the extent of hydrogen bonding. Recently Fujita, Nakamoto and Kobayashi (90) observed that water molecules in some solid aquo complexes give rise to a new vibrational band at about 800 cm^{-1} . Brame, Johnson, Larsen and Meloche (91) observed similarity of spectra for the isomorphous $\text{K}_4\text{Mo}(\text{CN})_8 \cdot 2\text{H}_2\text{O}$ and $\text{K}_4\text{W}(\text{CN})_8 \cdot 2\text{H}_2\text{O}$.

In the present study an attempt has been made to explain the different regions of the infrared spectrum for the compounds $\text{NiCl}_2 \cdot 6\text{H}_2\text{O}$, $\text{NiCl}_2 \cdot 4\text{H}_2\text{O}$ and $\text{NiCl}_2 \cdot 2\text{H}_2\text{O}$. Infrared spectra of some isomorphous hydrates whose structures are known have also been taken to determine the relationship between isomorphism and the infrared spectra.

Objectives of the Present Work

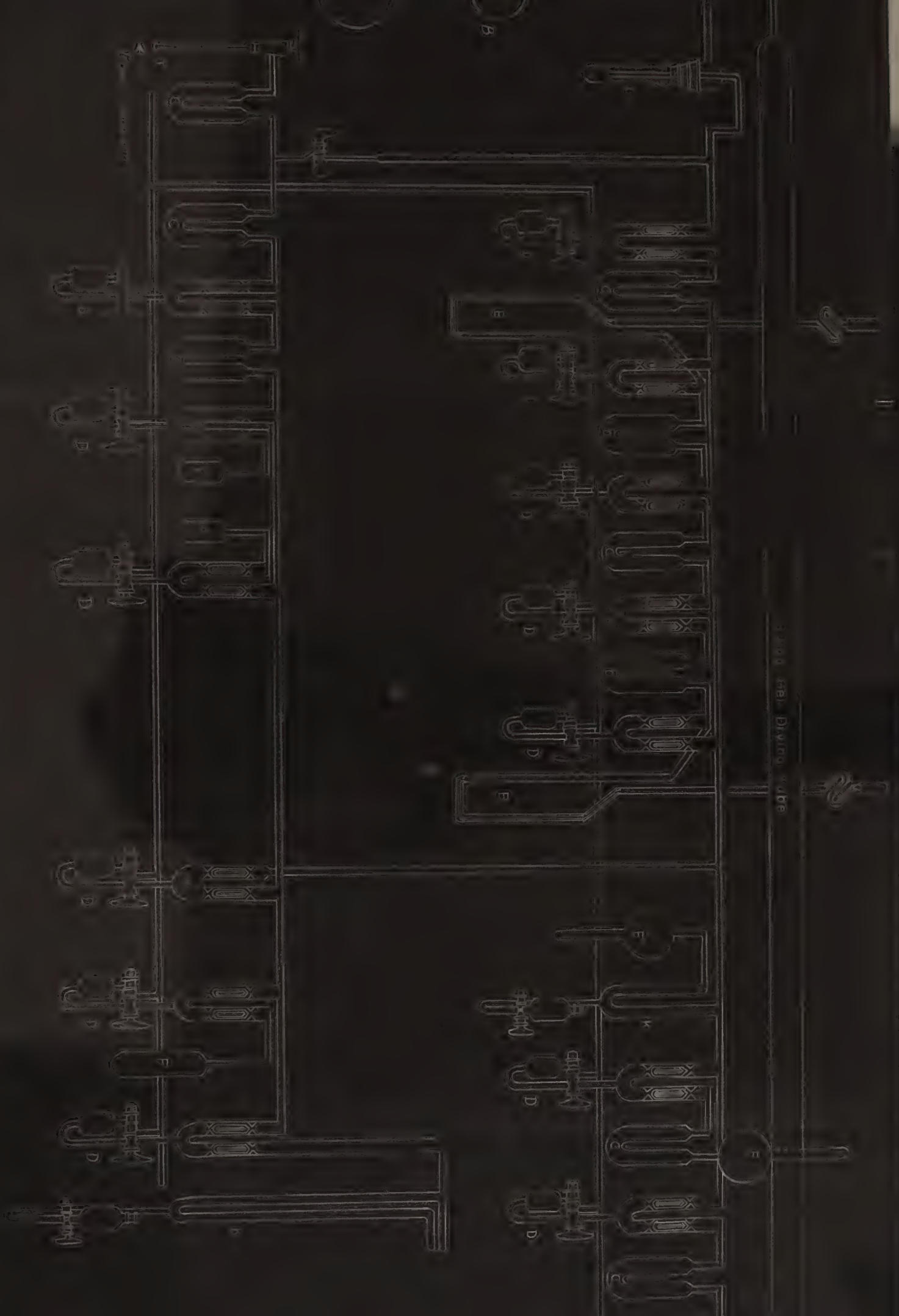
It is the purpose of the present work to firmly establish the identity of the hydrates of nickel(II) chloride. Once this is established it proposes to show that the energetics of the decomposition process have relevance to the problem of the binding of water molecules by transitional metal ions.

EXPERIMENTAL

Equilibrium Studies

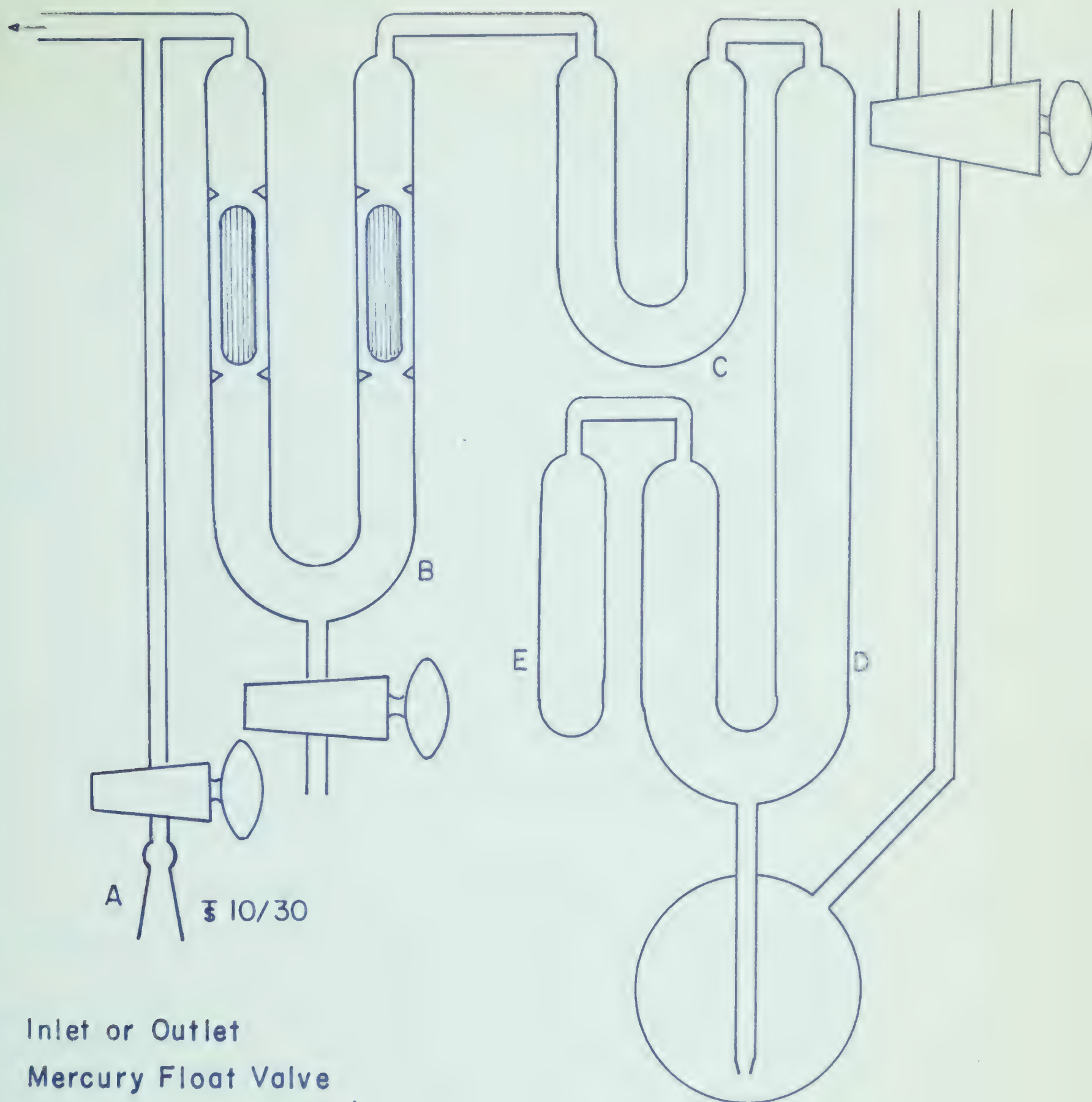
The $\text{NiCl}_2\text{-H}_2\text{O}$ System:- The vapour pressure measurements were carried out in a Stock-type high vacuum apparatus as described by Sanderson (92a), with the modifications evolved in these laboratories (see Fig. 17). A modification of the dissociation tensimeter, described by Brown, Taylor and Gerstein (92b) was made. The modified tensimeter is shown in Fig. 18(D). It consists of a U-tube manometer made from 18 mm O.D. tubing connected to a mercury reservoir. One limb of the manometer is connected to a tube which holds the sample and the other limb to the vacuum system. The mercury in the manometer can be either raised or lowered by connecting the two-way stopcock to either air or rough vacuum. Thus, when the mercury is raised in the manometer it can act both as a seal to isolate the system to be measured from the remainder of the line and as a manometer fluid. When a sample is placed in the sample tube, the difference in height of mercury in the two limbs of the manometer signifies the vapour pressure of the sample.

An aqueous nickel chloride solution was prepared by dissolving BDH Analar nickel chloride hexahydrate in water. This solution was analyzed for its nickel and chloride content by the conventional cyanide method for nickel and conductometric titration of chloride with silver nitrate. Knowing the



pe high vacuum
Fig. 17

To Mercury Float Valve
and High Vacuum System



- A Inlet or Outlet
- B Mercury Float Valve
- C Condensation Trap
- D Dissociation Tensimeter
- E Sample Tube

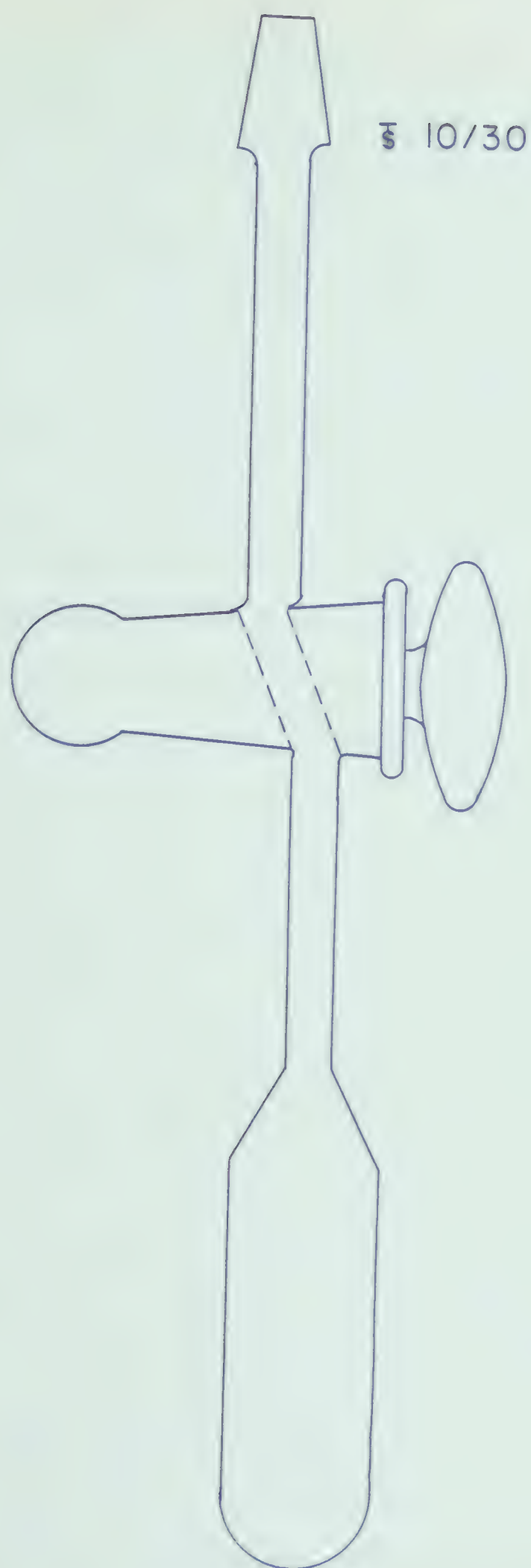
Fig. 18

weight of the liquid sample and subtracting the weight due to nickel chloride, the weight due to water was calculated and thus the $\text{H}_2\text{O}/\text{NiCl}_2$ ratio was computed. The nickel chloride solution was stored in, and dispensed from, a dropping bottle. The male joint ended in a long stem touching the bottom of the bottle. A rubber teat was attached to the opening of the male joint. This prevented change of composition due to evaporation and functioned as a dropper. By squeezing the rubber teat the solution can be delivered to any desired container. The nickel chloride solution was taken in this dropping bottle and weighed. After delivering the desired quantity of solution, the weight of the weighing bottle was taken. The difference between the initial and final weight gave the weight of the solution taken. To ensure an additional check on the initial composition, a sample of similar size was taken for complete analysis.

A 3.0169 gm. sample of nickel chloride solution was placed in the tube E, shown in Fig. 18, through the open tap. The opening was then sealed quickly with a hand torch. The capacity of the tube was about 30 ml. Inside the tube a magnet sealed in glass functioned as a stirrer.

After the solution was introduced and the opening sealed, the sample tube was immersed in liquid nitrogen and opened to the high vacuum line, and pumped down to the best obtainable vacuum. Dissolved air was removed by freezing the

solution in liquid nitrogen opening it to a high vacuum, isolating and then thawing the sample, refreezing it followed by evacuation. By repeating this process several times most of the dissolved air was eliminated. The last traces of dissolved air were removed by pumping on the unfrozen solution for about a minute. The volatilized water was collected in the U-trap (C) which was immersed in liquid nitrogen. The sample tube E was then immersed in liquid nitrogen and mercury raised in the manometer to cut off the solution from the U-trap C. The mercury float valve B was then closed to separate this section from the rest of the vacuum line. The water volatilized was taken into the weighing tube shown in Fig. 19. The procedure involves attaching the weighing tube to the vacuum line by a 10/30 ground glass joint lubricated with Apiezon L grease and evacuating it. The vacuum achieved was of the order of 10^{-6} mm Hg. measured by the McLeod gauge. The weighing tube after evacuation was detached from the vacuum line. The grease on the joints was removed by Kleenex soaked in ether, and the tube then weighed. It has been found that by repeating the process of greasing, degreasing by ether, and weighing, that the uncertainty introduced into the weight by this operation was negligible (<1 mg). After determining the initial weight of the weighing tube it was again attached to the vacuum line. When a vacuum of the order of magnitude of 10^{-6} mm. Hg was achieved, this section of the line was isolated



WEIGHING TUBE

Fig. 19

from the pump by a mercury float valve (not shown in Fig. 18). The mercury float valve (B) was then opened and the liquid nitrogen dewar used to condense water in the U-trap (C) was removed. The weighing tube was now cooled in liquid nitrogen. By this operation the water collected in U-trap (C) was transferred to the weighing tube. The completeness of the transfer was checked by measuring the residual pressure in the vacuum line by McLeod gauge. After ensuring complete transfer the weighing tube was closed, detached from the vacuum line, and after careful removal of grease weighed. The gain in weight represents the water removed. Thus, knowing the weight of the water removed, the composition of the system was computed. In an effort to check the reliability of this procedure, the water sample was returned to the vacuum line and the procedure repeated several times. The variation in sample weight was negligible and showed no trend. The tensimeter and sample were completely immersed in a Pyrex glass water bath whose temperature could be controlled at any value from ambient to 100°C . to within $\pm 0.1^{\circ}$ by a Fisher Unitized Bath Electronic Control unit. The temperature of the bath was measured by a NBS calibrated thermometer (Fisher 2A 1706) to the nearest 0.05°C . The equilibrium vapour pressure of the sample at a particular temperature could then be measured to the nearest 0.05 mm with a Gaertner Cathetometer (M-911). The pressure values reported were corrected for the density

of mercury at the temperature of measurement and for the capillarity depression.

Once a sample of known composition was isolated in the tensimeter, its pressure was measured at all the selected temperatures with the exception of 75° . Each individual temperature was attained by allowing the bath to warm from the next lower temperature. Sufficient time, ranging from 4 to 6 hours, was allowed for equilibration before any pressure values were recorded. The system was considered to be in equilibrium when, at a particular temperature, it gave three identical pressure values at consecutive intervals of 30 minutes. When the sample became solid after withdrawal of water, it usually took much longer times to attain equilibrium. Usually for the solid sample, the time elapsed for reaching equilibrium ranged from 6 to 24 hours depending on the temperature of the bath. At lower temperatures equilibrium was attained less rapidly than at higher temperatures. When three readings of vapour pressure gave identical values at intervals of one hour, it was considered to be the equilibrium value. Then, once the equilibrium values were approached from lower temperature, the bath was allowed to warm a degree or two above the equilibrium temperature, readjusted to the equilibrium temperature, and observations of the pressure continued until the constant value was obtained. In all cases the equilibrium values obtained by approaching from above and below agreed

within 0.05 mm Hg.

The composition of the sample was changed by lowering the water bath to make the sample tube (E) accessible for cooling in liquid nitrogen. After cooling, the mercury in the manometer of the tensimeter (D) was lowered, the U-trap (C) was immersed in liquid nitrogen, the float valve B closed, and the liquid nitrogen dewar removed from E. Water from the sample would volatilize and collect in the U-trap C. The time allowed for this operation depends on the composition desired for the sample. Although this can be only very crudely controlled, the final composition would be known accurately. After an appropriate time, the sample tube E was again immersed in liquid nitrogen and the mercury raised in the manometer. The water collected in the U-trap C was taken out and weighed by the manipulation described above. Once the composition was changed, the vapour pressure measurements were again made for the different temperatures.

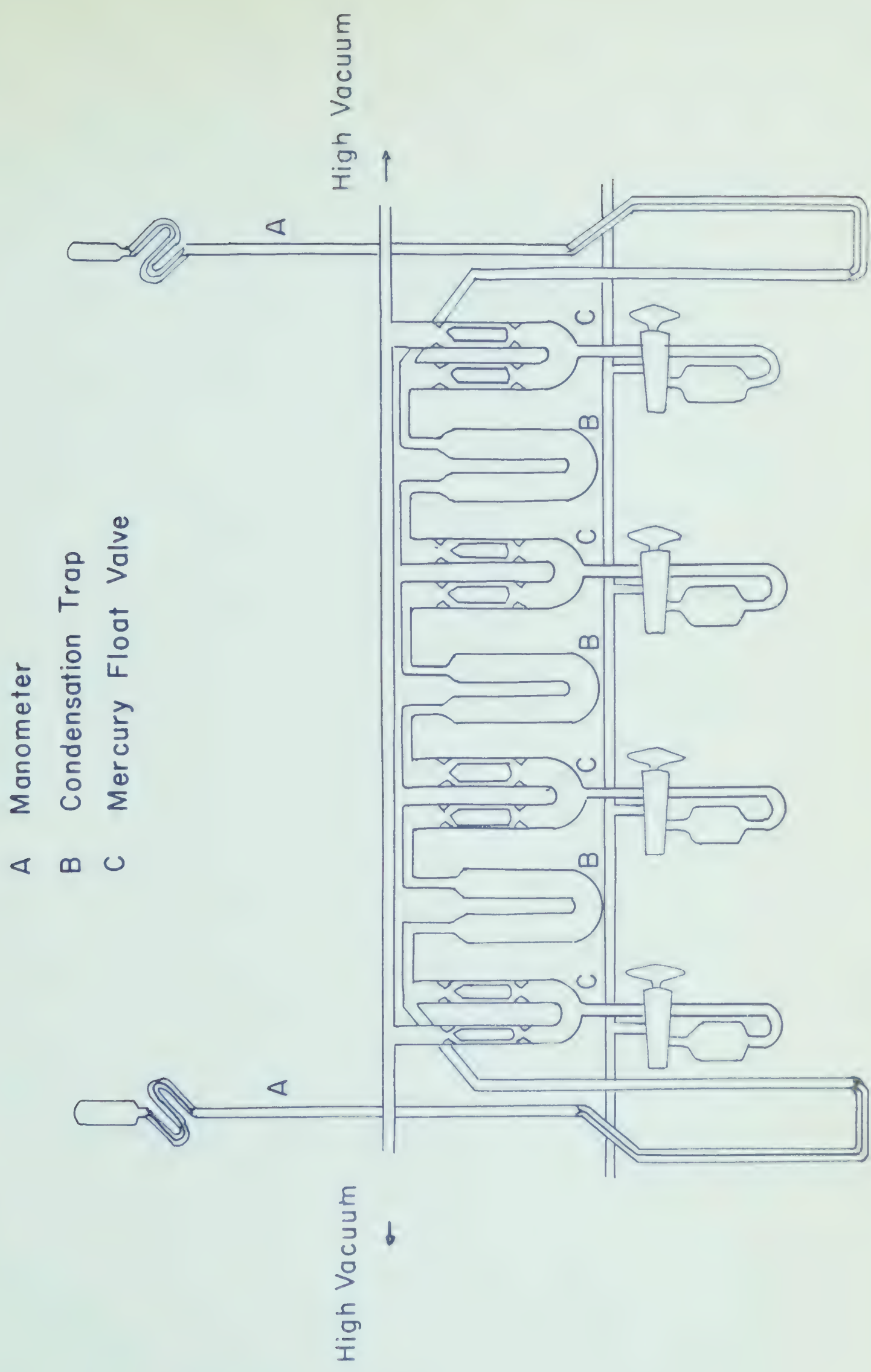
The composition of the sample was varied in this way in convenient steps. At each step the vapour pressure of the sample was determined at each of the selected temperatures as described above. The sample, at the last series of measurements, was estimated to have an H_2O to NiCl_2 ratio of 2.16. This sample was removed from the vacuum line, weighed, dissolved in water, and aliquots of the resultant solution analyzed for nickel and chloride by the cyanide and conductometric

chloride titrations respectively. These results showed that the material removed actually had a composition corresponding to $\text{NiCl}_2 \cdot 2.05\text{H}_2\text{O}$.

The $\text{NiCl}_2 \cdot \text{H}_2\text{O}$ - ethylenediamine System:- Ethylenediamine 98% (Eastman Organic Chemicals) was taken into the vacuum line (Fig. 17) and subjected to trap to trap distillation in the U-trap system shown in Fig. 20. A final cut was then allowed to stand in contact with a sodium mirror in the bulb, shown in Fig. 21. After this treatment further fractionation was carried out, and a middle fraction from this treatment was taken in the dissociation tensimeter shown in Fig. 18, and its vapour pressure measured at three temperatures as shown in Table 1. This sample was stored in the vacuum line and used in the later measurements.

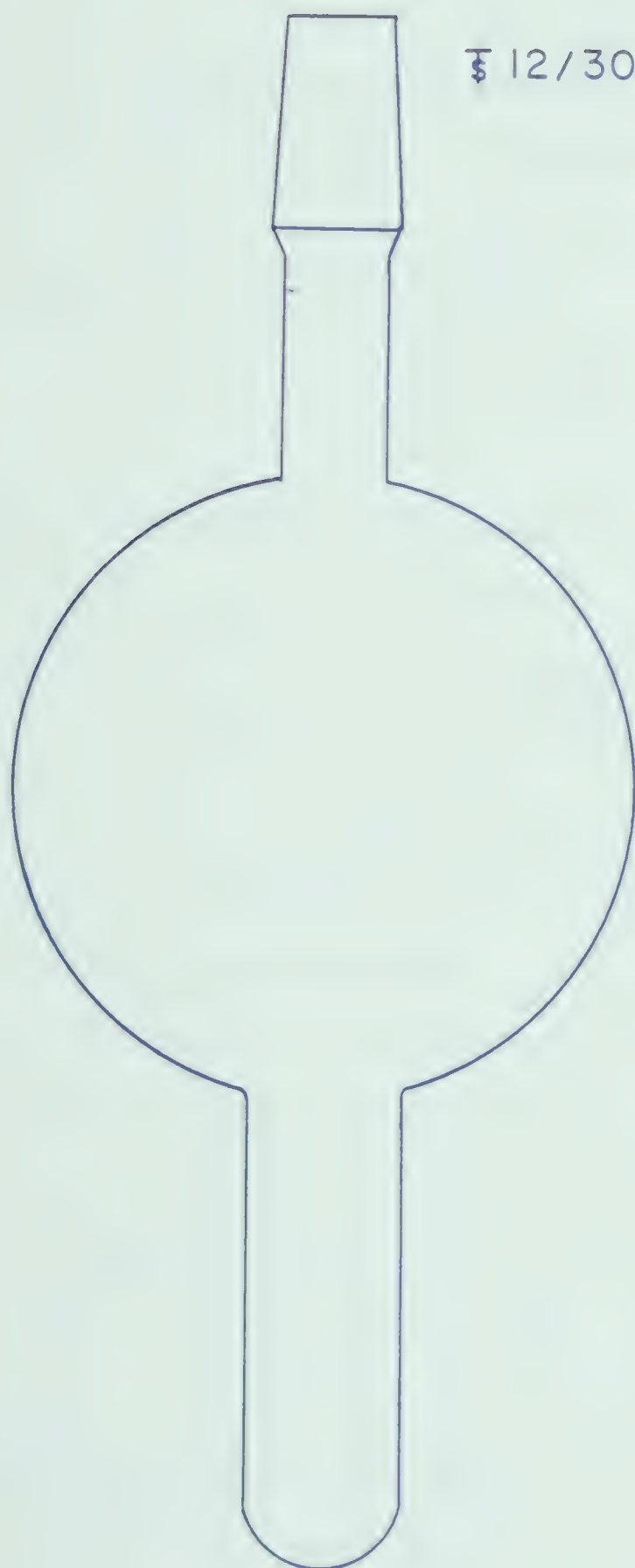
TABLE 1
Vapour pressure of ethylenediamine
at different temperatures

Temp. °C.	Vapour Pressure Observed	Vapour Pressure Literature (37)
30.0	16.85	16.75
40.0	30.20	30.25
50.0	53.00	52.90



FRACTIONATION TRAIN

Fig. 20



SODIUM MIRROR BULB

A 3.6420 gm sample of an aqueous solution of nickel chloride analyzed immediately before use was placed in the sample tube E, shown in Fig. 18, of about 30 ml capacity. The tube was sealed immediately, immersed in liquid nitrogen, and after about 5 minutes evacuated. After the removal of dissolved air the composition of the solution was brought to an H_2O to NiCl_2 ratio of 13.49 by removal of water. The vapour pressure of this solution was measured at a series of temperatures.

The weighing tube shown in Fig. 19 was connected to the vacuum line through a 10/30 ground glass joint lubricated with ApiezonL grease. After ensuring a vacuum of the order of 10^{-6} mm Hg, purified ethylenediamine was distilled into the weighing tube which was then closed, removed from the line, and weighed. The weighed tube was returned to the vacuum line and the vacuum of the system re-established. Then by opening the stopcock of the weighing tube containing ethylenediamine, a desired quantity was distilled in the U-trap C. After ensuring complete transfer, the weighing tube was detached from the vacuum line and weighed. From the loss in weight the amount of ethylenediamine introduced into the nickel chloride solution was calculated.

The ethylenediamine transferred to the U-trap C was taken into the solution contained in sample tube E by cooling E in liquid nitrogen, pulling down the mercury in the

manometer, and allowing the U-trap C to warm. Complete transfer was achieved rapidly and after allowing about 15 minutes the pressure in the line was checked by the McLeod gauge. After withdrawing the liquid nitrogen dewar from the sample tube E, the ethylenediamine was mixed completely with the nickel chloride solution by stirring with the glass enclosed magnet provided in the sample tube E. After this operation the mercury in the manometer was raised. To make sure that the solution was completely free from entrained air, the solution was again cooled in liquid nitrogen and the mercury was pulled down from the manometer and the system connected to the high vacuum line. After ensuring a vacuum of the order of 10^{-6} mm Hg, the mercury in the manometer of the tensimeter was raised, the water bath raised into position, and the system equilibrated overnight at 23°C . The addition of subsequent quantities of ethylenediamine was carried exactly the way mentioned above. Great care needs to be taken with the weighing tube containing ethylenediamine. This was always immersed in liquid nitrogen and evacuated to the order of 10^{-6} mm Hg and then brought to room temperature before taking its initial weight.

The temperature of the solution and the entire measuring system was maintained by immersing it in a Pyrex glass water bath with thermostatically controlled temperature to within $\pm 0.1^{\circ}\text{C}$ by a Fisher Unitized Bath Electronic Control

unit. The temperature of the bath was measured to the nearest 0.05°C by a magnifying arrangement attached to a calibrated NBS thermometer (Fisher 2A - 1706). The vapour pressure was measured by using a Gaertner Cathetometer (M-911) to the nearest 0.05 mm.

Kinetic Studies

Nickel(II) chloride hexahydrate (BDH Analar Reagent) was desiccated by spreading powdered samples evenly in 3 cm diameter petri dishes inside 6 inch desiccators containing different desiccants. Investigation of the behaviour of the "as received" material over sulphuric acid solutions of various specific gravities established that $\text{NiCl}_2 \cdot 6\text{H}_2\text{O}$ could be obtained and maintained in a desiccator which was maintained at a humidity corresponding to sulphuric acid of 1.35 specific gravity. The composition of the final equilibrium phase was established by nickel and chloride analyses. The results of these analyses were: Ni 24.60%, Cl 29.85%, and H_2O 45.55%; calculated for $\text{NiCl}_2 \cdot 6\text{H}_2\text{O}$: Ni 24.69%, Cl 29.83%, and H_2O 45.48%. Samples maintained in a sulphuric acid desiccant of specific gravity 1.35 were then always taken as starting material for other dehydration studies. The dehydrations in sulphuric acid desiccants of specific gravities 1.40, 1.50, 1.60, 1.70 and 1.80 were carried out in 3 cm diameter petri dishes inside 6 inch desiccators containing 100 ml of the

appropriate desiccant. The rate of loss of weight was determined by removing the petri dish from its desiccator at intervals and weighing it. Tests showed that exposure to the atmosphere for times equivalent to those required for weighing did not cause the sample to change in weight by more than 1 mg. By careful judgement the weighing operation does not take more than one minute. After weighing, the sample was returned to the appropriate desiccator.

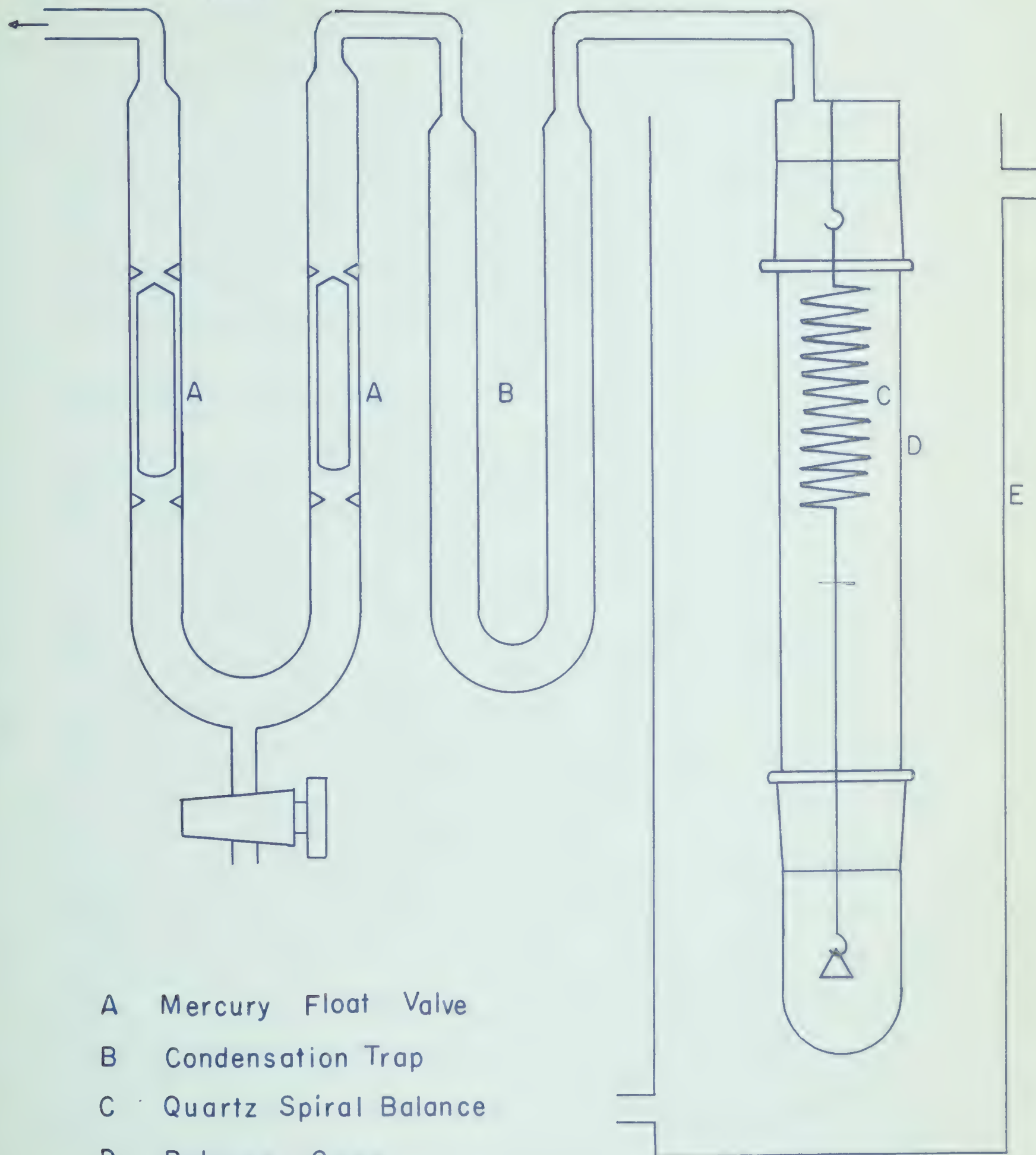
In the case of dehydrations carried out over phosphorous pentoxide and magnesium perchlorate desiccant, the precaution of desiccating the balance by placing a petri dish containing the appropriate desiccant inside the balance case was taken. Again, any change in weight due to exposure to the atmosphere was shown to amount to less than 1 mg. Since the dehydrations over sulphuric acid desiccants of low specific gravities were slow, they were followed in detail for only about 8 to 9 hours and then periodically for a week or more in order to determine the composition of the end product. This latter was done on the basis of both weight loss and chemical analysis. The dehydrations over phosphorous pentoxide desiccant were carried to their final stages. Attempts to control the atmospheric temperature were not made.

The arrangements for following the dehydration on the quartz spiral balance were more elaborate. A Misco quartz helix balance having 0.5 mm extension for 4.9 mg was suspended

from the top of a glass tube which served as a balance case. The balance case was connected through a U-trap B and a mercury float valve A to the high vacuum line. The arrangement of the apparatus is shown in Fig. 21(a). The quartz spiral was calibrated in vacuum with the balance case immersed in a thermostatically controlled water bath at $25.0 \pm 0.1^\circ$, by adding known standard weight on an aluminium foil pan of one inch diameter, and measuring the extension of the helix with the cathetometer to the nearest 0.05 mm. The extension of the spiral was found to be linear with respect to the amount of weight added. It was considered important that the quartz helix and the cathetometer did not change their relative positions during a series of measurements. This was ensured by referring back to the fixed index on the quartz spiral.

A sample of $\text{NiCl}_2 \cdot 6\text{H}_2\text{O}$ was sieved through ASTM standard sieves. The cut between 105 and 150 microns was retained and conditioned in a desiccator whose humidity was maintained by sulphuric acid of 1.35 sp. gr. A sample of this material was placed on an aluminum foil pan, weighed, and transferred immediately to the quartz helix. The system was allowed to come to the temperature of the bath before being evacuated. The bath was maintained by circulating a constant temperature water controlled by a Fisher Unitized Bath Electronic Control unit to $\pm 0.1^\circ\text{C}$. The movement of the pointer was followed after about 3 to 5 minutes, when the system had attained a vacuum

High Vacuum System



- A Mercury Float Valve
- B Condensation Trap
- C Quartz Spiral Balance
- D Balance Case
- E Water Bath

Fig. 21a

of the order of 10^{-6} mm Hg. The temperature of the bath was measured to the nearest 0.05°C by an NBS calibrated thermometer (Fisher 58 - 630). The water evolved during dehydration was collected in a U-trap immersed in liquid nitrogen. Thus, the whole system was kept open to the vacuum line so that the water liberated was immediately withdrawn from the system. The progress of dehydration was followed by the upward movement of the index fiber.

Infrared and X-ray Studies

Preparation of materials:- The hydrates of nickel chloride were prepared by desiccating BDH Analar $\text{NiCl}_2 \cdot 6\text{H}_2\text{O}$ in an atmosphere of controlled humidity. The product was nickel chloride hexahydrate when sulphuric acid of specific gravity 1.35 was used as the desiccant, nickel chloride tetrahydrate when sulphuric acid of specific gravity 1.40 was used, and nickel chloride dihydrate when phosphorous pentoxide was used. The intermediate hydrates, presumably mixtures of hydrates, were obtained from the dehydration of $\text{NiCl}_2 \cdot 6\text{H}_2\text{O}$ over P_2O_5 for different times. The composition was calculated from the loss in weight of the sample. $\text{CoCl}_2 \cdot 6\text{H}_2\text{O}$ (Mallinckrodt Analytical Reagent) was used without further treatment. $\text{CoCl}_2 \cdot 2\text{H}_2\text{O}$ was obtained by desiccating finely powdered $\text{CoCl}_2 \cdot 6\text{H}_2\text{O}$ over P_2O_5 until the weight loss indicated that the sample composition corresponded to $\text{CoCl}_2 \cdot 2\text{H}_2\text{O}$. $\text{MnCl}_2 \cdot 4\text{H}_2\text{O}$ (May and Baker grade)

was used without further treatment. $\text{MnCl}_2 \cdot 2\text{H}_2\text{O}$ was obtained by desiccating $\text{MnCl}_2 \cdot 4\text{H}_2\text{O}$ over P_2O_5 until the sample had lost sufficient weight that the empirical formula corresponded to $\text{MnCl}_2 \cdot 2\text{H}_2\text{O}$.

Infrared Absorption Measurements:- The infrared spectra were obtained on a Perkin-Elmer Model 21 double beam infrared spectrophotometer using an NaCl prism. Higher resolution in the O-H stretching region was obtained with a Perkin-Elmer Model 221-G infrared spectrophotometer with an NaCl prism-grating interchange. Wavelength was calibrated using the polystyrene band at 6.238μ .

Considering the influence of adsorbed water and the chance of chemical interaction during pelleting under high pressure, it was decided to mount the samples as mulls for obtaining the infrared spectra rather than as potassium bromide discs. Two different mulling agents were used. Fluorolube S-30 (Hooker Electrochemical Corporation) was used for the 3500 to 1600 cm^{-1} regions and Nujol for the 800 cm^{-1} region. These two mulling agents were necessary because of the limitations associated with each. Overlap in the stretching frequency of the C-H and O-H limits the use of Nujol in 3500 cm^{-1} region, and Fluorolube S-30 is quite absorbing in the 800 cm^{-1} region. Combining the spectra obtained from samples in two mulling agents, a clear picture of the spectral regions of interest was obtained.

X-ray Diffraction Measurements:- X-ray powder diffraction patterns were taken at room temperature $\approx 25^{\circ}\text{C}$. The samples of $\text{NiCl}_2 \cdot 6\text{H}_2\text{O}$, $\text{NiCl}_2 \cdot 4\text{H}_2\text{O}$, and $\text{NiCl}_2 \cdot 2\text{H}_2\text{O}$ were prepared under the proper conditions of humidity established earlier. The hydrates were milled to a fine paste in an Agate mortar with Fluorolube S-30 (Hooker Electrochemical Corporation). Changes in composition due to exposure to atmosphere was minimum because of the protective action of the oil over the samples. The mull was evenly spread on a microscope slide and exposed to the X-ray beam on a Norelco X-ray Diffractometer. A copper target X-ray tube using a nickel filter was employed as the source of radiation.

RESULTS

Equilibrium Studies

The vapour pressures of nickel chloride-water mixtures of various compositions are given in Tables 2, 3, 4 and 5. The vapour pressure-composition isotherms obtained from these data are displayed graphically in Figs. 22, 23 and 24. These isotherms show that the vapour pressure decreases normally as the concentration of the solution increases up to the first appearance of a solid phase. Upon appearance of the solid, the pressure becomes and remains constant so long as any liquid phase is present. Upon disappearance of the liquid phase there is a discontinuous change in the pressure of the system. The pressure then maintains a constant value through a subsequent range of compositions until eventually a second discontinuous decrease in the pressure of the system is observed. This stepwise variation of the pressure continues in some cases for as many as three such steps. The actual number of steps present in a particular isotherm depends upon the temperature. In the temperature range 27-36° (Fig. 22) there are three steps and these occur at mole ratios of H_2O to NiCl_2 of 6, 4 and 2. In the temperature range 37-70°C (Figs. 23, 24) two steps, at mole ratios of 4 and 2, are apparent.

TABLE 2

Vapour Pressure - Composition Data for the $\text{NiCl}_2\text{-H}_2\text{O}$ System
at 27, 30, 33, 35, 36°C

$$\text{Mmoles NiCl}_2 = 3.84$$

Mmoles H_2O	Mmole Ratio $\text{H}_2\text{O/NiCl}_2$	Vapour Pressure in mm Hg. at				
		27°C	30°C	33°C	35°C	36°C
91.53	23.83	23.90	27.95	33.15	36.65	39.00
62.92	16.38	18.85	22.65	26.75	30.10	32.05
49.23	12.82	16.25	19.60	23.20	26.05	27.65
42.13	10.97	14.80	17.65	21.05	23.60	25.10
37.12	9.66*	14.30 ^S	16.65 ^S	19.20 ^S	21.15 ^S	22.80 ^S
37.12	9.66	13.30	15.70	19.00	21.15	22.40
37.12	9.66	14.30	16.65	19.20	21.15	22.40
32.17	8.38	14.30	16.65	19.20	21.15	22.40
28.25	7.35	14.30	16.65	19.20	21.15	22.40
23.65	6.15	14.30	16.65	19.20	21.15	22.40
21.44	5.58	13.50	16.20	18.80	20.75	21.70
19.51	5.08	13.50	16.20	18.80	20.75	21.70
17.97	4.68	13.50	16.20	18.80	20.75	21.70
16.78	4.37	13.50	16.20	18.80	20.75	21.70
16.78	4.37*	12.50	14.90	18.20	20.30	-
16.44	4.28	13.50	16.20	18.80	20.75	21.70
14.94	3.89	7.0	7.85	10.35	11.90	13.45
13.75	3.58	7.0	7.85	10.35	11.90	13.45
12.68	3.30	7.0	7.85	10.35	11.90	13.45
9.68	2.52	7.0	7.85	10.35	11.90	13.45
8.29	2.16	7.0	7.85	10.35	11.90	13.45

* Vapour Pressure Heating Direction

S Solid Appears

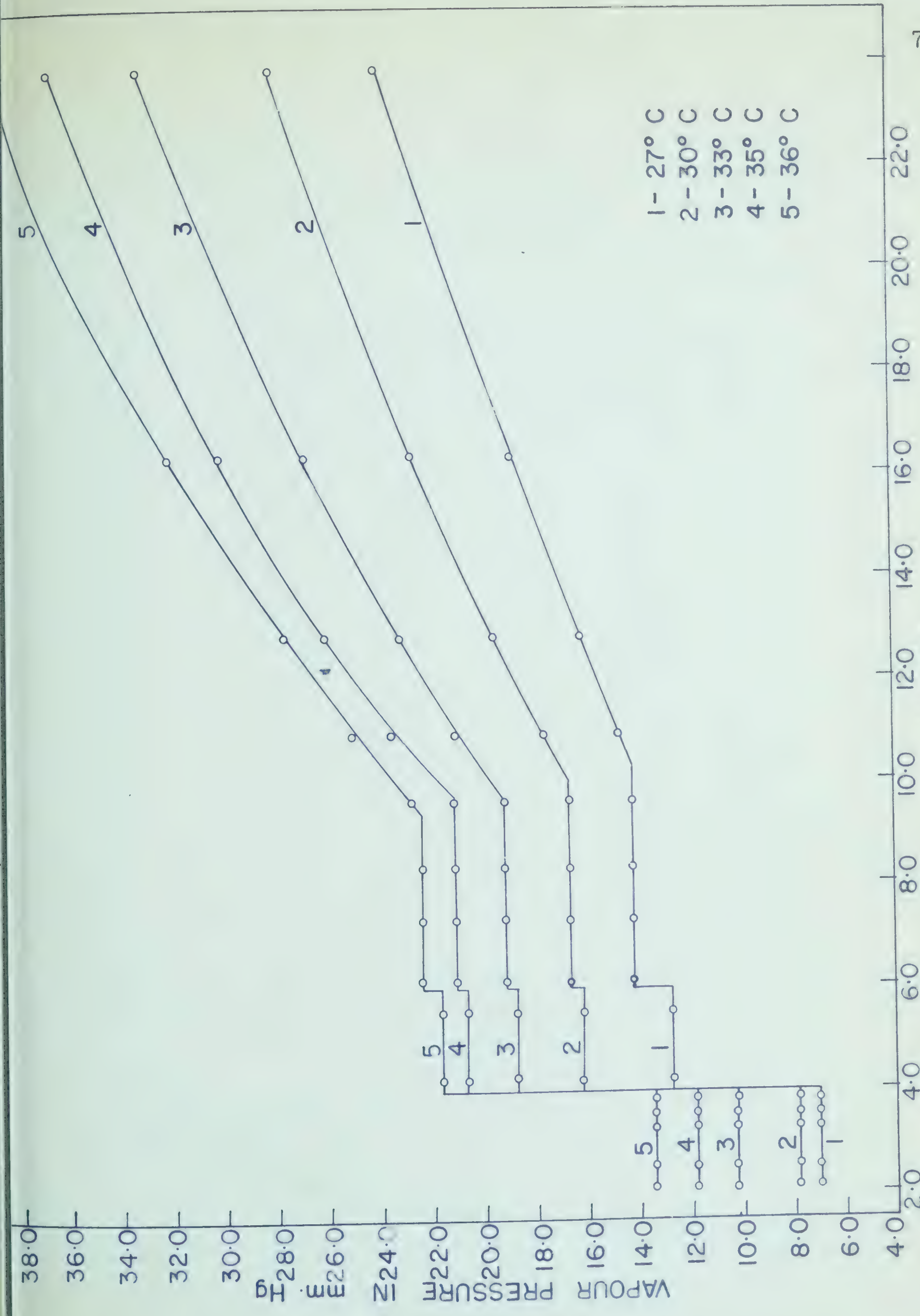


Fig. 22
 $H_2O/NiCl_2$
 VAPOUR PRESSURE—COMPOSITION DIAGRAMS FOR 27°C, 30°C, 33°C, 35°C & 36°C.

TABLE 3

Vapour Pressure - Composition Data for the $\text{NiCl}_2\text{-H}_2\text{O}$ System
 at 37, 40, 45, 50, 55°C
 Mmoles $\text{NiCl}_2 = 3.84$

Mmoles H_2O	Mmole Ratio $\text{H}_2\text{O}/\text{NiCl}_2$	Vapour Pressure in mm Hg.				
		37°C	40°C	45°C	50°C	55°C
91.53	23.83	40.65	47.70	62.00	79.85	
62.92	16.38	33.40	39.75	52.15	67.70	86.80
49.23	12.82	29.35	34.75	45.65	59.35	76.45
42.13	10.97	26.30	31.50	41.05	53.75	69.55
37.12	9.66	23.85	28.75	37.10	48.90	63.40
32.17	8.38	23.30 ^S	26.70 ^S	35.85	45.70 ^S	58.60 ^S
28.25	7.35	23.30	26.70	35.85	45.70	58.60
23.65	6.15	23.30	26.70	35.85	45.70	58.60
21.44	5.58	23.25	26.70	35.80	45.70	58.55
19.51	5.08	23.25	26.70	35.80	45.70	58.55
17.97	4.68	23.25	26.70	35.80	45.70	58.55
16.78	4.37	23.25	26.70	35.80	45.70	58.55
16.78	4.37*	22.50	26.70	35.80	45.70	58.55
16.44	4.28	23.25	26.70	35.80	45.70	58.55
14.94	3.89	14.70	19.0	23.30	30.30	42.30
13.75	3.58	14.70	19.0	23.30	30.30	42.30
12.68	3.30	14.70	19.0	23.30	30.30	42.30
9.68	2.52	14.70	19.0	23.30	30.30	42.30
8.29	2.16	14.70	19.0	23.30	30.30	42.30

* Vapour Pressure - Heating Direction

S Solid Appears

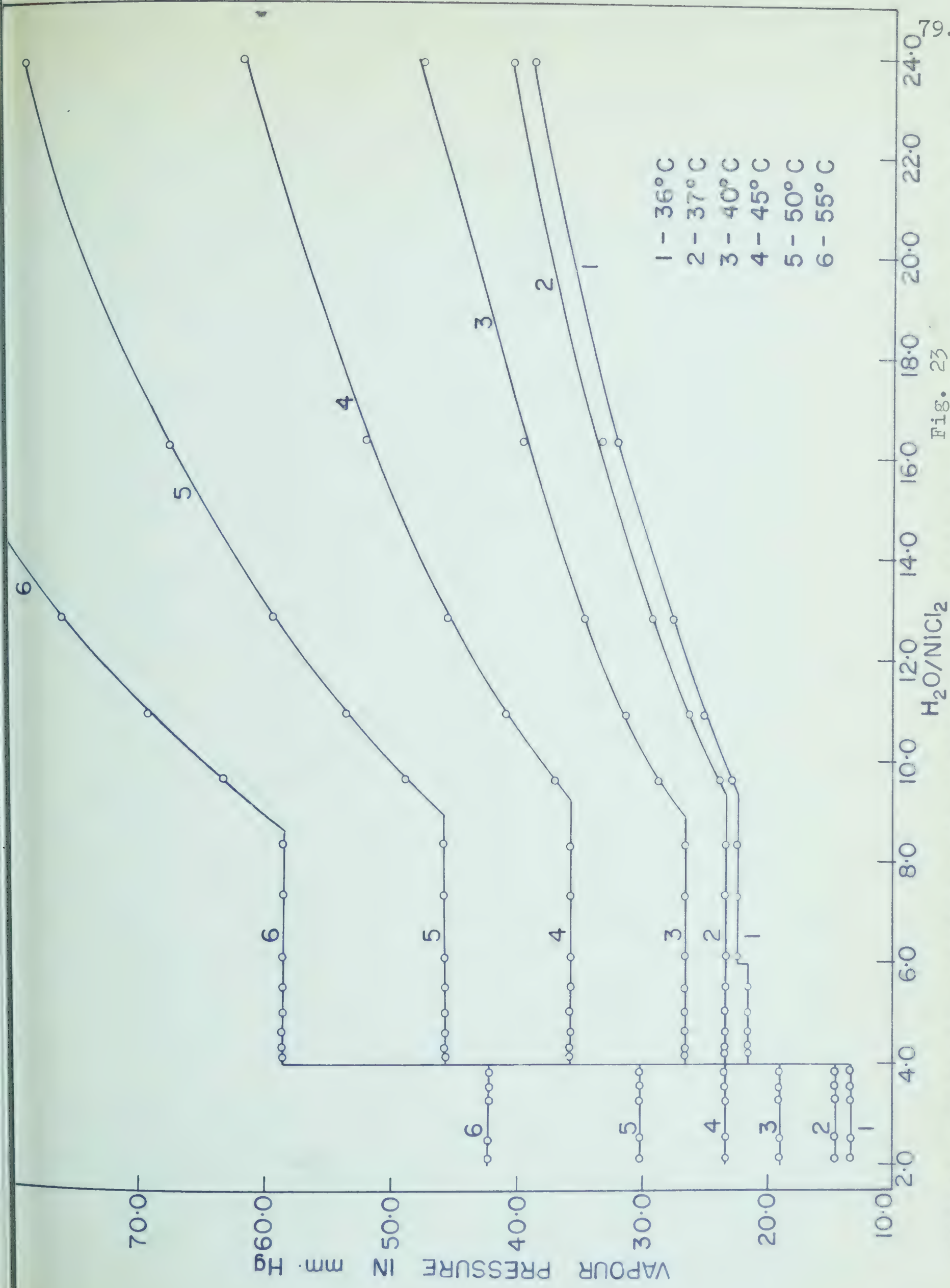


Fig. 23

VAPOUR PRESSURE--COMPOSITION DIAGRAMS FOR 36°C, 37°C, 40°C, 45°C, 50°C, & 55°C.

TABLE 4

Vapour Pressure - Composition Data for the $\text{NiCl}_2\text{-H}_2\text{O}$ System
at 60, 65, 70°C

Mmoles $\text{NiCl}_2 = 3.84$

Mmoles H_2O	Mmole Ratio $\text{H}_2\text{O}/\text{NiCl}_2$	Vapour Pressure in mm Hg. **		
		60°C	65°C	70°C
32.17	8.38	73.85 ^S	93.20	
28.25	7.35	73.85	92.00 ^S	
23.65	6.15	73.85	92.00	114.3
21.44	5.58	73.80	92.00	114.3
19.51	5.08	73.80	92.00	114.3
17.97	4.68	73.80	92.00	114.3
16.78	4.37	73.80	92.00	114.3
16.78	4.37 [*]	73.80	92.00	114.3
16.44	4.28	73.80	92.00	114.3
14.94	3.89	58.50	79.30	107.0
13.75	3.58	58.50	79.30	107.0
12.68	3.30	58.50	79.30	107.0
9.68	2.52	58.50	79.30	107.0
8.29	2.16	58.50	79.30	107.0

* Vapour Pressure - Cooling Direction

** Corrected for thermal expansion of mercury

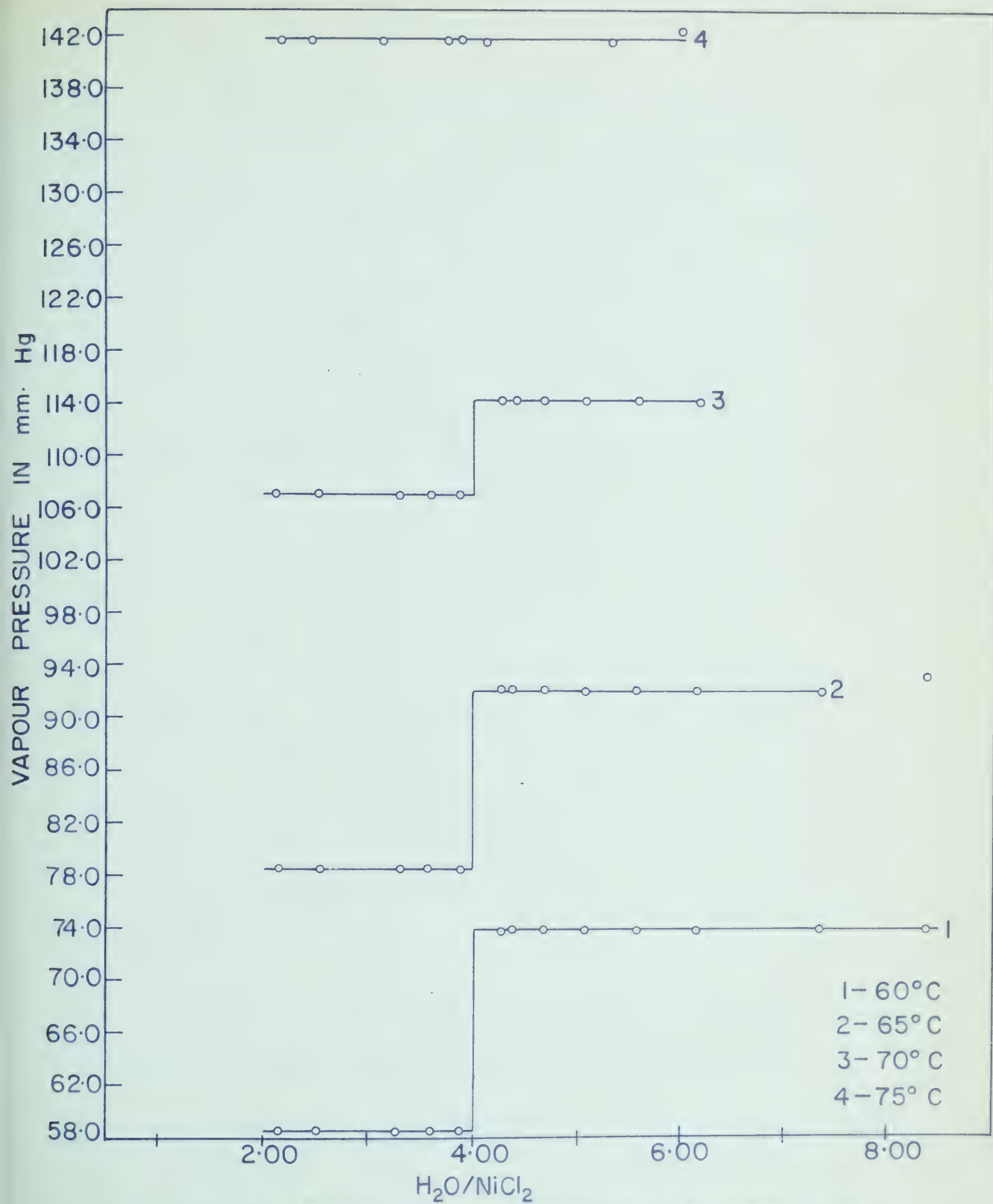
S Solid Appears

TABLE 5

Vapour Pressure - Composition Data for the $\text{NiCl}_2\text{-H}_2\text{O}$ System
at 75°C .

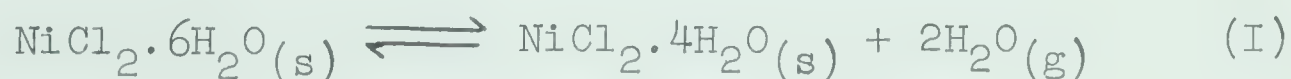
Mmoles $\text{NiCl}_2 = 3.84$

Mmoles H_2O	Mmole Ratio $\text{H}_2\text{O}/\text{NiCl}_2$	Vapour Pressure in mm Hg
23.04	6.00	142.55
20.62	5.37	141.50
15.86	4.13	141.50
14.86	3.87	141.50
14.32	3.73	141.50
13.06	3.14	141.50
9.42	2.45	141.50
8.30	2.16	141.50



VAPOUR PRESSURE—COMPOSITION DIAGRAM FOR
60°C, 65°C, 70°C, & 75°C.

The data in Table 6, plotted in Figure 25, produces a family of straight lines of approximately equal slopes displaced to lower pressures as the concentration of the solution increases. Presumably this indicates that the essential process occurring is independent of both the concentration of the solution and the temperature at which it is carried out. This is not surprising since all of these measurements were carried out in homogeneous solutions. However, as the composition of the system is changed so that a solid phase makes its appearance, the data of Table 7 and Figs. 26 and 27 are obtained. In each of Fig. 26 and 27 there is a discontinuity in the $\log p$ vs $1/T$ plots at a temperature of 36.25° . Below this temperature the systems represented in both figures consist of saturated solution in equilibrium with $\text{NiCl}_2 \cdot 6\text{H}_2\text{O}$. The portion of the curve above this temperature in Fig. 26 corresponds to unsaturated solution whereas that in Fig. 27 corresponds to a saturated solution in equilibrium with $\text{NiCl}_2 \cdot 4\text{H}_2\text{O}$. The data in Table 8 and Fig. 28 reveal the same discontinuity at 36.25° C. Below this temperature the process concerned is the equilibrium (I)



Above 36.25°C equilibrium (II) is involved.



TABLE 6

Logarithm of Vapour Pressure - $1/T$ for $\text{NiCl}_2\text{-H}_2\text{O}$ System
at Different Compositions

$1/T \times 10^3$	Logarithm of Vapour Pressure at Different $\text{H}_2\text{O/NiCl}_2$ Ratios			
	23.83	16.38	12.82	10.97
3.331	1.3784	1.2753	1.2109	1.1703
3.298	1.4464	1.3551	1.2923	1.2467
3.266	1.5204	1.4273	1.3655	1.3232
3.245	1.5641	1.4786	1.4158	1.3729
3.234	1.5911	1.5058	1.4417	1.3997
3.224	1.6090	1.5237	1.4676	1.4200
3.193	1.6785	1.5993	1.5409	1.4983
3.143	1.7924	1.7172	1.6595	1.6133
3.094	1.9023	1.8306	1.7735	1.7304
3.047	--	1.9385	1.8834	1.8423

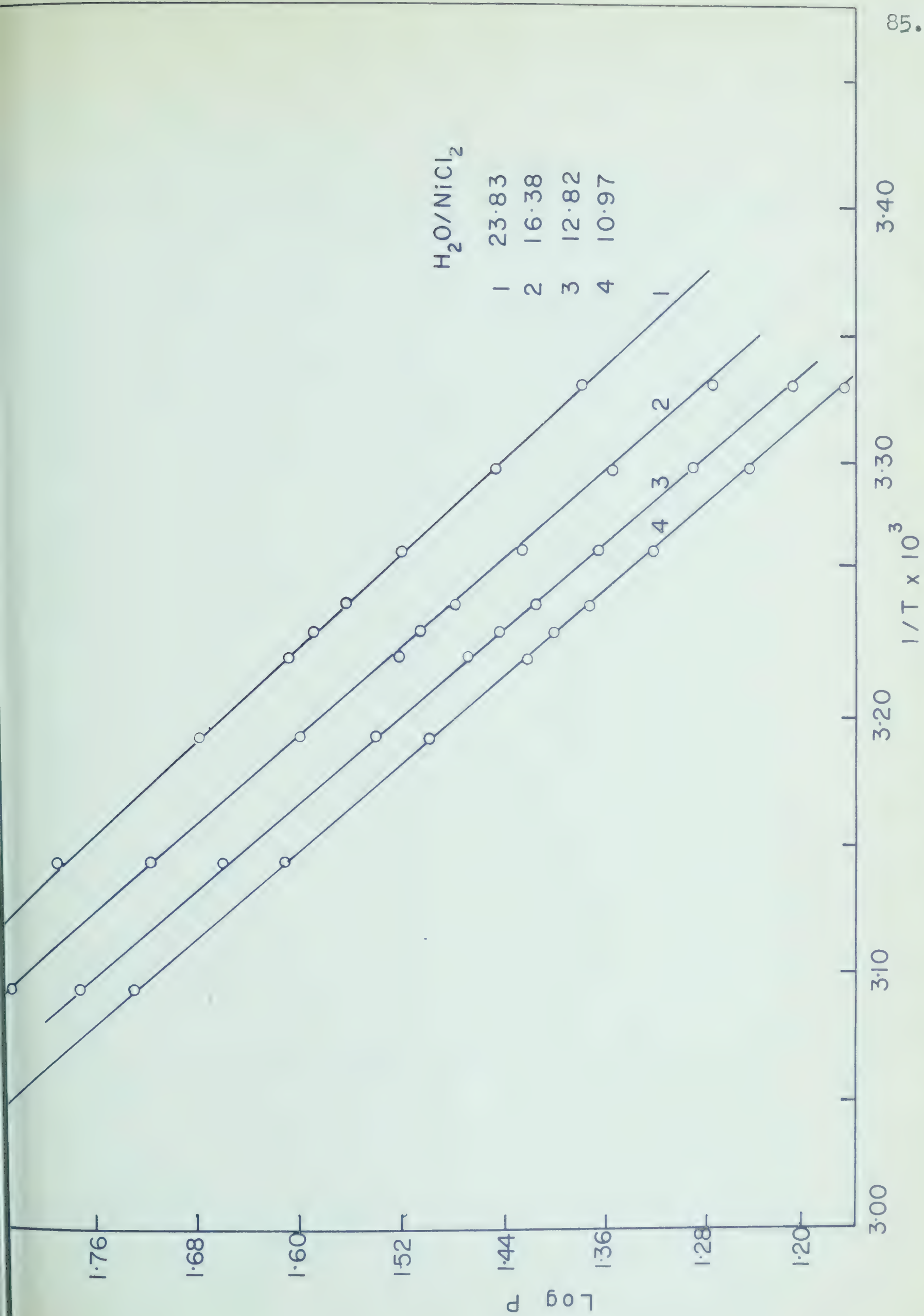


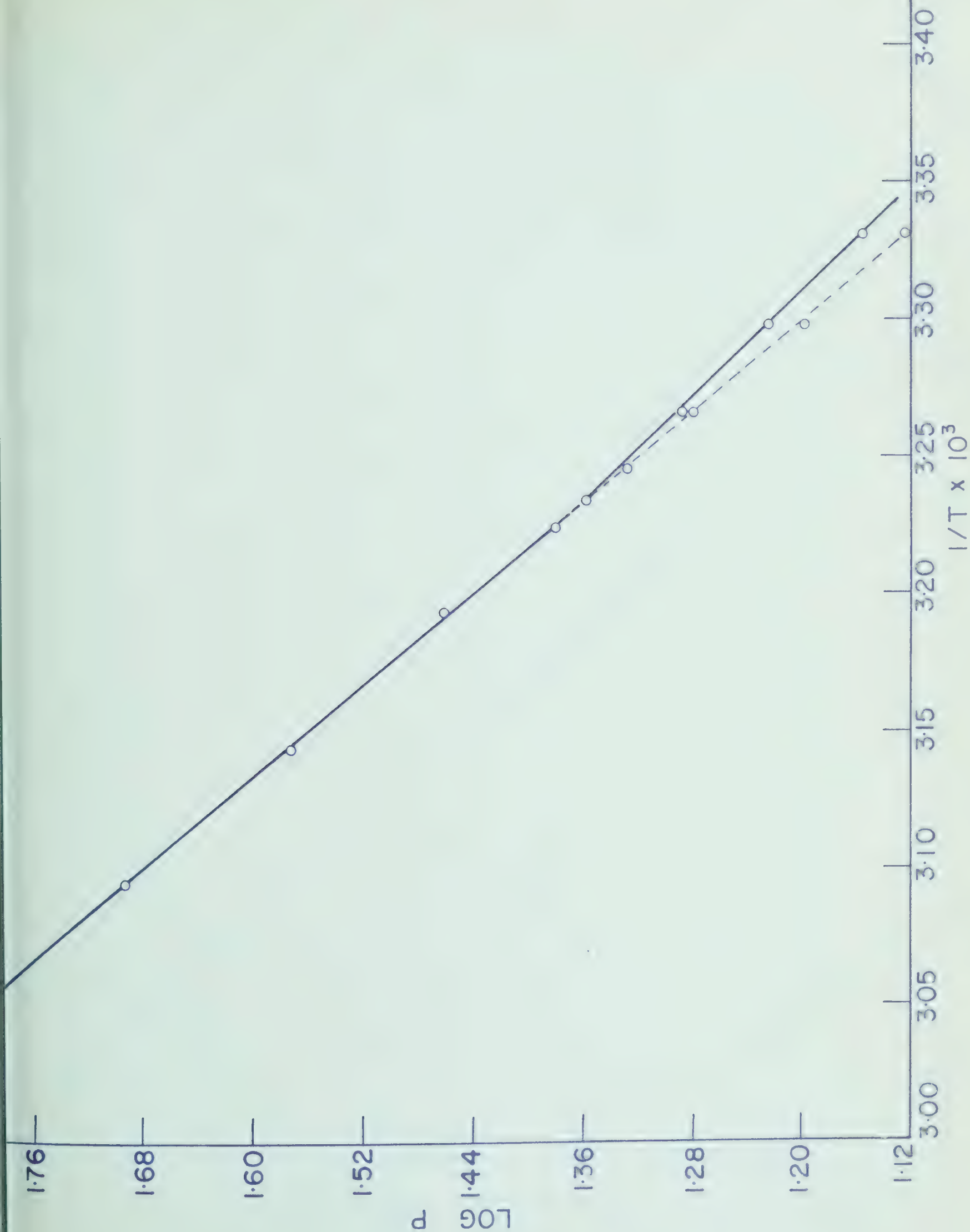
Fig. 25 $\log P$ as a function of $1/T$ for different $H_2O/NiCl_2$ ratio

TABLE 7

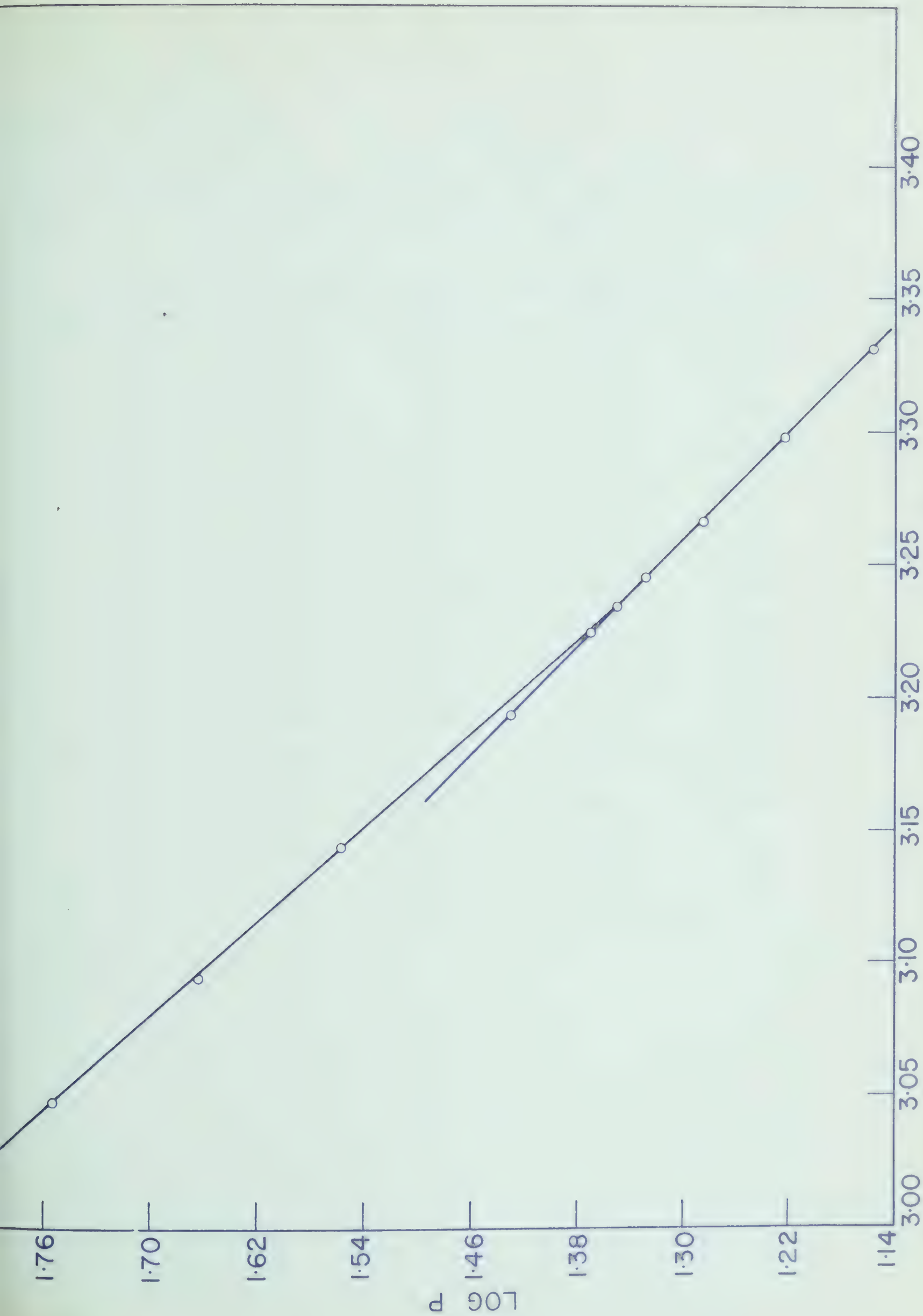
Logarithm of Vapour Pressure - $1/T$ Data for $\text{NiCl}_2\text{-H}_2\text{O}$ System
at Different Compositions

$1/T \times 10^3$	Logarithm of Vapour Pressure at Different $\text{H}_2\text{O}/\text{NiCl}_2$ Ratios			
	9.66	8.38	7.35	6.15
3.331	1.1553 1.1239 ^a	1.1553	1.1553	1.1553
3.298	1.2214 1.1959 ^a	1.2214	1.2214	1.2214
3.266	1.2833 1.2788 ^a	1.2833	1.2833	1.2833
3.245	1.3253	1.3253	1.3253	1.3253
3.234	1.3502	1.3502	1.3502	1.3502
3.224	1.3775	1.3674	1.3674	1.3674
3.193	1.4587	1.4265	1.4265	1.4265
3.143	1.5694	1.5545	1.5545	1.5545
3.094	1.6893	1.6599	1.6599	1.6599
3.047	1.8021	1.7679	1.7679	1.7679
3.001	--	1.8684	1.8684	1.8684
2.957	--	1.9638	1.9638	1.9638

(a) Vapour pressure cooling direction



Log P as a function of $1/T$ for $\text{H}_2\text{O}:\text{NiCl}_2 = 9.66:1$
Fig. 26



$1/T \times 10^3$

Fig. 27

$\log P$ as a function of $1/T$ for $H_2O : NiCl_2 = 8.38, 7.35, 8.6.15$

TABLE 8

Logarithm of Vapour Pressure - I/T Data for $\text{NiCl}_2\text{-H}_2\text{O}$ System
at Different Compositions

I/T x 10^3	Logarithm of Vapour Pressure at Different $\text{H}_2\text{O/NiCl}_2$ Ratios				
	5.58	5.08	4.68	4.37	4.28
3.331	1.1303	1.1303	1.1303	1.1303	1.1303
3.298	1.2095	1.2095	1.2095	1.2095	1.2095
3.266	1.2742	1.2742	1.2742	1.2742	1.2742
3.245	1.3171	1.3171	1.3171	1.3171	1.3171
3.234	1.3365	1.3365	1.3365	1.3365	1.3365
3.224	1.3654	1.3654	1.3654	1.3654	1.3654
3.193	1.4265	1.4265	1.4265	1.4265	1.4265
3.143	1.5539	1.5539	1.5539	1.5539	1.5539
3.094	1.6599	1.6599	1.6599	1.6599	1.6599
3.047	1.7676	1.7676	1.7676	1.7676	1.7676
3.001	1.8681	1.8681	1.8681	1.8681	1.8681
2.957	1.9638	1.9638	1.9638	1.9638	1.9638
2.914	2.0581	2.0581	2.0581	2.0581	2.0581

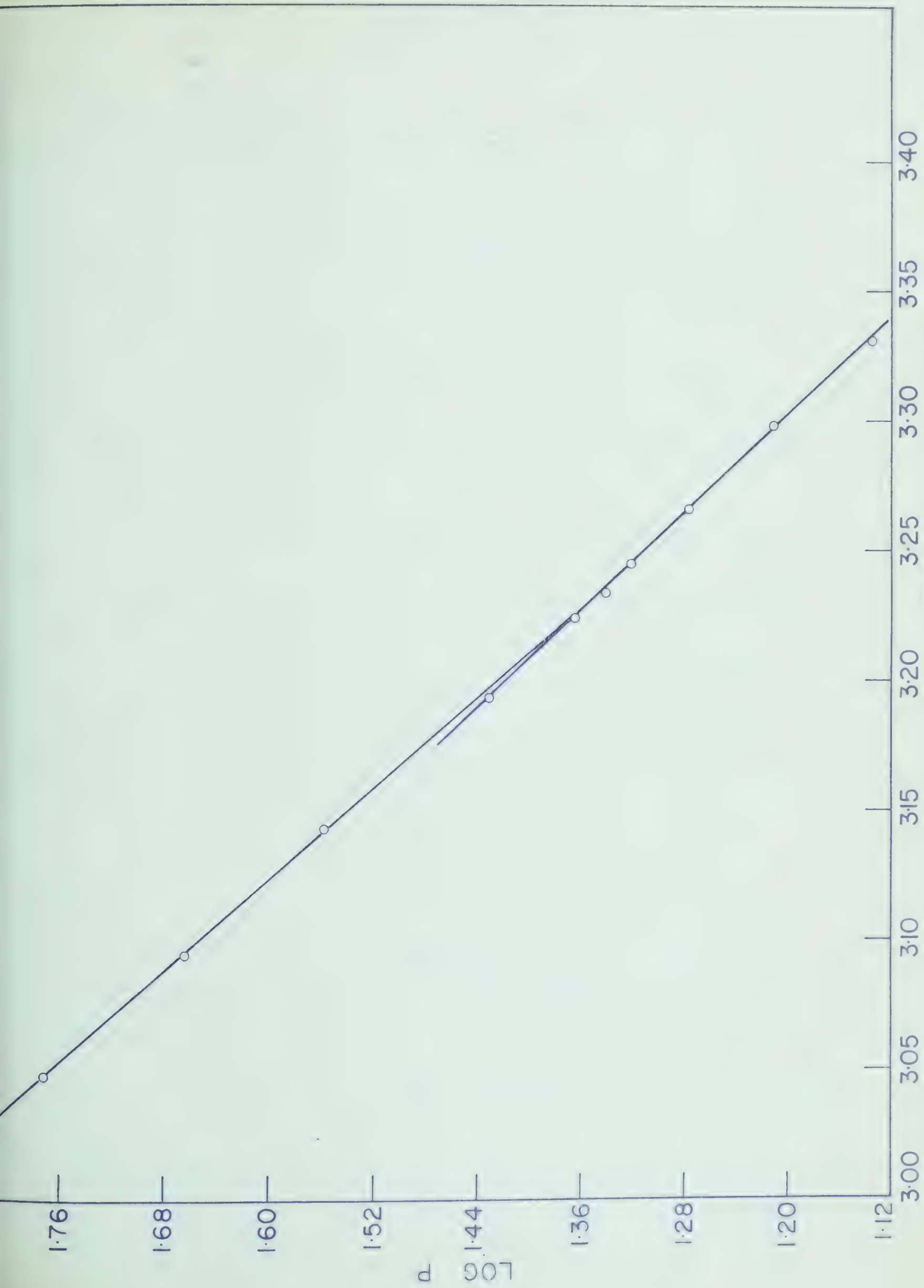


Fig. 28

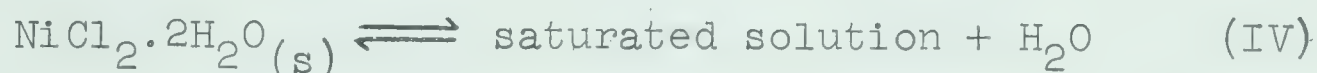
Log P as a function of $1/T$ for $H_2O:NiCl_2 = 5.58, 5.08, 4.68, 4.37$ & 4.28

Hence, in each of these cases the stable solid phase is seen to be transformed from $\text{NiCl}_2 \cdot 6\text{H}_2\text{O}$ to $\text{NiCl}_2 \cdot 4\text{H}_2\text{O}$ at 36.25°C .

In a similar way the data in Tables 9 and 10 and Fig. 29 shown the temperature induced transition between $\text{NiCl}_2 \cdot 4\text{H}_2\text{O}$ and $\text{NiCl}_2 \cdot 2\text{H}_2\text{O}$ which occurs at 75°C . At temperatures below 75°C the equilibrium (III) is observed



whereas above this temperature the equilibrium corresponds to that represented by (IV)



At least this is true when the system has a composition which lies between an H_2O to NiCl_2 mole ratio of 2 to 4. Should the mole ratio lie on the high side of this range the equilibrium would be between two saturated solutions with different solid phases. On the low side of this ratio the equilibrium would be between the dihydrate and the anhydrous material.

It is observed in Figs. 26 and 29 that the set of points obtained on the heating cycle does not correspond to the set obtained in the cooling cycle, provided the system passes through a transition point. Apparently the system is able to remain in the metastable high temperature state for indefinite periods of time even though the system is cooled to bring it back through the transition point. However, if the system is subjected to severe thermal shock such as quenching in liquid

TABLE 9

Logarithm of Vapour Pressure - I/T Data for $\text{NiCl}_2\text{-H}_2\text{O}$ System
at Different Compositions

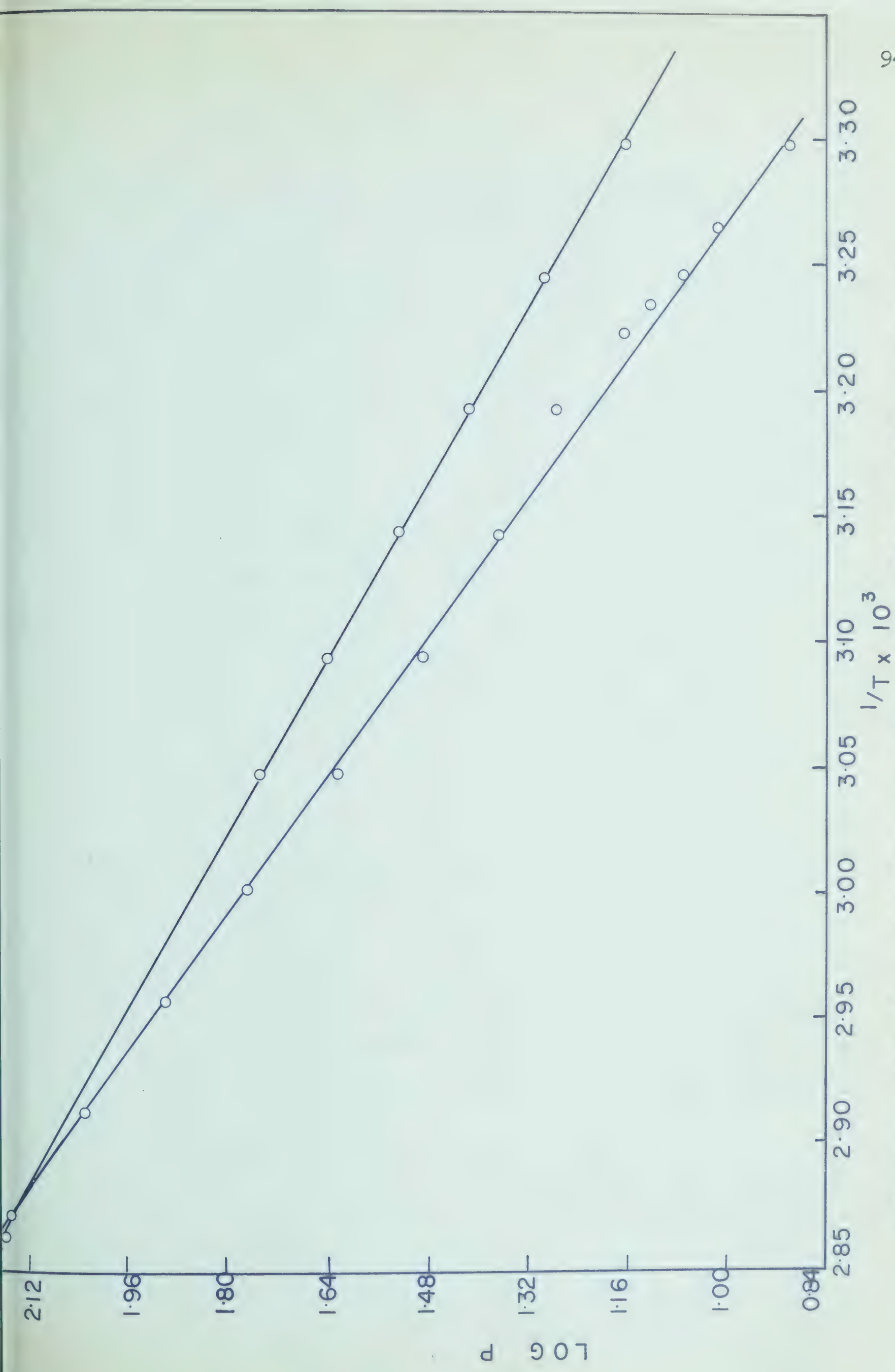
$1/T \times 10^3$	Logarithm of Vapour Pressure at Different $\text{H}_2\text{O}/\text{NiCl}_2$ Ratios				
	3.89	3.58	3.30	2.52	2.16
3.331	0.8451	0.8451	0.8451	0.8451	0.8451
3.298	0.8949	0.8949	0.8949	0.8949	0.8949
3.266	1.0149	1.0149	1.0149	1.0149	1.0149
3.245	1.0755	1.0755	1.0755	1.0755	1.0755
3.234	1.1287	1.1287	1.1287	1.1287	1.1287
3.224	1.1673	1.1673	1.1673	1.1673	1.1673
3.193	1.2788	1.2788	1.2788	1.2788	1.2788
3.143	1.3674	1.3674	1.3674	1.3674	1.3674
3.094	1.4814	1.4814	1.4814	1.4814	1.4814
3.047	1.6263	1.6263	1.6263	1.6263	1.6263
3.001	1.7672	1.7672	1.7672	1.7672	1.7672
2.957	1.8993	1.8993	1.8993	1.8993	1.8993
2.914	2.0294	2.0294	2.0294	2.0294	2.0294

TABLE 10

Vapour pressures of $\text{NiCl}_2 - \text{H}_2\text{O}$ systems a)

Temp ($^{\circ}\text{K}$) Heating Direction	$\frac{1}{T} \times 10^3$	Vapour Pressure in mm Hg	Log P
348.16	2.872	141.50	2.1507
349.16	2.864	146.05	2.1644
349.66	2.859	149.30	2.1741
350.16	2.855	152.40	2.1828
<u>Cooling Direction</u>			
300.16	3.331	12.05	1.0810
303.16	3.298	14.65	1.1655
306.16	3.266	17.75	1.2492
308.16	3.245	18.90	1.2967
310.16	3.224	22.25	1.3464
313.16	3.193	26.10	1.4166
318.16	3.143	33.50	1.5350
323.16	3.094	43.75	1.6410

a) Composition $\text{H}_2\text{O}/\text{NiCl}_2$ 3.89



LOG P vs. $1/T$ for $\text{H}_2\text{O}\cdot\text{NiCl}_2 = 3.89, 3.58, 3.30, 2.52, \text{ and } 2.16.$

Fig. 29

nitrogen, it returns to its normal room temperature condition upon being allowed to warm up. This system can again be taken through the heating cycle to reproduce the original data. Upon cooling through the transition point the system repeats its former behaviour by cooling along the non-equilibrium curve. It may be returned to the low temperature equilibrium condition by again quenching in liquid nitrogen and warming to room temperature. This cycle has been repeated for as many as a dozen cycles for the data of Fig. 26.

In general, each point reported in this section was obtained as the average of at least two values; one obtained by reaching equilibrium from a slightly lower temperature, and the other obtained by reaching equilibrium from a slightly higher temperature. The pressure reported never varies by more than 0.05 mm from either of the two values.

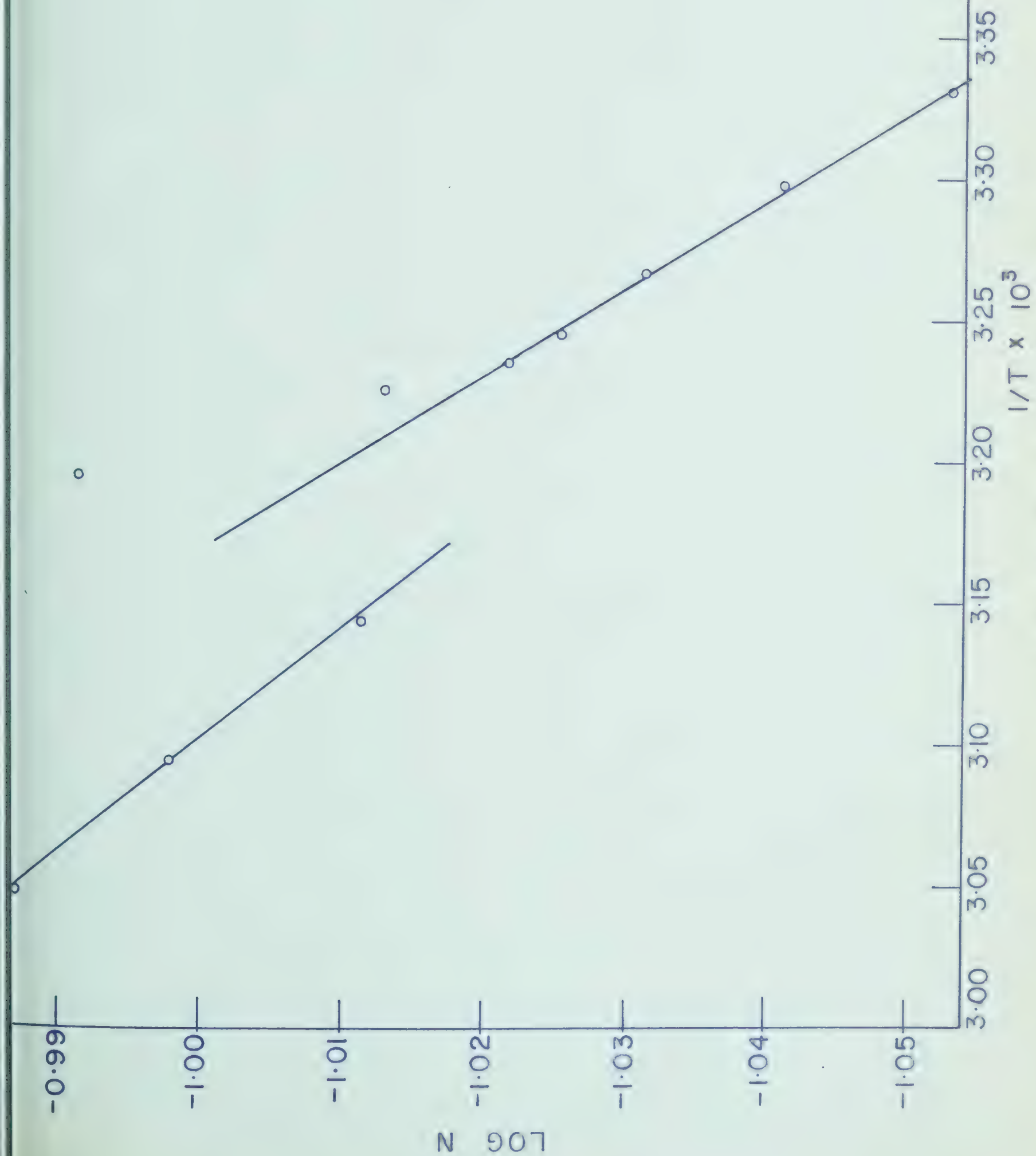
In Table 11 are the solubilities of nickel chloride in water at various temperatures determined from the intersection of the vapour pressure curves for saturated and unsaturated solutions shown in Figs. 22 and 23. It should be noted that below 36.25° the solid phase in equilibrium with the solution is $\text{NiCl}_2 \cdot 6\text{H}_2\text{O}$ whereas above this temperature the solid phase is $\text{NiCl}_2 \cdot 4\text{H}_2\text{O}$. The data given in Table 11 have been plotted in Fig. 30.

TABLE 11
Solubility Limits, of NiCl_2 in Water

Temp. (°C)	$I/T \times 10^3$	$\text{H}_2\text{O}/\text{NiCl}_2$	Mole Fraction NiCl_2	Log N
27.0	3.331	10.30 ^a	0.08849	-1.0531
30.0	3.298	10.00 ^a	0.09090	-1.0414
33.0	3.266	9.75 ^a	0.09304	-1.0313
35.0	3.245	9.60 ^a	0.09434	-1.0253
36.0	3.234	9.50 ^a	0.09587	-1.0213
37.0	3.224	9.30 ^b	0.09709	-1.0128
40.0	3.193	8.80 ^b	0.1020	-0.9914
45.0	3.143	9.27 ^b	0.09738	-1.0115
50.0	3.094	8.95 ^b	0.1005	-0.9979
55.0	3.047	8.70 ^b	0.1031	-0.9868

a) Solid phase in equilibrium with the solution is
 $\text{NiCl}_2 \cdot 6\text{H}_2\text{O}$

b) Solid phase in equilibrium with the solution is
 $\text{NiCl}_2 \cdot 4\text{H}_2\text{O}$.



Log N as a function of $1/T$
Fig. 30

The vapour pressure - composition data for the reaction of aqueous nickel chloride solution with ethylenediamine for different temperatures from 23°C to 50°C are given in Tables 12 and 13, and are plotted in Figs. 31, 32 and 33. The pressures for the corresponding aqueous nickel chloride solution are given in Table 14 and plotted in Fig. 34.

The maximum vapour pressure observed in these measurements is seen to be 82.5 mm of Hg at a temperature of 50°C . The total volume of the measuring bulb was found to be 40 ml (exclusive of the volume occupied by the solution and stirrer). Consequently it is possible to estimate a maximum correction which must be applied to the concentration of the solution to account for the water which is in the vapour phase. Assuming the ideal gas law to be applicable to this system, the correction is 0.165 mmole. This maximum correction is of the order of 0.25% of the total amount of water present in the system. As a consequence corrections of this type have been ignored in all measurements.

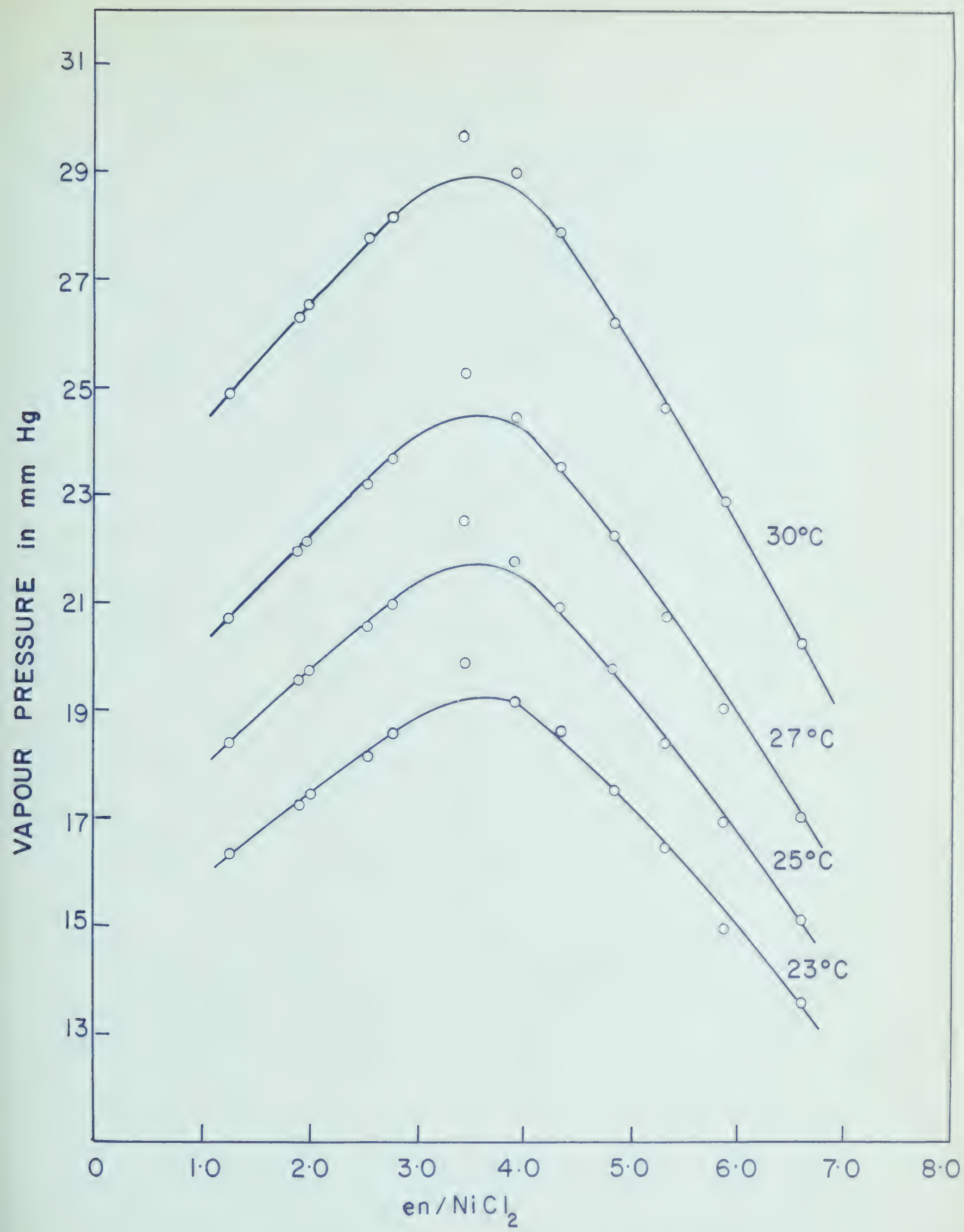
TABLE 12

Vapour Pressure - Composition Data for Aqueous NiCl_2^{a} - en System

M moles en	M mole ratio en/ NiCl_2	Vapour Pressure in mm Hg. at Different Temperatures ^a			
		23°C	25°C	27°C	30°C
6.02	1.26	16.25	18.40	20.70	24.85
9.08	1.91	17.25	19.55	21.95	26.25
9.52	2.00	17.40	19.70	22.10	26.50
12.19	2.56	18.10	20.55	23.20	27.75
13.20	2.77 ^b	18.55	20.90	23.60	28.15
16.36	3.44	19.85	22.55	25.25	29.60
18.65	3.92	19.15	21.75	24.40	28.95
20.69	4.35	18.60	20.90	23.50	27.85
23.14	4.86	17.50	19.80	22.20	26.15
25.38	5.33	16.35	18.40	20.70	24.60
27.97	5.87	14.85	16.90	19.05	22.85
31.05	6.52	13.55	15.10	17.00	20.25

a) Solution contains 4.76 mmole of NiCl_2 and 64.1 mmole of H_2O

b) Solid $[\text{Ni en}_3]\text{Cl}_2$ separates from the solution.



VAPOUR PRESSURE - COMPOSITION DIAGRAM FOR AQUEOUS
NICKEL CHLORIDE - en SYSTEM AT DIFFERENT TEMPERATURES

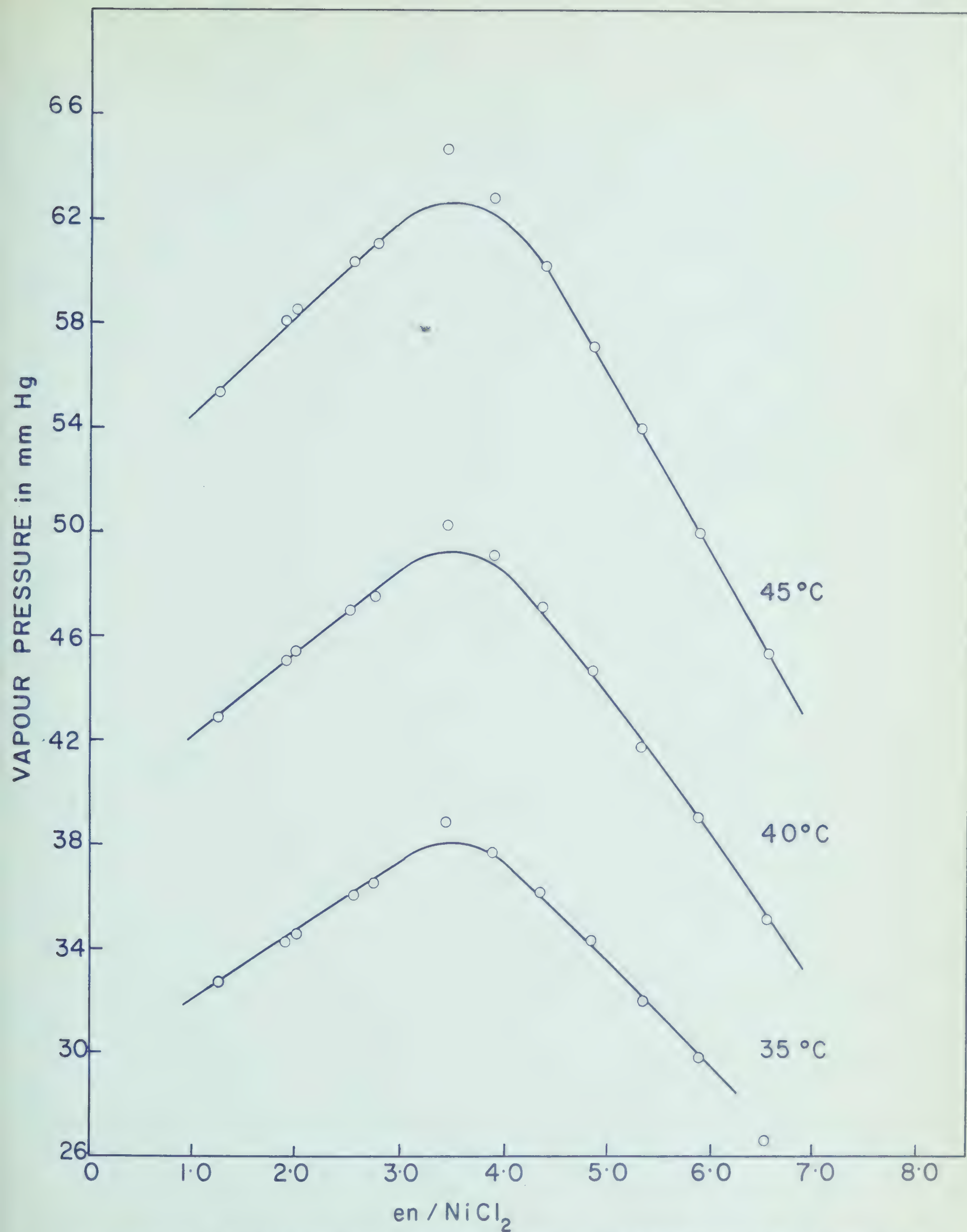
TABLE 13

Vapour Pressure - Composition Data for Aqueous NiCl_2 - en^a System

M moles en	M mole ratio en/ NiCl_2	Vapour Pressure in mm Hg. at Different Temperatures			
		35°C	40°C	45°C	50°C
6.02	1.26	32.70	42.35	55.35	72.30
9.08	1.91	34.25	45.05	58.00	75.10
9.52	2.00	34.55	45.35	58.50	75.70
12.19	2.56	36.00	46.70	60.30	77.50
13.20	2.77 ^b	36.55	47.15	60.70	78.35
16.36	3.44	38.80	50.35	64.75	82.50
16.65	3.92	37.75	49.15	62.85	80.10
20.69	4.35	36.25	47.10	60.25	76.80
23.14	4.86	34.35	44.75	57.05	73.10
25.38	5.33	32.00	41.70	53.90	69.20
27.97	5.87	29.80	39.10	50.00	64.60
31.05	6.52	26.70	35.15	45.35	58.65

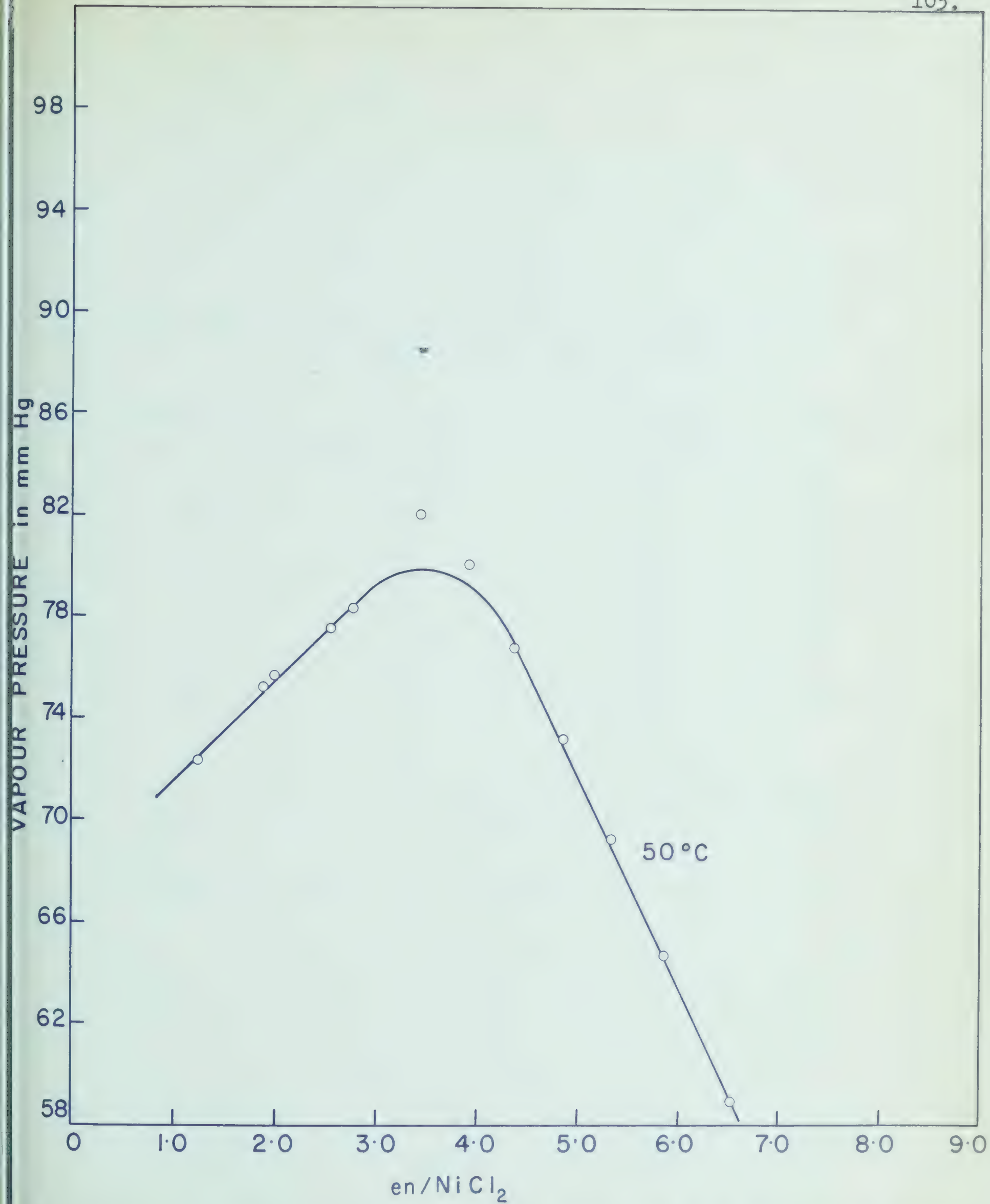
a) Solution contains 4.76 mmole NiCl_2 and 64.1 mmole H_2O

b) Solid $[\text{Ni en}_3]\text{Cl}_2$ separates from the solution.



VAPOUR PRESSURE - COMPOSITION DIAGRAM FOR AQUEOUS
NICKEL CHLORIDE - en SYSTEM AT DIFFERENT TEMPERATURES

Fig. 32



VAPOUR PRESSURE - COMPOSITION DIAGRAM FOR AQUEOUS NICKEL
CHLORIDE-en SYSTEM AT 50 °C

Fig. 33

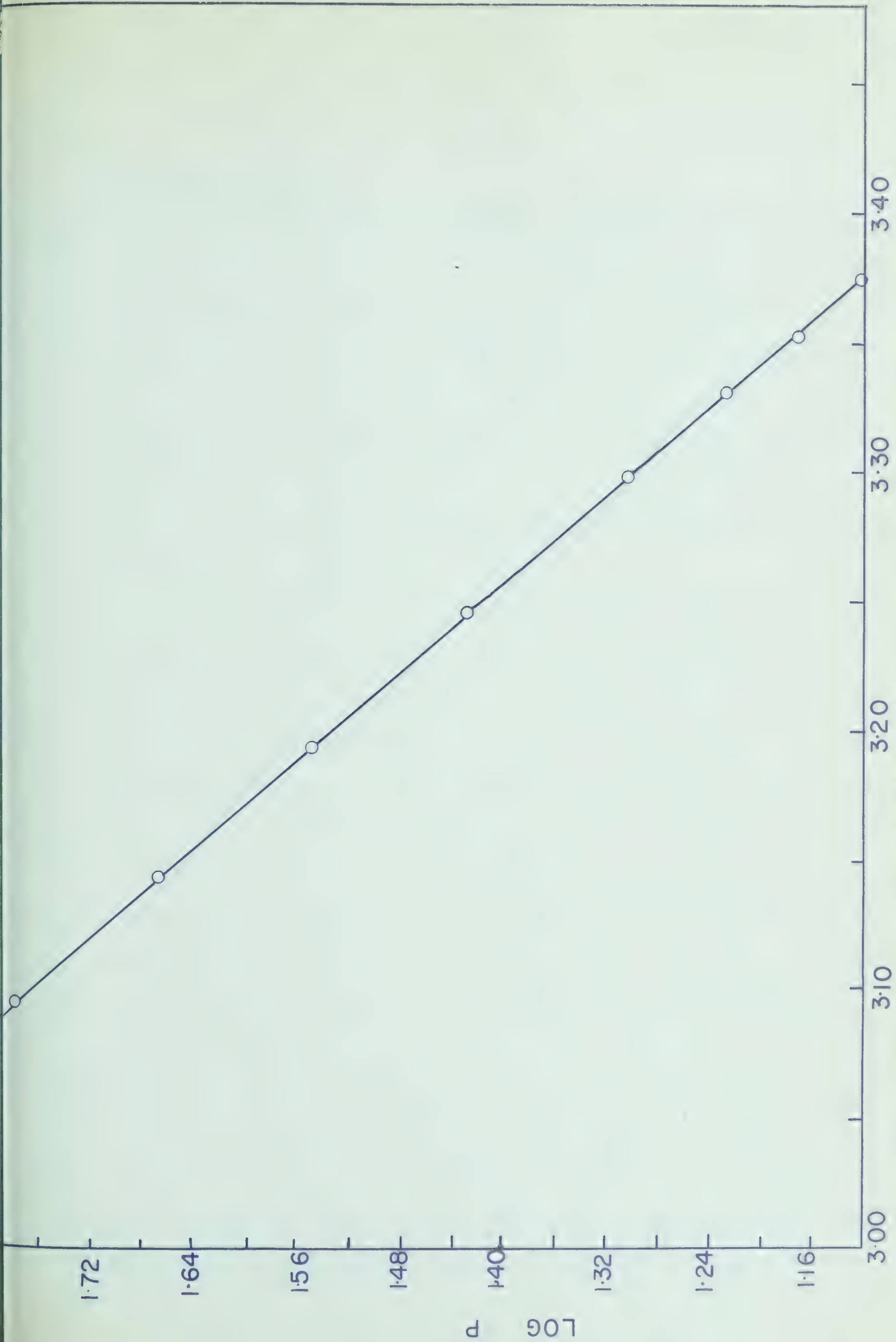
TABLE 14

Vapour Pressure of Aqueous Nickel Chloride Solution^a at
Different Temperatures

Temperature	$1/T \times 10^3$	Pressure* (mm Hg)	Log P
23°C	3.376	13.25	1.1222
25°C	3.353	14.85	1.1717
27°C	3.331	16.95	1.2292
30°C	3.298	20.20	1.3054
35°C	3.245	26.90	1.4298
40°C	3.193	35.40	1.5490
45°C	3.143	46.40	1.6665
50°C	3.094	60.15	1.7793

a) Solution contains 4.76 mmole of NiCl_2 and 64.1 mmole of H_2O

* Corrected for thermal expansion of mercury.



Log P as a function of $1/T$

Fig. 34

Kinetic Studies

Dehydration of various quantities of $\text{NiCl}_2 \cdot 6\text{H}_2\text{O}$ was carried out in phosphorous pentoxide desiccant in a closed static system at atmospheric pressure. A typical set of results, for a sample weight of 2.8542 gms., is given in Table 15a. The decomposition curve is shown in Fig. 35. The differential rate curves for water lost per one hour and per two hours are shown in Fig. 36. The differential rate for a sample weight of 1.6892 gms., results of which are given in Table 15b, are also shown in Fig. 36.

Dehydration on a quartz spiral balance containing magnesium perchlorate in the balance case was carried out by evacuating the system and isolating the part containing the quartz spiral balance from the rest of the vacuum line by a mercury float valve. The extent of dehydration was obtained by following the upward movement of the index fiber of the quartz spiral. No rigorous precaution was made for maintaining a constant temperature. The results are given in Table 16. The decomposition curve is shown in Fig. 37. The differential rate curves for water lost for different time intervals are shown in Fig. 38.

The results of the dehydration on a quartz spiral balance in vacuum at 25°C , 35°C and 45°C are given in Tables 17, 18 and 19. The decomposition curves are shown in Figs. 39, 40 and 41. The differential rate for water lost for different time intervals are shown in Figs. 42, 43 and 44.

TABLE 15 a

*Dehydration of $\text{NiCl}_2 \cdot 6\text{H}_2\text{O}$ at Room Temperature $\approx 25^\circ\text{C}$

Weight of $\text{NiCl}_2 = 1.5568$ gms.

Time in Hours	Wt. of the Sample (gm)	Wt. of Total H_2O Lost (gm)	Ratio $\text{H}_2\text{O}/\text{NiCl}_2$	Rate $\text{mgH}_2\text{O}/\text{Hr}$
0	2.8542	0	6.00	0
1.0	2.8382	0.0160	5.93	16.0
2.0	2.8242	0.0300	5.86	14.0
3.0	2.8109	0.0433	5.80	13.3
4.0	2.7965	0.0577	5.73	14.4
5.0	2.7807	0.0735	5.66	15.8
6.0	2.7642	0.0900	5.58	16.5
7.0	2.7476	0.1066	5.51	16.6
8.0	2.7297	0.1245	5.42	17.9
9.0	2.7131	0.1411	5.35	16.6
10.0	2.6960	0.1582	5.26	17.1
11.0	2.6794	0.1748	5.19	16.6
12.0	2.6626	0.1916	5.11	16.8
13.0	2.6468	0.2074	5.03	15.8
14.0	2.6303	0.2239	4.96	16.5
15.0	2.6166	0.2376	4.89	13.7
16.0	2.6015	0.2527	4.83	15.1

Time in Hours	Wt. of the Sample (gm)	Wt. of Total H ₂ O Lost (gm)	Ratio H ₂ O/NiCl ₂	Rate mgH ₂ O/Hr
17.0	2.5867	0.2675	4.76	14.8
18.0	2.5717	0.2825	4.69	15.0
19.0	2.5573	0.2969	4.62	14.4
20.0	2.5419	0.3123	4.55	15.4
21.0	2.5260	0.3282	4.48	15.9
22.0	2.5107	0.3435	4.41	15.3
23.0	2.4967	0.3575	4.34	14.0
24.0	2.4826	0.3716	4.28	14.1
25.0	2.4688	0.3854	4.21	13.8
26.0	2.4551	0.3991	4.15	13.7
27.0	2.4417	0.4125	4.09	13.4
28.0	2.4284	0.4258	4.03	13.3
29.0	2.4143	0.4399	3.96	14.1
30.0	2.4002	0.4540	3.90	14.1
31.0	2.3852	0.4690	3.83	15.0
32.0	2.3697	0.4845	3.75	15.5
33.0	2.3562	0.4980	3.69	13.5
34.0	2.3422	0.5120	3.63	14.0
35.0	2.3272	0.5270	3.56	15.0
36.0	2.3121	0.5421	3.49	15.1

Time in Hours	Wt. of the Sample (gm)	Wt. of Total H ₂ O Lost (gm)	Ratio H ₂ O/NiCl ₂	Rate mgH ₂ O/Hr.
37.0	2.2961	0.5581	3.41	16.0
38.0	2.2821	0.5721	3.35	14.0
39.0	2.2676	0.5866	3.28	14.5
40.0	2.2546	0.5996	3.22	13.0
41.0	2.2443	0.6099	3.17	10.3
42.0	2.2341	0.6201	3.13	10.2
43.0	2.2237	0.6305	3.08	10.4
44.0	2.2129	0.6413	3.03	10.8
45.0	2.2009	0.6533	2.97	12.0
46.0	2.1903	0.6639	2.92	10.6
47.0	2.1780	0.6762	2.87	12.3
48.0	2.1659	0.6891	2.81	12.9
49.0	2.1546	0.7004	2.76	11.3
50.0	2.1444	0.7106	2.71	10.2
51.0	2.1348	0.7202	2.67	9.6
52.0	2.1265	0.7285	2.63	8.3
53.0	2.1195	0.7355	2.59	7.0
54.0	2.1138	0.7412	2.57	5.7
55.0	2.1102	0.7448	2.55	3.6
56.0	2.1067	0.7483	2.54	3.5

Time in Hours	Wt. of the Sample (gm)	Wt. of Total H ₂ O Lost (gm)	Ratio H ₂ O/NiCl ₂	Rate mgH ₂ O/Hr.
57.0	2.1025	0.7525	2.52	4.2
58.0	2.0984	0.7566	2.50	4.1
59.0	2.0945	0.7605	2.48	3.9
60.0	2.0900	0.7650	2.46	4.5
61.0	2.0854	0.7696	2.44	4.6
62.0	2.0808	0.7742	2.42	4.6
63.0	2.0768	0.7782	2.40	4.0
64.0	2.0726	0.7824	2.38	4.2
65.0	2.0691	0.7859	2.36	3.5
66.0	2.0657	0.7893	2.35	3.4
67.0	2.0629	0.7921	2.33	2.8
68.0	2.0606	0.7944	2.32	2.3
69.0	2.0573	0.7967	2.32	2.3
70.0	2.0550	0.7990	2.31	2.3
71.0	2.0532	0.8008	2.30	1.8
72.0	2.0512	0.8028	2.29	2.0

* Dehydration carried out in a glass stopper weighing bottle 4 cm diameter and 2.5 cm high in a 6 in. desiccator containing phosphorous pentoxide as desiccant.

TABLE 15 b

*Dehydration of $\text{NiCl}_2 \cdot 6\text{H}_2\text{O}$ at Room Temperature $\approx 25^\circ\text{C}$ Weight of $\text{NiCl}_2 = 0.9209$ gms.

Time in Hours	Wt. of the Sample (gm)	Wt. of Total H_2O Lost (gm)	Ratio $\text{H}_2\text{O}/\text{NiCl}_2$	Rate $\text{mgH}_2\text{O}/\text{Hr.}$
0	1.6892	0	6.00	0
1.0	1.6710	0.0182	5.86	18.2
2.0	1.6568	0.0324	5.75	14.2
3.0	1.6417	0.0475	5.63	15.1
4.0	1.6263	0.0629	5.51	15.4
5.0	1.6092	0.0800	5.38	17.1
6.0	1.5925	0.0967	5.24	16.7
7.0	1.5778	0.1114	5.13	14.7
8.0	1.5629	0.1263	5.01	14.9
9.0	1.5472	0.1420	4.89	15.7
10.0	1.5317	0.1575	4.77	15.5
11.0	1.5188	0.1704	4.67	12.9
12.0	1.5079	0.1813	4.58	10.9
13.0	1.4970	0.1922	4.50	10.9
14.0	1.4828	0.2064	4.39	14.2
15.0	1.4686	0.2206	4.28	14.2
16.0	1.4560	0.2332	4.18	12.6
17.0	1.4420	0.2472	4.07	14.0
18.0	1.4279	0.2613	3.96	14.1
19.0	1.4147	0.2745	3.85	13.2

Time in Hours	Wt. of the Sample (gm)	Wt. of Total H ₂ O Lost (gm)	Ratio H ₂ O/NiCl ₂	Rate mgH ₂ O/Hr.
20.0	1.4010	0.2882	3.74	13.7
21.0	1.3899	0.2993	3.66	11.1
22.0	1.3775	0.3117	3.56	12.4
23.0	1.3663	0.3229	3.48	11.2
24.0	1.3551	0.3341	3.39	11.2
25.0	1.3454	0.3438	3.31	9.7
26.0	1.3344	0.3548	3.23	11.0
27.0	1.3232	0.3660	3.14	11.2
28.0	1.3118	0.3774	3.05	11.4
29.0	1.3013	0.3879	2.97	10.5
30.0	1.2897	0.3995	2.88	11.6
31.0	1.2809	0.4083	2.81	8.8
32.0	1.2702	0.4190	2.72	10.7
33.0	1.2592	0.4300	2.64	11.0
34.0	1.2488	0.4404	2.56	10.4
35.0	1.2394	0.4498	2.48	9.4
36.0	1.2300	0.4592	2.41	9.4
37.0	1.2216	0.4676	2.35	8.4
38.0	1.2147	0.4745	2.29	6.9
39.0	1.2099	0.4793	2.25	4.8
40.0	1.2049	0.4843	2.21	5.0
41.0	1.2000	0.4892	2.18	4.9

* Dehydration carried out in a glass stopper weighing bottle 4 cm diameter and 2.5 cm high in a 6 in. desiccator containing phosphorous pentoxide as desiccant.

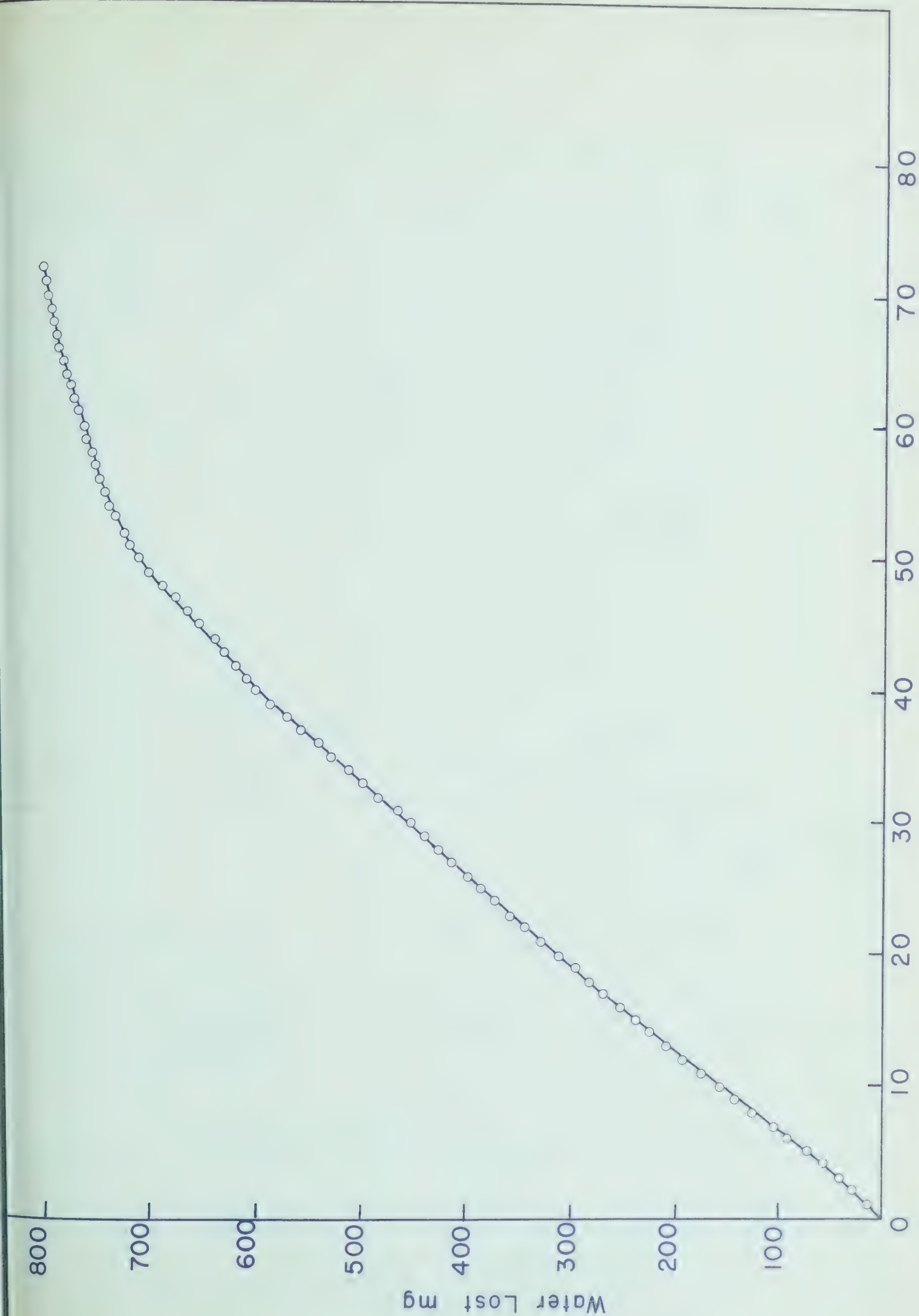
DEHYDRATION OF $\text{NiCl}_2 \cdot 6\text{H}_2\text{O}$ AT ROOM TEMPERATURE — 25°C

Fig. 35

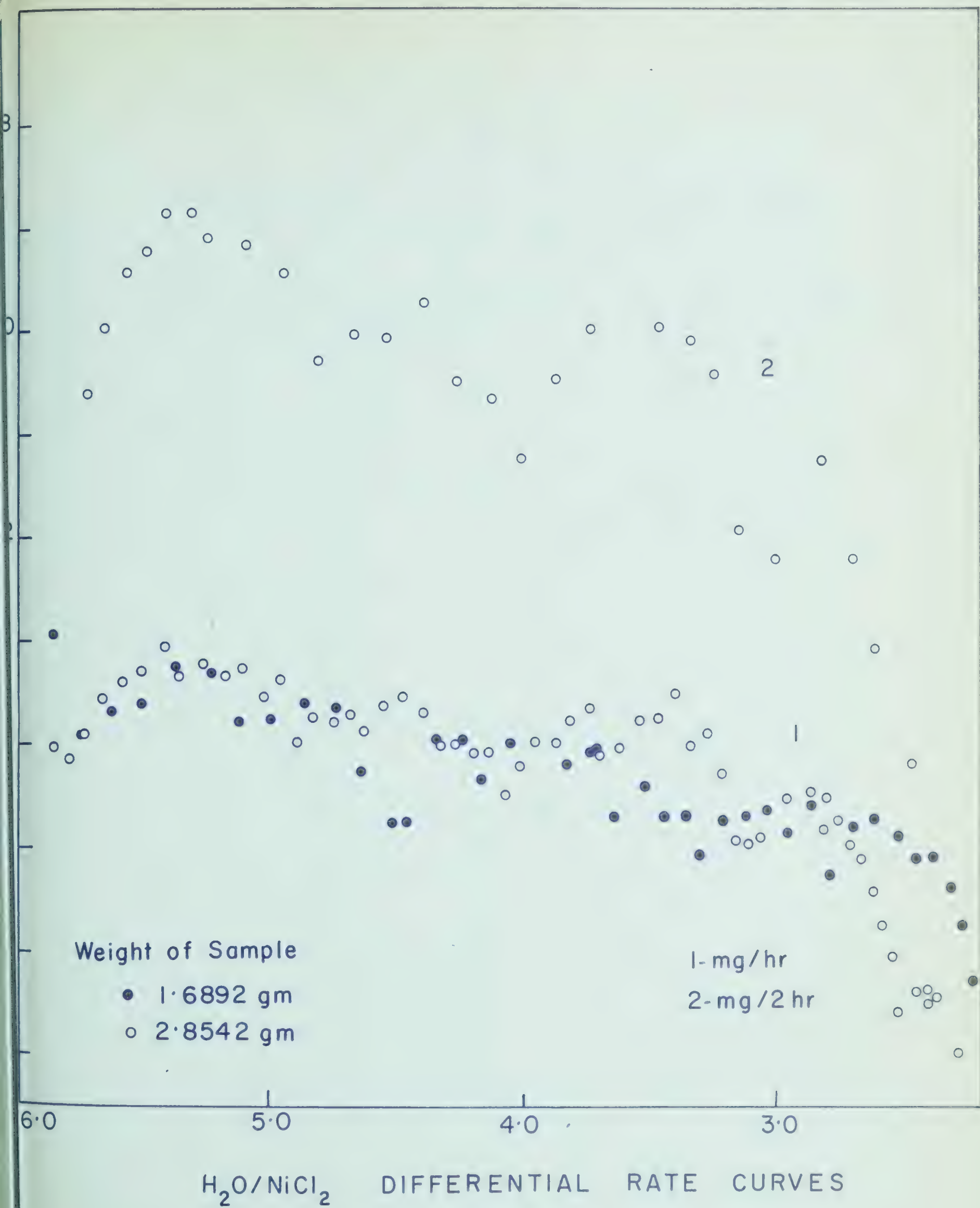


Fig. 36

TABLE 16

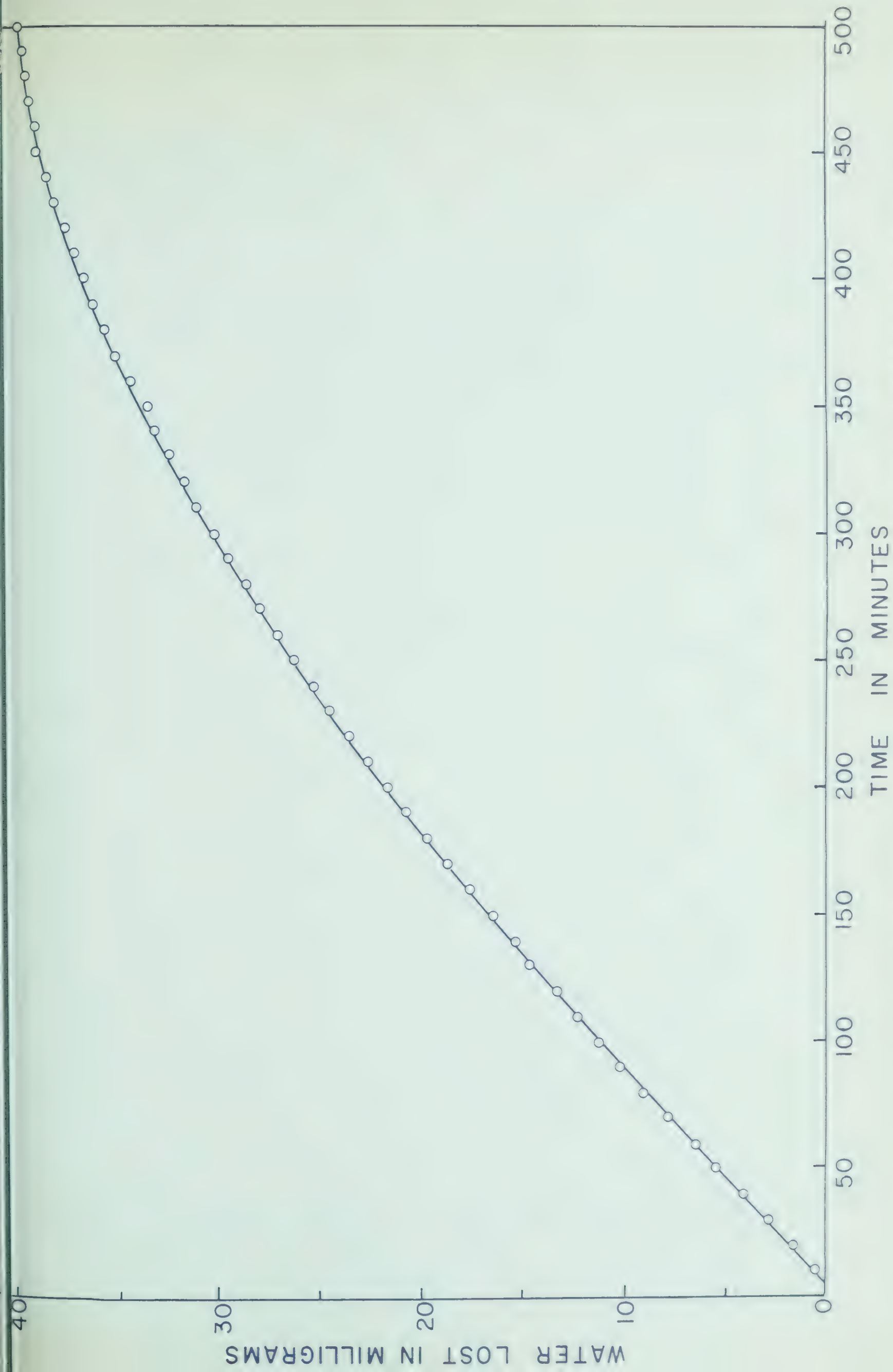
Dehydration of $\text{NiCl}_2 \cdot 6\text{H}_2\text{O}$ at Room Temperature $\approx 25^\circ\text{C}$ Weight of $\text{NiCl}_2 = 72.14$ mg.

Time in Minutes	Wt. of the Sample (mg.)	Wt. of Total H_2O Lost	$\text{H}_2\text{O}/\text{NiCl}_2$ Mole Ratio	Rate $\text{mgH}_2\text{O}/10$ Mins.
0	132.3	0	6.00	0
10	131.9	0.4	5.96	0.4
20	130.8	1.5	5.85	1.1
30	129.6	2.7	5.73	1.2
40	128.3	4.0	5.60	1.3
50	127.1	5.2	5.48	1.2
60	125.9	6.4	5.36	1.2
70	124.6	7.7	5.23	1.3
80	123.4	8.9	5.11	1.2
90	122.2	10.1	4.99	1.2
100	121.2	11.1	4.89	1.0
110	120.0	12.3	4.77	1.2
120	119.0	13.3	4.67	1.0
130	117.6	14.7	4.53	1.4
140	117.1	15.2	4.48	0.5
150	115.8	16.5	4.35	1.3
160	114.7	17.6	4.24	1.1

Time in Minutes	Wt. of the Sample (mg.)	Wt. of Total H ₂ O Lost	H ₂ O/NiCl ₂ Mole Ratio	Rate mgH ₂ O/10 Mins.
170	114.0	18.3	4.17	0.7
180	112.7	19.6	4.05	1.3
190	111.7	20.6	3.94	1.0
200	110.8	21.5	3.86	0.9
210	109.8	22.5	3.76	1.0
220	108.9	23.4	3.67	0.9
230	108.1	24.2	3.59	0.8
240	107.2	25.1	3.49	0.9
250	106.2	26.1	3.39	1.0
260	105.3	27.0	3.31	0.9
270	104.6	27.7	3.24	0.7
280	103.8	28.5	3.16	0.8
290	102.9	29.4	3.07	0.9
300	102.2	30.1	3.00	0.7
310	101.3	31.0	2.92	0.9
320	100.9	31.4	2.87	0.4
330	100.0	32.3	2.78	0.9
340	99.2	33.1	2.70	0.8
350	98.7	33.6	2.65	0.5
360	98.0	34.3	2.58	0.7

Time in Minutes	Wt. of the Sample (mg.)	Wt. of Total H ₂ O Lost	H ₂ O/NiCl ₂ Mole Ratio	Rate mgH ₂ O/10 Mins.
370	97.2	35.1	2.50	0.8
380	96.8	35.5	2.46	0.4
390	96.2	36.1	2.40	0.6
400	95.8	36.5	2.36	0.4
410	95.2	37.1	2.30	0.6
420	94.8	37.5	2.26	0.4
430	94.3	38.0	2.21	0.5
440	94.0	38.3	2.18	0.3
450	93.5	38.8	2.13	0.5
460	93.3	39.0	2.11	0.2
470	93.1	39.2	2.09	0.2
480	92.8	39.5	2.06	0.3
490	92.5	39.8	2.03	0.3
500	92.4	39.9	2.02	0.1

* Dehydration carried out on a quartz spiral, suspended in a balance case containing magnesium perchlorate desiccant.



DEHYDRATION OF $\text{NiCl}_2 \cdot 6\text{H}_2\text{O}$ AT ROOM TEMPERATURE $\approx 25^\circ\text{C}$

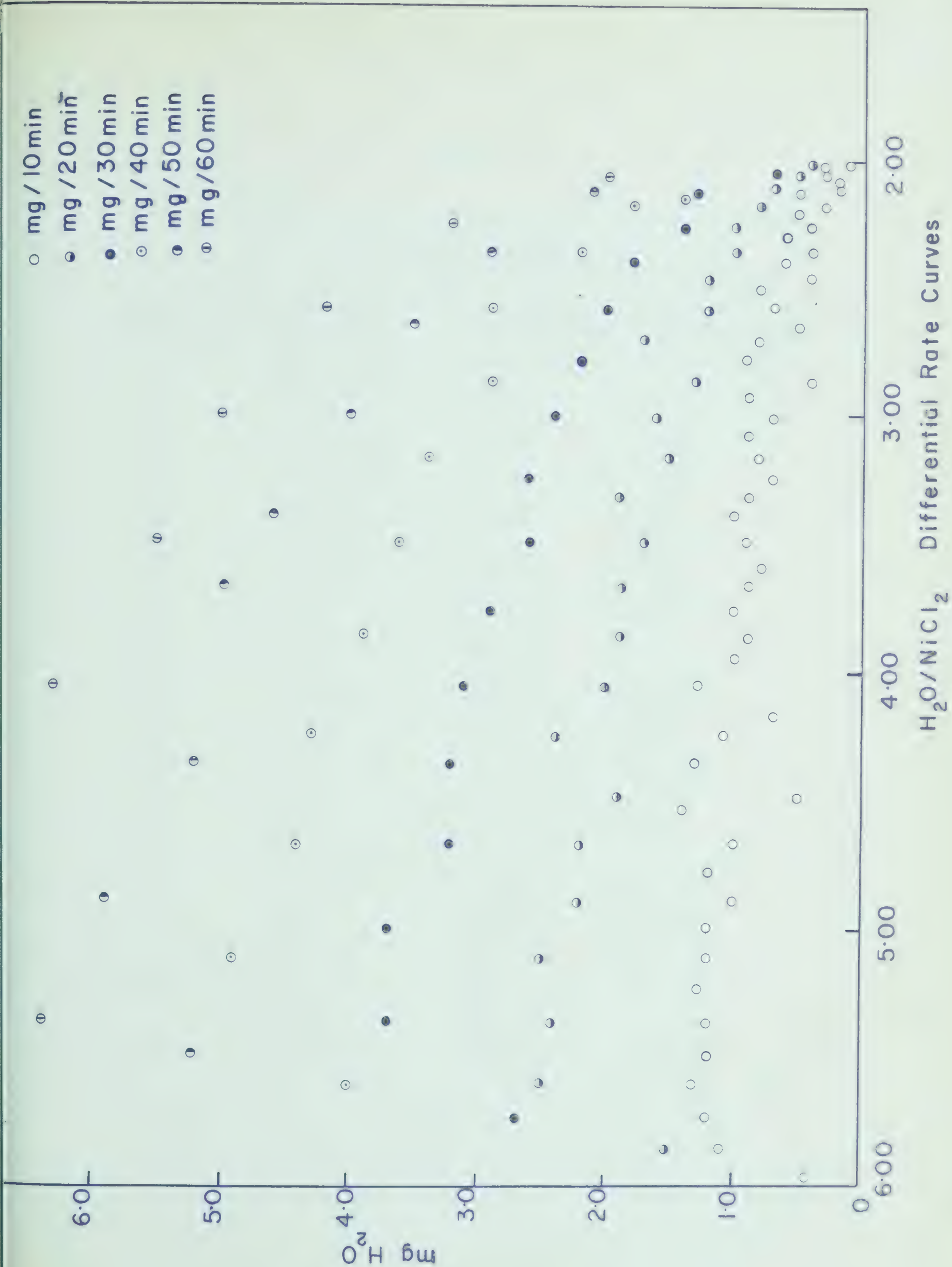


TABLE 17

Dehydration of $\text{NiCl}_2 \cdot 6\text{H}_2\text{O}$ at 25°C (Quartz Spiral)Weight of $\text{NiCl}_2 = 259.3$ mg.

Time in Minutes	Wt. of the Sample (mg.)	Wt. of Total H_2O Lost (mg)	Ratio $\text{H}_2\text{O}/\text{NiCl}_2$	Rate $\text{mgH}_2\text{O}/10$ Min.
0	475.5	0	6.00	0
10	470.6	4.9	5.86	4.9
20	465.7	9.8	5.73	4.9
30	459.9	15.6	5.56	5.8
40	454.5	21.0	5.42	5.4
50	449.6	25.9	5.28	4.9
60	444.8	30.7	5.15	4.8
70	439.9	35.6	5.01	4.9
80	435.0	40.5	4.87	4.9
90	430.1	45.4	4.74	4.9
100	424.8	50.7	4.59	5.3
110	419.9	55.6	4.45	4.9
120	415.0	60.5	4.32	4.9
130	410.6	64.9	4.20	4.4
140	406.7	68.8	4.09	3.9
150	402.8	72.7	3.98	3.9

Time in Minutes	Wt. of the Sample (mg.)	Wt. of Total H ₂ O Lost (mg)	Ratio H ₂ O/NiCl ₂	Rate mgH ₂ O/10 min.
160	398.9	76.6	3.87	3.9
170	395.0	80.5	3.76	3.9
180	391.6	83.9	3.67	3.4
190	388.2	87.3	3.57	3.4
200	384.8	90.7	3.48	3.4
210	381.8	93.7	3.40	3.0
220	378.9	96.6	3.32	2.9
230	376.0	99.5	3.23	2.9
240	373.1	102.4	3.15	2.9
250	370.1	105.4	3.07	3.0
260	367.2	108.3	2.99	2.9
270	364.7	110.8	2.92	2.5
280	361.8	113.7	2.84	2.9
290	359.8	115.7	2.79	2.0
300	357.9	117.6	2.73	1.9
310	356.0	119.5	2.68	1.9
320	354.2	121.3	2.63	1.8
330	352.1	123.4	2.57	2.1
340	350.6	124.9	2.53	1.5
350	349.1	126.4	2.49	1.5

Time in Minutes	Wt. of the Sample (mg.)	Wt. of Total H ₂ O Lost (mg)	Ratio H ₂ O/NiCl ₂	Rate mgH ₂ O/10 min.
360	347.7	127.8	2.45	1.4
370	346.2	129.3	2.41	1.5
380	344.7	130.8	2.37	1.5
390	343.2	132.3	2.33	1.5
400	341.8	133.7	2.29	1.4
410	340.8	134.7	2.26	1.0
420	339.9	135.6	2.23	0.9
430	338.9	136.6	2.20	1.0
440	338.0	137.5	2.18	0.9
450	337.5	138.5	2.16	0.5
460	336.9	138.6	2.15	0.6
470	336.4	139.1	2.14	0.5
480	335.9	139.6	2.12	0.5

TABLE 18

Dehydration of $\text{NiCl}_2 \cdot 6\text{H}_2\text{O}$ at 35°C (Quartz Spiral)Weight of $\text{NiCl}_2 = 259.5$ mg.

Time in Minutes	Wt. of the Sample (mg.)	Wt. of Total H_2O Lost (mg)	Ratio $\text{H}_2\text{O}/\text{NiCl}_2$	Rate $\text{mgH}_2\text{O}/5$ min.
0	476.0	0	6.00	0
5	472.1	3.9	5.90	3.9
10	467.2	8.8	5.76	4.9
15	460.9	15.1	5.58	6.3
20	454.6	21.4	5.51	6.3
25	449.2	26.8	5.26	5.3
30	443.8	32.2	5.11	5.4
35	438.0	38.0	4.95	5.8
40	433.1	42.9	4.81	4.9
45	428.2	47.8	4.68	4.9
50	423.3	52.7	4.54	4.9
55	417.9	58.1	4.39	5.4
60	412.6	63.4	4.24	5.3
65	407.2	68.8	4.09	5.4
70	402.3	73.7	3.96	4.9
75	398.4	77.6	3.85	3.9

Time in Minutes	Wt. of the Sample(mg.)	Wt. of Total H ₂ O Lost (mg)	Ratio H ₂ O/NiCl ₂	Ratio mgH ₂ O/10 min.
80	394.0	82.0	3.73	4.4
85	390.1	85.9	3.62	3.9
90	386.2	89.8	3.51	3.9
95	382.3	93.7	3.40	3.9
100	378.4	97.6	3.30	3.9
105	375.0	101.0	3.20	3.4
110	372.1	103.9	3.12	2.9
115	369.2	106.8	3.04	2.9
120	366.2	109.8	2.96	3.0
125	363.3	112.7	2.90	2.9
130	360.4	115.6	2.79	2.9
135	357.9	118.1	2.73	2.5
140	355.5	120.5	2.66	2.4
145	353.5	122.5	2.60	2.0
150	351.6	124.4	2.55	1.9
155	349.6	126.4	2.50	2.0
160	348.6	127.4	2.47	1.0
165	347.1	128.9	2.43	1.5
170	345.7	130.3	2.39	1.4
175	344.3	131.7	2.35	1.4

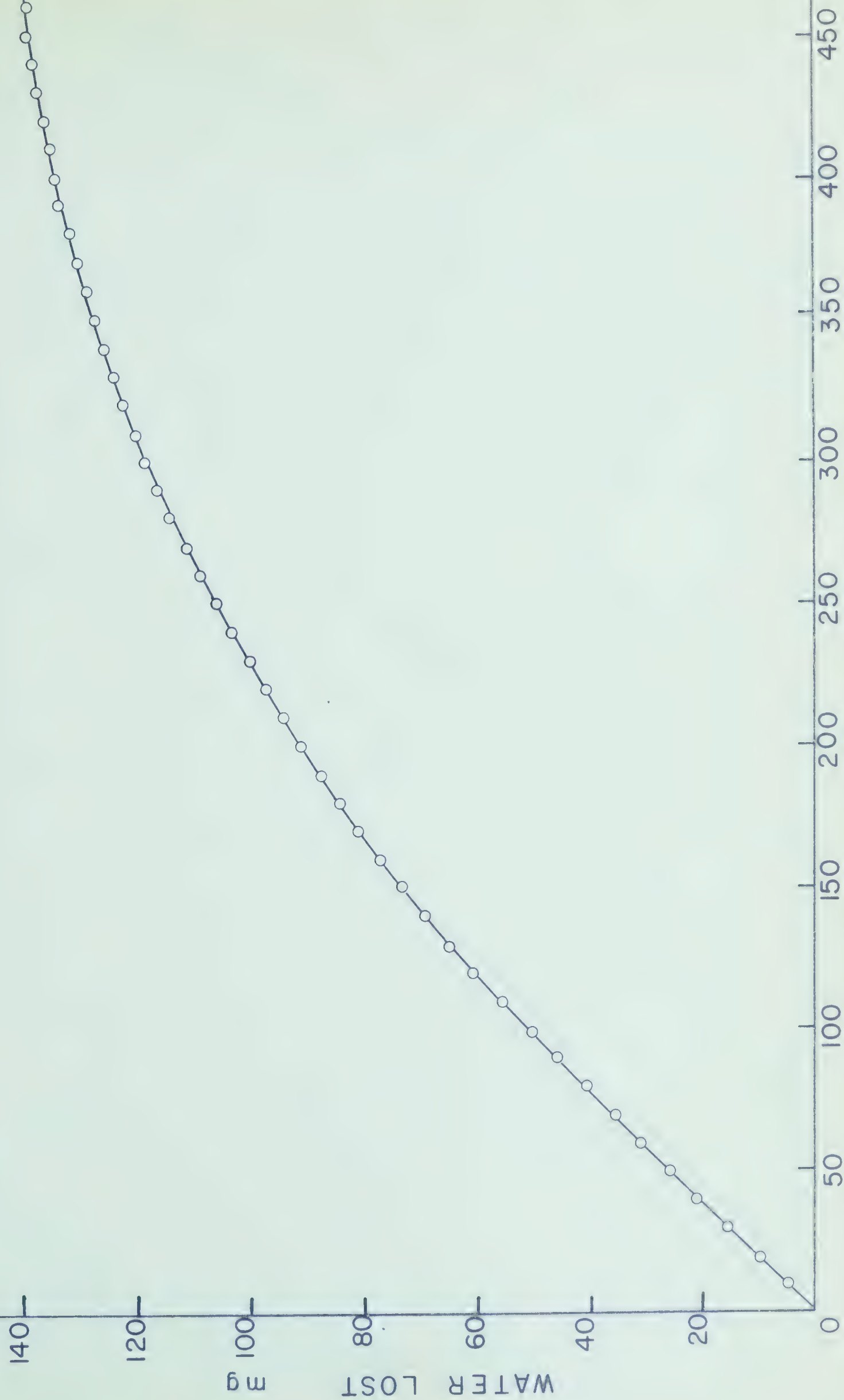
Time in Minutes	Wt. of the Sample (mg.)	Wt. of Total H ₂ O Lost (mg)	Ratio H ₂ O/NiCl ₂	Rate mgH ₂ O/5 min.
180	342.8	133.2	2.31	1.5
185	341.8	134.2	2.28	1.0
190	340.8	135.2	2.25	1.0
195	339.9	136.1	2.22	0.9
200	338.9	137.1	2.20	1.0
205	337.9	138.1	2.17	1.0
210	336.9	139.1	2.14	1.0
215	336.0	140.0	2.12	0.9
220	335.5	140.5	2.10	0.5
225	335.0	141.0	2.09	0.5
230	334.5	141.5	2.07	0.5
235	334.0	142.0	2.06	0.5

TABLE 19

Dehydration of $\text{NiCl}_2 \cdot 6\text{H}_2\text{O}$ at 45°C (Quartz Spiral)Weight of $\text{NiCl}_2 = 261.2$ mg.

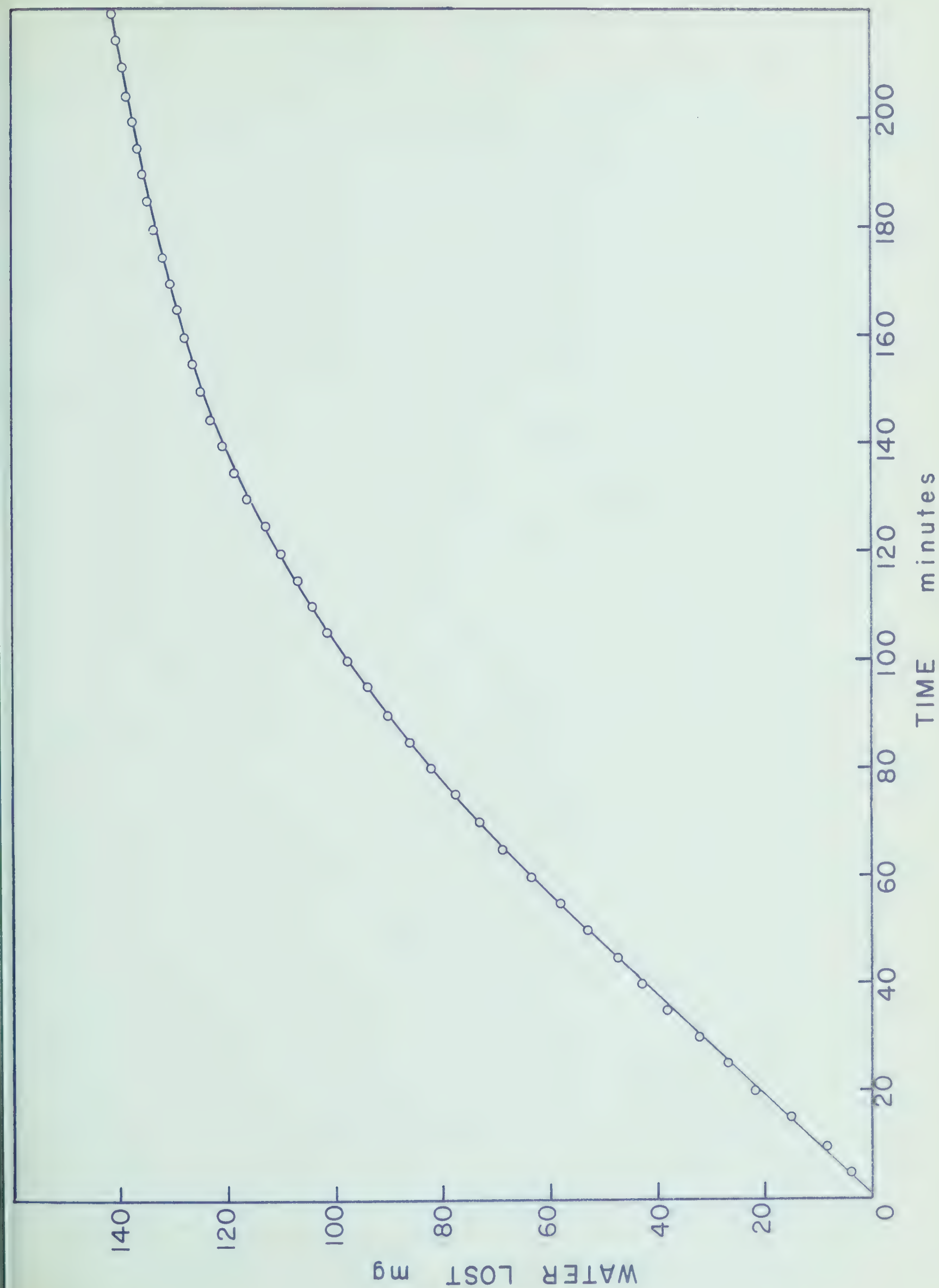
Time in Minutes	Wt. of the Sample (mg.)	Wt. of Total H_2O Lost (mg)	Ratio $\text{H}_2\text{O}/\text{NiCl}_2$	Rate $\text{mgH}_2\text{O}/5$ min.
0	479.0	0	6.00	0
5	471.2	7.8	5.78	7.8
10	462.9	16.1	5.55	8.3
15	454.6	24.4	5.33	8.3
20	445.3	33.7	5.07	9.3
25	434.6	44.4	4.77	10.7
30	424.8	54.2	4.51	9.8
35	415.6	63.4	4.25	9.2
40	406.3	72.7	3.99	9.3
45	398.0	81.0	3.77	8.3
50	390.7	87.3	3.56	7.3
55	384.3	93.7	3.42	6.4
60	378.0	100.0	3.24	6.3
65	372.1	105.9	3.11	5.9
70	366.3	111.7	2.92	5.8
75	361.4	116.6	2.78	4.9

Time in Minutes	Wt. of the Sample (mg.)	Wt. of Total H ₂ O Lost (mg)	Ratio H ₂ O/NiCl ₂	Rate mgH ₂ O/5 min.
80	357.5	120.5	2.68	3.9
85	353.6	124.4	2.57	3.9
90	350.2	127.8	2.47	3.4
95	347.2	130.8	2.39	3.0
100	344.3	133.7	2.31	2.9
105	342.3	135.7	2.26	2.0
110	340.4	137.6	2.21	1.9
115	338.9	139.1	2.17	1.5
120	338.0	140.0	2.14	0.9
125	337.0	141.0	2.11	1.0
130	336.0	142.0	2.08	1.0
135	335.0	143.0	2.06	1.0
140	334.5	143.5	2.04	0.5



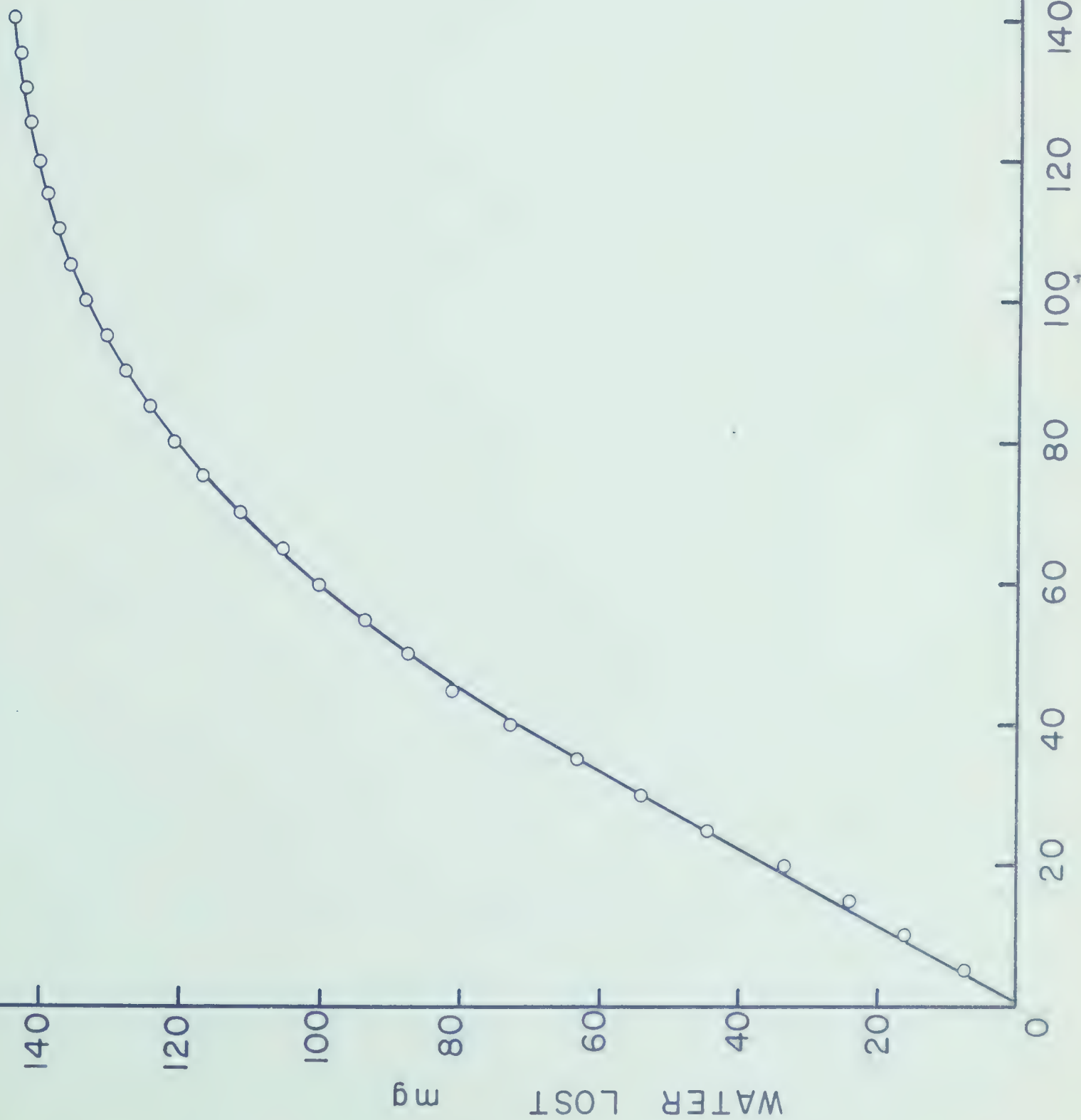
DEHYDRATION OF $\text{NiCl}_2 \cdot 6\text{H}_2\text{O}$ at 35°C

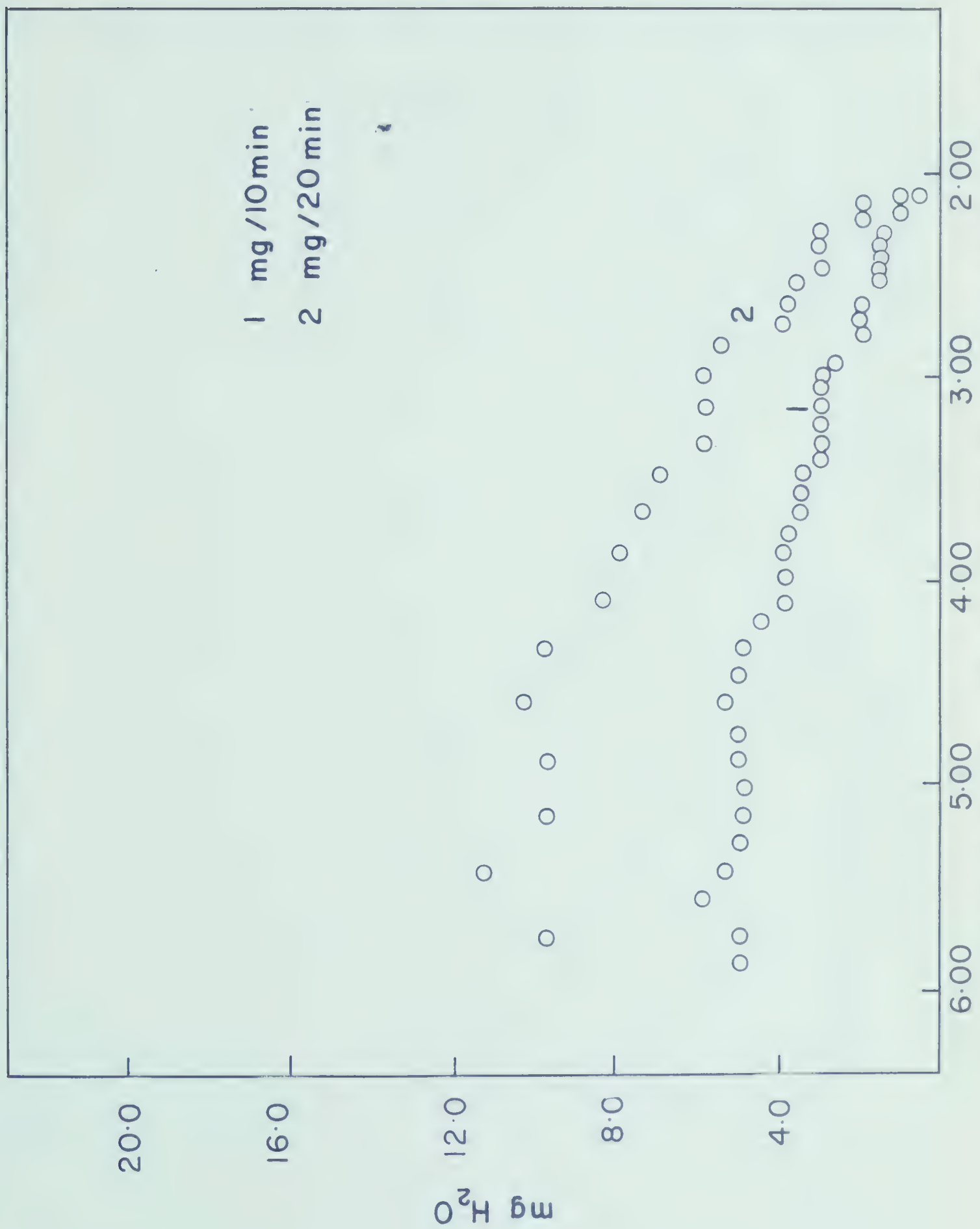
Fig. 40



DEHYDRATION OF $\text{NiCl}_2 \cdot 6\text{H}_2\text{O}$ at 45°C

TIME minutes





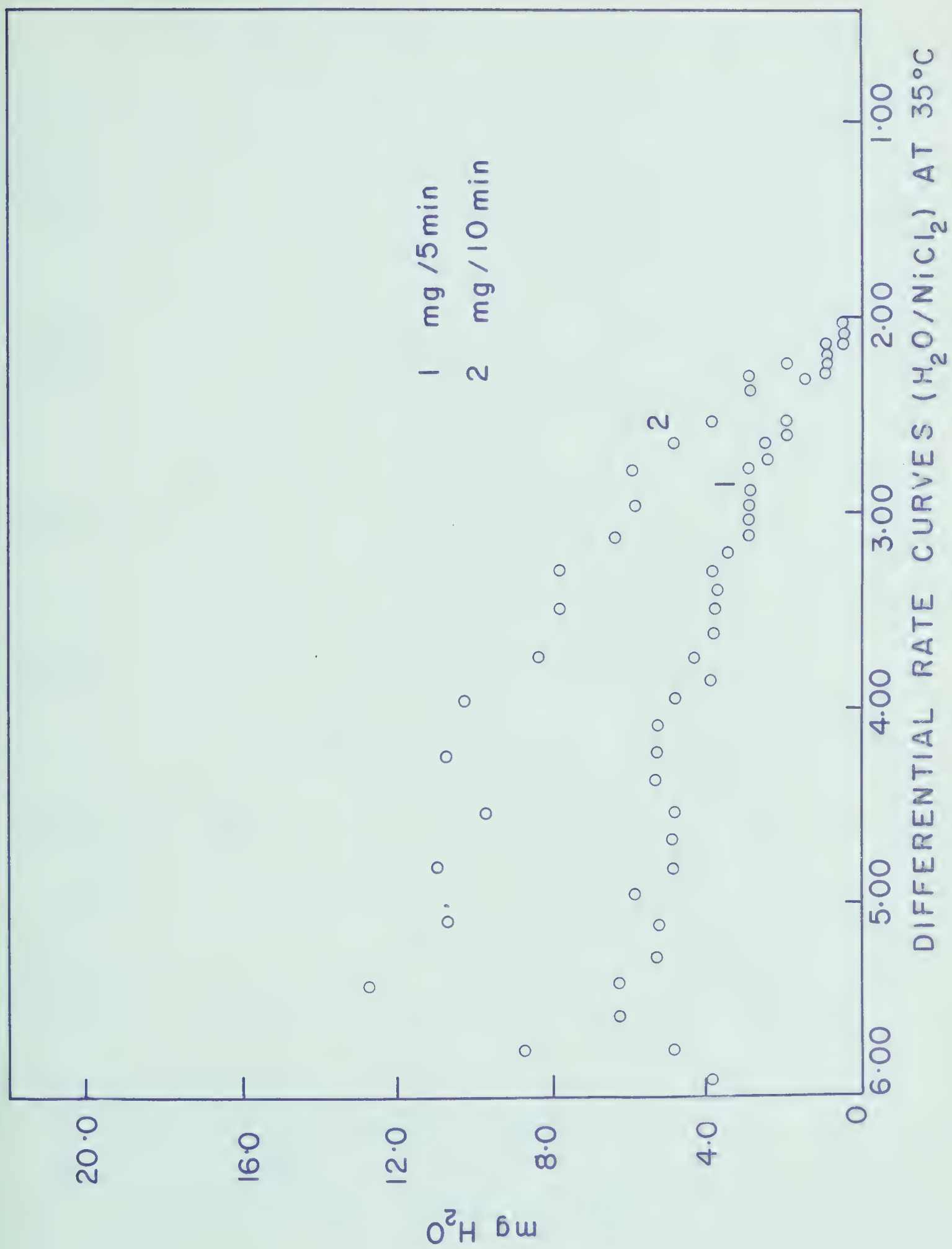
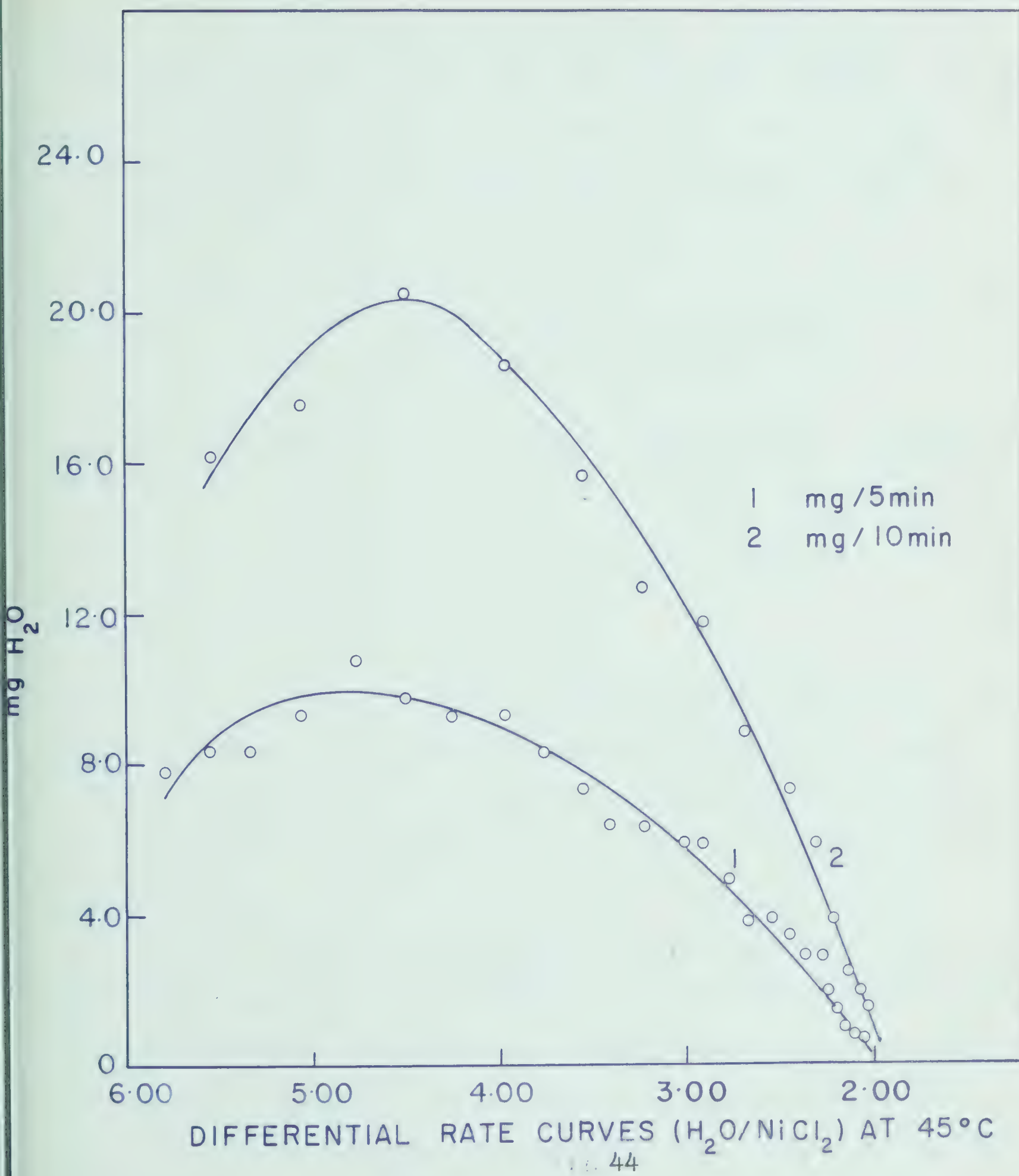


Fig. 43



From the linear part of the decomposition curves for 25°C, 35°C and 45°C as shown in Figs. 39, 40 and 41, the rate of loss of water for these temperatures was calculated from their slopes. The values obtained are given in Table 20.

TABLE 20

Rate of Loss of Water for $\text{NiCl}_2 \cdot 6\text{H}_2\text{O}$
at Different Temperatures

<u>Temperature</u>	<u>$1/T \times 10^3$</u>	<u>Rate mg/min.</u>	<u>Log rate</u>
25°C	3.353	0.50	- 0.3010
35°C	3.245	1.05	0.0212
45°C	3.143	1.89	0.2765

The plot of the logarithm of the rate versus the reciprocal of the absolute temperature yields a straight line as shown in Fig. 45. From the slope of the straight line the activation energy of the process was calculated to be 12.7 Kcals.

The results obtained for the dehydration of $\text{NiCl}_2 \cdot 6\text{H}_2\text{O}$ desiccated in atmospheres of different relative humidities are given in Table 21. The integral decomposition curves are shown in Figs. 46 and 47. The rate was calculated from the slopes of the linear part of the curves. The results for the rates at different relative humidities are given in Table 22,

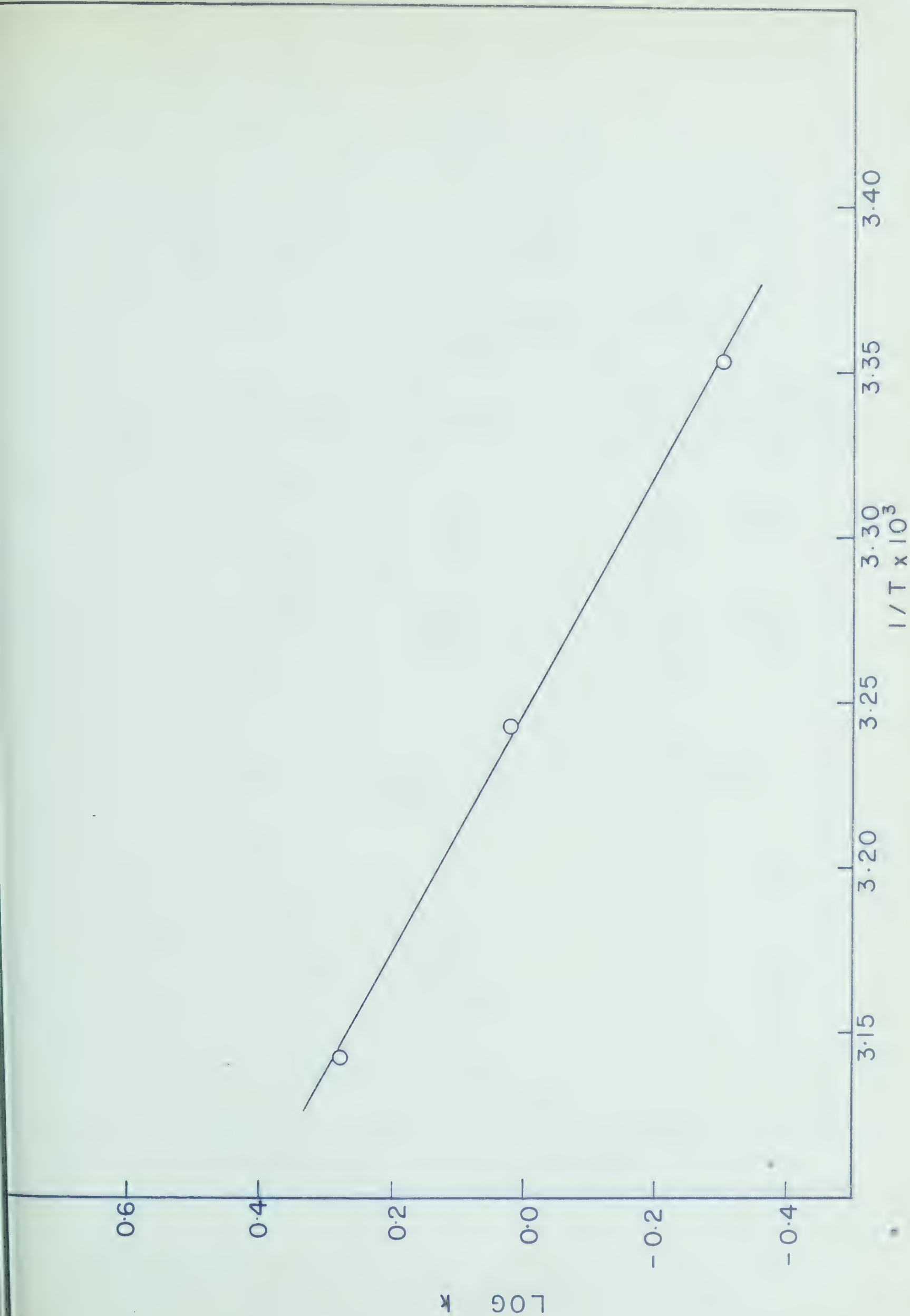
LOG k AS A FUNCTION OF $1/T$

Fig. 45

TABLE III

Dehydration of $\text{NiCl}_2 \cdot 6\text{H}_2\text{O}$ at Different Relative Humidities at Room Temperature $\approx 25^\circ \text{C}^a$

Specific Gravity of H_2SO_4 Desiccant = 1.40
Relative Humidity = 37.1 (74)

Time in Hours	Wt. of the Sample (gm)	Wt. of Total H_2O Lost (mg)	Ratio $\text{H}_2\text{O}/\text{NiCl}_2$	Rate $\text{mgH}_2\text{O}/\text{Hr}$
0	5.0000	0	6.00	0
1	4.9620	38.0	5.90	38.0
3	4.8910	109.0	5.71	35.5
5	4.8677	132.3	5.66	11.6
7	4.8668	133.2	5.65	0.5
9	4.8662	133.8	5.64	0.3

Specific Gravity of H_2SO_4 Desiccant = 1.50
Relative Humidity = 18.8 (74)

0	5.0003	0	6.00	0
1	4.9421	58.2	5.84	58.2
3	4.8793	121.0	5.68	31.4
5	4.8484	151.9	5.60	15.5
7	4.8148	185.5	5.51	16.8
9	4.7779	222.4	5.41	18.4

a Dehydration carried out in petri dish 6 cm diameter and 1 cm high in a 6 in. desiccator containing 100 ml of desiccant

TABLE 21 (Continued)

Dehydration of $\text{NiCl}_2 \cdot 6\text{H}_2\text{O}$ at Different Relative Humidities at Room Temperature $\approx 25^\circ\text{C}^a$

Specific Gravity of H_2SO_4 Desiccant = 1.60
Relative Humidity = 8.5 (74)

Time in Hours	Wt. of the Sample (gm)	Wt. of Total H_2O Lost (mg)	Ratio $\text{H}_2\text{O}/\text{NiCl}_2$	Rate $\text{mgH}_2\text{O}/\text{Hr}$
0	5.0000	0	6.00	0
2	4.8876	112.4	5.70	56.2
4	4.8297	170.3	5.55	28.9
6	4.7717	228.3	5.39	29.0
8	4.7129	287.1	5.24	29.4

Specific Gravity of H_2SO_4 Desiccant = 1.70
Relative Humidity = 3.2 (74)

0	5.0007	0	6.00	0
1	4.9349	65.8	5.82	65.8
3	4.8587	142.0	5.62	38.1
5	4.7892	210.5	5.44	34.2
7	4.7024	298.3	5.21	43.9

a Dehydration carried out in petri dish 6 cm. diameter and 1 cm high in a 6 in. desiccator containing 100 ml desiccant

TABLE 21 (Continued)

Dehydration of $\text{NiCl}_2 \cdot 6\text{H}_2\text{O}$ at Different Relative
Humidities at Room Temperature $\approx 25^\circ\text{C}$ ^a

Specific Gravity of H_2SO_4 Desiccant = 1.80

Time in Hours	Wt. of the Sample (gm)	Wt. of Total H_2O Lost (mg)	Ratio $\text{H}_2\text{O}/\text{NiCl}_2$	Rate $\text{mgH}_2\text{O}/\text{Hr}$
0	5.0000	0	6.00	0
1	4.9216	78.6	5.79	78.6
3	4.8171	183.1	5.51	52.2
5	4.7296	270.6	5.28	43.7
7	4.6454	354.8	5.06	42.1

a Dehydration carried out in petri dish 6 cm diameter and
1 cm high in a 6 in. desiccator containing 100 ml of
desiccant

TABLE 21 (Continued)

Dehydration of $\text{NiCl}_2 \cdot 6\text{H}_2\text{O}$ at Different Relative Humidities at Room Temperature $\approx 25^\circ\text{C}^a$

Magnesium Perchlorate Desiccant				
Time in Hours	Wt. of the Sample (gm)	Wt. of Total H_2O Lost (mg)	Ratio $\text{H}_2\text{O}/\text{NiCl}_2$	Rate $\text{mgH}_2\text{O}/\text{Hr}$
0	5.0000	0	6.00	0
1	4.8893	110.7	5.70	110.7
3	4.7986	201.4	5.47	45.4
5	4.7017	298.3	5.21	48.5
7	4.5901	409.9	4.91	55.8
9	4.4921	507.9	4.66	49.0
Phosphorous Pentoxide Desiccant				
0	5.0000	0	6.00	0
1	4.8874	112.6	5.70	112.6
3	4.7950	205.0	5.46	46.2
5	4.6958	304.2	5.19	49.6
7	4.5837	416.3	4.90	56.0
9	4.4815	518.5	4.63	51.1

^a Dehydration carried out in petri dish 6 cm diameter and 1 cm high in a 6 in. desiccator containing about 100 gms of desiccant

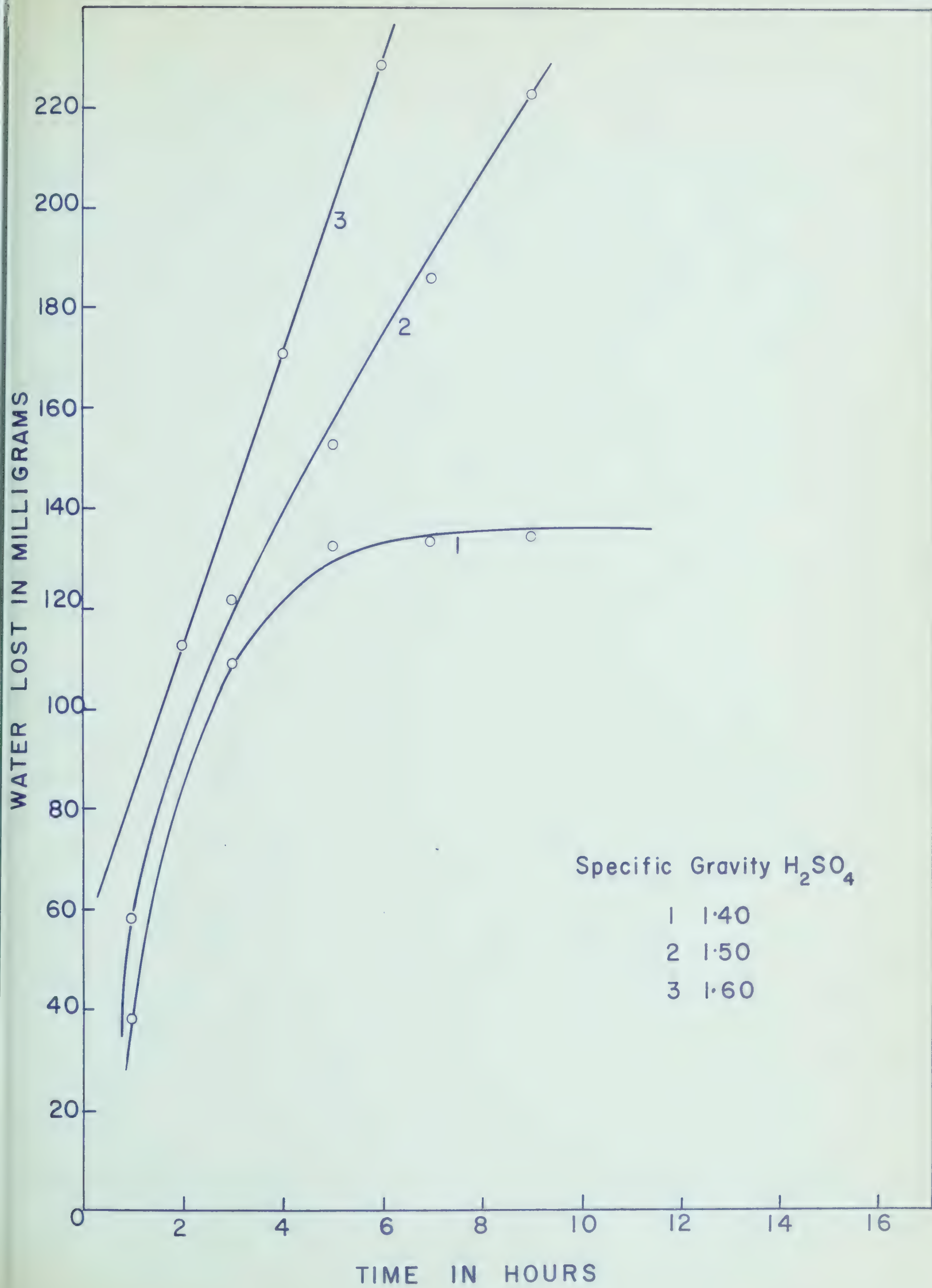


Fig. 46

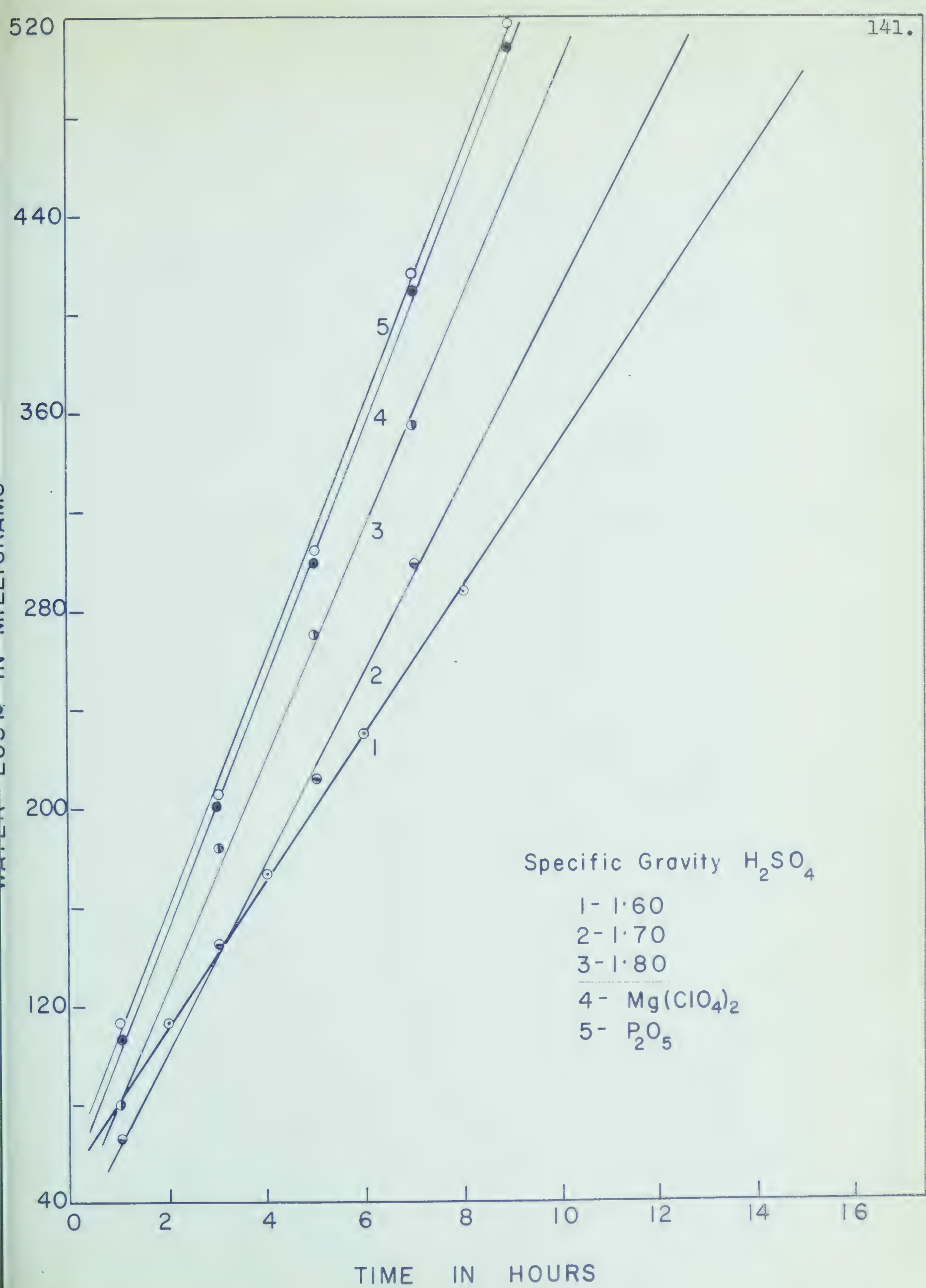


Fig. 47

TABLE 22

Rate of Dehydration of $\text{NiCl}_2 \cdot 6\text{H}_2\text{O}$ Under Different
Relative Humidities

Desiccant	Rate of Loss of H_2O (mg/Hr)
H_2SO_4 (Sp. Gr. 1.50)	18.0
H_2SO_4 (Sp. Gr. 1.60)	30.0
H_2SO_4 (Sp. Gr. 1.70)	38.5
H_2SO_4 (Sp. Gr. 1.80)	46.6
$\text{Mg} (\text{ClO}_4)_2$	50.7
P_2O_5	51.4

and their plot with respect to the efficiency of the desiccants is shown in Fig. 48. It can be seen that the reaction was followed for only 8 to 9 hours to determine the trend; but in each case the end product was analyzed to ascertain the hydrate which was stable at that humidity. The results of these analyses are given in Table 23.

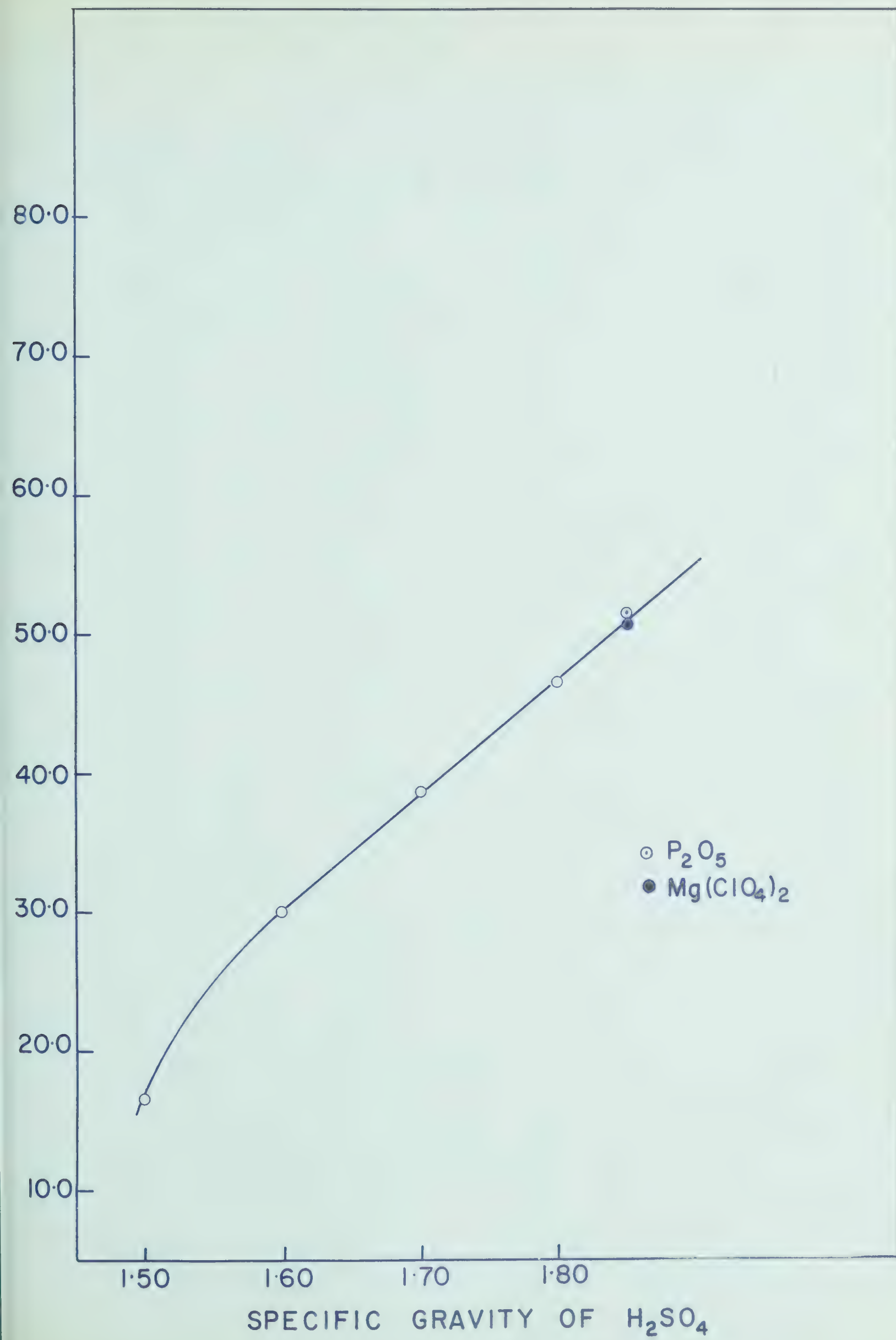


Fig. 48

TABLE 23

Stable Hydrates of Nickel Chloride in Atmospheres of
Different Relative Humidity

Sp. Gr. H_2SO_4	Relative Humidity	Time Obs.	Form of Hydrate
1.20	80.4	-	a
1.25	70.40	-	a
1.30	58.2	-	b
1.31	55.6	-	c
1.32	53.6	48 hrs.	6.08
1.33	51.4	48 hrs.	6.05
1.34	49.3	48 hrs.	6.01
1.35	47.2	24 hrs.	5.99
1.36	45.1	24 hrs.	5.98
1.37	43.1	24 hrs.	6.01
1.38	41.1	1 week	5.52

a Absorbs water from the desiccant. Solid finally turns into solution.

b Initially loses water. After 24 hours starts absorbing water from the desiccant.

c Initially loses water. After a week starts absorbing water from the desiccant.

TABLE 23 (Continued)

Sp. Gr. H_2SO_4	Relative Humidity	Time Obs.	Form of Hydrate
1.38	41.1	2 weeks	3.98
1.39	39.0	1 week	4.97
1.39	39.0	2 weeks	4.05
1.40	37.1	1 week	4.01
1.40	37.1	3 weeks	3.99
1.42	33.2	1 week	4.01
1.44	29.4	1 week	3.98
1.46	25.8	1 week	3.92
1.48	22.2	1 week	3.92
1.50	18.8	96 hrs.	2.02
1.80	--	48 hrs.	1.99

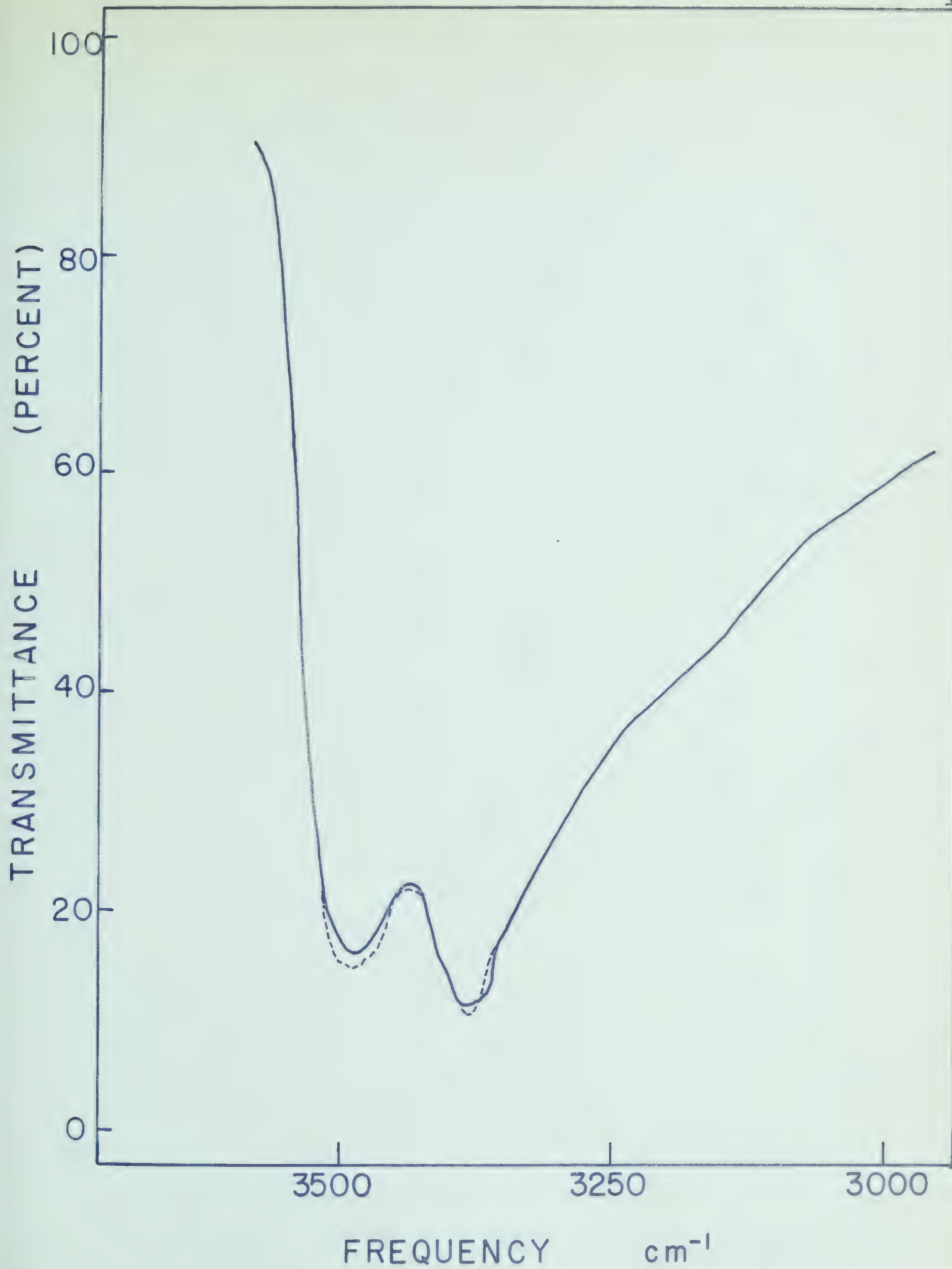
Using phosphorous pentoxide or anhydrous magnesium perchlorate as desiccant, the end product obtained was $\text{NiCl}_2 \cdot 2\text{H}_2\text{O}$. From Table 23 it is evident that for the preparation of $\text{NiCl}_2 \cdot 6\text{H}_2\text{O}$, the best humidity is 47.2% and for $\text{NiCl}_2 \cdot 4\text{H}_2\text{O}$, 37.1%, corresponding to sulphuric acid of specific gravity 1.35 and 1.40 respectively. For the preparation of $\text{NiCl}_2 \cdot 2\text{H}_2\text{O}$ any effective desiccants, e.g., concentrated sulphuric acid (Sp. Gr. 1.84), anhydrous magnesium perchlorate or phosphorous pentoxide, may be used. These observations confirm that the stable hydrates for nickel chloride are $\text{NiCl}_2 \cdot 6\text{H}_2\text{O}$, $\text{NiCl}_2 \cdot 4\text{H}_2\text{O}$ and $\text{NiCl}_2 \cdot 2\text{H}_2\text{O}$.

Infrared and X-ray Studies

An attempt was made to obtain a quantitative suspension of the hydrates. The major difficulties associated with the preparation of mulls of quantitatively known concentration are initial dispersal and subsequent suspension. Uniform dispersions of the lower hydrates were prepared in a vibrating ball mill (Hilger and Watts). The higher hydrates had a tendency to agglomerate during milling and were finally prepared by hand grinding in an Agate mortar. The hand ground mulls were generally less uniform than those which were mechanically ground. These mulls were all prepared by mixing together a weighed amount of salt and a weighed amount of the mulling agent. It was found most convenient to use an amount of salt such that the concentration of nickel in the mull was the same for all samples. Assuming that a uniform dispersion was obtained which incorporated all the salt and all the mulling agent into the final mixture, the suspensions contained nickel at a concentration of 0.2 molal. This particular concentration was chosen as a compromise between the ease of preparation of a uniform mull and the ease with which the mull could be introduced into the infrared cell. At higher concentration it was difficult to transfer to the absorption cells while at lower concentrations the chance of solid particles separating from the medium increases. By trial a 0.2 molal suspension was found to be convenient for a cell thickness of 0.1 mm. The

suspension was transferred to a 0.1 mm cell, with sodium chloride windows, with a hypodermic syringe. By careful manipulation of the syringe most of the trapped air bubbles were eliminated before the samples were introduced into the cell. A homogeneous suspension in the path of the light beam, free from minute traces of trapped air, was obtained by manipulating the stoppers of the cell. Once the samples had been introduced into the absorption cell further difficulty of settling of the suspended particles was encountered. It was found that this could be partly overcome by the use of a high density, high viscosity suspending medium. Fluorolube S-30 served this purpose very well while Nujol did not. Consequently the fluorolube mulls gave reproducible transmittance as shown in Fig. 49.

The spectra obtained from Nujol mulls were not quantitatively reproducible. The spectra for 0.2 molal suspensions of $\text{NiCl}_2 \cdot 6\text{H}_2\text{O}$, $\text{NiCl}_2 \cdot 4\text{H}_2\text{O}$ and $\text{NiCl}_2 \cdot 2\text{H}_2\text{O}$ in Fluorolube S-30 are shown in Fig. 50, for the O-H stretching region, at normal and at five times expansion. The transmittance scale for each spectrum has been shifted to give a clear representation of the spectra. The spectra for the O-H bending region are shown in Fig. 51. The Nujol mulls were prepared by hand in an Agate mortar and the spectra were run in a demountable cell with sodium chloride windows. The spectra obtained for $\text{NiCl}_2 \cdot 6\text{H}_2\text{O}$, $\text{NiCl}_2 \cdot 4\text{H}_2\text{O}$ and $\text{NiCl}_2 \cdot 2\text{H}_2\text{O}$ for the 800 cm^{-1} region are shown in Fig. 52.



REPRODUCIBILITY OF INFRARED ABSORPTION SPECTRA
OF $\text{NiCl}_2 \cdot 2\text{H}_2\text{O}$

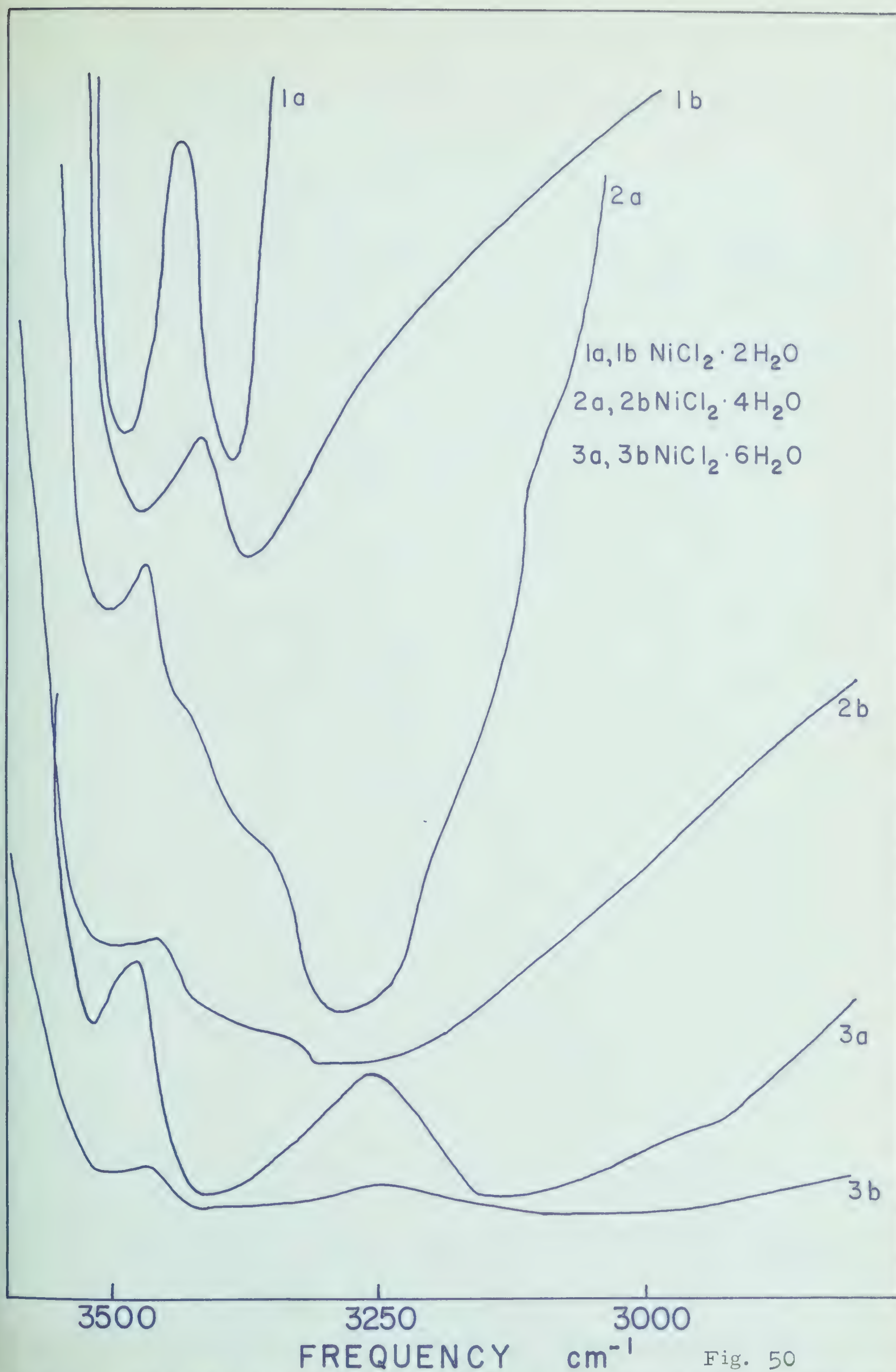
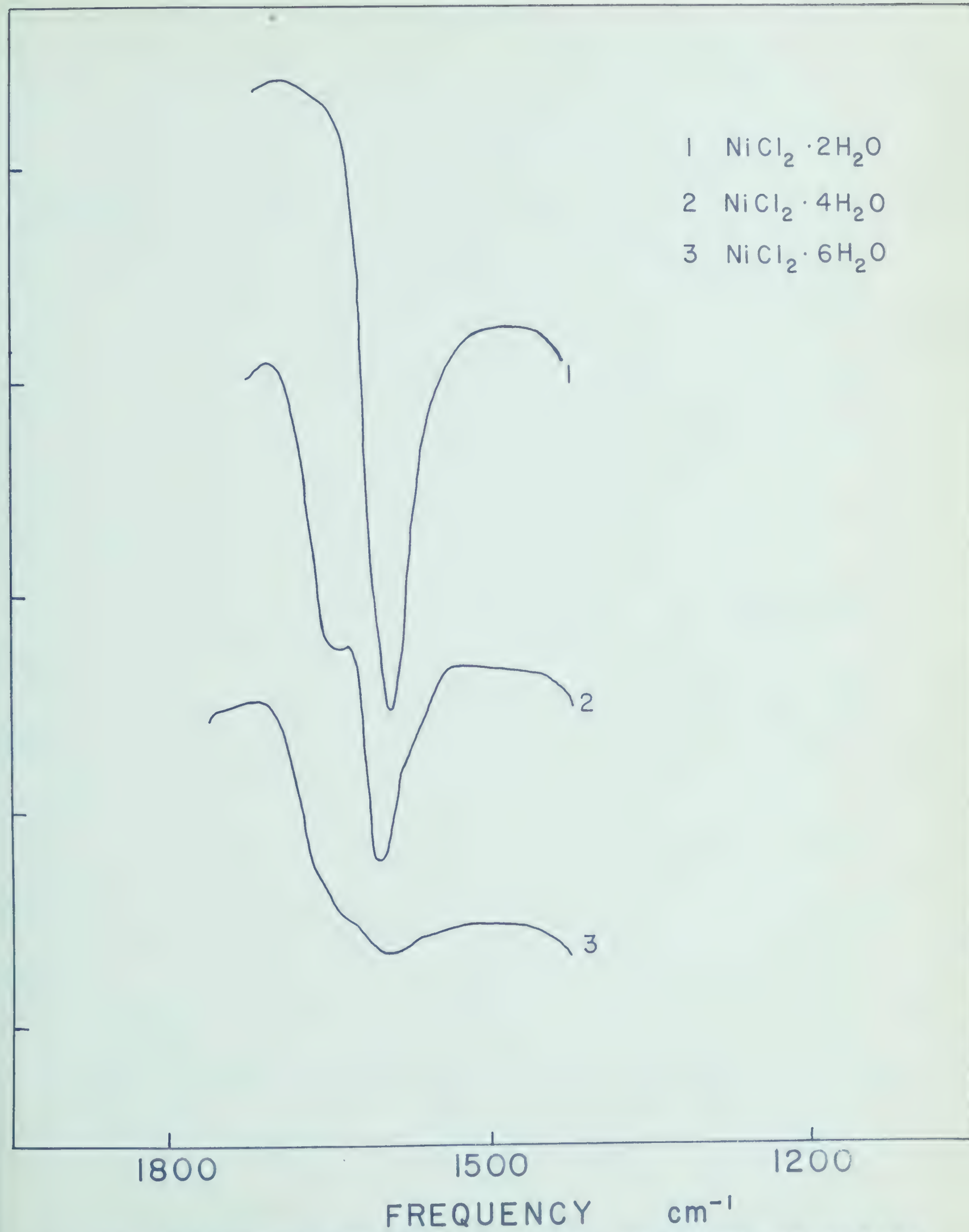
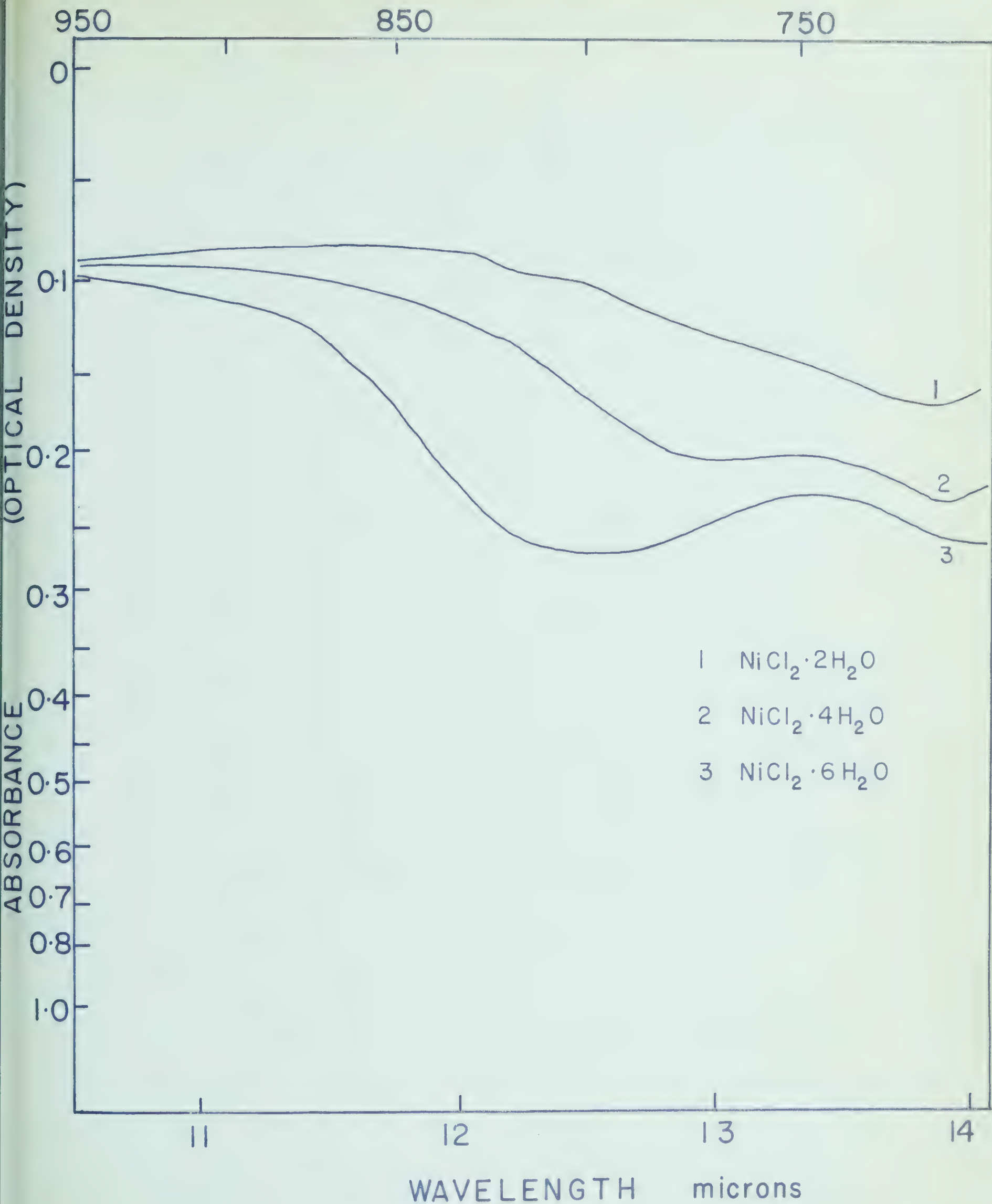


Fig. 50



INFRARED ABSORPTION SPECTRA OF NICKEL CHLORIDE HYDRATES



INFRARED ABSORPTION SPECTRA OF NICKEL CHLORIDE
HYDRATES

The spectra of the various stages of hydration of nickel chloride in Fluorolube S-30 for the O-H stretching and bending regions with normal expansion are shown in Figs. 53 and 54. The spectra at five times expansion of the O-H stretching region are shown in Fig. 55. The transmittance scale in each case has been shifted for clarity in presentation. An attempt was not made to obtain the integrated intensity of the absorption bands since they were so broad. The bands which were identifiable in the spectra of the partially dehydrated salts are catalogued in Table 24. Table 25 gives the positions of the bands identifiable in the O-H stretching region for a series of different transition metal hydrates.

Typical X-ray powder patterns were determined on samples prepared by grinding material of appropriate composition under fluorolube oil in a mortar. These suspensions were then mounted on plates and placed in the sample holder of a Norelco Diffractometer. The patterns obtained by irradiation with X-rays from a copper target are shown in Figs. 56 - 58.

TABLE 24

Prominent Bands of the Infrared Spectra of
Hydrated Nickel Chloride in cm^{-1}

Hydrates	Stretching region ^a			Bending region	
$\text{NiCl}_2 \cdot 6\text{H}_2\text{O}$	3515	3415	3135	--	1600
$\text{NiCl}_2 \cdot 5.5\text{H}_2\text{O}$	3516	3405	3140	1636(s)	1600
$\text{NiCl}_2 \cdot 5\text{H}_2\text{O}$	3515	3395	3138	1633	1595
$\text{NiCl}_2 \cdot 4.5\text{H}_2\text{O}$	3505	3390 ^(s)	3250	1645	1595
$\text{NiCl}_2 \cdot 4\text{H}_2\text{O}$	3515	3385 ^(s)	3290	1655	1605
$\text{NiCl}_2 \cdot 3.5\text{H}_2\text{O}$	3505	3380	3290	1640	1600
$\text{NiCl}_2 \cdot 3\text{H}_2\text{O}$	3500	3390	3295	--	1605
$\text{NiCl}_2 \cdot 2.5\text{H}_2\text{O}$	3495	3390	--	--	1605
$\text{NiCl}_2 \cdot 2\text{H}_2\text{O}$	3495	3385	--	--	1605

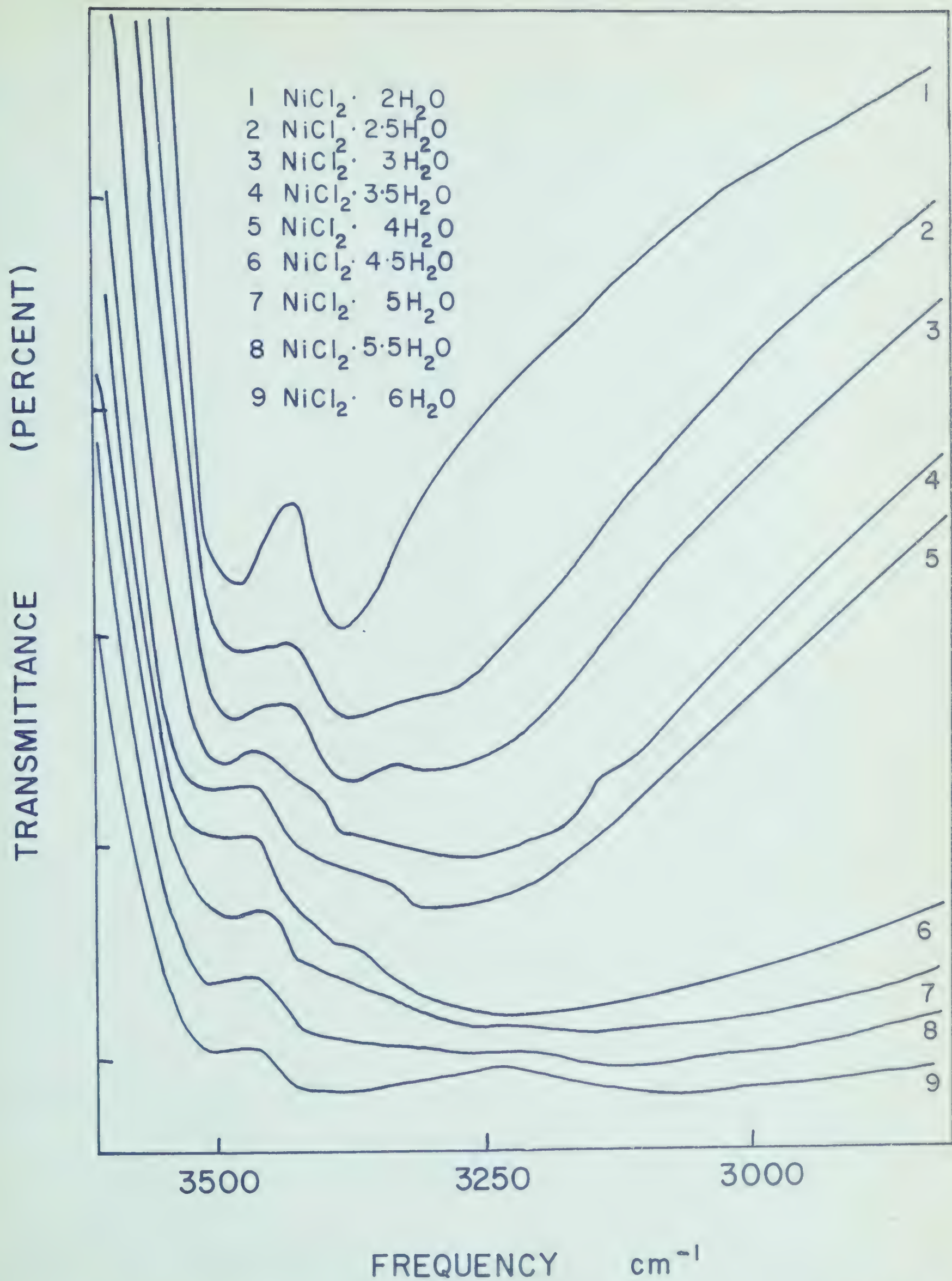
(a) Values reported on the basis of 5 times scale expansion

(s) Shoulder

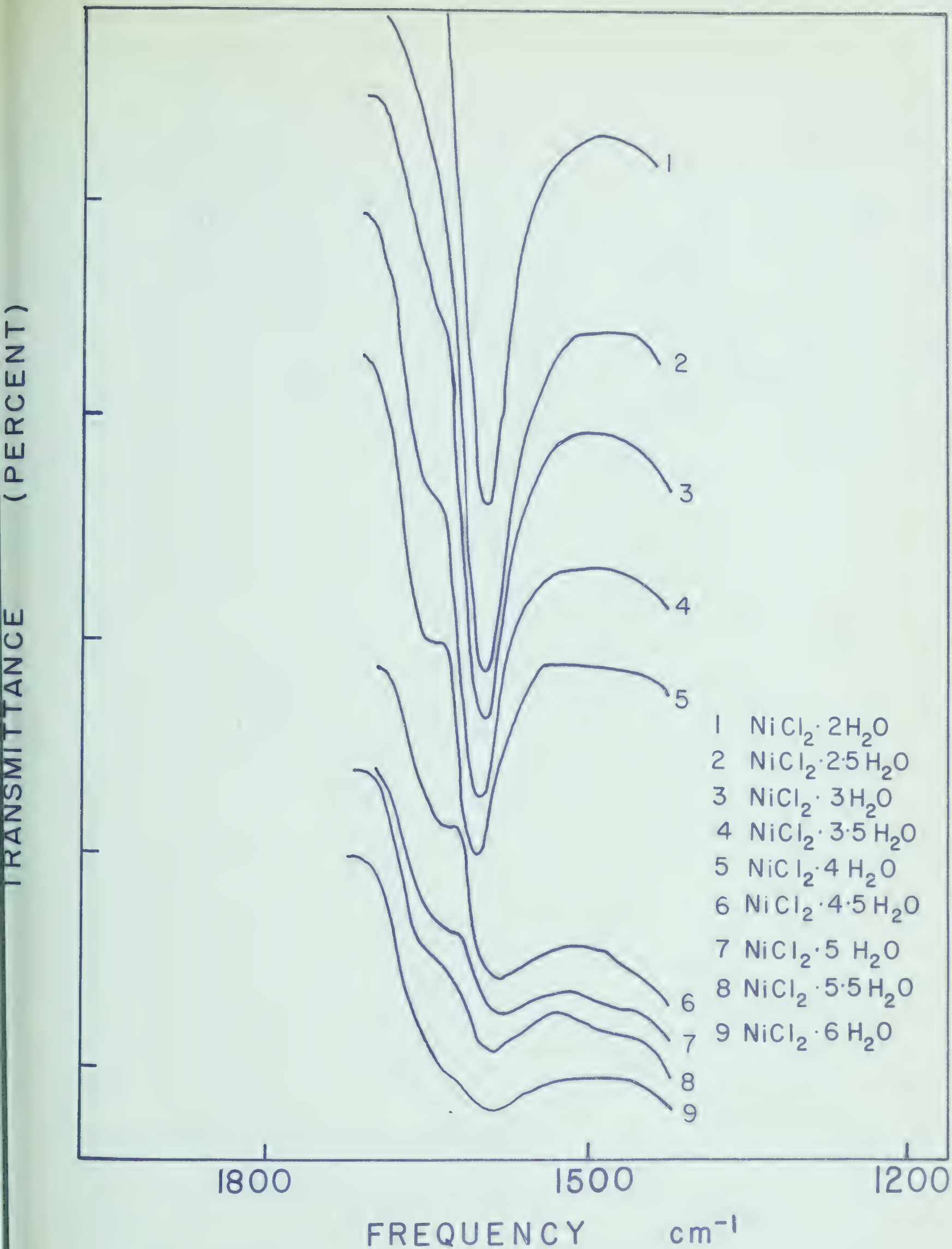
TABLE 25

Prominent O-H Stretching Frequencies
of Different Hydrates in cm^{-1}

$\text{NiCl}_2 \cdot 6\text{H}_2\text{O}$	3515	3415	3135	$\text{NiCl}_2 \cdot 2\text{H}_2\text{O}$	3495	3385
$\text{CoCl}_2 \cdot 6\text{H}_2\text{O}$	3528	3393	3133	$\text{CoCl}_2 \cdot 2\text{H}_2\text{O}$	3403	3178
$\text{NiCl}_2 \cdot 4\text{H}_2\text{O}$	3515	3385	3290	$\text{MnCl}_2 \cdot 2\text{H}_2\text{O}$	3443	3188
$\text{MnCl}_2 \cdot 4\text{H}_2\text{O}$	3508	3388	3308			



INFRARED ABSORPTION SPECTRA OF NICKEL CHLORIDE HYDRATES



INFRARED ABSORPTION SPECTRA OF NICKEL CHLORIDE HYDRATES

Fig. 54

TRANSMITTANCE (PERCENT)

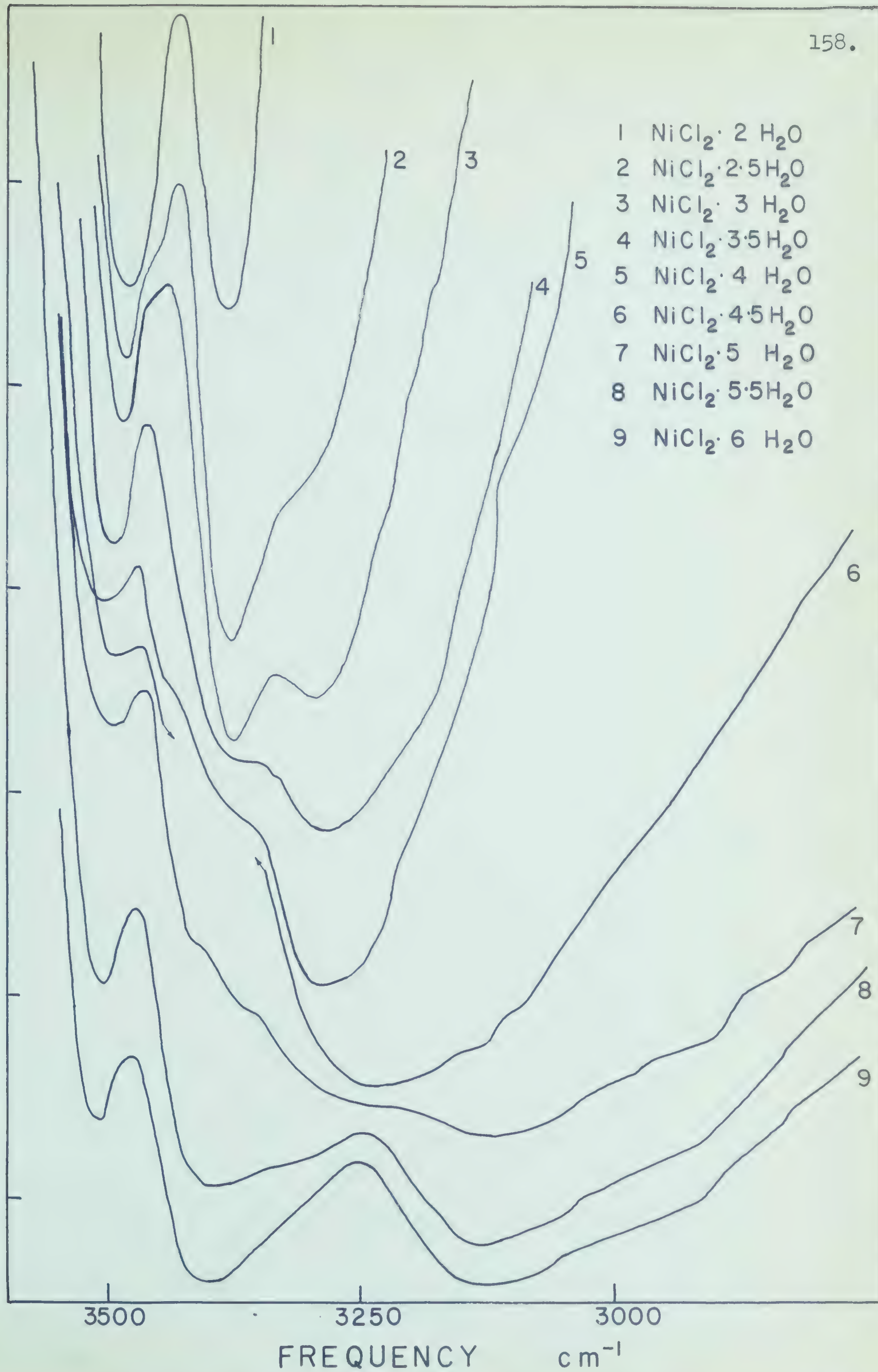
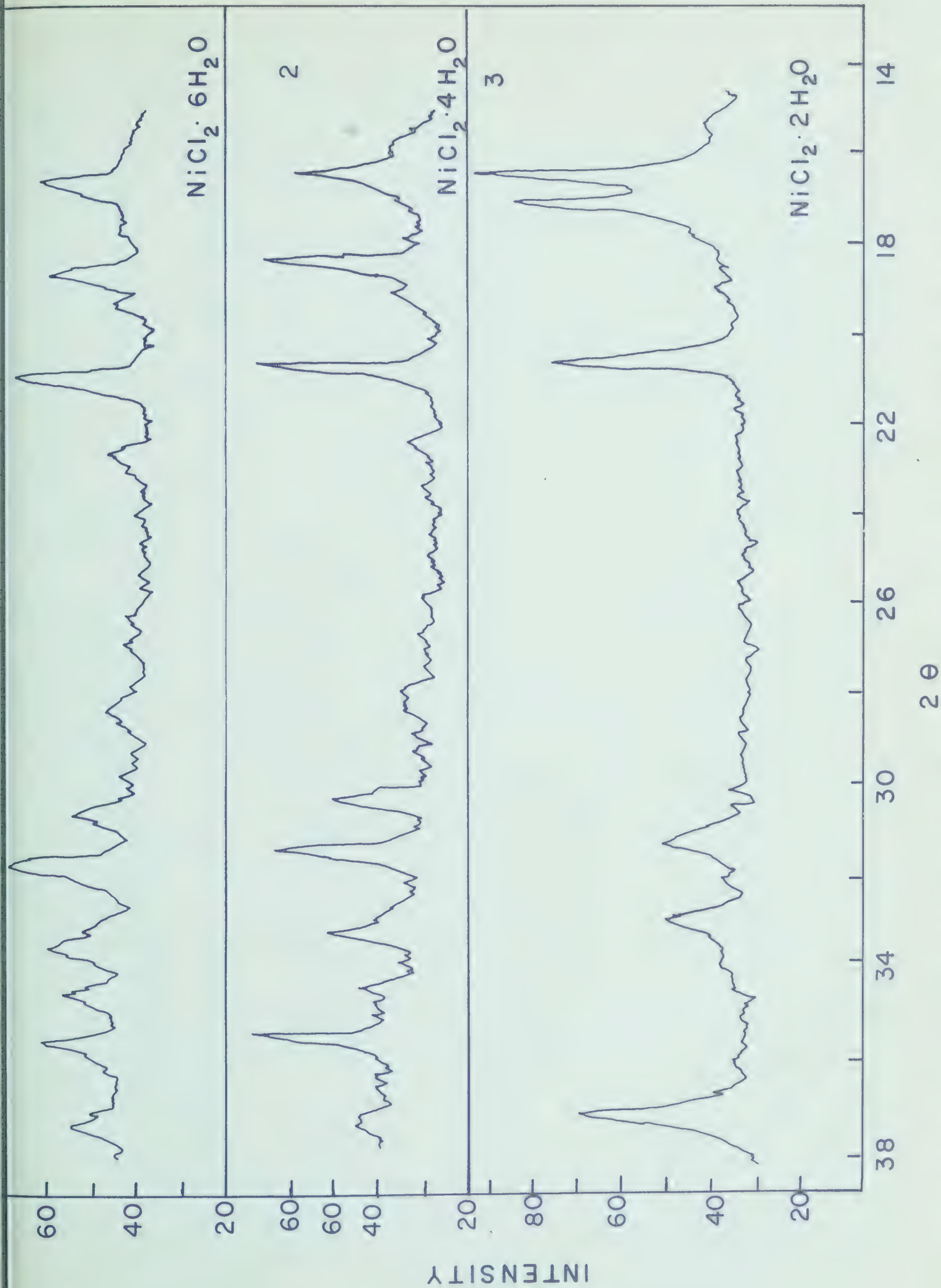
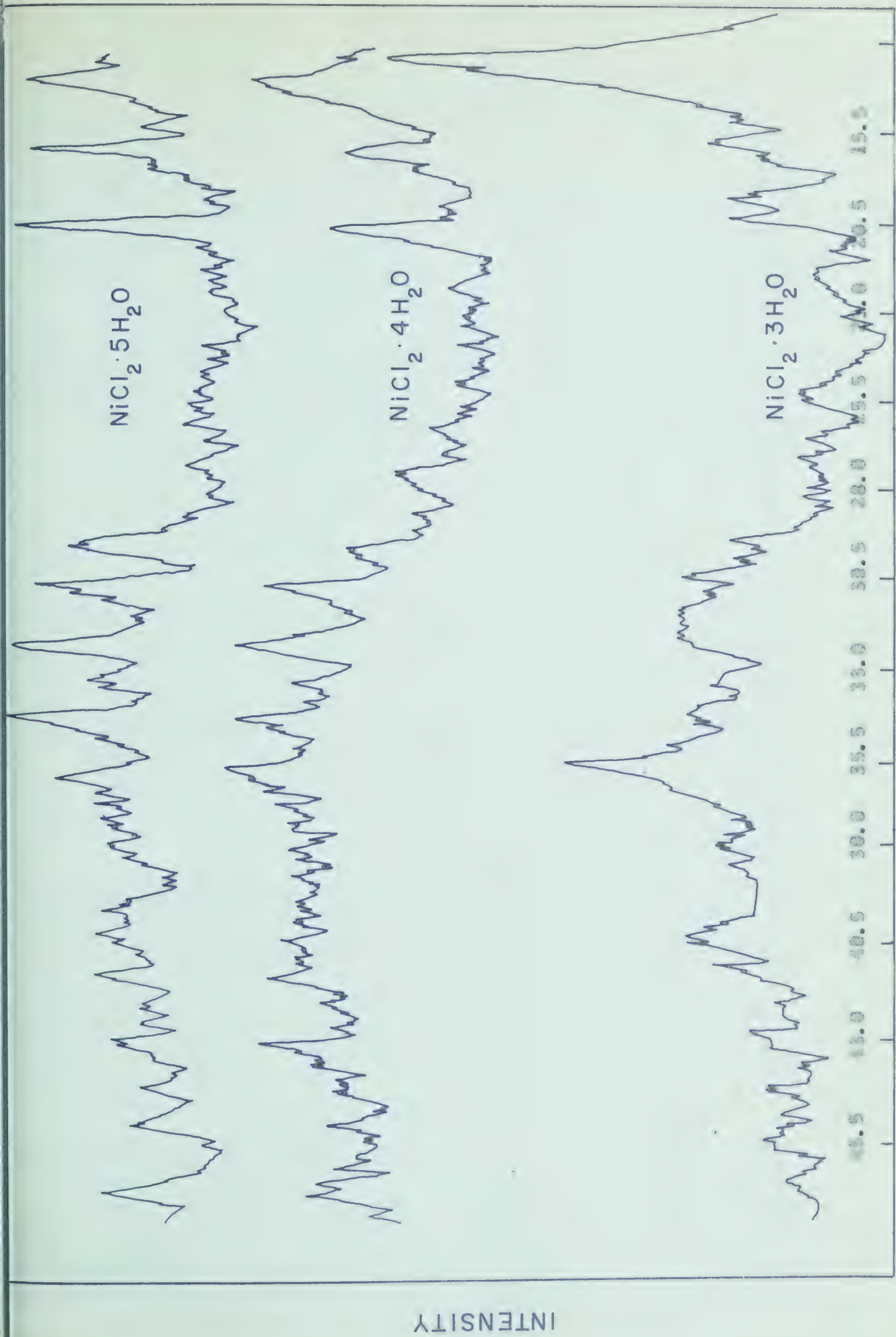


Fig. 55

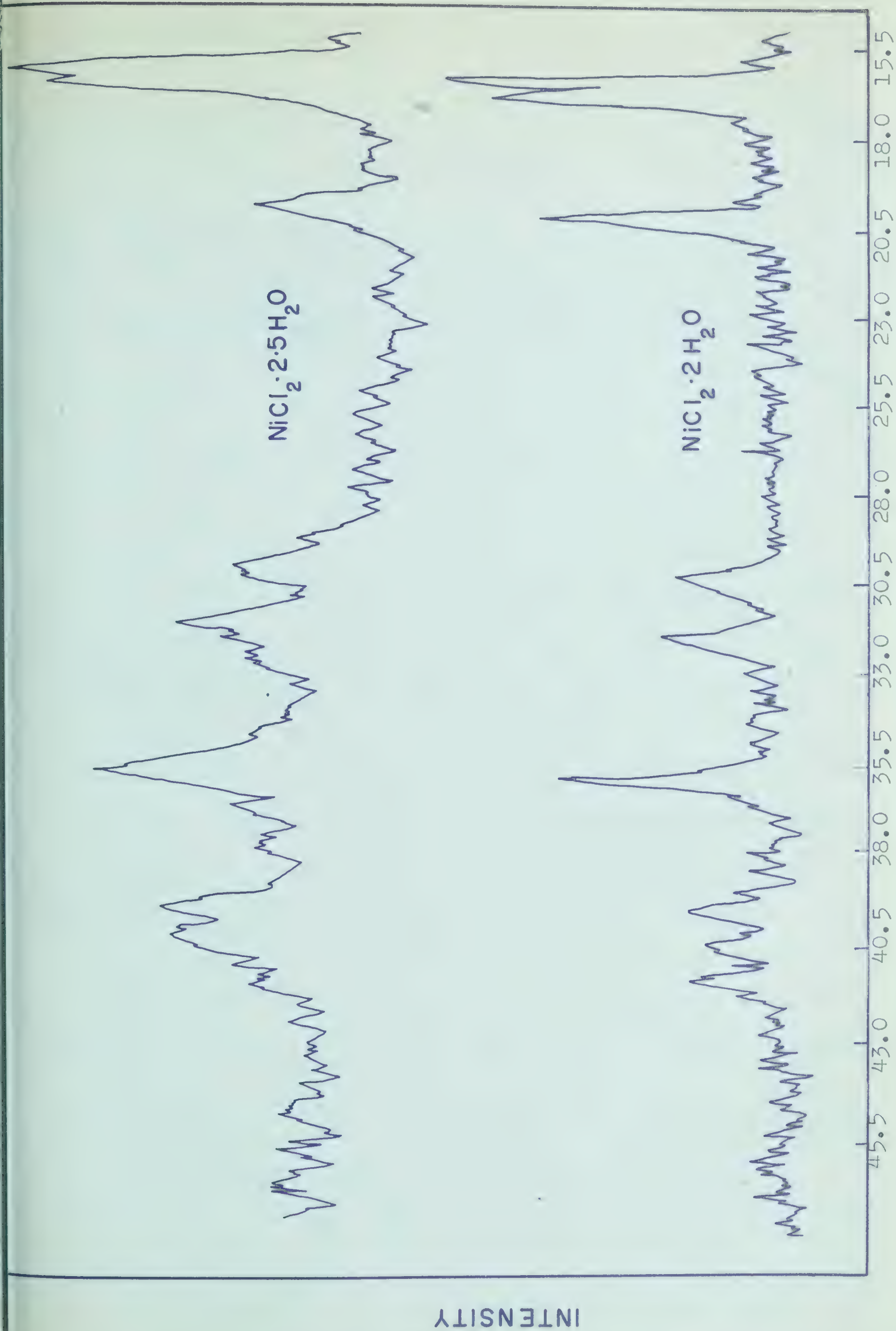


X-RAY DIFFRACTOMETER TRACES FOR $\text{NiCl}_2 \cdot 6\text{H}_2\text{O}$, (1), $\text{NiCl}_2 \cdot 4\text{H}_2\text{O}$, (2) AND $\text{NiCl}_2 \cdot 2\text{H}_2\text{O}$, (3)



X-RAY DIFFRACTOMETER TRACES FOR NICKEL CHLORIDE HYDRATES

Fig. 57



X-RAY DIFFRACTOMETER TRACES FOR NICKEL CHLORIDE HYDRATES

Fig. 58

DISCUSSION

Equilibrium Studies

Application of the phase rule criterion to the data presented graphically in Figs. 22, 23, 24 shows quite clearly that there are only three hydrates of nickel(II) chloride which have significant ranges of stability. These are $\text{NiCl}_2 \cdot 6\text{H}_2\text{O}$, $\text{NiCl}_2 \cdot 4\text{H}_2\text{O}$ and $\text{NiCl}_2 \cdot 2\text{H}_2\text{O}$. Of these $\text{NiCl}_2 \cdot 6\text{H}_2\text{O}$ is stable up to about 36° , $\text{NiCl}_2 \cdot 4\text{H}_2\text{O}$ is stable in the temperature range $37 - 75^\circ$, and $\text{NiCl}_2 \cdot 2\text{H}_2\text{O}$ is stable above 75° . An effort was made to pinpoint the transition temperatures through the variation of $\log P$ as a function of $1/T$ as shown in Figs. 25, 26, 27, 28 and 29. The intersections of the portions of these curves of different slopes reveal the positions of the transition points. These were found to occur at 36.3° for the transition between hexa- and tetrahydrate and at 75.0° for the transition between the tetra- and the dihydrate. The first of these transition temperatures had been determined quite accurately by Derby and Yngve (8). The present value is in excellent agreement with that reported previously. The second transition temperature had been estimated by the same workers to be about 75° . The present work confirms the earlier estimate, and a somewhat more accurate value of 75.0° is reported here.

Perhaps the most significant conclusion from the

$\log P$ vs $1/T$ plots for this system can be drawn from the number of discontinuities rather than their positions. The fact that the only discontinuities observed throughout the temperature range studied are known to correspond to the transformation of hexahydrate to tetrahydrate and of tetrahydrate to dihydrate strongly suggests that these are the only hydrates which are able to form in this system. This seems a reasonable conclusion for with very few exceptions these have been the only hydrates reported for the halides of the divalent metals of the first transition series. There are two notable exceptions to this generalization. The first of these is the result of some observations on cobalt(II) chloride in mixed solvents by Katzin and Ferraro (94). In this case the ternary phase diagram showed evidence for the existence, in a very narrow stability range, of a trihydrate. The existence of a trihydrate in the present instance would have been of great advantage in some of the calculations to be reported a little later in this work. However, the evidence discussed above suggests that if such a hydrate is present it cannot differ in stability from that of the tetrahydrate by more than 100 to 200 cal., if it has as much as a 10^0 stability range. This is the estimated discontinuity in the slope that could have been dismissed as experimental uncertainty. Of course, if the stability range was only a few degrees, then the uncertainty of the slope would have fallen completely on a

single point and could easily have been missed. However, analyses of solid phases failed to reveal the presence of such a material in the range of 36 to 75°. Similarly, infra-red and X-ray measurements to be discussed later showed no evidence for a trihydrate.

The other notable exception was a report by Castor and Basolo (55) of $\text{NiCl}_2 \cdot 5.5\text{H}_2\text{O}$ and $\text{NiCl}_2 \cdot 5\text{H}_2\text{O}$. These phases were reported on the basis of differential kinetics of dehydration measurements, and will be discussed in a subsequent section.

The curves of Figs. 25, 26, 27, 28 and 29 are useful from another aspect inasmuch as they yield information which is of thermodynamic significance. In Fig. 28, the low-temperature portion of the curve refers to the equilibrium represented by the equation



The equilibrium constant (K_p) for this reaction is given by

$$K_p = P^2 \quad 3$$

Insertion of 3 in the Clausius-Clapeyron equation [4] gives an expression 6 for the variation of the equilibrium constant with the temperature. Consequently, the slope of the linear plot

$$\frac{d \ln K_p}{dT} = \frac{\Delta H^\circ}{RT^2} \quad 4$$

$$\frac{d \ln P^2}{dT} = \frac{\Delta H^\circ}{RT^2} \quad 5$$

$$\frac{d \ln P}{dT} = \frac{\Delta H^\circ}{2RT^2} \quad 6$$

of $\log P$ as a function of $1/T$ allows ΔH° for the reaction 2 to be calculated. In a similar way ΔH° could be calculated for any other vaporization process which occurs in this system. The thermodynamic quantities which have been calculated in this way are given in Table 26.

TABLE 26
Enthalpy and Entropy of Decomposition
of the Hydrates of Nickel Chloride*

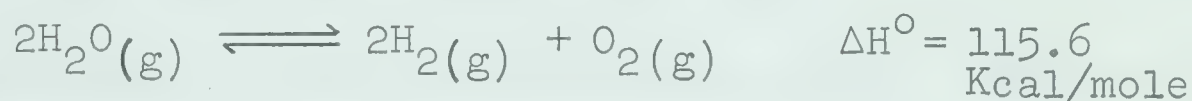
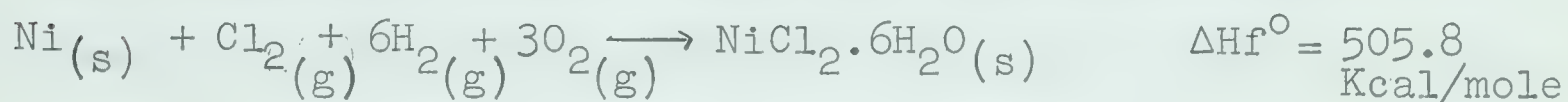
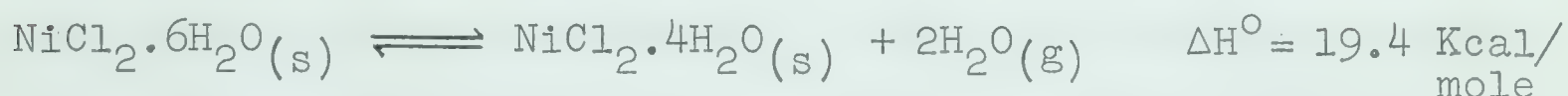
Hydrate	ΔH° Kcal/mole	ΔS° (eu)				
		27.0°C	36.0°C	37.0°C	55.0°C	70.0°C
$\text{NiCl}_2 \cdot 6\text{H}_2\text{O}$	9.70	32.3	31.4			
$\text{NiCl}_2 \cdot 4\text{H}_2\text{O}$	13.54			43.6	41.3	39.5

* Values reported as per mole of water lost

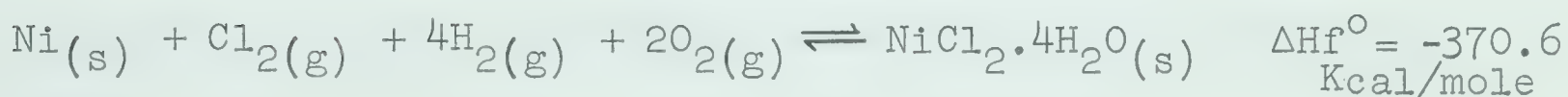
On the basis of the data in Table 26 it is apparent that the principal difference between the hexahydrate on the one hand and the tetrahydrate on the other resides in the degree of restriction which is placed upon the motion of the labile water molecules in the solid state. The restriction is considerably

less in the case of the hexahydrate.

Since the heats of decomposition of the hydrates as reported in Table 26 are reproducible to ± 0.2 Kcal/mole it was felt desirable to use these values, together with other thermochemical quantities available in the literature (95), to calculate heats of formation for nickel chloride hydrates. In this calculation ΔH_f° for $\text{NiCl}_2 \cdot 6\text{H}_2\text{O}(\text{s})$ will be taken as 505.8 Kcal/mole.



whence



This value of -370.6 Kcal/mole for the heat of formation of the tetrahydrate is in good agreement with the value of 364.6 Kcal/mole which is currently found in the literature (95). In view of the internal consistency of the present results this value is to be preferred over that which has been reported previously. In a similar way a value of -227.9 Kcal/mole is calculated for the heat of formation of the dihydrate. This value is in agreement with the literature (95) value of -220.8 Kcal/mole but should also be taken to represent a significant

improvement over that which is now available.

There are two apparent inconsistencies in the plots of $\log P$ as a function of $1/T$ in Figs. 26 and 29, which require comment. It was observed that when, during the course of observations at increasing temperatures, a transition temperature was passed, the pressure readings taken for increasing temperature did not correspond to those taken for decreasing temperature. In fact, the decreasing temperature curve was merely an extension of that obtained for a solution of the same composition on the high temperature side of the transition point. Thus, the transition back to the low temperature stable phase did not in fact take place at the transition temperature and this decreasing temperature branch of the curve represents a metastable equilibrium. It is, therefore, without significance for the system under discussion.

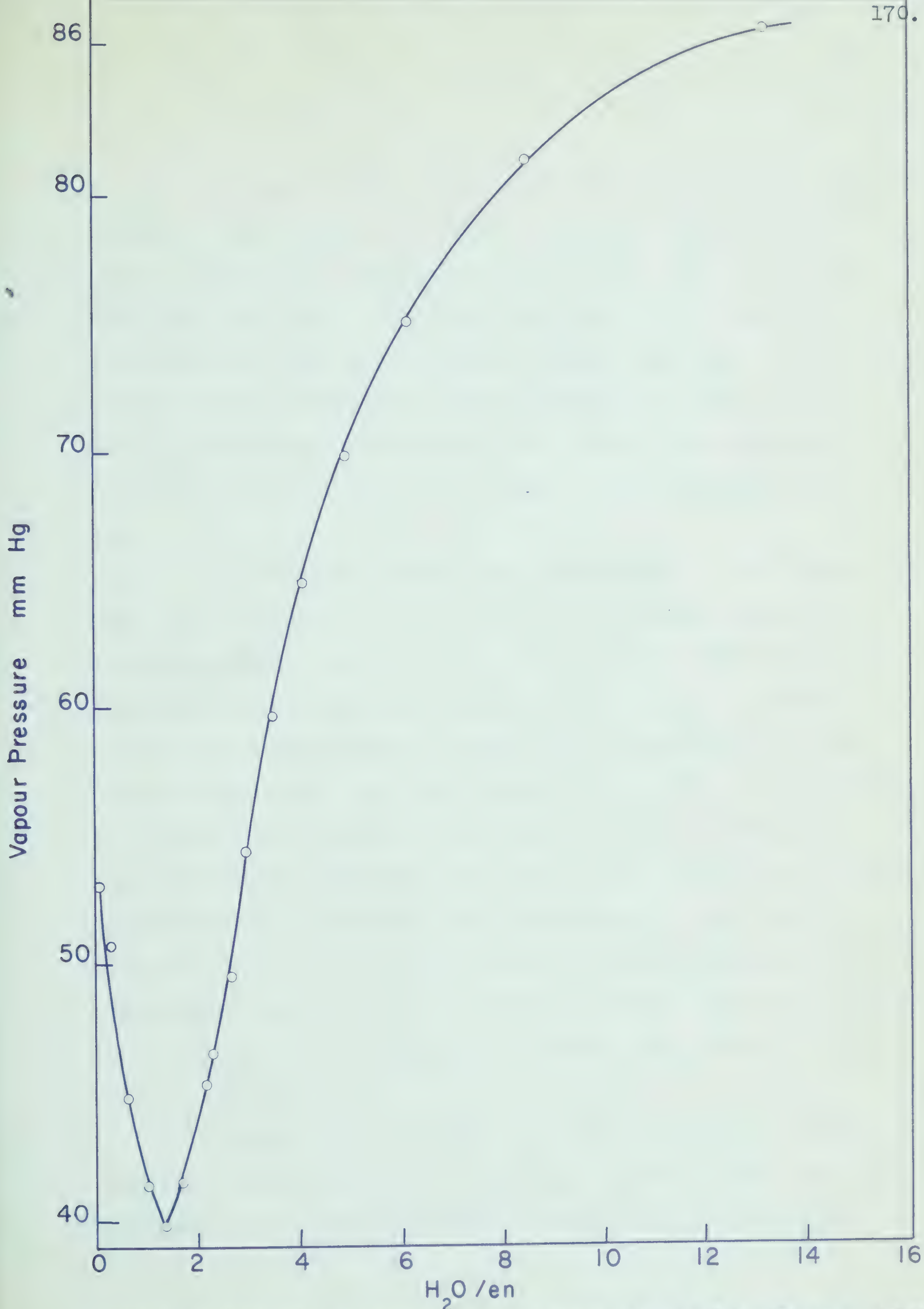
The other apparent inconsistency may also be traceable to a condition of metastability in the system. In Fig. 29 the pressure values recorded in the region of $37 - 40^{\circ}$ appear anomalously high. This will be shown below to be due to liquid crystal formation in the system in this temperature region.

The data shown in Table 11 can be substituted into the Clausius-Clapeyron equation to yield values for the heats of solution of the hydrates. From the slope of the line

representing the solubility behaviour from 27° to 36°C the heat of the solution of $\text{NiCl}_2 \cdot 6\text{H}_2\text{O}$ was calculated to be 1.46 Kcal./mole. From the slope of line representing the solubility behaviour from 40° to 55° the heat of the solution of $\text{NiCl}_2 \cdot 4\text{H}_2\text{O}$ was calculated to be 1.16 Kcal./mole.

If the solution phase is identical irrespective of whether the solid phase is $\text{NiCl}_2 \cdot 6\text{H}_2\text{O}$ or $\text{NiCl}_2 \cdot 4\text{H}_2\text{O}$ then it is possible to use a thermochemical cycle similar to the one used above, together with the heats of solution determined here, to obtain a completely independent check upon the heats of formation of the tetra- and dihydrates. A priori, no difference in the solution phases would be expected. However, it was shown in the course of the present work spectrophotometrically that as the temperature increases to around 90° there is a tendency for chloride to enter the inner coordination sphere. This can be seen from the effect of adding a soluble chloride to an aqueous nickel solution. The peak at 422 m μ gradually shifts upon addition of chloride to about 400 m μ . This same shift in λ_{max} can be observed upon heating a solution of nickel chloride to the vicinity of the boiling point. The spectrophotometric method is however, a very insensitive method for detecting such changes and as a consequence an alternative was sought. The alternative that was finally selected was the displacement of water from the vicinity of the nickel ion by ethylenediamine. It was thought

that the displacement of water molecules by ethylenediamine would result in an increase in the vapour pressure of the system whereas displacement of chloride ions by ethylenediamine should result in a decrease in the vapour pressure of the system. The experimental observations lead to the conclusion that only the former behaviour pattern is apparent. The vapour pressure of the solution increases smoothly until the mole ratio of ethylenediamine to nickel chloride is 2.77. At this mole ratio the solution becomes saturated with respect to tris-ethylenediaminenickel(II) chloride, and further increase of the vapour pressure of the solution beyond this mole ratio is not quantitatively interpretable. However, it should be pointed out that the vapour pressure curve goes through a maximum (Figs. 31, 32 & 33) near a mole ratio of three and then, when excess ethylenediamine is present in the solution, begins to fall in just the way expected for a water-ethylenediamine mixture (Fig. 59a). In spite of the difficulty associated with the separation of solid at the 2.77 mole ratio the use of such a concentrated solution ($\text{H}_2\text{O}/\text{NiCl}_2 = 13.49$) was justified by the objective of the experiment. This was, of course, to investigate the intimate atmosphere of the nickel ion near the solubility limit. This concentration represents a compromise between maintaining a homogeneous mixture over a reasonable range of mole ratio and proximity of the solution investigated to the saturation concentration.



Vapour Pressure - Composition Diagram for H_2O/en System at $50^\circ C$

Fig. 59a

If the initial assumption, that the ethylenediamine displaces water molecules from the solvation sheaths of the ions to the body of the medium, is correct, then it would be expected that, when water molecules bound to the nickel ions are displaced, the vapour pressure should increase. That this expectation is realized is fully evident from Figs. 31, 32 and 33. Evidently the maxima do not occur at the expected en/ NiCl_2 ratio 3:1. The maxima seem to be displaced to about 3.5.

Several conjectures can be offered for the displacement, shown in Figs. 31, 32 and 33, of the maxima above the expected en/ NiCl_2 ratio of 3:1. A part of the ethylenediamine may behave as a unidentate ligand. This assumption however cannot be substantiated and seems highly improbable. It has been observed that, when the composition of the system en/ NiCl_2 lies between 2.56 and 2.77, precipitation of the ethylenediamine complex of nickel chloride takes place and remains for all temperatures. A result of this precipitation would be displacement of water from the secondary solvation sheath. Ethylenediamine beyond the theoretical ratio would further reduce the solubility of the complex and release more solvent to the body of the solution.

Evidently the maxima observed for en/ NiCl_2 remains sensibly constant from 23°C to 50°C . This might mean that the environment of Ni(II) ion remains unaltered throughout this

temperature range. A satisfactory proof that the environment of Ni(II) ion remains unaltered is evident from the results given in Table 27.

From the thermodynamic measurements of the $\text{NiCl}_2\text{-H}_2\text{O}$ system the vapour pressures of homogeneous solutions of various compositions were known at different temperatures (vide Figs. 22 and 23). It was assumed that when the vapour pressures of two systems were identical at a given temperature, their $\text{H}_2\text{O/NiCl}_2$ ratio would be the same. Since vapour pressures corresponding to particular compositions of en/ NiCl_2 were determined in water solution, these were extrapolated to determine the value of $\text{H}_2\text{O/NiCl}_2$ corresponding to this vapour pressure, assuming tacitly that the only phenomenon operative was the release of water molecules to the body of the solution. Now, knowing the initial $\text{H}_2\text{O/NiCl}_2$ ratio and subtracting this from the value obtained by the reaction of aqueous nickel chloride solution with ethylenediamine, the extent of dilution due to release of water can be calculated. This would be made clearer by the sample calculation given below for 27°C .

Composition of initial solution - $\text{H}_2\text{O/NiCl}_2 = 13.49$
Addition of ethylenediamine yielding a ratio of en/ NiCl_2 of 1.26 shows a vapour pressure of 20.70 mm Hg. This corresponds to $\text{H}_2\text{O/NiCl}_2$ of 19.0. Subtracting this from 13.49 the value 5.5 is obtained.

TABLE 27

Release of Water to the Medium by the Reaction of Ethylenediamine with Aqueous Nickel Chloride Solution at Different Temperatures

Initial Mmole ratio $\text{H}_2\text{O}:\text{NiCl}_2$ 13.49:1

Temp ($^{\circ}\text{C}$)	Mmole ratio en/NiCl_2	Corresponding Mmole ratio $\text{H}_2\text{O}/\text{NiCl}_2$	Mean
27	1.26	19.0	
30	1.26	19.2	
35	1.26	19.1	19.0
40	1.26	19.1	
45	1.26	18.9	
50	1.26	19.0	
27	1.91	20.6	
30	1.91	21.1	
35	1.91	20.8	
40	1.91	21.1	20.8
45	1.91	20.6	
50	1.91	20.8	
27	2.00	21.1	
30	2.00	21.6	
35	2.00	21.1	21.3
40	2.00	21.4	
45	2.00	21.1	
50	2.00	21.2	

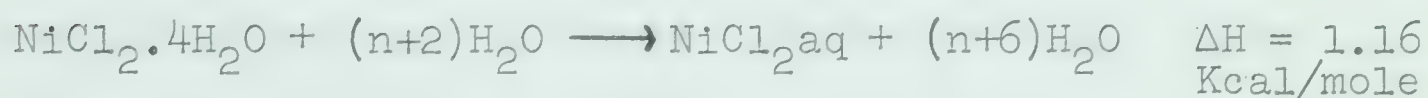
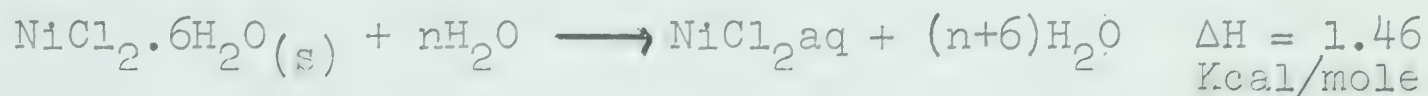
This means the 5.5 moles of water have been released for 1.26 moles of ethylenediamine. On the basis that for each ethylenediamine molecule there should be two water molecules released, the release in this case should be 2.52 moles of water. Thus, the relation between the observed and the expected water released is 2.2.

From Table 27, it can be seen that the water released to the medium remains constant, to a first approximation, throughout the temperature range. It can also be seen from Table 27 that for en/ NiCl_2 ratio of 1.26, 1.91 and 2.00 the ratio of calculated mean value for $\text{H}_2\text{O}/\text{NiCl}_2$ are 19.0, 20.8 and 21.3. On subtracting these values from the initial value of 13.49 the increase in values are 5.5, 7.3 and 7.8. The relation between the observed release of water molecules to those expected are 2.2, 1.92 and 1.95. Thus, the increase of vapour pressure corresponds to the release of approximately twice the expected amount of water. This must mean that the introduction of ethylenediamine causes the displacement of both intimately and tenuously bound water molecules.

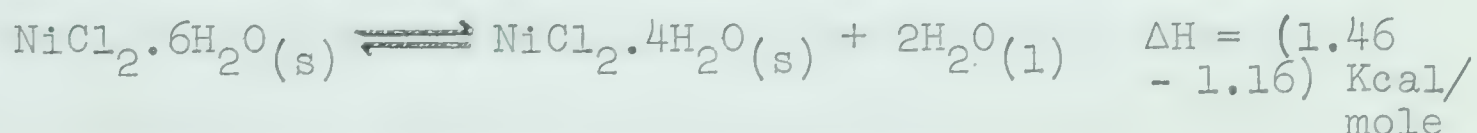
Though it is known that the temperature induced transition in the solid phase from $\text{NiCl}_2 \cdot 6\text{H}_2\text{O}$ to $\text{NiCl}_2 \cdot 4\text{H}_2\text{O}$ occurs around 36.3°C , there was no evidence for such a transition in solution. In solution there are two competing processes occurring, the association of Ni(II) ion with water

and the association with chloride ions. In order that there be a transition of one form into another it is necessary to change the relative free energy of these two association processes in such a way that the free energy decreases with chloride ion association than that with water. So long as the structure of the solid remains constant the free energy of water association remains approximately constant. Since the structure of water does not appreciably change with temperature up to its boiling point it is not surprising that the temperature induced transition was not visible.

In view of this demonstration of the substantial equivalence of the solution species throughout the temperature range of interest, the cycle shown below becomes valid



Since the heat of formation of the solution phase must be the same in each case,



Then, since $\Delta\text{Hf}^\circ_{\text{NiCl}_2 \cdot 6\text{H}_2\text{O}} = -505.8 \text{ Kcal/mole}$

and $\Delta\text{Hf}^\circ_{\text{H}_2\text{O}} = -68.4 \text{ Kcal/mole}$

it can be shown that $\Delta\text{Hf}^\circ_{\text{NiCl}_2 \cdot 4\text{H}_2\text{O}} = -368.7 \text{ Kcal/mole}$. This

value, obtained on the basis of a completely independent method, lends support to both the value for the heat of formation of $\text{NiCl}_2 \cdot 4\text{H}_2\text{O}$ obtained from the vapour pressure measurements (-370.6 Kcal/mole) and to the values for the heats of solution of these two phases. Now, since it was not experimentally convenient to determine a heat of solution value for $\text{NiCl}_2 \cdot 2\text{H}_2\text{O}$ it is probably reasonable to turn the calculation above around and use it to calculate a value for the heat of solution of the dihydrate. When this was done the heat of solution of $\text{NiCl}_2 \cdot 2\text{H}_2\text{O}$ was calculated to be -4.7 Kcal/mole. This does not represent unreasonable agreement with the value of -10.1 Kcal/mole reported for solution in 400 moles of water.

The data obtained from the equilibrium vapour pressure studies in the temperature range 25 to 77° are uniquely explicable on the basis of the existence of only three solid hydrates within this interval. These are $\text{NiCl}_2 \cdot 6\text{H}_2\text{O}$, $\text{NiCl}_2 \cdot 4\text{H}_2\text{O}$ and $\text{NiCl}_2 \cdot 2\text{H}_2\text{O}$. However, the claim has been made (55) that equilibrium studies are insufficiently sensitive to detect hydrates which are closely similar to adjacent hydrates. A differential kinetic technique has been suggested as being capable of supplying this additional sensitivity. The claims which have been made for this technique will be examined in the next section.

Kinetic Studies

From Fig. 36, it is evident that the differential

decomposition curves exhibit maxima and minima. The discontinuities in the rate curve are not very marked when the rate is plotted as weight loss per hour, but become more so when plotted as weight loss per two hours. From the curve it can be seen that such a method of determining whether or not particular hydrates exist would be quite approximate. Even though the temperature was not carefully controlled it can be seen that the type of minima observed by Castor and Basolo (55) for nickel chloride hydrates were not obtained in the present case. For the dehydration of a 6.5437 gm. sample of $\text{NiCl}_2 \cdot 6\text{H}_2\text{O}$ Castor and Basolo observed that, around $\text{NiCl}_2 \cdot 4\text{H}_2\text{O}$ the rate of loss of water was about 6 mg./hr. In the present case, for samples a little less than $1/2$ & $1/4$ of the size, the observed rate was about 12 mg./hr. and showed rather blurred minima. This latter observation is in sharp contrast to that of Castor and Basolo, shown in Fig. 11(1). The difference between the present study and that due to Castor and Basolo can be explained on the basis of the observations of Crowther and Coutts (52) who found that the particle size and the placement of the hydrate do influence the nature of the differential decomposition curve.

The differential decomposition curve obtained by carrying out the dehydration on a quartz spiral balance in an evacuated system containing $\text{Mg}(\text{ClO}_4)_2$ desiccant is even less conclusive. As is evident from Fig. 38, the minimum in

the differential rate curve changes its position with changing time interval. It is probable that the minima are related to the mechanism of the decomposition process rather than to the experimental imprecision and temperature fluctuations.

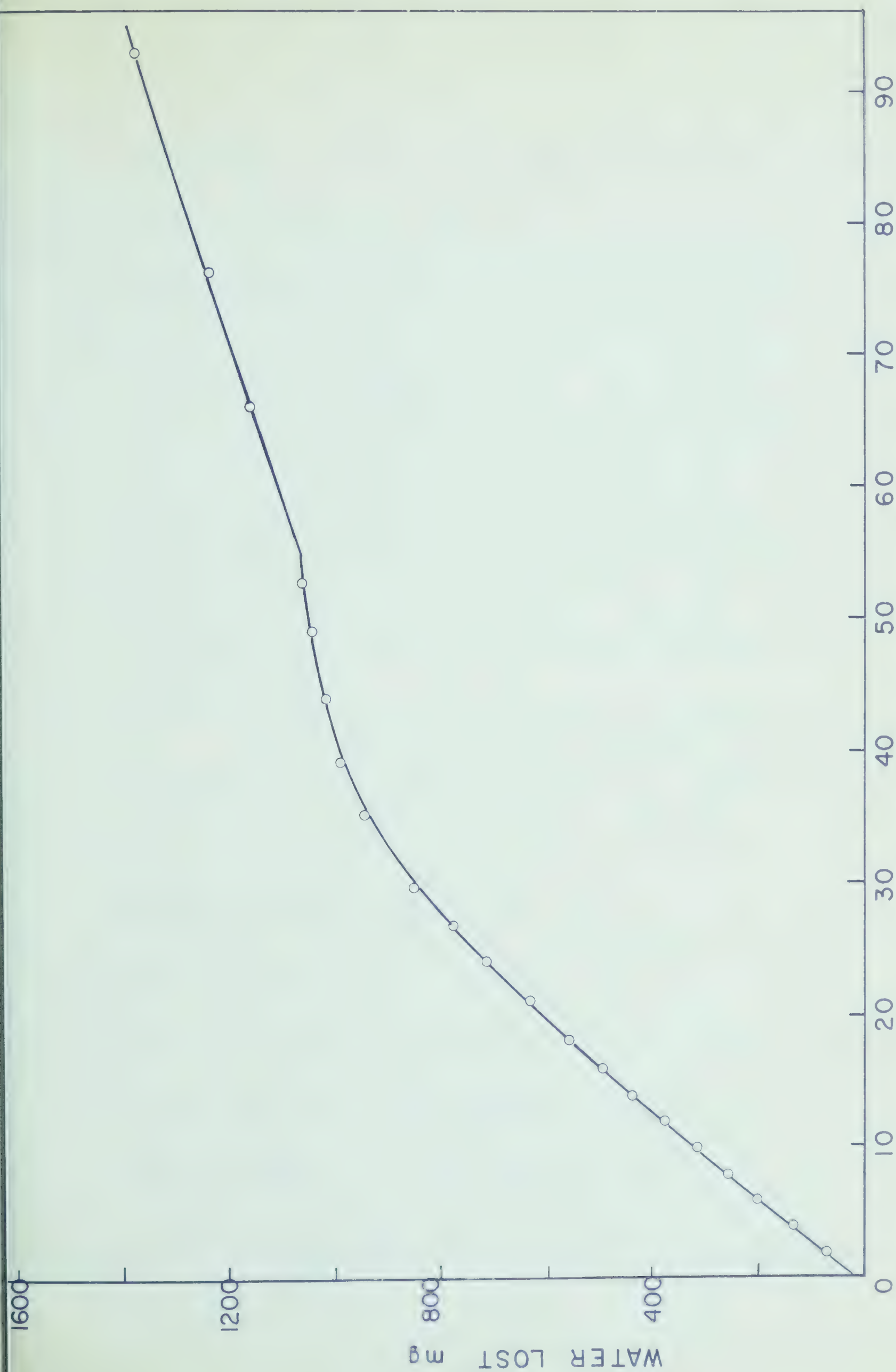
The differential decomposition curves for the controlled temperatures 25°C , 35°C and 45°C for the dehydrations carried out in vacuo on a quartz spiral balance shown in Figs. 42, 43 and 44 clearly demonstrate that the rate of decomposition starts at a low value, passes through a maximum and finally falls off again. Minima are observed to be superimposed on these curves but whether they can be associated with the existence of intermediate hydrates is uncertain. An explanation for the shape of the differential decomposition curve might be found in the changes in the reaction geometry. This suggestion was advanced by Allen (96(a)) for the thermal decomposition of AgO . In physical terms, the reaction occurs via rapid nucleation over the whole surface followed by a rate controlling movement of the reaction interface towards the center of the crystal. The changes in the rate of reaction at different stages were interpreted in terms of the diffuseness of the reaction interface. This interpretation was supported by measurements of surface area and by X-ray measurements. Thus, it is evident that the shape of the differential decomposition curve is markedly dependent on the geometry of the system and that the identification of parti-

cular hydrates on the basis of the position of the minima in the differential decomposition curve is at best uncertain and reporting new hydrates on this basis alone is rather presumptuous.

It is generally observed that the integral decomposition curves may be divided into a linear and a nonlinear part. It is seen in Figs. 39, 40, and 41 that the curves remain sensibly linear to the point corresponding approximately to 50% decomposition, considering the conversion of $\text{NiCl}_2 \cdot 6\text{H}_2\text{O}$ to $\text{NiCl}_2 \cdot 2\text{H}_2\text{O}$ to represent 100%. The linear part could then correspond to the decomposition of $\text{NiCl}_2 \cdot 6\text{H}_2\text{O}$ into $\text{NiCl}_2 \cdot 4\text{H}_2\text{O}$. For this portion of the decomposition an apparently zero order rate law is observed. Beyond 50% decomposition the curve bends and the overall shape is typically sigmoid. For the bent part of the decomposition curve a first order rate law is observed till about 75% decomposition ($\text{NiCl}_2 \cdot 3\text{H}_2\text{O}$) followed by a second first order portion which persists down to about 95% decomposition. If these are significant they could mean intermediate formation of $\text{NiCl}_2 \cdot 3\text{H}_2\text{O}$ which then decomposes by another first order process with a different rate constant. Since there is no other evidence to indicate the existence of $\text{NiCl}_2 \cdot 3\text{H}_2\text{O}$ this observation must be weighted only lightly and other explanations for the behaviour sought. There is a possibility that this behaviour is related to structure.

The structures of $\text{NiCl}_2 \cdot 4\text{H}_2\text{O}$ and $\text{NiCl}_2 \cdot 2\text{H}_2\text{O}$ are entirely dissimilar (vide Structural Studies) and as a result the transformation from one to the other would involve a considerable migration of ions and molecules. On this basis it is not difficult to conceive that the decomposition of the hexahydrate should occur by a different process from the decomposition of the tetrahydrate. Furthermore, if the rearrangement of the lattice is involved in the rate determining step of the tetrahydrate decomposition, the reaction could be extremely complex and the observation that this portion of the curve is separable into two first order portions purely fortuitous.

The integral decomposition curve plotted from the data of Castor (56) is shown in Fig. 59b. The portion corresponding to the conversion of $\text{NiCl}_2 \cdot 6\text{H}_2\text{O}$ to $\text{NiCl}_2 \cdot 4\text{H}_2\text{O}$ is sensibly linear and similar in appearance to that obtained in the present study. However, at a composition corresponding to approximately $\text{NiCl}_2 \cdot 3.5\text{H}_2\text{O}$ there is a conspicuous break in the curve. The second portion of the curve begins linearly and if extended further it would presumably appear similar in shape to the first part. Thus, the complete curve has the appearance of two superimposed sigmoid curves of the usually observed type. A distinction is apparent in the integral decomposition curves observed in this study and in that due to Castor and Basolo (55). The explanation offered for



the difference in the differential decomposition curves is equally applicable to the integral decomposition.

If the contracting envelope picture suggested by Taylor and Taylor is correct it should be possible to obtain a mathematical expression from such a model which reproduces the experimental results (96(b)). This envelope may have any shape, but it is convenient for the present purpose to assume some regular geometrical shape. A sphere has the most symmetrical shape and has the smallest surface area to volume ratio. Hence the decomposing particles of $\text{NiCl}_2 \cdot 6\text{H}_2\text{O}$ are probably closer to spherical than to any other regular shape. Consequently the derivation given below is based upon a spherical model.

Let n = number of molecular units in the surface area, $\frac{dn}{dt}$ = rate of change with time = kn , where k = Pseudo rate constant. Area = $4\pi r^2$; Volume = $\frac{4}{3}\pi r^3$

$$\frac{\text{Number on surface}}{\text{Number in total}} = \frac{4\pi r^2}{\frac{4}{3}\pi r^3} = \frac{3}{r} ;$$

$$\text{Number on surface} = \frac{3}{r} \cdot \text{total} = \frac{3}{r} \cdot N_T$$

$$\frac{dn}{dt} = k \cdot \frac{3}{r} \cdot N_T ; rdn = 3k \cdot N_T \cdot dt ; N = \text{number of particles}$$

$$N = \frac{4}{3} \cdot \frac{N \cdot \pi \cdot r^3 \cdot \rho}{M} \quad \begin{array}{l} N = \text{Avogadro's number;} \\ M = \text{Molecular weight} \end{array} \quad \rho = \text{density}$$

$$\text{Thus, } \frac{4}{3} \cdot \frac{N \cdot \pi \cdot \rho}{M} \cdot r \cdot dr^3 = 3k \cdot N_T \cdot dt$$

$$r \cdot dr^3 = \frac{9k \cdot M \cdot N_T \cdot dt}{4N \cdot \pi \cdot \rho} ; \quad 3r^3 \cdot dr = \frac{9k \cdot M \cdot N_T \cdot dt}{4N \cdot \pi \cdot \rho}$$

On integration between the limits 1 and 2;

$$\frac{3}{4}(r_2^4 - r_1^4) = \frac{9k \cdot M \cdot N_T}{4N \cdot \pi \cdot \rho} \cdot t$$

$$\frac{3}{4} r_2^4 - \frac{3}{4} r_1^4 = \frac{9kMN_T}{4N\pi\rho} \cdot t. \quad \text{Rearranging,}$$

$$\frac{3}{4} \cdot \frac{4\pi N \rho r_2^4}{M} - \frac{3}{4} \cdot \frac{4\pi N \rho r_1^4}{M} = 9kN_T \cdot t$$

$$\frac{9}{4} \cdot r_2 \cdot \frac{4}{3} \frac{\pi N \rho r_2^3}{M} - \frac{9}{4} r_1 \cdot \frac{4}{3} \frac{\pi N \rho r_1^3}{M} = 9kN_T \cdot t$$

N_1 = number of particles at time 1; N_2 = number of particles at time 2.

$$\frac{9}{4} r_2 \cdot N_2 - \frac{9}{4} r_1 \cdot N_1 = 9kN_T \cdot t; \quad r_2 \cdot N_2 - r_1 N_1 = 4kN_T \cdot t$$

$$r_2 \cdot N_2 = 4kN_T t + r_1 N_1. \quad (\text{At the start } N_1 = N_T) = 4kN_T \cdot t + r_1 N_T = N_T(4kt + r_1)$$

$$N_2 = \frac{N_T(4kt + r_1)}{r_2}$$

Let α = fraction decomposed

$\frac{N_1}{N_2}$ = ratio of total number of particles of nickel chloride hexahydrate.

$$\alpha = \frac{4kt + r_1}{r_2} = \frac{4kt}{r_2} + \frac{r_1}{r_2}$$

It can be shown that for 50% decomposition the deviation from linearity is small (ca 20%) provided that the decomposing particles all lie in narrow size range. In the

case in question the particles fell in the range 105 to 150 μ .

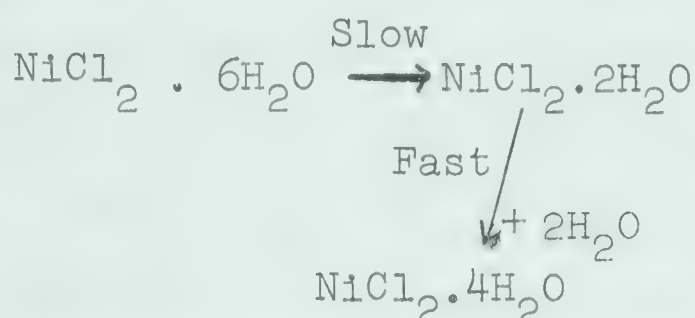
This expression fits a rate law similar in shape to that which is observed. However, such a rate law suggests continuous dehydration in proceeding from $\text{NiCl}_2 \cdot 6\text{H}_2\text{O}$ to $\text{NiCl}_2 \cdot 2\text{H}_2\text{O}$. Continuous dehydration, however, is not consistent with the present data.

The dehydration of $\text{NiCl}_2 \cdot 6\text{H}_2\text{O}$ to the final product $\text{NiCl}_2 \cdot 2\text{H}_2\text{O}$ might follow either of the two paths; direct decomposition or decomposition through intermediates. Evidence from X-ray diffraction powder patterns for different stages of dehydration (Figs. 57 and 58) from infrared absorption spectra (Figs. 54 and 55) and from the kinetic evidence (Figs. 39, 40 and 41), indicate that the decomposition scheme is:

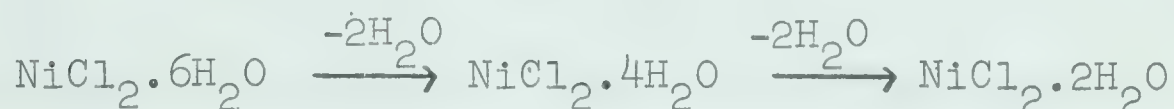


Thus, in each case there is evidence for the disappearance of $\text{NiCl}_2 \cdot 6\text{H}_2\text{O}$ and the concurrent appearance of $\text{NiCl}_2 \cdot 4\text{H}_2\text{O}$. In no case is there evidence for $\text{NiCl}_2 \cdot 2\text{H}_2\text{O}$ in the sample prior to the complete conversion of $\text{NiCl}_2 \cdot 6\text{H}_2\text{O}$ to $\text{NiCl}_2 \cdot 4\text{H}_2\text{O}$. Then, once the sample has passed through the first dehydration step, the dihydrate begins to appear as product. This stepwise decomposition scheme, at first glance, seems to be at variance with the near identity of the equilibrium vapour pressures of the hexahydrate and of the tetrahydrate. There

is, however, no apriori reason for a relationship between the equilibrium vapour pressure (a thermodynamic quantity) and the rate of decomposition (a kinetic quantity). The evidence to rule out the possibility of a reaction mechanism as:



is that the process of rehydration is very slow as seen in the present study. Obviously the mechanism would then be:



The rate of decomposition depends largely on the activation energies for the processes involved and the mechanism of the migration of water molecules through the solid phase.

The observations on the dehydrations performed under a variety of different relative humidities offer additional insight into the reaction mechanism.

Evidently the relative humidity of the atmosphere plays a very important role in determining both the rate of dehydration and the shape of the integral dehydration curve. When the specific gravity of the H_2SO_4 desiccant is 1.40 the extent of decomposition is initially linearly dependent

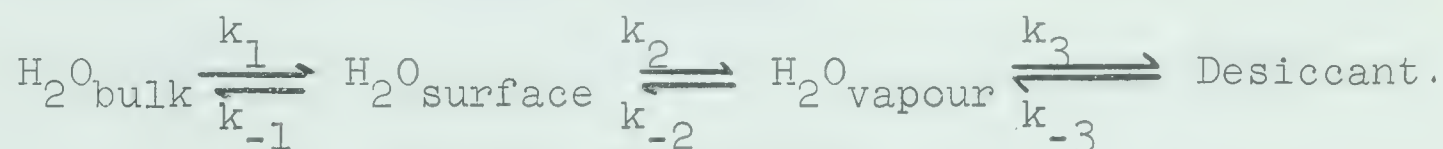
upon time. At a composition corresponding to $\text{NiCl}_2 \cdot 5.65\text{H}_2\text{O}$, there is a sharp decrease in the rate of decomposition which produces a marked discontinuity in the curve. This could be due to some adsorbed water present with the starting material and could also be due to a small change in the desiccant composition. The end product at room temperature is $\text{NiCl}_2 \cdot 4\text{H}_2\text{O}$. The decomposition curve for the H_2SO_4 desiccant of specific gravity 1.50, shown in Fig. 46(2), can be seen to possess some of the characteristics of the curves obtained at both higher and lower relative humidities. Superposition of curves 1 and 3 in Fig. 46 would result in curve 2. The final product was $\text{NiCl}_2 \cdot 2\text{H}_2\text{O}$, but about 96 hours were required for the sample to reach this composition. The decomposition curves for H_2SO_4 desiccants of specific gravity 1.60, 1.70 and 1.80 are shown in Fig. 47. These have the same general shape as those obtained with anhydrous magnesium perchlorate and phosphorous pentoxide desiccants.

From Table 21, it is evident that the rate of loss of water increases progressively with the decrease in the relative humidity.

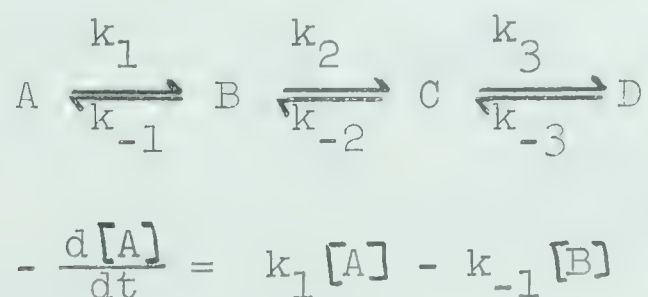
The equilibrium vapour pressures of water above H_2SO_4 (sp. gr. 1.84), $\text{Mg}(\text{ClO}_4)_2$ and P_2O_5 , in terms of $\text{mgH}_2\text{O}/\text{liter}$ at 25°C , are 3×10^{-3} , $< 5 \times 10^{-4}$ and $< 5 \times 10^{-5}$, respectively. Evidently the efficiencies of these desiccants are quite comparable and the difference will not be shown on

the relative humidity scale used here. With this in mind the dehydration rates for $\text{Mg}(\text{ClO}_4)_2$ and P_2O_5 are also shown in Fig. 48 to give an idea of their position relative to the other desiccants. These fall on the same curve. The points lie quite close to that for H_2SO_4 of specific gravity 1.84. This is quite understandable in terms of the low vapour pressure of water in equilibrium with the desiccants.

From this it can be inferred that the rate controlling step at higher humidity is the evaporation of the water molecules from the surface of the crystal. When the relative humidity is high the surface layers of the individual crystallites contain significant quantities of vapourizable water. It is suggested that loss of water by hydrate means loss of water from the surface of individual crystallites. The essential processes which occur can be represented as



In a physical sense, this means that water from the crystal hydrate diffuses to the surface, then becomes free vapour and is subsequently absorbed in the desiccant. For mathematical convenience let this be written as :



Assuming B, C and D in equilibrium, then

$$k_2[B] - k_{-2}[C] = 0 \quad \text{or} \quad [B] = \frac{k_{-2}}{k_2} [C]$$

$$k_3[C] - k_{-3}[D] = 0 \quad \text{or} \quad [C] = \frac{k_{-3}}{k_3} [D]$$

$$\frac{-d[A]}{dt} = k_1[A] - k_{-1} \times \frac{k_{-2}}{k_2} [C]$$

$$\frac{-d[A]}{dt} = k_1[A] - k_4[C] \quad \text{where } k_4 = \frac{k_{-1} \cdot k_{-2}}{k_2}$$

This means that a plot of $\frac{-d[A]}{dt}$ versus $[C]$ should give a straight line. The plot is shown in Fig. 60 and it can be seen that it is not a straight line. This means that simple evaporation from the surface cannot be rate controlling.

Assuming now a Langmuir type dependence to be valid for the process $B \rightleftharpoons C$, i.e. $H_2O_{\text{surface}} \rightleftharpoons H_2O_{\text{vapour}}$, the observations can be critically analyzed.

Suppose θ is the fraction of the surface covered, then $(1 - \theta)$ is the remaining surface and $[B]$ is proportional to θ . According to Langmuir type dependence:

$$k_2 = k_{-2}(1 - \theta) [C]$$

$$k_2 = k_{-2} \cdot [C] - k_{-2}\theta[C]$$

$$\theta(k_2 + k_{-2}[C]) = k_{-2}[C]$$

$$\theta = \frac{k_{-2}[C]}{k_2 + k_{-2}[C]}$$

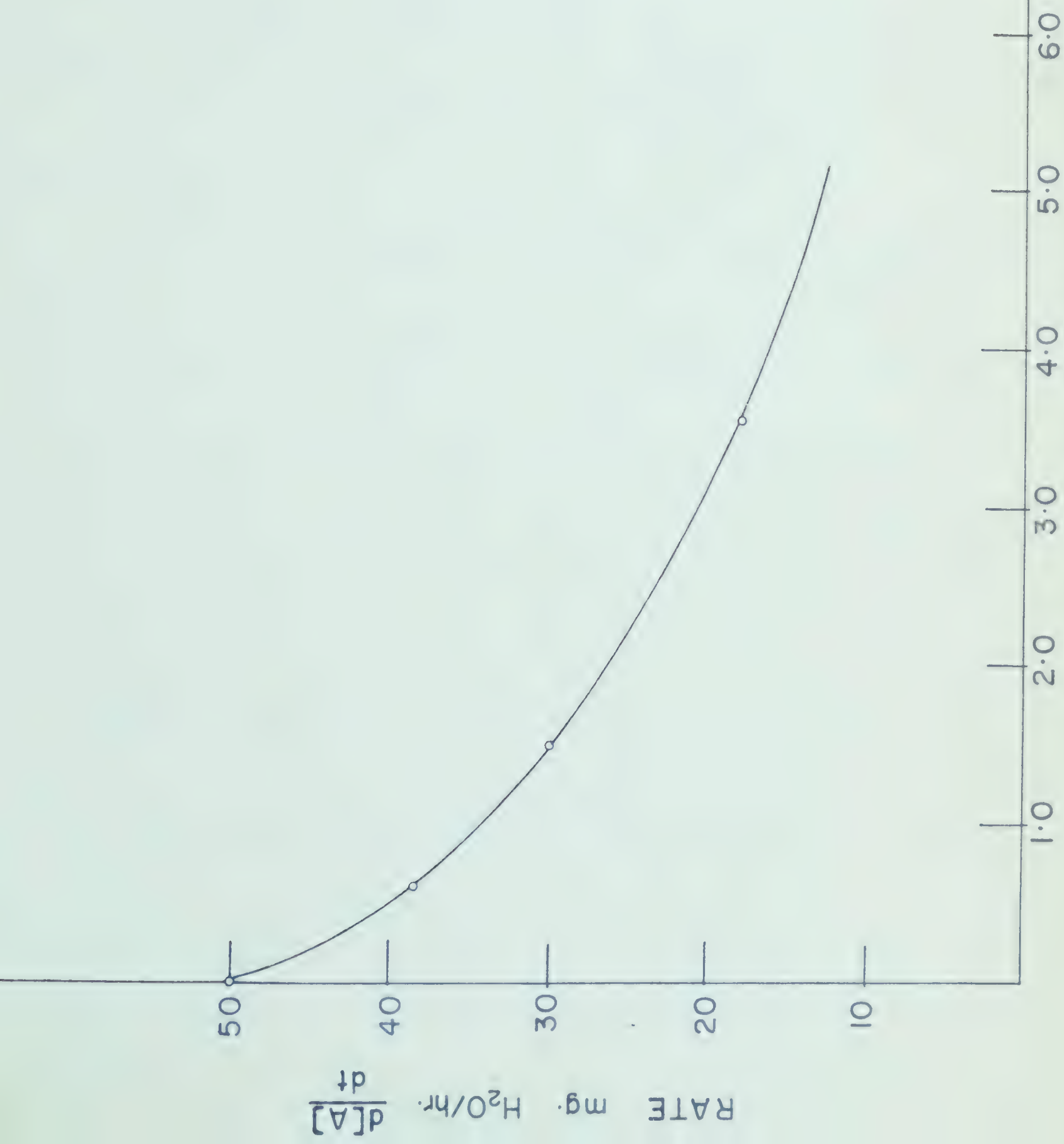


Fig. 60

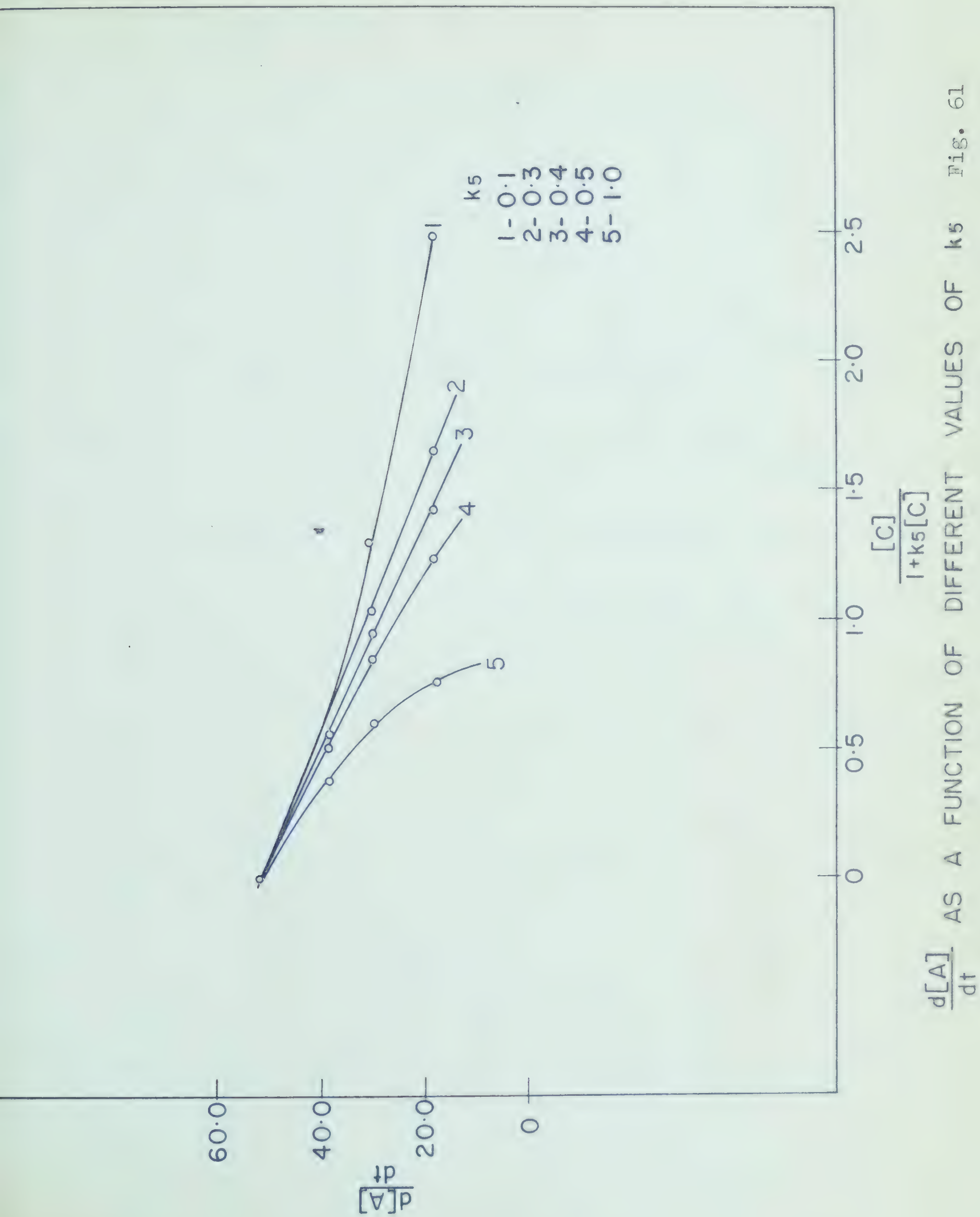
$$\theta = \frac{\frac{k_{-2}}{k_2} [C]}{1 + \frac{k_{-2}}{k_2} [C]}$$

Since $\theta \propto [B]$

$[B] = K \theta$ where K = proportionality constant

$$\begin{aligned} -\frac{d[A]}{dt} &= k_1[A] - k_{-1}[B] \\ &= k_1[A] - k_{-1} \times K \times \frac{\frac{k_{-2}}{k_2} [C]}{1 + \frac{k_{-2}}{k_2} [C]} \\ &= k_1[A] - \frac{K \cdot k_4 [C]}{1 + k_5 [C]} \quad \text{where } k_4 = \frac{k_{-1} \cdot k_{-2}}{k_2} \\ &\quad \text{and} \\ &= k_1[A] - K \cdot k_4 \cdot \frac{[C]}{1 + k_5 [C]} \quad k_5 = \frac{k_{-2}}{k_2} \end{aligned}$$

Now, the plot of $-\frac{d[A]}{dt}$ versus $\frac{[C]}{1 + k_5 [C]}$ where k_5 is arbitrarily assumed to have values between 0.1 and 1.0 is shown in Fig. 61. It is seen that when the value of k_5 lies between 0.3 to 0.4 a straight line relationship is observed whereas for higher or lower values a curvature of the line is observed. This must mean that the Langmuir type dependence is valid for $k_5 = 0.3$ or 0.4 . Since $k_5 = \frac{k_{-2}}{k_2}$ the equilibrium constant for the process $B \rightleftharpoons C$; $\frac{k_2}{k_{-2}} \approx 3$. The slope of the straight line is -20.4 mg/hr.mm.



$$\text{Thus, slope} = K.k_4 = 20.4$$

$$20.4 = K \cdot \frac{k_{-1}.k_{-2}}{k_2}$$

$$\text{For } \frac{k_{-2}}{k_2} = 0.4$$

$$K.k_{-1} = \frac{20.4}{0.4}$$

$$= 51 \text{ A.U.} \quad \text{A.U.} = \text{Arbitrary Unit}$$

$$\text{The intercept} = 51.4 \text{ mg/hr} = k_1[A]$$

$$\text{Thus } \frac{k_1[A]}{K.k_{-1}} = \frac{51.4}{51} \text{ A.U.} \quad \text{A.U.} = \text{Another Arbitrary Unit}$$

$$B \cdot \frac{k_1}{k_{-1}} \approx 1 \quad \text{where } B \text{ is another constant} = \frac{[A]}{K}$$

If the value of B were unity, the value of $\frac{k_1}{k_{-1}}$ would also be unity. This would mean that the rate constant for water molecules to diffuse out of the crystal would be equal to that for diffusion into the crystal. Since the values of K and [A] are not known, it is difficult to say anything more. K could be easily obtained by conventional gas absorption measurements for the determination of surface area.

The rate expression

$$-\frac{d[A]}{dt} = k_1[A] - k_4[C]$$

means that the greater is the value of [C], i.e. the greater

is the relative humidity, the slower is the rate of dehydration. At very low relative humidities the value of $[C]$ is so small that the rate expression reduces to

$$-\frac{1}{dt} [A] = k_1 [A]$$

These rate expressions have been substantiated by the experimental measurements. Thus, at higher desiccant efficiency the rate determining step is the rate of diffusion of water to the surface and at lower desiccant efficiency the rate determining step is the evaporation of water from the surface of the crystals.

In conclusion it can be said that there is no basis for the existence of hydrates like $\text{NiCl}_2 \cdot 5\text{H}_2\text{O}$ and $\text{NiCl}_2 \cdot 5.5\text{H}_2\text{O}$ as propounded by Castor and Basolo (55) and the differential kinetic technique does not appear to be a rigorously valid criteria to exhibit the presence of all decomposing hydrates. The evidence mentioned hitherto strongly suggests that the only hydrates of nickel chloride are: $\text{NiCl}_2 \cdot 6\text{H}_2\text{O}$, $\text{NiCl}_2 \cdot 4\text{H}_2\text{O}$ and $\text{NiCl}_2 \cdot 2\text{H}_2\text{O}$.

Structural Studies

Any attempt to come to grips with the factors underlying the course of dehydration and the reasons for the stability of one composition in relation to another must have its roots in an understanding of the structural parameters invol-

ved. This section is intended to point out and to estimate the importance of such factors. Particular stress will be laid upon hydrogen bonding.

In the hydrates of nickel chloride the possible hydrogen bonding interactions are O-H..O and O-H..Cl. The relative importance of each of these depends upon the orientation of water molecules and chloride ions in the unit cell. Consequently, before the infrared spectra associated with different hydrates are considered, it would be advantageous to discuss briefly the crystal structure of the hydrates of nickel chloride in terms of the orientation of water molecules and chloride ions to be able to decide the nature of hydrogen bonding present in each case.

The crystal structure of $\text{NiCl}_2 \cdot 6\text{H}_2\text{O}$ is known (97) and it has been shown to be isomorphous with $\text{CoCl}_2 \cdot 6\text{H}_2\text{O}$ (98) whose crystal structure is also known (57). In view of this isomorphism the orientation of water molecules and chloride ions are similar in both $\text{CoCl}_2 \cdot 6\text{H}_2\text{O}$ and $\text{NiCl}_2 \cdot 6\text{H}_2\text{O}$. A portion of a $\text{CoCl}_2 \cdot 6\text{H}_2\text{O}$ structural unit is shown in Fig. 62.

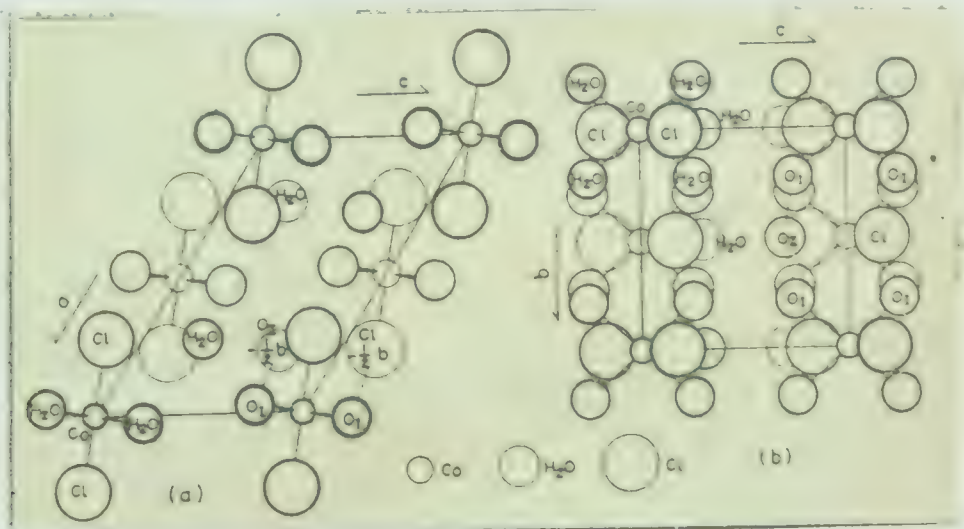


Fig. 62

The arrangement of atoms projected (a) on (010) and (b) on (100). Broken lines represent the hydrogen bond.

Four water molecules are seen to be arranged in a square plane around the cobalt(II) ion and the two chloride ions are placed one above and one below the plane and lying on a line perpendicular to the plane and passing through its center. Thus, four water molecules and two chloride ions surround the cobalt in an octahedral configuration. These octahedra and the remaining pair of water molecules pack together to produce the observed crystal lattice. The water molecules are seen to occupy two types of environment in the lattice. In the one water molecules are held primarily through interaction with the metal ion. In the other they are held primarily by dipole forces acting upon the adjacent chloride ions and water molecules. The units pack in such a way that both O-H...O and O-H...Cl interactions are possible.

The crystal structure of $\text{NiCl}_2 \cdot 4\text{H}_2\text{O}$ is not known nor is the crystal structure of any system isomorphous with it. However, it can be imagined to be derived from $\text{NiCl}_2 \cdot 6\text{H}_2\text{O}$ by removing the two water molecules not directly linked to the metal ion and sliding the octahedra of adjacent layers closer together. An approximate picture is shown in Fig. 63. The suggested similarity in the structure of $\text{NiCl}_2 \cdot 6\text{H}_2\text{O}$ and $\text{NiCl}_2 \cdot 4\text{H}_2\text{O}$ is substantiated by the similarity of their powder X-ray diffraction patterns (Fig. 56).

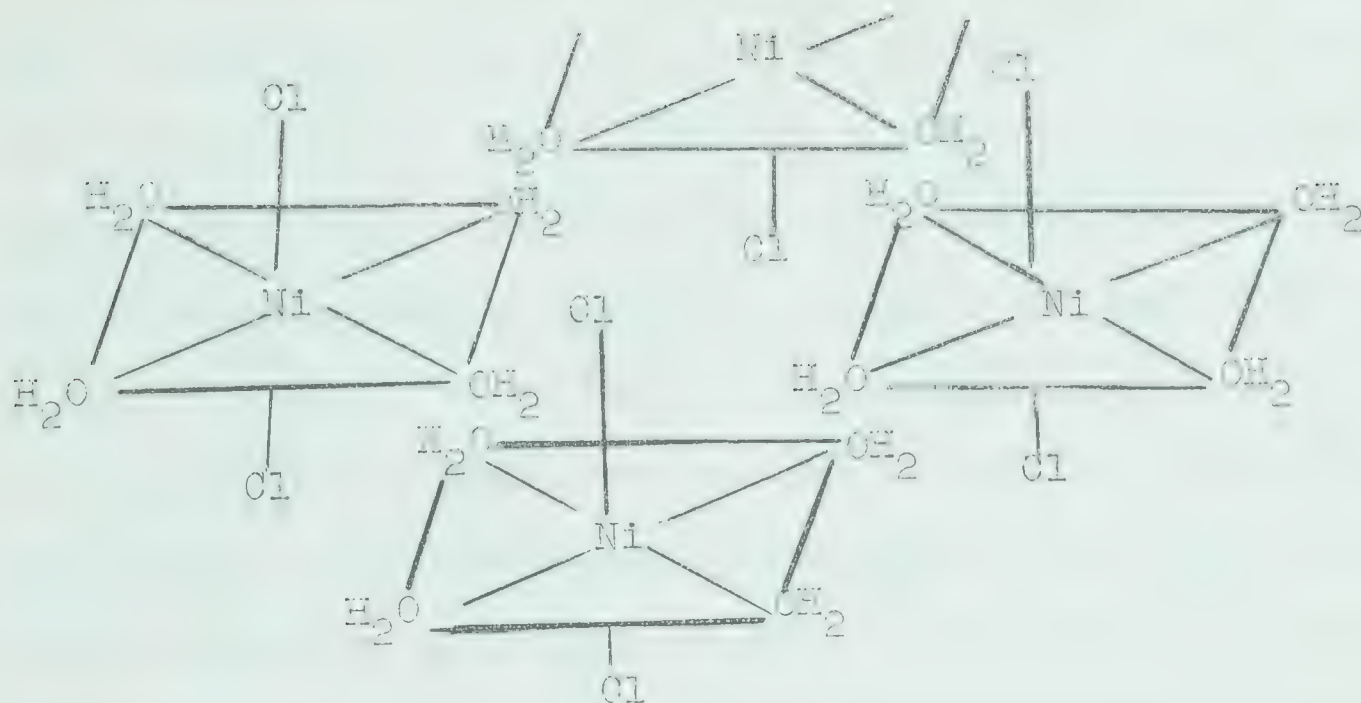


Fig. 63

The crystal structure of $\text{NiCl}_2 \cdot 2\text{H}_2\text{O}$ is known (99). The orientation of water molecules and chloride ions is shown in Fig. 64.

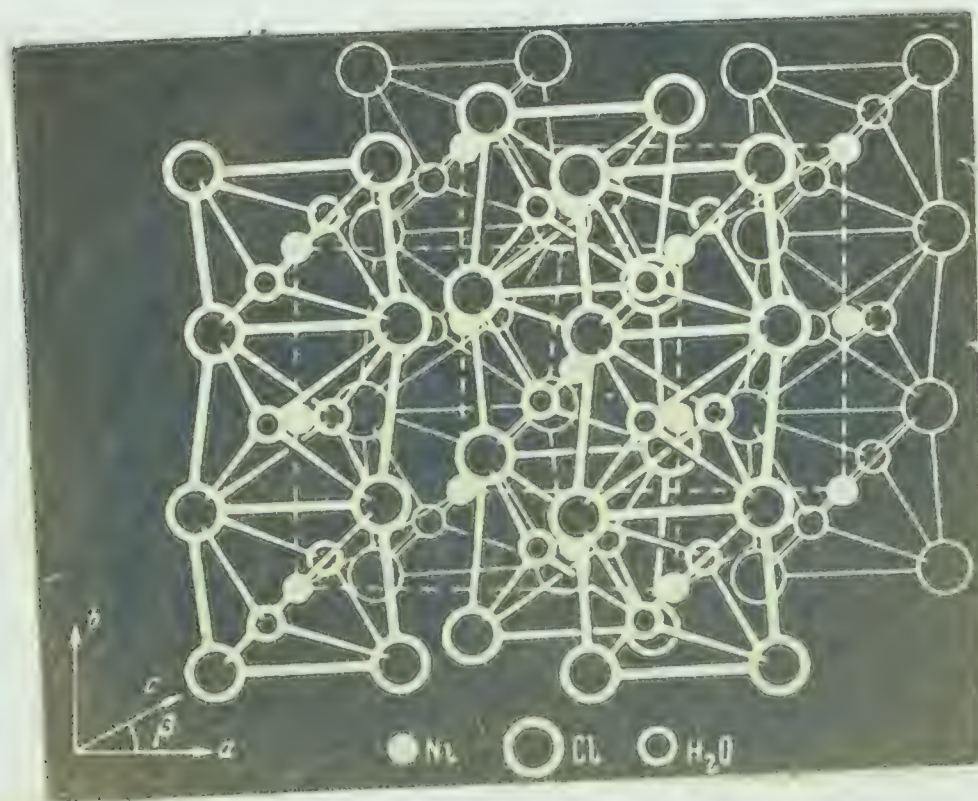


Fig. 64

In this case four chloride ions lie in one plane occupying four coordination positions and the two water molecules lie one above and the other below the plane in the other two octahedral positions. These linear chlorine bridged polymers are packed in the lattice in such a manner that each water has eight chloride ions as nearest neighbours. In a structure of this kind the likelihood of water to water interaction is very small. The predominant hydrogen bonding must be O-H...Cl. This interaction is weak compared to the O-H...O interaction and would not be expected to contribute greatly to the energy of the system. From the above discussions of the structure of the hydrates of nickel chloride it is evident that the three hydrates are closely related and transition from one structure to the next can be easily visualized as shown in Fig. 65.

There are three important regions in the infrared spectra of the hydrates of nickel chloride. A broad unassigned band at 800 cm^{-1} , the O-H bending region around 1600 cm^{-1} and the O-H stretching region around 3500 cm^{-1} .

The band at 810 cm^{-1} is seen, in Fig. 52, to be present in the absorption spectrum of $\text{NiCl}_2 \cdot 6\text{H}_2\text{O}$ but not in those of $\text{NiCl}_2 \cdot 4\text{H}_2\text{O}$ or $\text{NiCl}_2 \cdot 2\text{H}_2\text{O}$. There is an indication that the intensity of this band decreases as the composition of the system is altered in the direction indicated by the reaction

$$\text{NiCl}_2 \cdot 6\text{H}_2\text{O} \longrightarrow \text{NiCl}_2 \cdot 4\text{H}_2\text{O} .$$

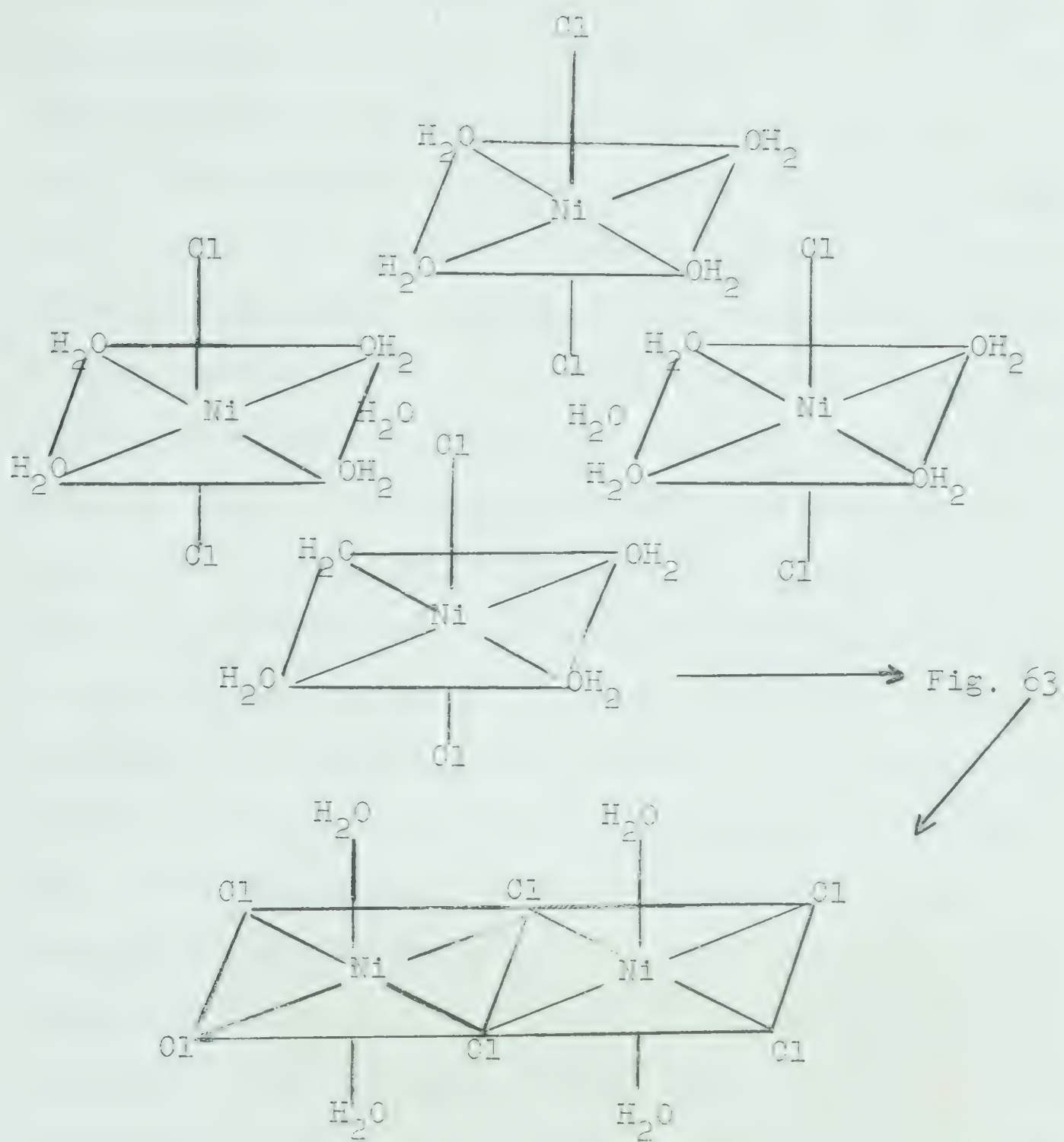
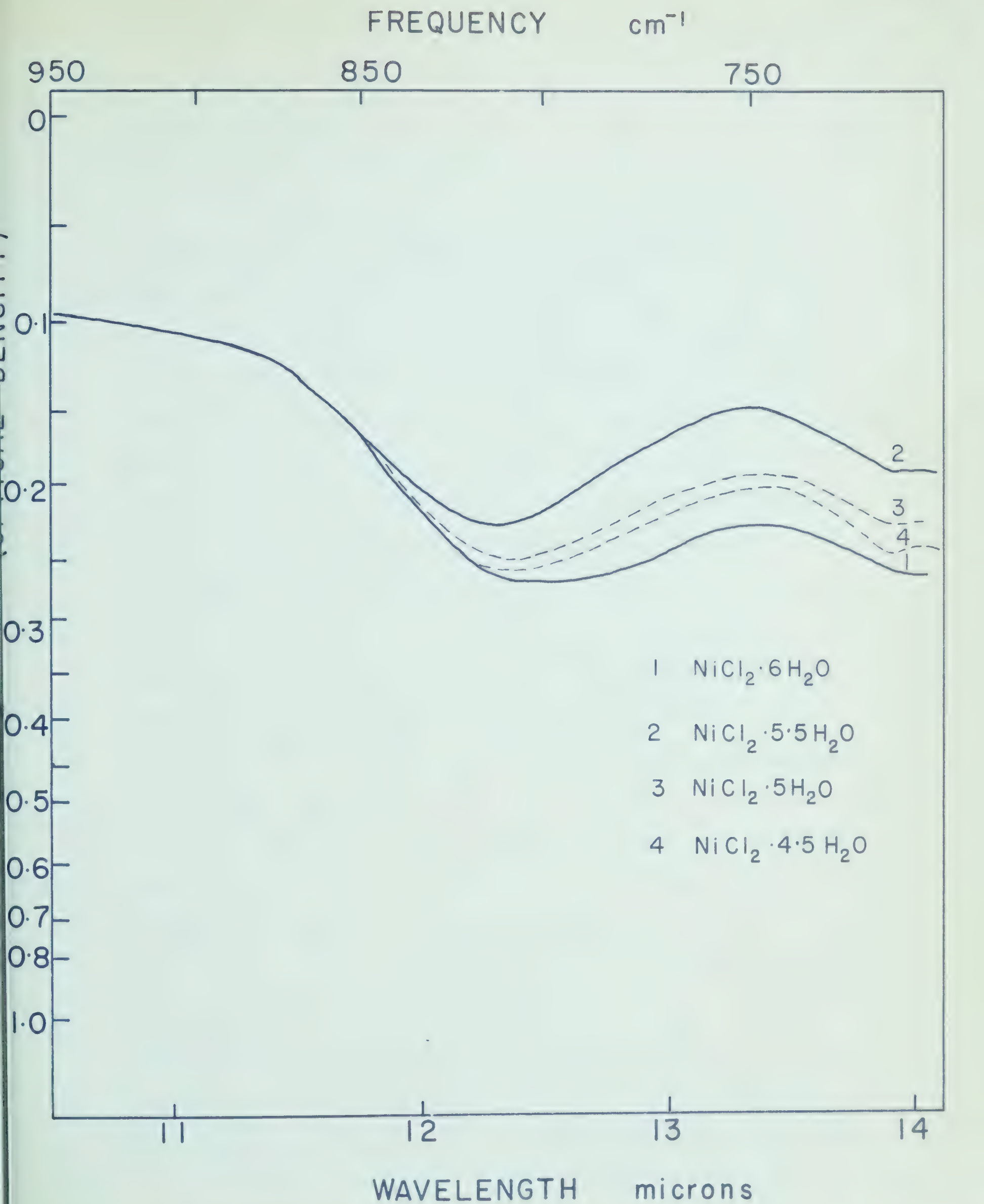


Fig. 65

Unfortunately, this intensity change is not well documented because of the difficulty of preparing Nujol mulls with quantitatively identical amounts of absorbing species in the light path. These spectra are shown in Fig. 66. The spectra shown in Fig. 52 indicate different placement of water molecules in $\text{NiCl}_2 \cdot 6\text{H}_2\text{O}$ as compared with $\text{NiCl}_2 \cdot 4\text{H}_2\text{O}$. Fujita, Nakamoto and Kobayashi (90) observed similar water band in solid aquo complexes. Although this band has not been identified, it seems to be associated with the metal-oxygen interaction and normally falls in the $300 - 500 \text{ cm}^{-1}$ region which is not accessible with NaCl optics. In those cases where it is observed in the 800 cm^{-1} region, there is structural evidence for the presence of two kinds of water molecules, one situated in such a position as to be able to interact directly with the metal ion and the other in a position particularly favourable for hydrogen bonding. Thus, the band at 800 cm^{-1} region has been ascribed to a kind of cooperative effect of coordination and hydrogen bonding responsible for shifting the band from its normal position. When either of these two conditions are absent the absorption band does not appear in the sodium chloride region. Consequently the appearance of this band should represent a sensitive test for non-coordinated water and an indication of two types of water molecules in the system. The presence of the band at 800 cm^{-1} region in the infrared spectrum of $\text{NiCl}_2 \cdot 6\text{H}_2\text{O}$ is additional direct evidence



INFRARED ABSORPTION SPECTRA OF NICKEL CHLORIDE HYDRATES

for both coordinated and hydrogen bonded water in the structure of this material.

The spectra at different stages of hydration are shown in Fig. 54, for the O-H bending region shifted in the transmittance scale for clear representation. For $\text{NiCl}_2 \cdot 6\text{H}_2\text{O}$ the band at 1600 cm^{-1} is quite broad. The broadening may be due to strong hydrogen bonding facilitated by favourable orientation of water molecules or overlap of two O-H bending modes originating from two different environments of water molecules in the crystal lattice. As the water content approaches $\text{NiCl}_2 \cdot 4\text{H}_2\text{O}$ the band becomes less diffuse and finally a shoulder appears at 1655 cm^{-1} and a sharp band at 1605 cm^{-1} . As the water content falls below that corresponding to $\text{NiCl}_2 \cdot 4\text{H}_2\text{O}$, the shoulder decreases in intensity and finally disappears at a composition corresponding to $\text{NiCl}_2 \cdot 2\text{H}_2\text{O}$. The band at 1605 cm^{-1} for $\text{NiCl}_2 \cdot 2\text{H}_2\text{O}$ is sharp and intense compared to all other hydrates. These observations are consistent with the successive preferential disappearance of two kinds of modifying environments. The sharpness of the band indicates increasing isolation of the water molecules within the structural unit. In $\text{NiCl}_2 \cdot 2\text{H}_2\text{O}$ there is only a remote possibility of strong hydrogen bonding of the O-H...O type. Finally the progressive nature of the changes indicate that there is no time dependence in the interconversion between structure types. As a consequence one is always dealing with essentially an

equilibrium mixture of the two structures or at least of the two structural environments.

The effect of hydrogen bonding is more prominent in the region of O-H stretching frequency than at any other frequency. It is the bands at this region that have been most used for correlation with other physicochemical properties of hydrogen bonded systems. Considerable changes take place in the frequency and the intensity of vibrations. The frequency shifts to smaller values from that observed for the free hydroxyl group and there is an increase in intensity. In all the nickel chloride hydrates, the frequency of the O-H stretching region is lower than it is for free O-H. Changes in this band seem to be easier to relate to changes in environment than do those in any other band. Thus, Nakamoto, Margoshes and Rundle (100) have correlated the shift in the stretching frequency with the hydrogen bond distances in a number of compounds.

The prominent band maxima for the different stages of hydration are given in Table 24. The band positions for the O-H stretching regions were determined by five times expansion of the spectra.

From the spectra of different hydrates it is seen that the bands near 3500 cm^{-1} and 3400 cm^{-1} remain sensibly unaltered in spite of the change in composition of the solid from $\text{NiCl}_2 \cdot 6\text{H}_2\text{O}$ to $\text{NiCl}_2 \cdot 2\text{H}_2\text{O}$. Since these bands are present

in $\text{NiCl}_2 \cdot 2\text{H}_2\text{O}$ where hydrogen bonding of the type $\text{O}-\text{H} \cdots \text{O}$ is less favourable on the basis of its structure than $\text{O}-\text{H} \cdots \text{Cl}$, these may be assigned to an $\text{O}-\text{H} \cdots \text{Cl}$ interaction. Another support for such an assignment is provided by the fact that an $\text{O}-\text{H} \cdots \text{O}$ interaction, being much stronger than $\text{O}-\text{H} \cdots \text{Cl}$ interaction, would lead to a greater frequency shift than that observed for these bands at the same internuclear distance (101). The two bands can be assigned as a symmetric and anti-symmetric vibrations on the basis of the observations of Van Thiel, Becker and Pimentel (102) in their matrix isolation study of the hydrogen bonding interaction of water molecules. An additional band at 3290 cm^{-1} is observed for $\text{NiCl}_2 \cdot 4\text{H}_2\text{O}$ and one at 3135 cm^{-1} is observed for $\text{NiCl}_2 \cdot 6\text{H}_2\text{O}$. The gradual emergence of these bands can be seen in the spectra shown in Figs. 54 and 55, for the gradual transformation of one hydrate into the next, and shows that the different hydrates of nickel chloride are $\text{NiCl}_2 \cdot 6\text{H}_2\text{O}$, $\text{NiCl}_2 \cdot 4\text{H}_2\text{O}$ and $\text{NiCl}_2 \cdot 2\text{H}_2\text{O}$, and that the intermediates are mixtures of hydrates. As the water content decreases the bands in the stretching region become sharp. Since the sharpness of the band may be related to the extent of hydrogen bonding, this is a further indication of the increased importance of this kind of interaction in the more highly hydrated salts. Qualitatively then, the conclusions drawn from the infrared spectra produced by the water molecules in a solid metal hydrate are in agreement with the structural

information which is available. On this basis it might be possible to draw some conclusions regarding the placement of water in solid hydrates on the basis of the observations of their infrared spectra in the absence of other structural information.

If the bands at 3500 cm^{-1} and 3400 cm^{-1} are due to symmetric and antisymmetric O-H stretching vibrations influenced by hydrogen bonding to a chloride ion, the O-H...Cl bond distance can be estimated from the graph given by Nakamoto, Margoshes and Rundle (100) for the stretching frequency as a function of distance in hydrogen bonds. The O-H...Cl distance obtained by taking the mean of the symmetric and antisymmetric vibrations for $\text{NiCl}_2 \cdot 6\text{H}_2\text{O}$, $\text{NiCl}_2 \cdot 4\text{H}_2\text{O}$ and $\text{NiCl}_2 \cdot 2\text{H}_2\text{O}$ are 3.19 \AA , 3.19 \AA and 3.18 \AA respectively. This can be compared with the bond distance observed for $\text{CoCl}_2 \cdot 6\text{H}_2\text{O}$ which is isomorphous with $\text{NiCl}_2 \cdot 6\text{H}_2\text{O}$ (98). In $\text{CoCl}_2 \cdot 6\text{H}_2\text{O}$ the $\text{H}_2\text{O}-\text{Cl}$ distance is 3.22 \AA and in $\text{NiCl}_2 \cdot 2\text{H}_2\text{O}$ (69) it is 3.17 \AA . The agreement seems to justify the assignment of this band.

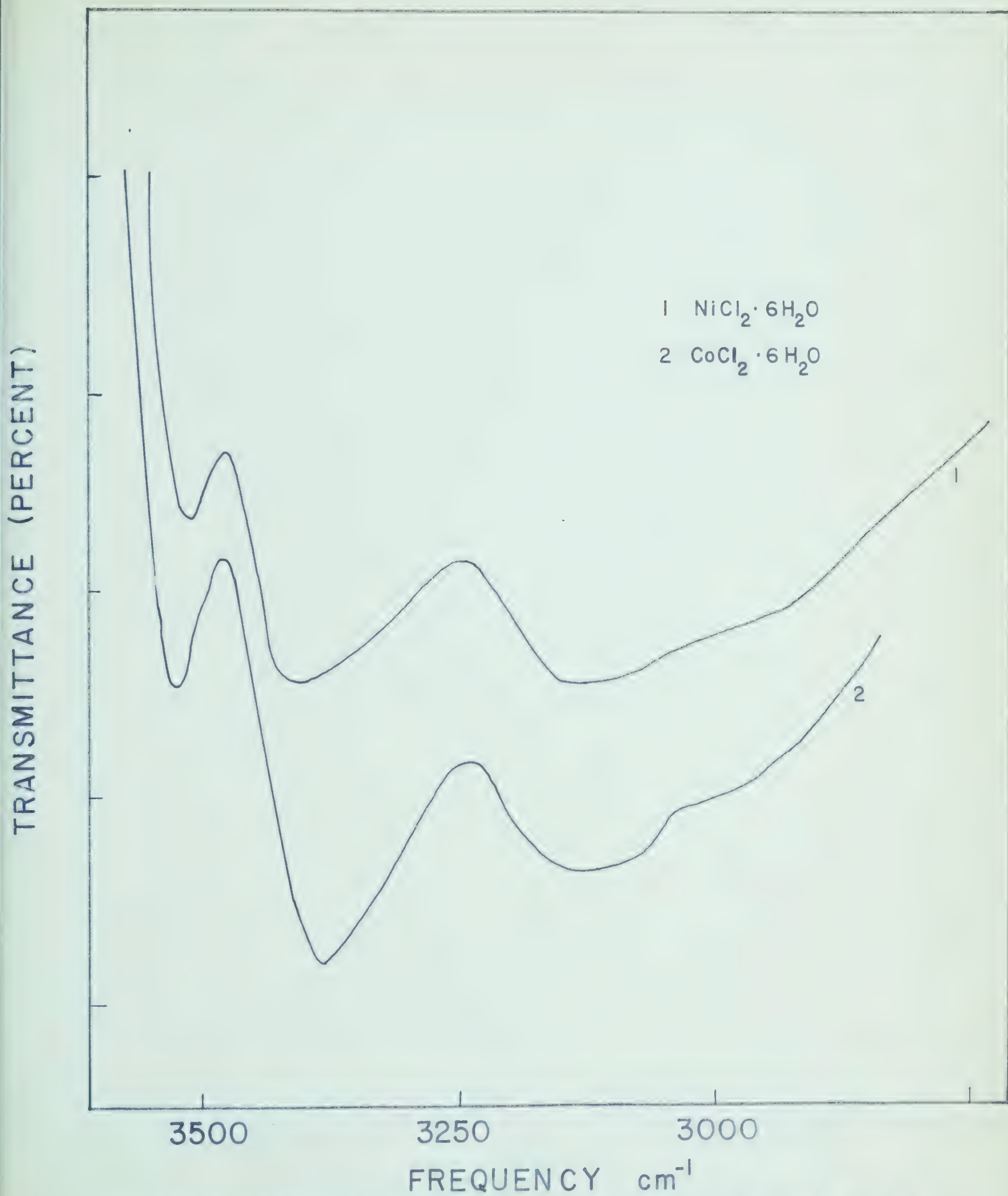
The band at 3290 cm^{-1} for $\text{NiCl}_2 \cdot 4\text{H}_2\text{O}$ may be assigned to O-H frequency influenced by O-H...O bond. This frequency corresponds to a distance of 2.78 \AA . Since $\text{H}_2\text{O}-\text{H}_2\text{O}$ distance in $\text{NiCl}_2 \cdot 4\text{H}_2\text{O}$ is not known it cannot be compared.

The band at 3135 cm^{-1} appears for $\text{NiCl}_2 \cdot 6\text{H}_2\text{O}$. This may be assigned to the O-H stretching frequency influenced by the interaction of free water with the water coordinated

to the metal ion. This frequency corresponds to an O-H...O distance of 2.70 \AA . Assuming the distance of free water to coordinated water in $\text{NiCl}_2 \cdot 6\text{H}_2\text{O}$ to be similar to $\text{CoCl}_2 \cdot 6\text{H}_2\text{O}$, the hydrogen bond distance can be compared. In $\text{CoCl}_2 \cdot 6\text{H}_2\text{O}$ (57) the distance of nonbonded water to the water bonded to the metal ion has been found to be 2.69 \AA . The agreement seems to be fairly satisfactory.

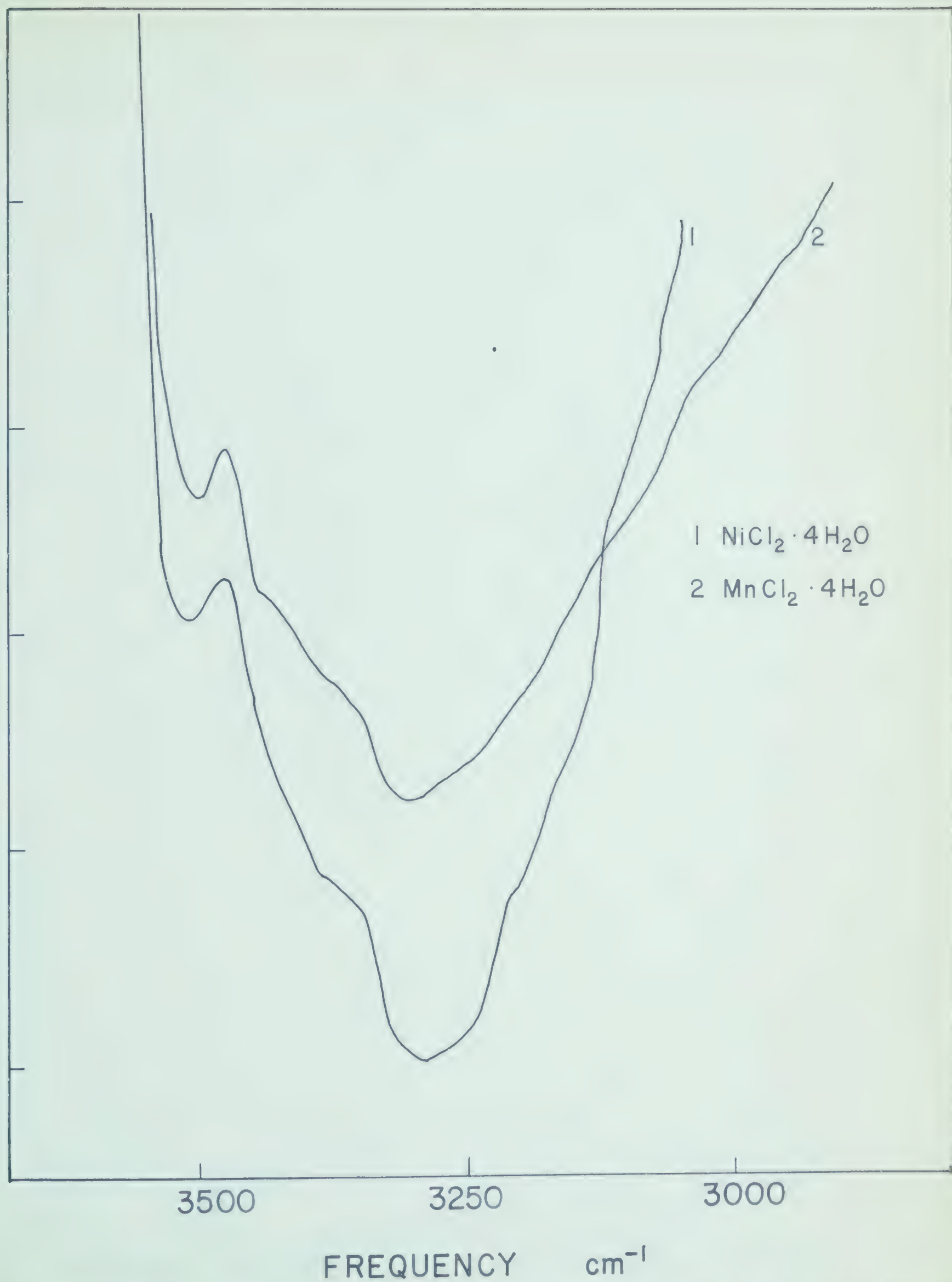
When the crystal structure of a hydrate is not known and the structure of an isomorphous hydrate is known, it should be possible to rationalize the infrared observations in terms of the known structure. Conversely, similarity in the infrared spectra of two hydrated crystals may signify isomorphism. The infrared spectra of some isomorphous and nonisomorphous crystal hydrates are shown in Figs. 67, 68 and 69. $\text{NiCl}_2 \cdot 6\text{H}_2\text{O}$ is isomorphous with $\text{CoCl}_2 \cdot 6\text{H}_2\text{O}$ and $\text{CoCl}_2 \cdot 2\text{H}_2\text{O}$ with $\text{MnCl}_2 \cdot 2\text{H}_2\text{O}$.

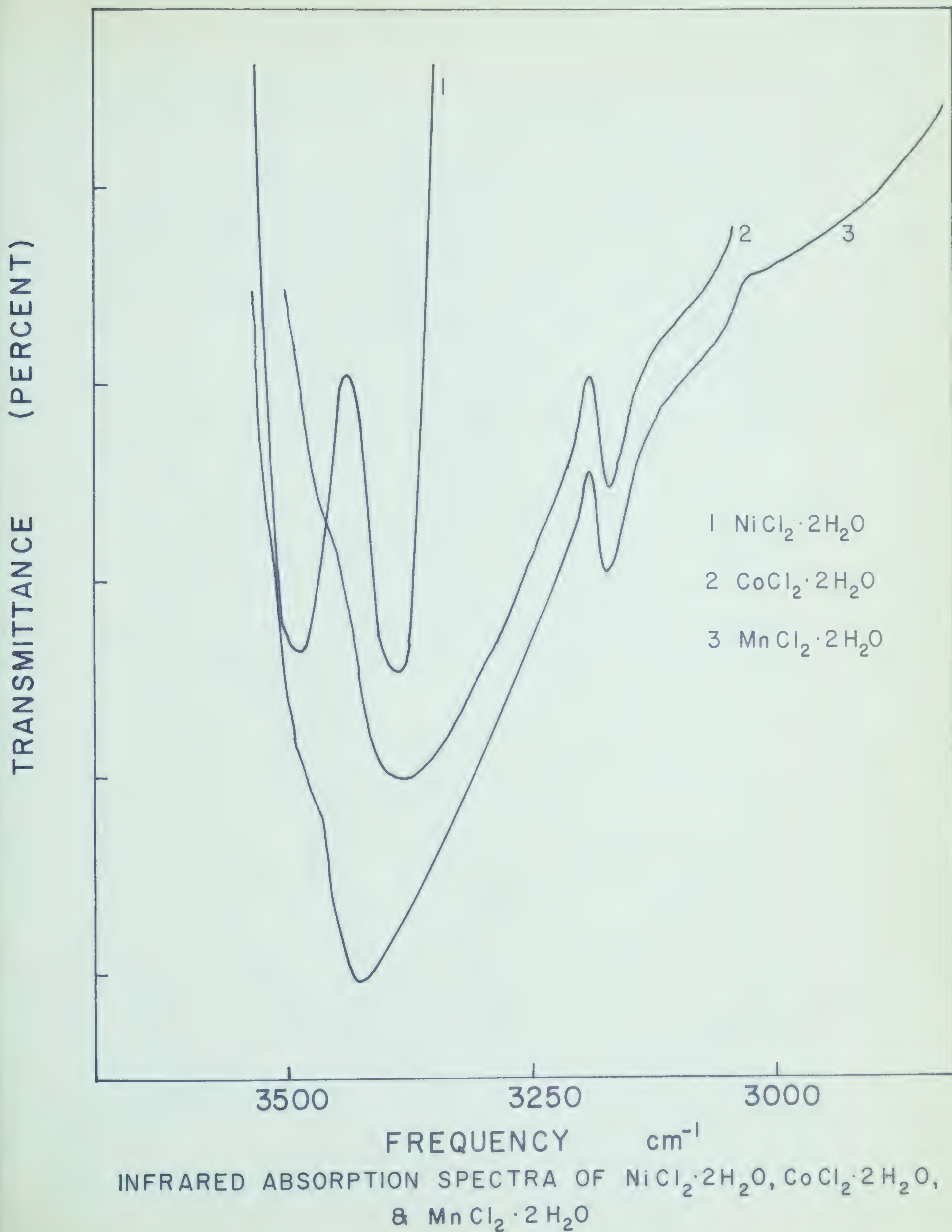
Comparison of the spectra of $\text{NiCl}_2 \cdot 6\text{H}_2\text{O}$ and $\text{CoCl}_2 \cdot 6\text{H}_2\text{O}$, shown in Fig. 67, reveals a close similarity in the shape of the band. The only difference is a slight shift in the positions of the bands, which is due presumably to small changes in the internuclear distances. The spectra of $\text{NiCl}_2 \cdot 4\text{H}_2\text{O}$ and $\text{MnCl}_2 \cdot 4\text{H}_2\text{O}$ are shown in Fig. 68. The similarity in the shape of the spectra of these compounds suggests that they are isomorphous even in the absence of structural information. The spectra of $\text{NiCl}_2 \cdot 2\text{H}_2\text{O}$, $\text{CoCl}_2 \cdot 2\text{H}_2\text{O}$ and $\text{MnCl}_2 \cdot 2\text{H}_2\text{O}$ are shown in Fig. 69. The similarity in the shapes of the

INFRARED ABSORPTION SPECTRA OF $\text{NiCl}_2 \cdot 6\text{H}_2\text{O}$ & $\text{CoCl}_2 \cdot 6\text{H}_2\text{O}$



TRANSMITTANCE (PERCENT)

INFRARED ABSORPTION SPECTRA OF $\text{NiCl}_2 \cdot 4\text{H}_2\text{O}$ (1) & $\text{MnCl}_2 \cdot 4\text{H}_2\text{O}$ (2)



$\text{CoCl}_2 \cdot 2\text{H}_2\text{O}$ and $\text{MnCl}_2 \cdot 2\text{H}_2\text{O}$ spectra is apparent. This similarity is in marked contrast with their dissimilarity to the $\text{NiCl}_2 \cdot 2\text{H}_2\text{O}$ spectrum. It is perhaps significant that $\text{CoCl}_2 \cdot 2\text{H}_2\text{O}$ and $\text{MnCl}_2 \cdot 2\text{H}_2\text{O}$ are isomorphous while $\text{NiCl}_2 \cdot 2\text{H}_2\text{O}$ has a different crystal structure. The positions of the band maxima for the O-H stretching frequencies are given in Table 25.

The infrared absorption spectra of $\text{NiCl}_2 \cdot 6\text{H}_2\text{O}$ at different temperatures, shown in Fig. 70, give structural evidence that the thermodynamic transition temperatures for the conversion of $\text{NiCl}_2 \cdot 6\text{H}_2\text{O} \longrightarrow \text{NiCl}_2 \cdot 4\text{H}_2\text{O} \longrightarrow \text{NiCl}_2 \cdot 2\text{H}_2\text{O}$ are correct (cf. Fig. 50). Evidently the spectrum at 40°C possesses some contribution from $\text{NiCl}_2 \cdot 6\text{H}_2\text{O}$ which is understandable in view of the fact that at lower temperatures equilibrium is attained rather slowly, and sufficient time was not allowed before taking out a sample. The spectrum at 55°C clearly shows that it is that of $\text{NiCl}_2 \cdot 4\text{H}_2\text{O}$ and the spectrum at 75°C is that of $\text{NiCl}_2 \cdot 2\text{H}_2\text{O}$. Also pertinent to this study are the observations reported in Figs. 57 and 58 of the variation of the X-ray diffraction pattern as the extent of dehydration is changed. The patterns for the partially dehydrated species can be constructed by the simple appropriate superposition of the patterns for the known stable hydrates. Thus, these studies also support the conclusion that in the $\text{NiCl}_2\text{-H}_2\text{O}$ system the only hydrates formed are $\text{NiCl}_2 \cdot 6\text{H}_2\text{O}$, $\text{NiCl}_2 \cdot 4\text{H}_2\text{O}$ and $\text{NiCl}_2 \cdot 2\text{H}_2\text{O}$.

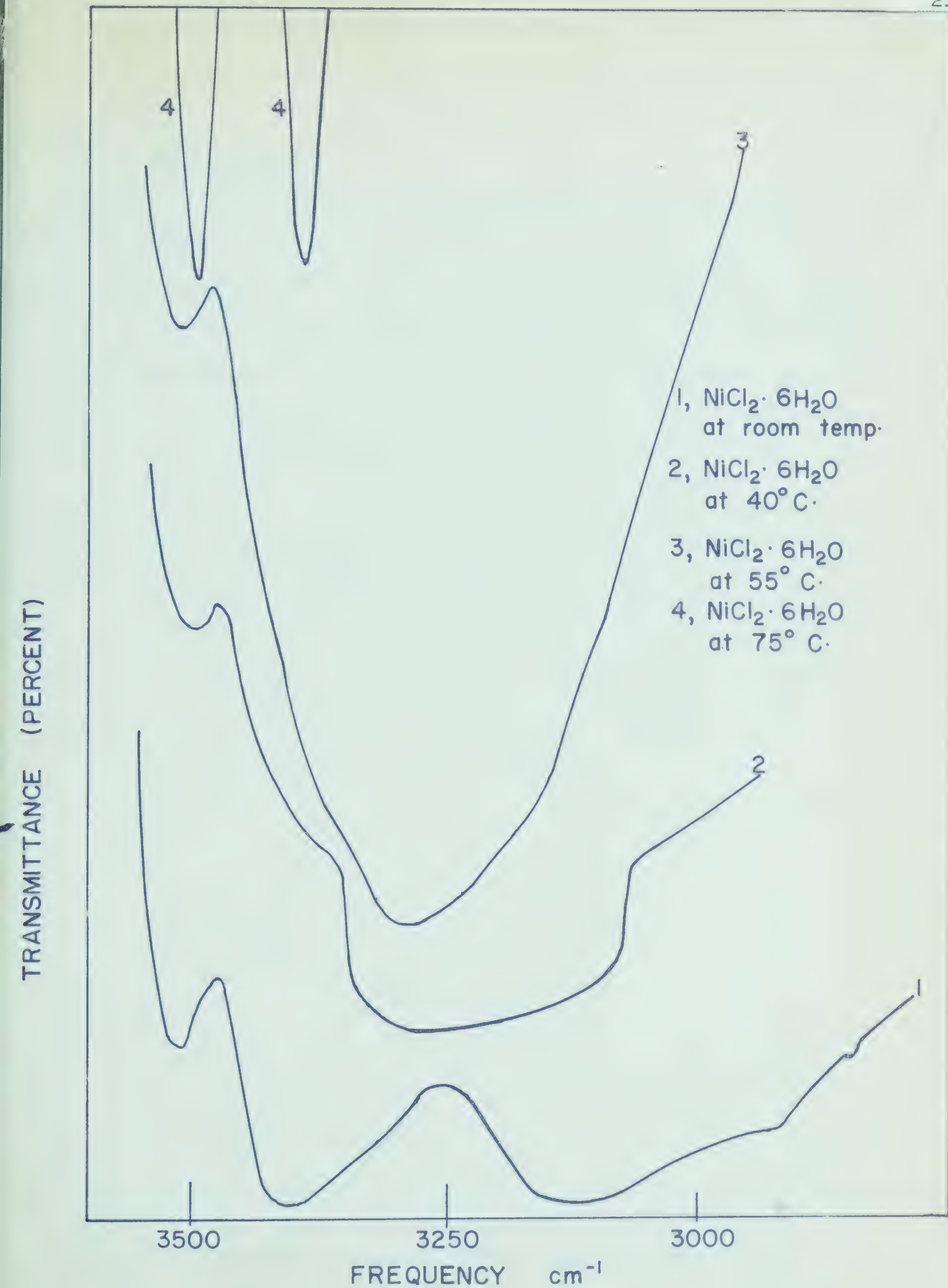
INFRARED ABSORPTION SPECTRA OF $\text{NiCl}_2 \cdot 6\text{H}_2\text{O}$ AT DIFFERENT TEMPERATURES

Fig. 70

Conclusions

The infrared measurements which were made on $\text{NiCl}_2 \cdot 6\text{H}_2\text{O}$ have been interpreted in an earlier section of this discussion in terms of an $\text{O-H}\cdots\text{O}$ interaction at an oxygen to oxygen distance of 2.70 \AA and an $\text{O-H}\cdots\text{Cl}$ interaction at an oxygen to chlorine distance of 3.19 \AA . In addition, there is an indication of a third peak in this spectrum (Fig. 50) which is covered by the $\text{O-H}\cdots\text{Cl}$ peak at 3415 cm^{-1} . The presence of this additional absorber was inferred from the observation that, in this case, the signal at 3415 cm^{-1} was stronger than that at 3515 cm^{-1} whereas, for $\text{NiCl}_2 \cdot 2\text{H}_2\text{O}$, when these two peaks are due to $\text{O-H}\cdots\text{Cl}$ interactions alone, they are of equal intensity. When a model was made these observations could be logically interpreted only in terms of the hydrogen positions shown in Fig. 71.

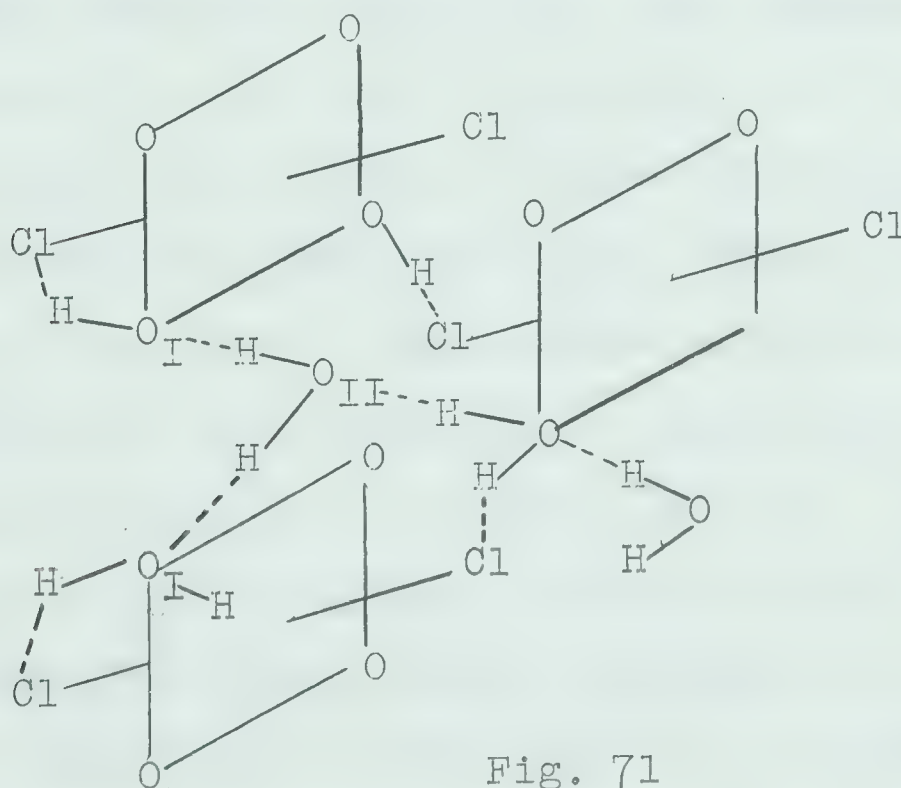


Fig. 71

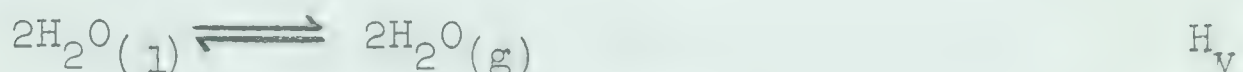
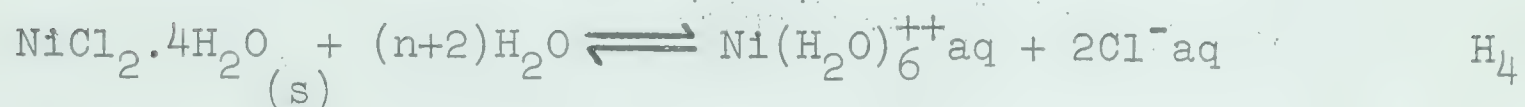
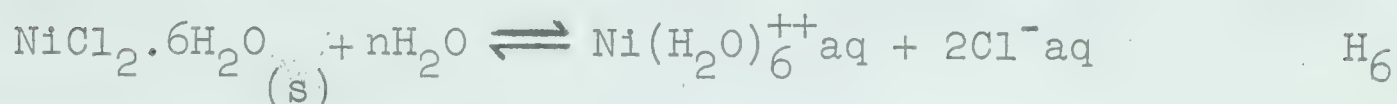
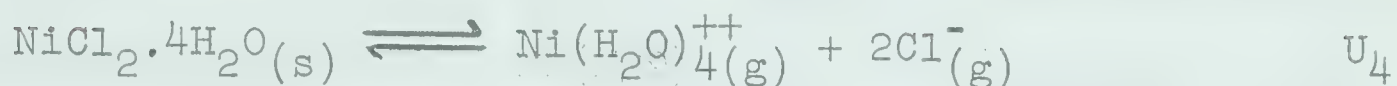
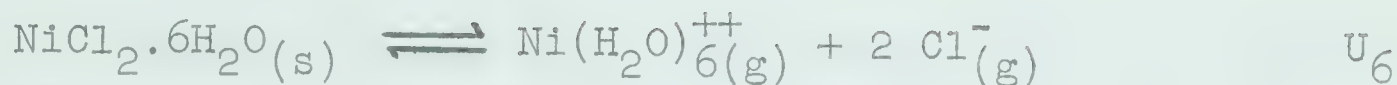
The Position of Hydrogen in $\text{NiCl}_2 \cdot 6\text{H}_2\text{O}$
 Estimated on the Basis of Infrared Observation

This model indicates that there are two kinds of O-H...Cl interaction. One with a chlorine in the same molecular or coordinate unit and the other with a chlorine of an adjacent molecular lattice unit (e.g. $\text{Ni}(\text{H}_2\text{O})_4\text{Cl}_2$). The distances involved in both of these are substantially identical (97), and give good agreement with the estimated distance of 3.19 \AA . Thus, this hydrogen bond makes a small contribution toward maintaining the lattice unit within the crystalline species. It would further appear that there are two kinds of O-H...O interactions. The first of these corresponds to the interaction of the hydrogens of the interstitial water molecule(II) with the oxygens of the inner sphere water molecules. The spacing of the octahedra with respect to one another and to the interstitial water molecule makes the angle $\text{O(I)} - \text{O(II)} - \text{O(I)} = 101^\circ$ and this of course allows the formation of unstrained hydrogen bonds of the type described. The distances involved (97), are also in agreement with the 2.70 \AA estimated previously. The second of these interactions also involves the interstitial water molecule. This time it is the oxygen of the interstitial water molecule interacting with a hydrogen from an inner sphere water molecule of an adjacent octahedral lattice unit as shown in Fig. 71. In this case the oxygen to oxygen distance is actually 3.3 \AA and in addition the hydrogen bond is bent at an angle of about 120° . Both of these factors would cause the O-H...O interaction to be less

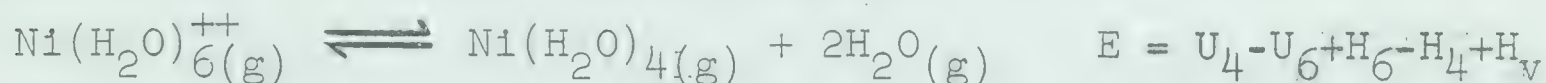
than in the previous case and where this is true the absorption maximum for the hydrogen bond is expected to fall at higher frequency. This then could be the postulated additional absorber at 3415 cm^{-1} . These three hydrogen bonds, formed by each interstitial water molecule, perform dual functions. They serve, at least partially, to maintain the lattice structure and, again at least partially, to hold the water molecules within the lattice. Both of these interactions will ultimately be of importance. However, let us first consider the problem of the binding of the water molecules within the lattice. The energy terms which are involved can be divided into roughly four classes. They are dipole-dipole attraction to other water molecules, ion-dipole attraction to the nickel ions, ion-dipole attraction to the chloride ions and van der Waal's repulsion effects. Using the procedure described by Garrick (103) these various terms were evaluated for a single water molecule and shown to be -16 Kcal/mole , -20 Kcal/mole , $+5\text{ Kcal/mole}$ and $+3.5\text{ Kcal/mole}$. Then, assuming that no rearrangement of the lattice occurred, 27.5 Kcal would be required to remove a single mole of water from the hexahydrate. This represents a crude, but perhaps not unrealistic value. An attempt will now be made to compare this value with a value obtained from the data of the present work.

The problem of the evaluation of the binding energy of the interstitial water molecules was attacked through the

the following cycle.



From these equations the following can be obtained:



The required values for H_6 and H_4 have been determined experimentally. Hence, the only doubtful feature of the portion of the cycle is involved in the cancellation of the solution phases corresponding to the two solutions. This has been shown to be justifiable in the section where the results of the vapour pressure-composition measurements on the system $\text{NiCl}_2\text{-H}_2\text{O}$ -en were discussed. The heat of vaporization of water $H_v/2$ was obtained from the literature (104). The only quantities which remain to be estimated are U_6 and U_4 . These are the lattice energies of $\text{NiCl}_2 \cdot 6\text{H}_2\text{O}$ and $\text{NiCl}_2 \cdot 4\text{H}_2\text{O}$ which are defined as the energy change in the process of bringing the ions infinitely separated from one another to the position

they occupy in the crystal.

Born and Lande (105, 106) assumed that in addition to Coulombic attractions between the ions there are intrinsic repulsive forces which change rapidly with distance. Thus, the potential function of a system consisting of two ions at a distance 'r' apart may be written as:

$$\phi = - \frac{Z_1 \cdot Z_2 e^2}{r} + \frac{b}{r^n}$$

Z_1 and Z_2 are valences of the ions

e is the unit of electrical charge

b and n are constants.

This potential function is to be regarded as a first approximation only. The van der Waal's attractive forces, forces due to polarization and contributions due to induced dipole moments have been neglected.

The methods proposed for the calculation of lattice energies may be conveniently classified as extended classical calculations in which Madelung, repulsive, dispersion, zero-point and permanent electrical multipole energy terms are taken into account, Kapustinskii and Templeton approximations, quantum mechanical prediction, and hydration enthalpies. Direct determination is possible in a few cases. These methods have been extensively reviewed by Sherman (107) and Waddington (108) and in recent years the calculation of lattice energies has attracted considerable attention (109 - 124).

Examination of Fig. 62 reveals that for the hexahydrate the arrangement of chloride ions in relation to the nickel ions is such that a distorted cadmium chloride layer structure is produced. The distortion is such that the polar chlorides are closer to the nickel ions than are the planar chlorides and the axis of the polar chlorides makes an angle of $122^{\circ}10'$ with the planar chlorides. As a first approximation then, it should be possible to treat this system as a cadmium chloride layer lattice. On the basis of this assumption the development suggested by Katzin and Ferraro was adopted (120, 121). The lattice energies were calculated from the molecular volume parameter, viz.

$$U = 279.0(\rho/M)^{1/3} A(1 - \frac{1}{n})$$

where ρ = density of the crystalline compound

M = molecular weight of the compound

A = Madelung constant

n is related to the ionic repulsion term

and is of the order of magnitude of 10.

The term ' n ' has been replaced by $\frac{0.345}{R}$ where R is an ion-distance parameter (in \AA) as proposed by Verwey and de Boer (125). Katzin and Ferraro (120) made the further substitution of replacing R by $10^8 / (3 \times 6.023 \times 10^{23} \times \rho/M)^{1/3}$, i.e. R = cube root of the mean ionic volume.

Thus the equation reduces to:

$$U = 279(\rho/M)^{1/3}A \left[1 - \frac{0.345(3 \times 6.023 \times 10^{23} \times \rho/M)^{1/3}}{10^8} \right]$$

Thus, the only experimentally determined parameter which is required is the density of the solid phase. The density of $\text{NiCl}_2 \cdot 6\text{H}_2\text{O}$ has been found to be 1.921 by Mizuno (97). Introduction of this value for the density and the value 6.21 for A in the equation leads to the value shown in column 2 of Table 28 for the lattice energy of $\text{NiCl}_2 \cdot 6\text{H}_2\text{O}$.

TABLE 28

Lattice Energy Values of Nickel Chloride Hydrates

	<u>U (Kcal/mole)</u>	<u>U corrected</u>
$\text{NiCl}_2 \cdot 6\text{H}_2\text{O}$	318	321
$\text{NiCl}_2 \cdot 4\text{H}_2\text{O}$	365	351
$\text{NiCl}_2 \cdot 2\text{H}_2\text{O}$	412	402
NiCl_2	488	488

Values for the lattice energies for the tetra- and dihydrates and the anhydrous salt obtained by this same procedure are also shown in Table 28. In obtaining these values, use has been made of the known cadmium chloride structure for anhydrous nickel chloride and of the cadmium chloride-like structure for nickel chloride dihydrate. It has also been assumed that the structure of nickel chloride tetrahydrate is

obtained from that of nickel chloride hexahydrate without major reorganization of the lattice units as shown in Fig. 56, and that the cadmium chloride approximation can be applied to this system also. The densities of these systems were therefore required. The density of nickel chloride dihydrate was found to be 2.56 by Vainshtein (99) and for NiCl_2 to be 3.55 (126). The only unknown density is that of $\text{NiCl}_2 \cdot 4\text{H}_2\text{O}$. It was found that there is, to a first approximation, a linear relationship between densities of $\text{CoCl}_2 \cdot 6\text{H}_2\text{O}$, $\text{CoCl}_2 \cdot 4\text{H}_2\text{O}$ and $\text{CoCl}_2 \cdot 2\text{H}_2\text{O}$ with the number of water molecules (120) as shown in Fig. 72 (1). Assuming this to be valid the density of $\text{NiCl}_2 \cdot 4\text{H}_2\text{O}$ was interpolated from the plot of densities of $\text{NiCl}_2 \cdot 6\text{H}_2\text{O}$ and $\text{NiCl}_2 \cdot 2\text{H}_2\text{O}$ against water content and found to be 2.24 as shown in Fig. 72(2).

The lattice energies shown in column 2 of Table 28 represent the energies of disruption of an anhydrous system into nickel(II) ions and chloride ions and should be in error by the contribution which the water molecules make to the stability of the lattice. An effort must then be made to apply appropriate corrections in order to bring the lattice energies in line with reality.

Individual $\text{Ni}(\text{H}_2\text{O})_4\text{Cl}_2$ units are held in the lattice by inter-unit forces of the O-H...Cl, O-H...O and Ni...O types. This is, of course, in addition to the $\text{Ni}^{++} - \text{Cl}^-$ forces which have already been accounted for. Examination of

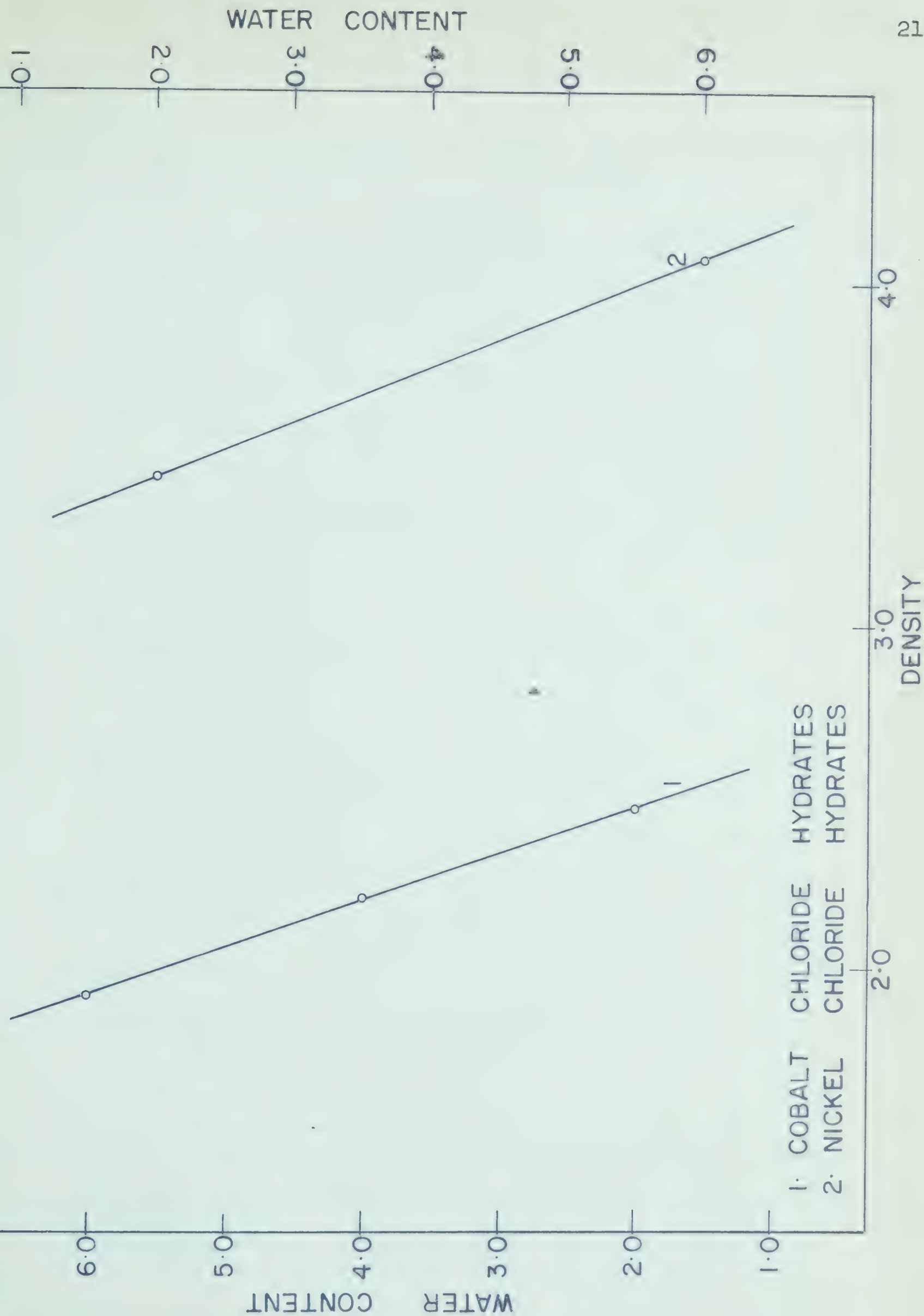


Fig. 72

Fig. 62, or more clearly of a model, reveals that the factors involved are 2 bent O-H...O bonds at a distance of 3.3 \AA , 4 linear O-H...O bonds at a distance of 2.70 \AA , 4 nearly linear O-H...Cl bonds at a distance of 3.19 \AA , 2 Ni...H₂O bonds at a distance of 4.05 \AA , and 8 Cl...OH₂ repulsion terms at a distance of 3.75 \AA . By applying the pure electrostatic procedure of Garrick (103), in just the way used previously in this discussion, these terms amount to a correction of +15 Kcal/mole of Ni(H₂O)₆Cl₂. Once this unit has been produced there still remain 4 O-H...Cl bonds at 3.17 \AA and 8 Cl...OH₂ repulsions at 3.17 \AA to be taken into account. These are estimated to be +8 Kcal and -20 Kcal respectively. Thus, the net result is that the calculated lattice energy for nickel chloride hexahydrate should be corrected by the addition 3 Kcal/mole. This corrected value is shown in column 3 of Table 28. In a similar way corrections may be applied to the lattice energies of the other hydrates. The correction for the tetrahydrate is less certain since the exact positions of the atoms are not known. However, the interaction terms being considered are not strongly dependent upon the distance at these internuclear separations. Hence the value deduced is based upon the structure of Fig. 63 in which water molecules have been lost from the interstitial positions and the Ni(H₂O)₄Cl₂ octahedra have moved closer together along the c axis. The estimated correction is -14 Kcal. The

corresponding correction for the more precisely understood dihydrate structure is -10 Kcal.

These values may now be introduced into the thermochemical cycle described above. The cycle is shown below for the hexa-to tetrahydrate transformation.

$$\begin{aligned} E &= U_4 - U_6 + H_6 - H_4 + H_V \\ &= 351 - 321 + 1.46 - 1.14 + 21.8 \\ &= 52 \text{ Kcal.} \end{aligned}$$

The value of 52 Kcal for the removal of the pair of interstitial water molecules is in remarkable agreement with that estimated above for the energy of removal of the pair of interstitial water molecules (55 Kcal). In fact, this order of agreement is likely fortuitous. Nevertheless, it does indicate that the general procedure is a valid one, and that it is applicable to the tetra- to dihydrate transformation to yield information about the bond energy of the directly coordinated water molecules. Upon substitution of the data into the cycle a value of 79.5 Kcal is obtained for the binding of the third and fourth water molecules in the solid hydrate. It is unfortunate that a trihydrate was not available so that individual values of the binding energy for the third and fourth water molecules could have been obtained. Even so, the average value of 40 Kcal for the binding energy of single water molecules is not in unreasonable agreement with

the 50 Kcal which is expected (121, 127). The somewhat low value is undoubtedly related to the extra repulsion terms due to the inclusion of chloride ions in the original octahedra.

Summary

The modes of decomposition of the hydrates of nickel chloride have been examined and it has been shown that all of the observed phenomena can be explained on the basis of three stable hydrates. These are $\text{NiCl}_2 \cdot 6\text{H}_2\text{O}$, $\text{NiCl}_2 \cdot 4\text{H}_2\text{O}$ and $\text{NiCl}_2 \cdot 2\text{H}_2\text{O}$. The decomposition of these appears to proceed through displacement reactions in which chloride ions from adjacent structural units move in to take the lattice positions vacated by the outgoing water molecules. The rate determining step for the decomposition then appears to be the diffusion of the water molecules to the surface from the interior or the evaporation of the water from the surface. These two processes appear to be of comparable magnitudes but at low humidities the former appears to govern whereas at high humidities it is the latter which governs.

The energetics of the decomposition have led to values for the heats of formation and heats of solution of the hydrates. These latter values have then been used to estimate a reasonable value for the energy of binding of water molecules in an unsymmetrical octahedral complex. This value is of interest in connection with studies of the rates of exchange of water molecules in such unsymmetrical environments.

BIBLIOGRAPHY

1. Eigen, M., "Advances in the Chemistry of Coordination Compounds", MacMillan Co., London (1961)
2. Hamer, W.J., "The Structure of Electrolytic Solutions", John Wiley & Sons, New York (1957)
3. Taube, H., and Rutenberg A.C., J. Am. Chem. Soc., 72, 5561 (1951)
4. Rundle, R.E., J. Chem. Phys. 23, 2450 (1955)
5. Orgel, L.E., "Transition Metal Chemistry", Methuen & Co. Ltd., London (1960)
6. Orgel, L.E., J. Chem. Soc., 4756 (1952)
7. Irving, H., and Williams, R.J.P., J. Chem. Soc., 3192 (1953)
8. Derby, I.H., and Yngve, V., J. Am. Chem. Soc., 38, 1439 (1916)
- 9(a). Pearce, J.N., and Eckstrom, H.C., J. Phys. Chem., 41, 563 (1937)
- 9(b). Mellor, J.W., "A Comprehensive Treatise on Inorganic and Theoretical Chemistry", Vol. 15, 412, Longmans Green and Co., London (1936)
10. Foote, H.W., J. Am. Chem. Soc., 45, 663 (1923)
11. Bull, R., Angew, Chem., 49, 145 (1936)
12. Chihara, H., and Nakatsu, K., Bull. Chem. Soc. Japan, 32, 903 (1959)

13. Grunwald, E., and Bacarella, A.L., J. Am. Chem. Soc., 80, 3840 (1958)
14. Basolo, F., and Pearson, R.G., "Mechanisms of Inorganic Reactions", John Wiley and Sons, New York, 1958, Page 65
15. Gurney, R.W., "Ionic Processes in Solution", McGraw-Hill Book Company, Inc., New York, 1953
16. Taylor, T.I., and Klug, H.D., J. Chem. Phys., 4, 601 (1936)
17. Colvin, J., and Hume, J., Trans. Faraday Soc., 34, 969 (1938)
18. Garner, W.E., and Tanner, M.G., J. Chem. Soc., 47, (1930)
19. Hume, J., and Colvin, J., Proc. Roy. Soc., 132A, 548 (1931)
20. Smith, M.L., and Topley, B., Proc. Roy. Soc., 134A, 224 (1932)
21. Rakuzin, M.A., and Brodski, D.A., Z. Angew. Chem., 40, 836 (1927)
22. Demassieux, N., and Federoff, B., Compt. rend., 206, 1649 (1938)
23. Simon, A., and Knauer, H., Z. anorg. Chem., 242, 375 (1939)
24. Plaksin, I.N., Ann. Secteur anal. Phys. Chim., Inst. Chim. gen (U.S.S.R.) 9, 271 (1936)

25. Membrauer, R., Z. Physik. Chem., 172A, 64 (1935)
26. Gapon, E.N., J. Chim. Phys., 25, 154 (1928)
27. Frost, G.B., Moon, K.A., and Tompkins, E.H., Can. J. Chem., 29, 604 (1951)
28. Wheeler, R.C., and Frost, G.B., Can. J. Chem., 33, 546 (1955)
29. Vallet, P. Ann. Chim., 7, 298, (1937)
30. Acock, G.P., Garner, W.E., Milsted, J., and Willavoys, H.J., Proc. Roy. Soc., 189A, 508 (1947)
31. Topley, B., and Smith, M.L., J. Chem. Soc., 321 (1935)
32. Cooper, M.M., Colvin, J., and Hume, J., Trans. Faraday Soc., 29, 576 (1933)
33. Garner, W.E., Trans. Faraday Soc., 34, 940 (1938)
34. Hume, J., and Colvin, J., Proc. Roy. Soc., 125A, 635 (1929)
35. Diev, N.P., Trudy Inst. Khim. i. Met., Akad. Nauk S.S.S.R., Ural Filial 3, 13 (1955)
36. Turco, A., and Salsilli, L., Gazz. chim. ital., 85, 192 (1955)
37. Bradley, R.S., Colvin, J., and Hume, J., Proc. Roy. Soc., 137A, 531 (1932)
38. Buckle, E.R., J. Phys. Chem., 63, 1231 (1959)
39. Reisman, A., and Karlak, J., J. Am. Chem. Soc., 80, 6500 (1958)

40. Borchardt, H.J., and Daniels, F., J. Phys. Chem., 61, 917 (1957)
41. Rabatin, J.G., Gale, R.H., and Newkirk, A.E., J. Phys. Chem., 64, 491 (1960)
42. Groves, W.O., and Edwards, J.W., J. Phys. Chem., 65, 645 (1961)
43. Flanagan, T.B., Trans. Faraday Soc., 57, 797 (1961)
44. Topley, B., Proc. Roy. Soc., 136A, 413 (1932)
45. Garner, W.E., "Chemistry of the Solid State", Butterworths Scientific Publications, London, 1955, Page 215
46. Garner, W.E., and Jennings, T.J., Proc. Roy. Soc., 224A, 460 (1954)
47. Ref. 45 page 185
48. Ref. 46 page 460
49. Volmer, M., and Seydel, G., Z. phys. Chem., 179, 153 (1937)
50. Smith, M.L., and Topley, B., Proc. Roy. Soc., 134A, 224 (1931)
51. Frost, G.B., and Campbell, R.A., Can. J. Chem., 31, 107 (1953)
52. Crowther, E.M., and Coutts, J.R.H., Proc. Roy. Soc., 106A, 215 (1924)
53. Tate, F.G.H., and Warren, L.A., Trans. Faraday Soc., 35, 1192 (1939)
54. Ghosh, B.N., J. Indian Chem. Soc., 18, 472 (1941)

55. Castor, W.S., and Basolo, F., J. Am. Chem. Soc., 75, 4804 (1953)
56. Castor, W.S., Ph.D. Thesis Northwestern University, 1950
57. Mizuno, J., J. Phys. Soc., Japan, 15, 1412 (1960)
58. Beevers, C.A., and Lipson, H., Proc. Roy. Soc., 146A, 570 (1934)
59. Harker, D., Z. Krist., 93, 136 (1936)
60. McGillavry, C.H., and Bijvoet, J.M., Z. Krist., 94, 231 (1936)
61. Vainshtein, B.K., Doklady Akad. Nauk S.S.S.R., 68, 301 (1949)
62. Herzberg, G., "Infrared and Raman Spectra of Polyatomic Molecules", D. van Nostrand Co., New York, 1956, Page 195
63. Gormen, M., J. Chem. Edn., 34, 304 (1957)
64. Cannon, C.G., Spec. Chim. Acta., 10, 341 (1958)
65. Linnett, J.W., Quart. Rev., 1, 73 (1947)
66. Coggeshall, N.D., J. Chem. Phys., 18, 978 (1950)
67. Badger, R.M., J. Chem. Phys., 8, 288 (1940)
68. Bratoz, S., and Hadzi, D., J. Chem. Phys., 27, 991 (1957)
69. Barrow, G.M., J. Phys. Chem., 59, 1129 (1955)
70. Tsubomura, H., J. Chem. Phys., 23, 2130 (1955)
24, 927 (1956)
71. Huggins, C.M., and Pimentel, G. C., J. Phys. Chem., 60, 1615 (1956)

72. Bellamy, L.J., Infrared Spectra of Complex Molecules, Methuen & Co., London, 1959, Page 379
73. Kletz, T.A., and Price, W.C., J. Chem. Soc., 644 (1947)
74. Ref. 72 Page 380
75. Ref. 72 Page 380
76. Coblentz, W.W., J. Franklin Inst. 172, 309 (1912)
77. Hunt, J.M., Wishered, M.P., and Bonham, L.D., Anal. Chem. 22, 1478 (1950)
78. Stimson, M.M., and O'Donnell, M.J., J. Am. Chem. Soc., 74, 1805 (1952)
79. Duyckaerts, G., Analysts., 84, 201 (1959)
80. Ref. 79, Page 209
81. Ketelaar, A.A., Haas, C., and van der Elsken, J., J. Chem. Phys., 24, 624 (1956)
82. Baker, A.W., J. Phys. Chem., 61, 450 (1957)
83. Stewart, J.E., J. Chim. Phys., 26, 248 (1957)
84. Ref. 82, Page 450
85. Coblentz, W.W., Bull. Bur. Stand., 7, 619 (1911)
86. Miller, F.A., and Wilkins, C.H., Anal. Chem., 24, 1253 (1952)
87. Frederikson, L.D., Anal. Chem., 26, 1883 (1954)
88. Corbridge, D.E.C., and Lowe, E.J., J. Chem. Soc., 493 (1954)
89. Lucchesi, P.J., and Glasson, W.A., J. Am. Chem. Soc., 78, 1347 (1956)

90. Fujita, J., Nakamoto, K., and Kobayashi, M., J. Am. Chem. Soc., 78, 3963 (1956)
91. Brame, E.G., Johnson, F.A., Larsen, E.M., and Meloche, V.W., J. Inorg. Nuclear Chem. 6, 99 (1958)
- 92(a). Sanderson, R.T., "Vacuum Manipulation of Volatile Compounds", John Wiley & Sons, Inc., New York, 1948
- 92(b). Brown, H.C., Taylor, M.D., and Gerstein, M., J. Am. Chem. Soc., 66, 431 (1944)
93. Argue, G.R., M.Sc. Thesis, University of Alberta, 1956
94. Katzin, L.I., and Ferraro, J.R., J. Am. Chem. Soc., 72, 5451 (1950)
95. Rossini, F.D., Wagman, D.D., Evans, W.H., Levine, S., and Jaffe, I., "Selected Values of Chemical Thermodynamic Properties, NBS Circular 500", National Bureau of Standards, U.S. Department of Commerce, U.S. Government Printing Office, Washington (1952)
- 96(a). Allen, J.A., Aust. J. Chem., 14, 20 (1961)
- 96(b). Taylor, T.I., and Taylor, G.G., Ind. Eng. Chem., 27, 672 (1935)
- 97(a). Stroganov, E.V., Kozhina, I.I., Andreyeva, S.N., and Kolyadin, A.B., Vestnik Leningrad Univ., 4, 130 (1960)
- 97(b). Mizuno, J., J. Phys. Soc., Japan, 16, 1574 (1961)
98. Mizuno, J., Ukei, K., and Sugawara, T., J. Phys. Soc., Japan, 14, 383 (1959)
99. Vainshtein, B.K., Zhur. Fiz. Khim., 26, 1774 (1952)
100. Nakamoto, K., Margoshes, M., and Rundle, R.E., J. Am. Chem. Soc., 77, 6480 (1955)

101. Ref. 100, Page 6482
102. Van Thiel, M., Becker, E.D., Pimentel, G.C., J. Chem. Phys., 27, 486 (1957)
103. Garrick, F.J., Phil. Mag. 9, 131 (1930)
104. Lange, N.A., "Handbook of Chemistry", Handbook Publishers Inc., Sandusky, Ohio (1946)
105. Born, M., and Lande, A., Ber. Preuss, Akad. Wiss., Berlin, 45, 1048 (1918)
106. Born, M., and Lande, A., Verhandl. deut. Physik. Ger. 20, 210 (1918)
107. Sherman, J., Chem. Rev., 11, 93 (1932)
108. Waddington, T.D., "Advances in Inorganic Chemistry and Radio-chemistry", Vol. I, Academic Press Inc., New York, 1959, Page 157
109. Cotton, F.A., Acta Chem. Scand., 10, 1520 (1956)
110. Beven, S.C., and Morris, D.F.C., J. Chem. Soc., 516 (1960)
111. Harries, H.J., and Morris, D.F.C., Acta. Cryst., 12, 657 (1959)
112. Cubicciotti, D., J. Chem. Phys., 31, 1646 (1959)
113. Kapustinskii, A.F., Quart. Rev., 10, 283 (1956)
114. Altshuller, A.P., J. Am. Chem. Soc., 77, 5455 (1955)
115. Ladd, M.F.C., and Lee, W.H., J. Inorg. Nucl. Chem. 13, 218 (1960)

116. Ladd, M.F.C., and Lee, W.H., Trans. Faraday Soc., 54, 34 (1958)
 117. Morris, D.F.C., J. Inorg. Nuclear Chem., 6, 295 (1958)
 118. Ladd, M.F.C., and Lee, W.H., J. Inorg. Nuclear Chem., 14, 14 (1960)
 119. Brewer, L., and Mastik, D.F., J. Am. Chem. Soc., 73, 2045 (1951)
 120. Katzin, L.I., and Ferraro, J.R., J. Am. Chem. Soc., 74, 6040 (1952)
 121. Katzin, L.I., and Ferraro, J.R., J. Am. Chem. Soc., 75, 3821 (1953)
 122. Yatsimirskii, K.B., "Thermochemie von Komplexverbindungen", Akademie-Verlag, Berlin, 1956
 123. Waddington, T.C., Trans. Faraday Soc., 54, 25 (1958)
 124. Gray, P., and Waddington, T.C. Proc. Roy. Soc., 235A, 481 (1956)
 125. Verwey, J.W., de Boer, J.H., Rec. trav. chim., 55, 431 (1936)
 126. Ref. 37, Page 565
 127. Basolo, F., and Pearson, R.G., "Mechanisms of Inorganic Reactions", John Wiley & Sons, Inc., New York (1958)
- Page 50.

B29799